2009

DESIGN, DEVELOPMENT, AND APPLICATION OF A TRANSDUCER TO QUANTIFY TENSION IN THE MEDIAL COLLATERAL LIGAMENT OF THE ELBOW

Katherine E. Fay

DESIGN, DEVELOPMENT, AND APPLICATION OF A TRANSDUCER TO QUANTIFY TENSION IN THE MEDIAL COLLATERAL LIGAMENT OF THE ELBOW

(Spine Title: A Transducer to Quantify Tension in the Medial Collateral Ligament of the Elbow)

(Thesis Format: Integrated-Article)

by

Katherine E. Fay

Graduate Program in Biomedical Engineering

A thesis submitted in partial fulfillment
of the requirements for the degree of
Master of Engineering Science

School of Graduate and Postdoctoral Studies
The University of Western Ontario
London, Ontario, Canada

THE UNIVERSITY OF WESTERN ONTARIO
School of Graduate and Postdoctoral Studies

CERTIFICATE OF EXAMINATION

Joint-Supervisor

Dr. James Johnson, PhD, PEng
Department of Mechanical and Materials Engineering
Department of Medical Biophysics
Department of Surgery

Joint-Supervisor

Dr. Graham King, MD, MSc, FRCSC
Department of Medical Biophysics
Department of Surgery

Examiners

Dr. George Athwal

Dr. James Dickey

Dr. James Lacefield

The thesis by

Katherine Elizabeth Fay

entitled:

Design, Development, and Application of a Transducer to Quantify Tension in the Medial Collateral Ligament of the Elbow

is accepted in partial fulfillment of the
requirements for the degree of
Master of Engineering Science

Date_____

Chair of the Thesis Examination Board

ABSTRACT

Techniques have evolved for quantifying human tendon and ligament forces in the lower extremity; however, custom developed systems for the upper extremity, particularly the elbow, are not well described. Consequently, ligament forces of the human elbow joint have not been reported. Knowledge of the magnitudes of tension of the primary valgus stabilizer, the anterior bundle of the medial collateral ligament (AMCL), would allow for an improved understanding of the load environment of this tissue. Mechanisms of AMCL injury include chronic high intensity overuse, radial head fracture, and elbow dislocations. This work focused on the design and development of a custom designed E-form frame buckle transducer to quantify AMCL tension *in vitro*. To understand the basic biomechanical characteristics of the AMCL, a series of *in vitro* studies employing this device were conducted. The specific objectives of this work were: (1) to quantify the magnitude of AMCL tension through the arc of elbow flexion; (2) to determine the effect of wrist flexor muscle loading on the magnitude of AMCL tension through the arc of elbow flexion; and (3) to evaluate the effect of radial head excision and arthroplasty on the magnitude of AMCL tension through the arc of elbow flexion. The chief findings were: (1) AMCL tension increased with increasing angles of elbow flexion (*i.e.* AMCL tension was greater at full flexion than at full extension); (2) increased wrist flexor muscle loading caused AMCL tension levels to decrease; and (3) radial head excision increased AMCL tension levels, whereas metallic radial head arthroplasty restored near-normal AMCL tension levels. Furthermore, for all investigations, AMCL tension levels were greater with the arm oriented in the valgus position than in the dependent (*i.e.* vertical) position. Improved knowledge of AMCL tissue biomechanics will allow for the design and evaluation of improved methods of AMCL repair/reconstruction and rehabilitation, and assist in the development of an artificial AMCL and *in vitro* biomechanical models of the elbow. Furthermore, this transducer will permit numerous additional projects to be explored that will investigate the ligament and soft tissue loading at the elbow, shoulder, and wrist.

Keywords: elbow, biomechanics, force transducer, ligament force, medial collateral ligament

CO-AUTHORSHIP

My primary contribution to this study was the design and development of the buckle transducer, including strain gauge selection. Dr. Jim Johnson, Dr. Graham King, and Louis Ferreira provided suggestions as to how to improve and refine the design of the buckle transducer. Karin Hirooka was instrumental in the design of the buckle transducer – he assisted with all phases of the mathematical modelling design process. The University of Western Ontario Machine Services manufactured several iterations of the buckle transducer. Brendon Beaton applied the specialty ordered strain gauges to the transducer, and Josh Giles assisted with signal conditioning and data acquisition for the transducer's calibration and hysteresis investigations.

Dr. Johnson, Dr. King, and myself conceived the study, and I developed the testing protocol with their guidance, as well as with Louis Ferreira's input. Dr. King prepared all specimens for testing and performed all surgical techniques. The specialized testing apparatus, and all of its supporting software, was previously designed by Louis Ferreira. I performed the testing and Emily Lalone operated the simulator. I analysed all elbow kinematic data using a custom developed LabVIEW software program, designed by Louis Ferreira, as well as through the use of Microsoft Office Excel 2002, and SPSS. I filtered all source tension data using a Matlab program, written by Petar Seslija, and analysed it using Microsoft Office Excel 2002 and SPSS. Dr. Johnson and Dr. King provided suggestions as to how to analyse the data, and Louis Ferreira provided assistance with SPSS data interpretation. I composed the manuscript, which was reviewed by all co-authors.

DEDICATION

To my best friend, Karin,

who held my hand through every comma, semicolon, period, i.e., and however

(i.e. microscopic step) of my thesis. I cannot thank you enough!

ACKNOWLEDGEMENTS

I would like to express my profound gratitude to several individuals who enabled me to complete my work successfully.

First and foremost, I would like to thank my mentors, Dr. James Johnson and Dr. Graham King, for giving me the opportunity to work under their supervision – it has truly been a privilege. I was extremely fortunate to have had two advisors who were so approachable, amusing, and enthusiastic about my research. For your unending guidance, expertise, support, and encouragement, I am forever thankful. You motivated me to excel and to deliver. Thank you for always finding the time to fit me and my project into your busy schedules.

Louis Ferreira (a.k.a. Papa Bear), you are a wealth of knowledge. I wish I had your patience! The most obvious thank you is for your troubleshooting; however, thank you for always finding the time to help and teach me, especially in the midst of a panic attack.

A sincere thank you to my lab buddy and testing partner, Emily Lalone, for making our long test days fun – I mean, our test days would have made record time if the placement of your fiducial markers didn't take so long! Anyways, *Tegan and Sara* got us through it all. I will miss everything about your ridiculousness, but in particular, I will miss Dr. King making fun of you and your personalized match boxes.

In general, I would like to thank the entire HULC Team for creating such a collaborative, stimulating, and pleasant work environment!

Finally, I would like to thank my family and my best friends, Christine and Karin, with whom I have shared the ups and downs of research. Your continued love and encouragement was vital.

TABLE OF CONTENTS

LIST OF TABLES

Chapter 2

LIST OF FIGURES

Chapter 1

Chapter 2

Chapter 3

Chapter 4

Chapter 5

LIST OF APPENDICES

LIST OF ABBREVIATIONS

AL	Annular ligament of the LCL
AMCL	Anterior bundle of the MCL
DVRT	Differential variable reluctance transducer
ECR	Extensor carpi radialis longus and brevus
ECU	Extensor carpi ulnaris
EDC	Extensor digitorum communis
ESM	Extensor-supinator mass
FCR	Flexor carpi radialis
FCU	Flexor carpi ulnaris
FDS	Flexor digitorum superficialis
FPM	Flexor-pronator mass
LCL	Lateral collateral ligament
LUCL	Lateral ulnar collateral ligament of the LCL
MCL	Medial collateral ligament
PMCL	Posterior bundle of the MCL
PT	Pronator teres
RCL	Radial collateral ligament of the LCL
RH	Radial head
WF	Wrist flexor(s)

CHAPTER 1

Introduction

Overview: The objective of this thesis was to quantify the magnitude of tension experienced by the medial collateral ligament (MCL) in the elbow through the arc of flexion. The magnitude of MCL tension under wrist flexor muscle loading, as well as under radial head excision and arthroplasty, were also of interest. This chapter reviews the anatomy, kinematics, and stability of the elbow joint. Mechanisms of MCL injury as well as ligament/tendon strain and force measurement techniques are also outlined. This chapter concludes with study rationale, objectives, and hypotheses.

1.1 ELBOW ANATOMY*

The elbow is a complex structure whose function is to position and stabilize the hand in space; it functions as the mechanical link in the upper extremity between the hand, the wrist, and the shoulder.[1] This joint is one of the most congruous of the body and, hence, inherently very stable.[2] Static or passive stability of the elbow joint is provided by the mechanical linkages of the three bones which form the joint, the ligaments that connect the bones together, and the joint capsule, whereas active or dynamic stability is provided by the muscles that cross the elbow joint.[1-5]

1.1.1 Osteology

The elbow joint is composed of three bones: the distal humerus, the proximal radius, and the proximal ulna (Figure 1.1).[1,4] The articulation between these three bones function to

* Appendix 1 has been provided to assist the reader with nomenclature.

form a trochoginglymoid ("pivoting hinge") joint where primarily two degrees of freedom exist – flexion-extension and pronation-supination (Figure 1.2 and Figure 1.3, respectively).[1,6] Important anatomical landmarks of these three bones are shown in Figure 1.4.

The medial and lateral epicondyles are osseous protrusions of the distal humerus, which lie near the elbow's axis of flexion.[7] The medial epicondyle is the attachment site of the medial collateral ligament and the flexor-pronator mass (or wrist flexor muscles); this epicondyle also provides protection for the ulnar nerve.[1,4] The lateral epicondyle is where the lateral collateral ligament and the extensor-supinator mass (or wrist extensor muscles) originate.[1,4] The medial and lateral epicondyles extend superiorly to form the medial and lateral supracondylar ridges, respectively.[4]

The humerus terminates distally with the formation of two articulations: the ulnohumeral joint and the radiocapitellar joint (Figure 1.5).[1,4] The saddle-shaped (or spool-shaped) trochlea of the distal-medial humerus articulates with the greater sigmoid notch of the proximal ulna; this bony articulation is the hinge-like ulnohumeral joint and is the prime osseous stabilizer of the elbow due to its complex interlocking geometry.[1,4] The shallow ball-and-socket articulation of the radiocapitellar joint is comprised of the almost sphere-shaped capitellum of the distal-lateral humerus and the slightly concave dish of the radial head (a depression that is not fully cylindrical but is slightly oval).[4] The third articulation of the elbow is the proximal radioulnar joint (Figure 1.5); the outer circumference of the radial head pivots about the proximal ulna at the lesser sigmoid notch. The ulnohumeral and radiocapitellar joints permit the forearm to flex and extend, whereas the radiocapitellar and proximal radioulnar joints permit forearm rotation (*i.e.* forearm pronation and supination).[1,4]

Independent of the collateral ligaments, the elbow joint is inherently stable in full flexion and extension where the bony articulations and joint capsule provide stability.[2,5,8-10] During elbow extension, the olecranon fossa (a depression located superior to the posterior trochlea) receives the olecranon process (the most proximal structure of the ulna, which cups the trochlea).[1,4] Similarly, the coronid fossa (a depression located superior to the anterior trochlea) receives the coronoid process of the ulna during elbow

flexion, whereas the radial fossa (a depression located superior to the anterior capitellum) accommodates a portion of the radial head during elbow flexion.[1,4]

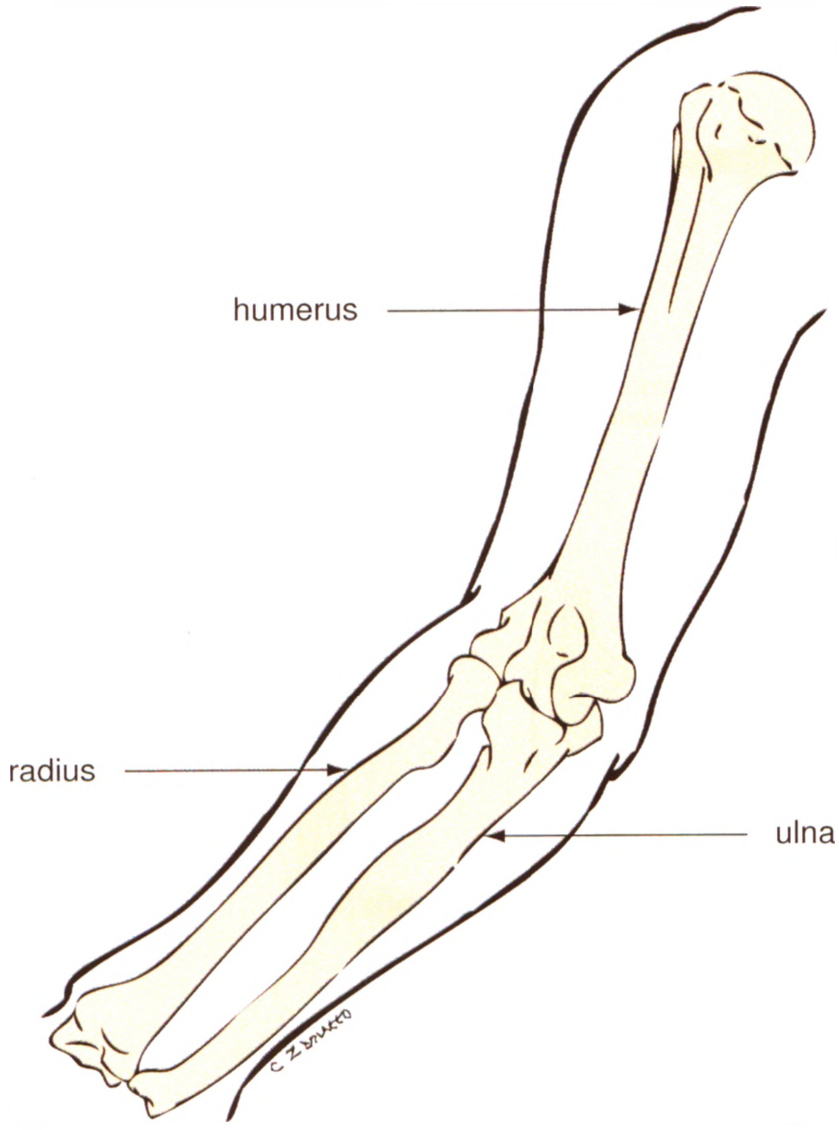

Figure 1.1: The three bones which comprise the elbow

An anterior view of a right arm showing the humerus, the radius, and the ulna.

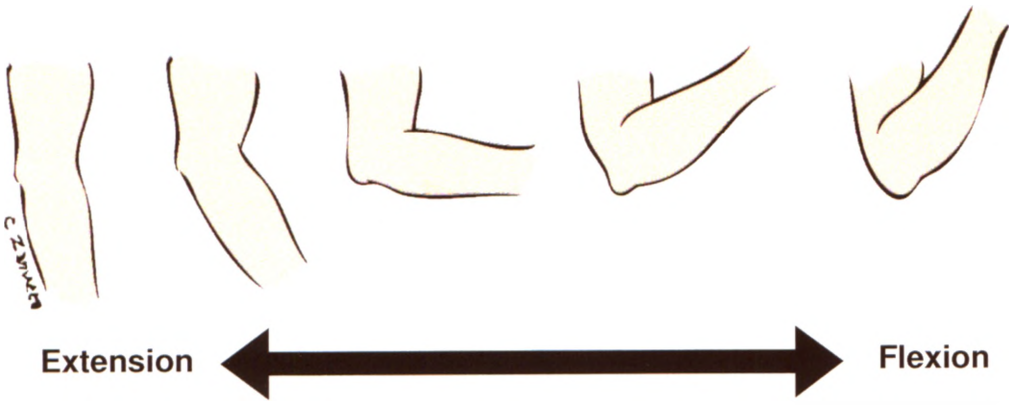

Figure 1.2: Elbow extension and flexion

Full extension (left) is defined as zero degrees of elbow flexion. Flexion angle increases as the elbow is flexed (right) (*i.e.* as the angle between the forearm and arm decreases).

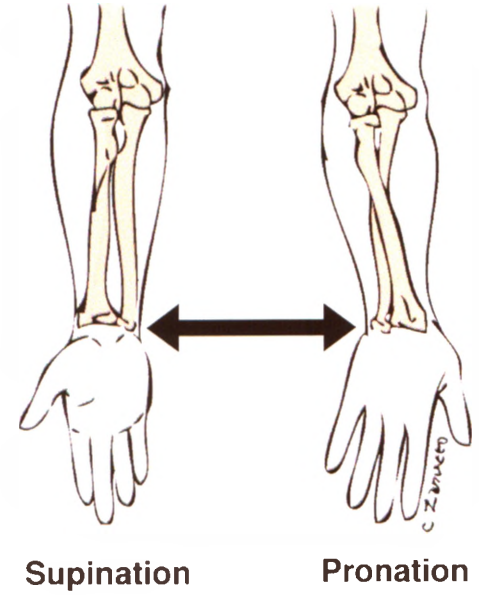

Figure 1.3: Elbow pronation and supination

Rotation of the forearm causing the palm of the hand to face downward or backward is called pronation, whereas rotation of the forearm causing the palm of the hand to face upward is called supination.

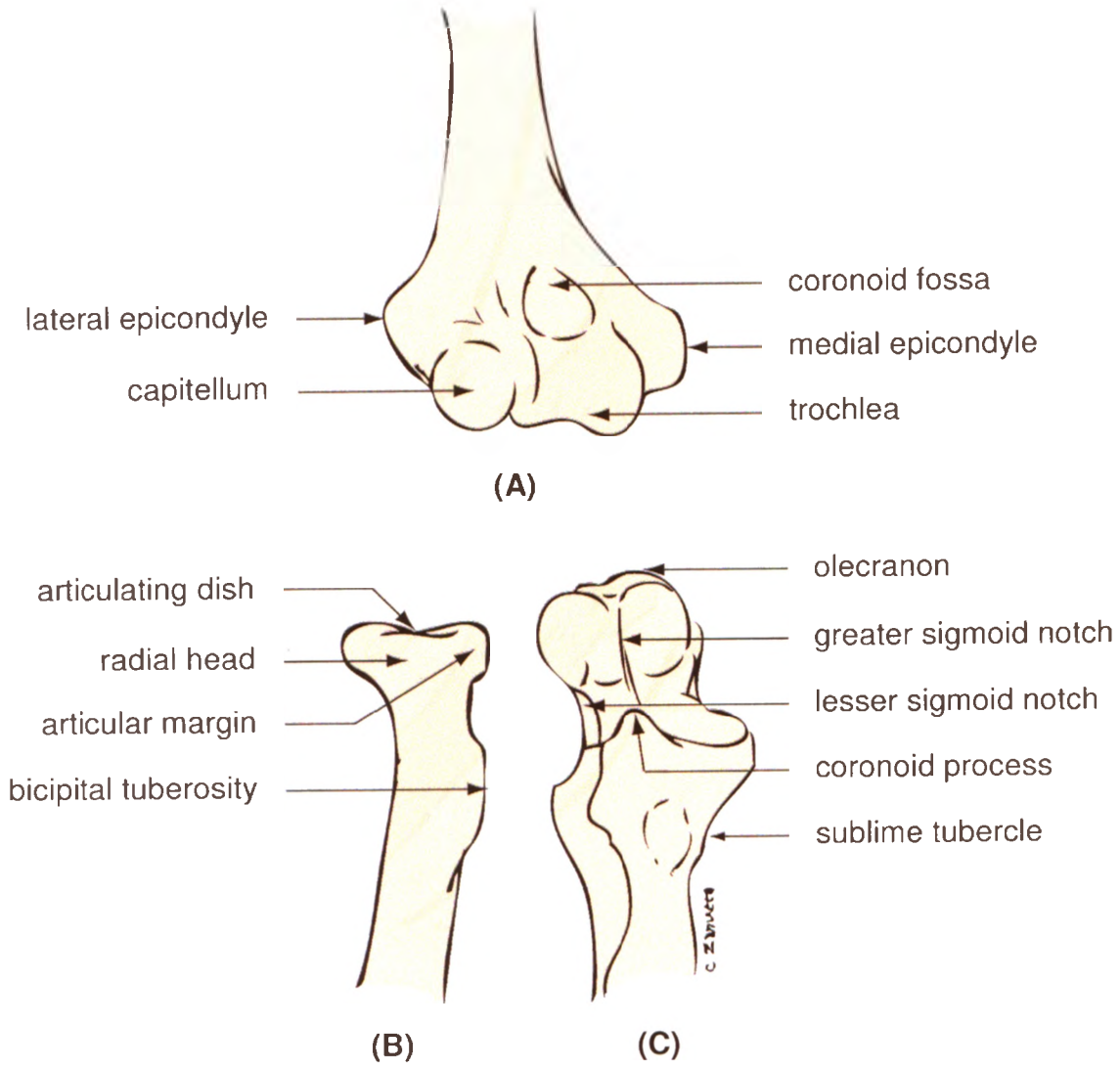

Figure 1.4: The morphological features of the three bones of the elbow joint

An anterior view of a disarticulated right elbow joint illustrating important osseous landmarks of the distal humerus (A), the proximal radius (B), and the proximal ulna (C).

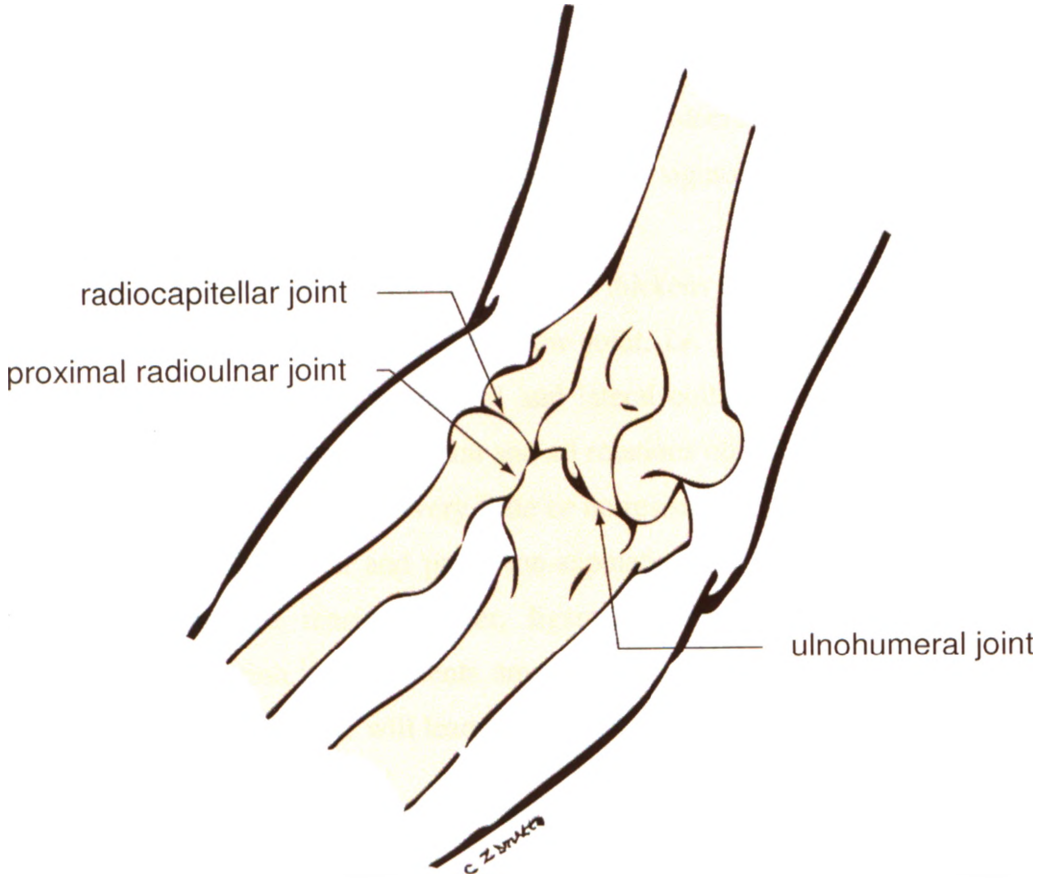

Figure 1.5: Articulations of the elbow joint

The humerus, the ulna, and the radius articulate together to form three separate joints. The distal humerus articulates with both the proximal ulna and the proximal radius to form the ulnohumeral joint and the radiocapitellar joint, respectively; the proximal radius and proximal ulna articulate together to form the proximal radioulnar joint.

1.1.2 Joint Capsule and Ligaments

Static or passive joint constraint is also provided by the soft tissue structures surrounding the elbow joint, which include the joint capsule as well as the medial and lateral collateral ligaments.[1,3-5]

The articular surfaces of the elbow joint are connected by the capsule (Figure 1.6). The anterior joint capsule extends proximally to the coronoid and radial fossae and distally to the anterior margin of the coronoid process and the annular ligament.[6] The posterior joint capsule extends proximally to the olecranon fossa and distally to the medial and lateral articular margins of the greater sigmoid notch and laterally becomes continuous with the annular ligament.[6]

Medially and laterally, the joint capsule thickens to become ligaments that prevent medial and lateral translation of the elbow joint, *i.e.* the medial and lateral collateral ligaments, respectively.[11] The medial and lateral collateral ligaments are arranged to resist nearly all translation of the joint and all rotations other than the primary rotations of the joint; the ligaments provide very little or no resistance to rotations about the primary axes (*i.e.* flexion-extension and pronation-supination).[12] Unlike muscles, ligaments do not actively produce tension; rather, ligaments develop tension as they passively constrain joint motion.[12] Ligaments are relatively inextensible when loaded and rapid loading to a high magnitude will lead to their failure, which is a common sports injury.[12]

1.1.2.1 *Medial Collateral Ligament*

The medial collateral ligament (MCL) consists of three major components: the anterior bundle (AMCL), the posterior bundle (PMCL), and the transverse ligament (Figure 1.7).[1,4,5,7-9,13-16]

The AMCL is the most discrete ligament of the MCL; it is well defined, robust, and easily distinguished from the medial joint capsule.[5,7,8,13,15] It originates from the inferior aspect of the medial epicondyle and inserts on the medial aspect of the coronoid process of the ulna at the sublime tubercle.[1,4,7,8,13,14,16,17] The AMCL can be divided into two functional components, anterior and posterior bands.[4,7,8,14,15,17]

Less prominent than the AMCL is the PMCL, which is described as a thickening or reinforcement of the posterior-medial joint capsule with a fibre density lower than the

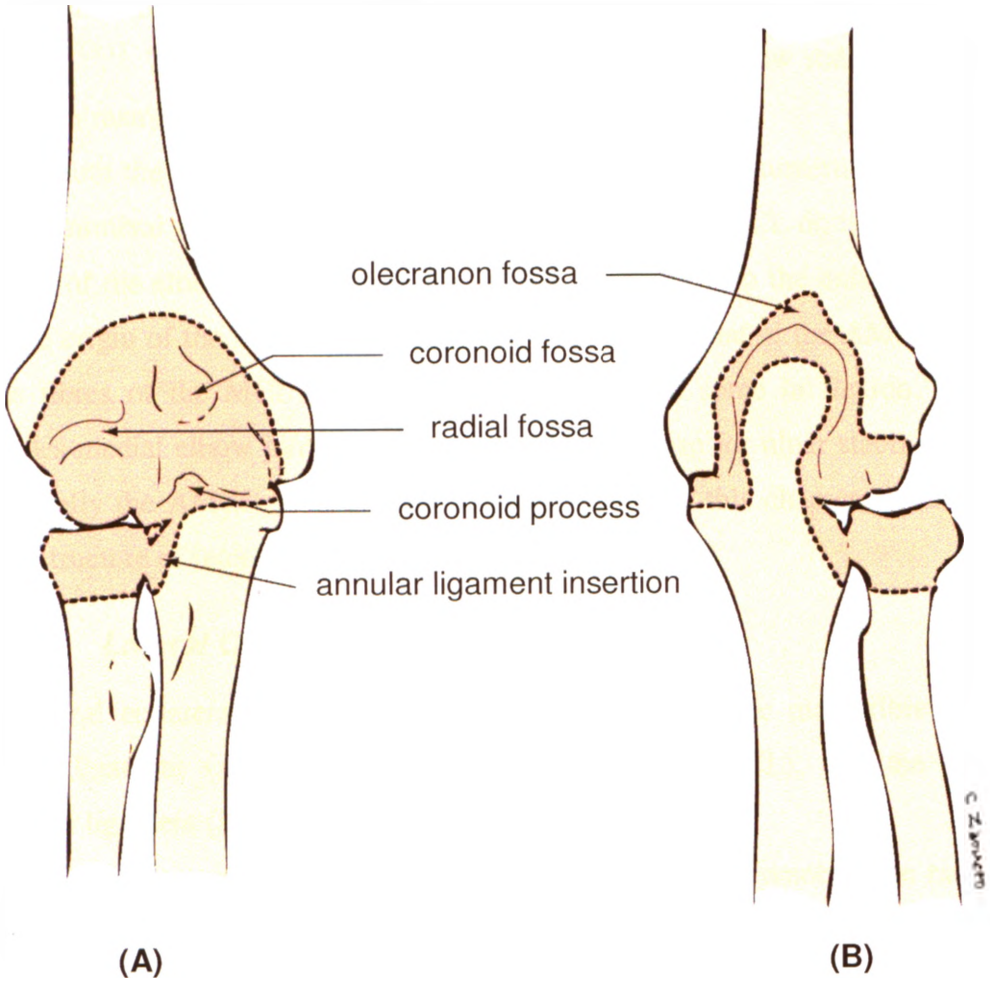

Figure 1.6: The elbow joint capsule

Anterior (A) and posterior (B) views of a right elbow illustrating the boundary of the joint capsule.

AMCL.[1,5,8,13-15] The PMCL originates from the inferior-posterior edge of the medial epicondyle and inserts on the posterior-medial aspect of the olecranon process in a broad fan-shaped fashion.[4,8,13,16,17]

The transverse ligament originates and inserts on the ulna, it covers the medial margin of the trochlear notch (*i.e.* it originates from the tip of the olecranon process and inserts into the coronoid process) and often cannot be separated from the medial joint capsule.[4,7,8,13] This ligament appears to contribute little to elbow stability and is not well defined in many specimens.[1,4,5,7,8,13-16]

Both the AMCL and PMCL stabilize the ulna to the humerus (*i.e.* they stabilize the ulnohumeral joint). The origin of the AMCL and the PMCL do not lie on the axis of rotation of the elbow; the origin of the AMCL is posterior to the axis of elbow rotation and the origin of the PMCL is slightly more posterior to that of the AMCL.[7] Therefore, some fibres of the MCL are taught in extension and some in flexion.[15] The MCL provides medial elbow joint constraint and acts as a base for ulnar stability. The MCL, specifically the AMCL, is discussed in greater detail in this chapter, as this is the soft tissue structure of interest in this thesis.

1.1.2.2 *Lateral Collateral Ligament*

The lateral collateral ligament (LCL) is composed of three main fibre bundles: the annular ligament (AL), the radial collateral ligament (RCL), and the lateral ulnar collateral ligament (LUCL) (Figure 1.8).[7,10,15,18-22]

The AL encircles approximately 80% of the circumference of the radial head; it originates and inserts on the anterior and posterior margins of the lesser sigmoid notch of the ulna and tapers distally, giving it a funnel-like shape.[1,4,17,21,22] This ligament stabilizes the radial head to the ulna (*i.e.* the proximal radioulnar joint) throughout the range of forearm pronation and supination.[1,4,17,21]

The RCL, a fan-shaped structure, originates from the inferior aspect of the lateral epicondyle and inserts into and blends with the AL, thereby preventing the distal migration of the AL and in turn the radial head; it promotes joint stability by maintaining close apposition of the humeral and radial articular surfaces.[1,4,7,10,15,17,21,22] None of the fibres of the RCL attach directly to either the radius or ulna.[17]

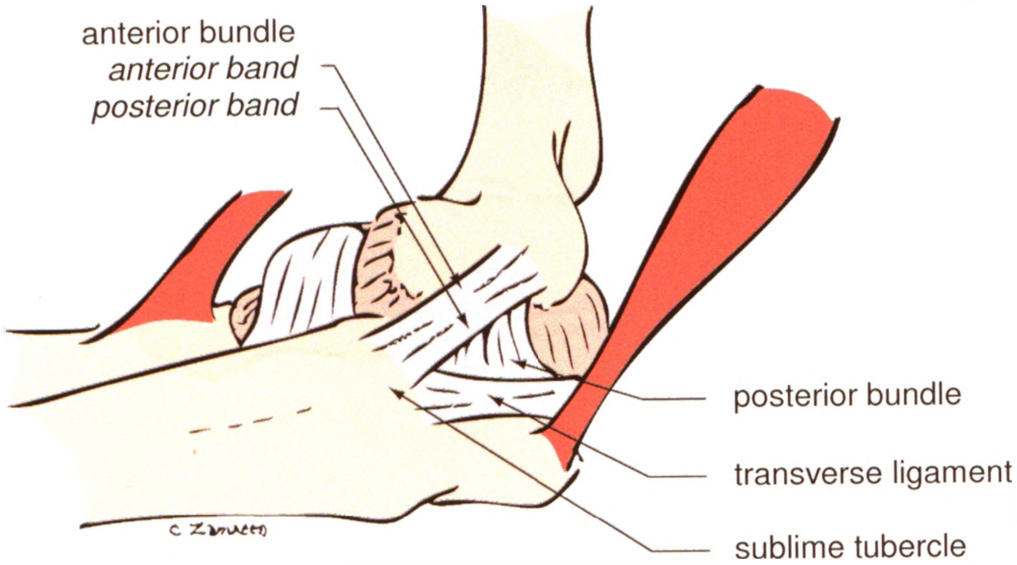

Figure 1.7: The medial collateral ligament (MCL)

The MCL is comprised of the anterior bundle (AMCL, which contains anterior and posterior bands), the posterior bundle (PMCL), and the transverse ligament.

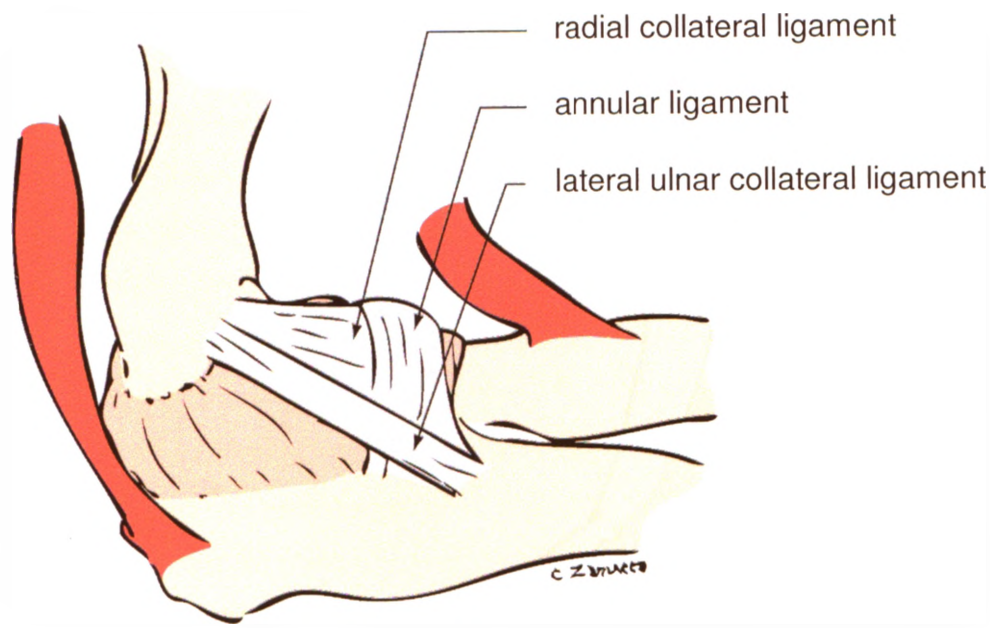

Figure 1.8: The lateral collateral ligament (LCL)

The LCL is comprised of the annular ligament (AL), the radial collateral ligament (RCL), and the lateral ulnar collateral ligament (LUCL).

The LUCL, observed as the posterior fibres of the RCL, originates from the more inferior surface of the lateral epicondyle, blends with the intermediary fibres of the AL, and inserts on a tubercle of the supinator crest of the ulna (the crista supinatoris).[1,4,7,10,20-22] This ligament laterally stabilizes the ulna to the humerus (*i.e.* it functions as the primary lateral stabilizer of the ulnohumeral joint).[1,4]

The LCL provides the primary constraint to varus instability and external (posterolateral) rotatory instability (Figure 1.9) and acts as a base for radial head stability and rotation.[10,18]

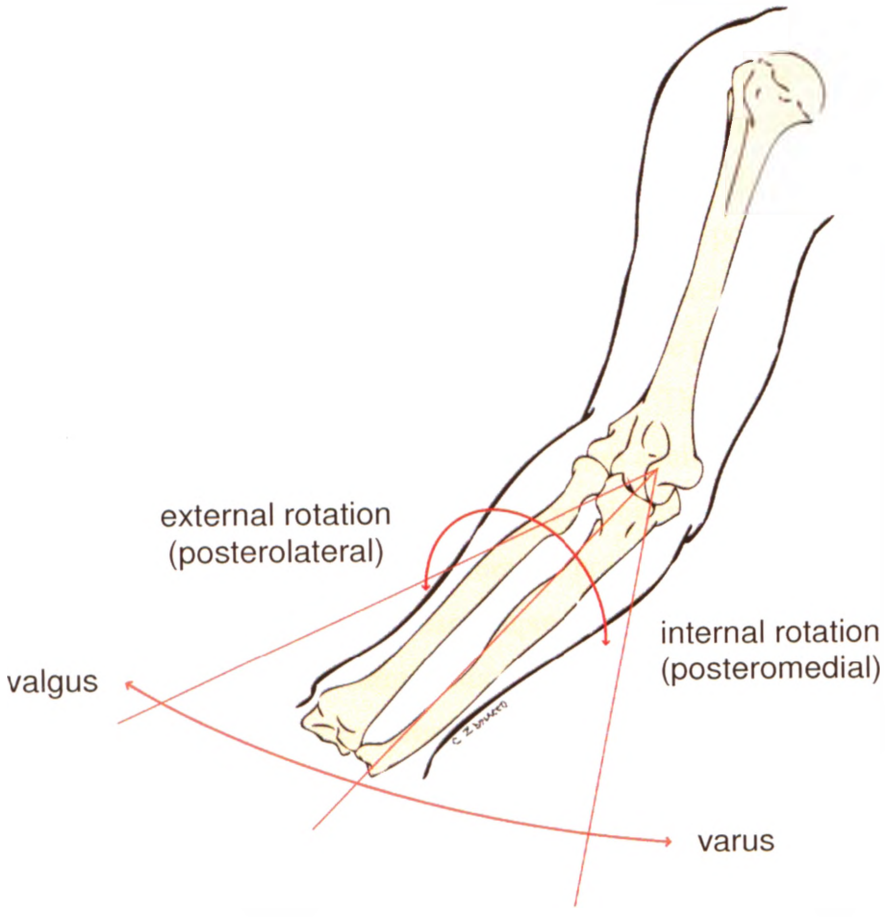

Figure 1.9: Varus-valgus angulation and external-internal rotation

Elbow instability is described in terms of valgus/varus instability and internal/external rotatory instability.

1.1.3 Muscles

The muscles provide dynamic stability to the elbow and enable the hand to perform skilled, precise motions.[4] The muscles that cross the elbow joint, which enable elbow flexion-extension (Figure 1.2) as well as forearm pronation-supination (Figure 1.3), can be classified into four groups: (1) elbow flexors; (2) elbow extensors; (3) common forearm flexors or flexor-pronator mass; and (4) common forearm extensors or extensor-supinator mass.[1,4,6] Relevant muscle origins and insertions are illustrated in Figure 1.10.

Anteriorly, the elbow flexors cross the elbow joint.[1,23] The elbow flexors include the brachialis, biceps brachii, and brachioradialis muscles.[4,23] Both the brachialis and biceps brachii have large cross-sectional areas, giving them the potential for greater force, and attach close to the axis of elbow rotation.[4,24] The brachialis muscle is active in flexing the elbow in all forearm positions, which makes it the prime elbow flexor.[4,25]

Posteriorly, the elbow extensors cross the joint.[1,23] The triceps brachii is the main elbow extensor, whereas the anconeus muscle only plays a minor role in this motion.[4,23]

The primary muscles that produce forearm rotation include the pronator teres (PT) and the pronator quadratus, which produce forearm pronation, and the biceps brachii and the supinator muscle, which produce forearm supination.[4,23]

Medially, the common forearm flexors, also known as the flexor-pronator mass, cross the elbow joint.[1] The flexor-pronator mass consists of the flexor carpi ulnaris (FCU), flexor carpi radialis (FCR), flexor digitorum superficialis (FDS), and PT.[3,4,23] All of these muscles originate from a common tendon attached to the medial epicondyle of the humerus and serve secondary roles as elbow flexors.[1,4,23] The PT acts to pronate the forearm, as previously mentioned, while the other muscles are primarily responsible for wrist and finger flexion.[4,23]

Laterally, the common forearm extensors, or extensor-supinator mass, cross the elbow joint.[1] The extensor-supinator mass includes the extensor carpi ulnaris (ECU), extensor carpi radialis longus and brevus (ECR), extensor digitorum communis (EDC), and brachioradialis.[3,4,23] All muscles originate from a common tendon attached to the lateral epicondyle of the humerus and are primarily responsible for wrist and finger extension.[1,4,23]

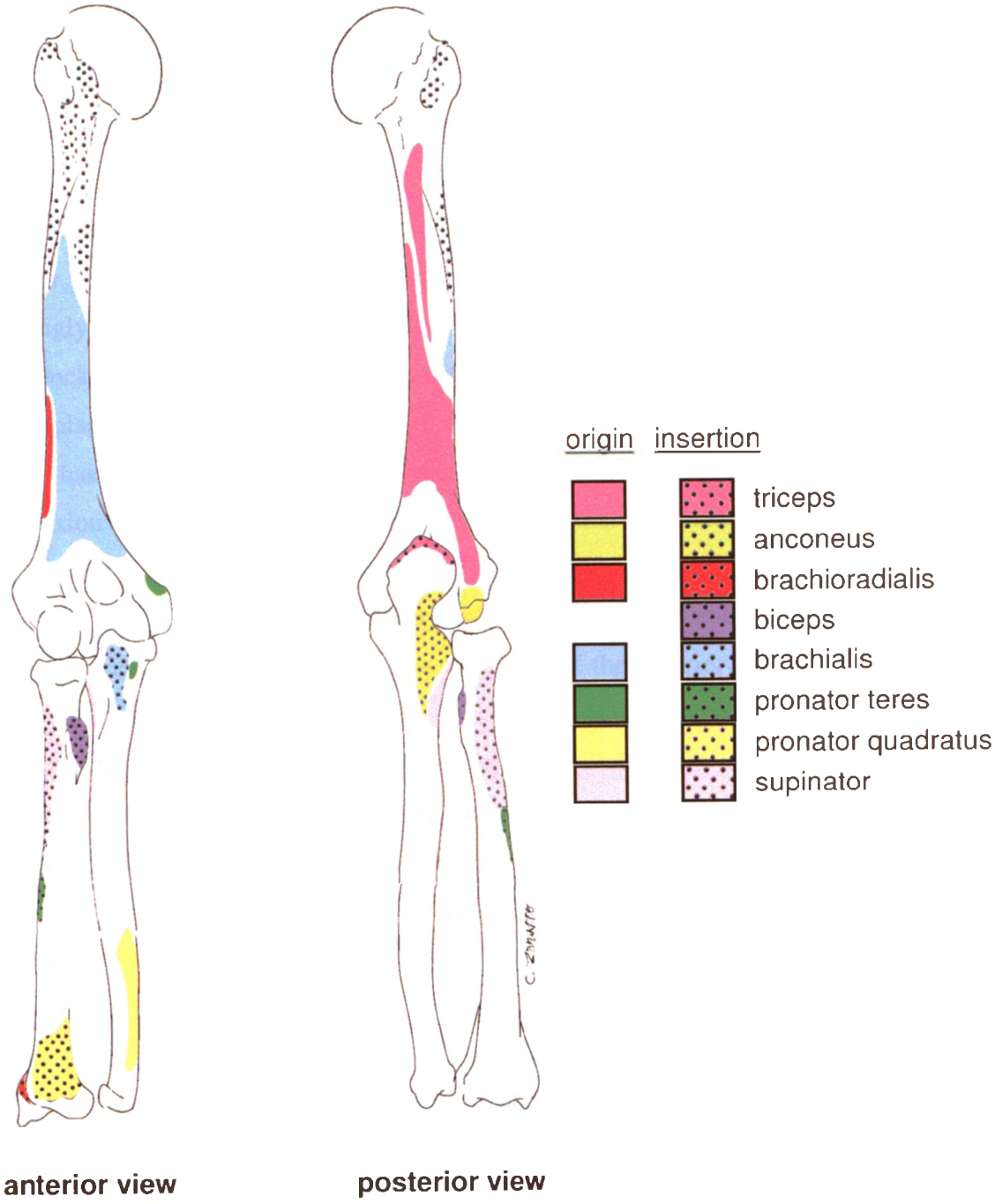

Figure 1.10: Muscles contributing to elbow motion

Anterior and posterior views of the bones of the elbow illustrating the origins and insertions of the muscles that are most important to elbow flexion-extension and forearm rotation. The origin of the biceps brachii is not shown as it originates on the scapula.

1.2 ELBOW KINEMATICS

The elbow joint is composed of two types of articulations that enable motion in primarily two-degrees-of-freedom: flexion-extension and pronation-supination of the forearm (Figure 1.2 and Figure 1.3, respectively). Flexion and extension are permitted by the hinge-like ulnohumeral joint and the shallow ball-and-socket radiocapitellar joint, whereas axial rotation of the forearm is permitted by the radiocapitellar and proximal radioulnar joints (Figure 1.5).[1,4] Therefore, the elbow joint has been classified as a trochoginglymoid ("pivoting hinge") joint.[1,6]

Duck et al.[26] have shown that the instantaneous axis of elbow rotation, termed the screw displacement axis (SDA), varies throughout the arc of elbow flexion. Analysis of the SDA has shown that the elbow behaves similar to a loose hinge joint throughout elbow flexion (Figure 1.11).[26] It has also been shown that the forearm rotates internally during the early part of flexion and then externally during the latter part.[27] The axis of rotation of the elbow joint has been shown to pass through the centre of the arcs of the trochlea and capitellum, and is located in the plane of the anterior border of the distal humerus (Figure 1.12).[27]

The plane of flexion and extension is not entirely within the sagittal plane.[28] This can be explained by the valgus angulation, or carrying angle, which is the lateral deflection of the forearm with respect to the humerus when the elbow is in full extension (*i.e.* the angle formed by the longitudinal axis between the humerus and the ulna when the elbow is in full extension).[1,4] The average carrying angle is larger in females (14°) than males (11°), which presumably accommodates gender differences in pelvic width (Figure 1.13).[1,29]

The elbow has a normal range of motion from 0° to 160° of elbow flexion, and 75°-80° of pronation to 85°-90° of supination.[30] However, the functional range of flexion and forearm rotation required to perform most daily activities is less, ranging from 30° to 130° degrees of elbow flexion and 50° of pronation to 50° of supination.[1,30]

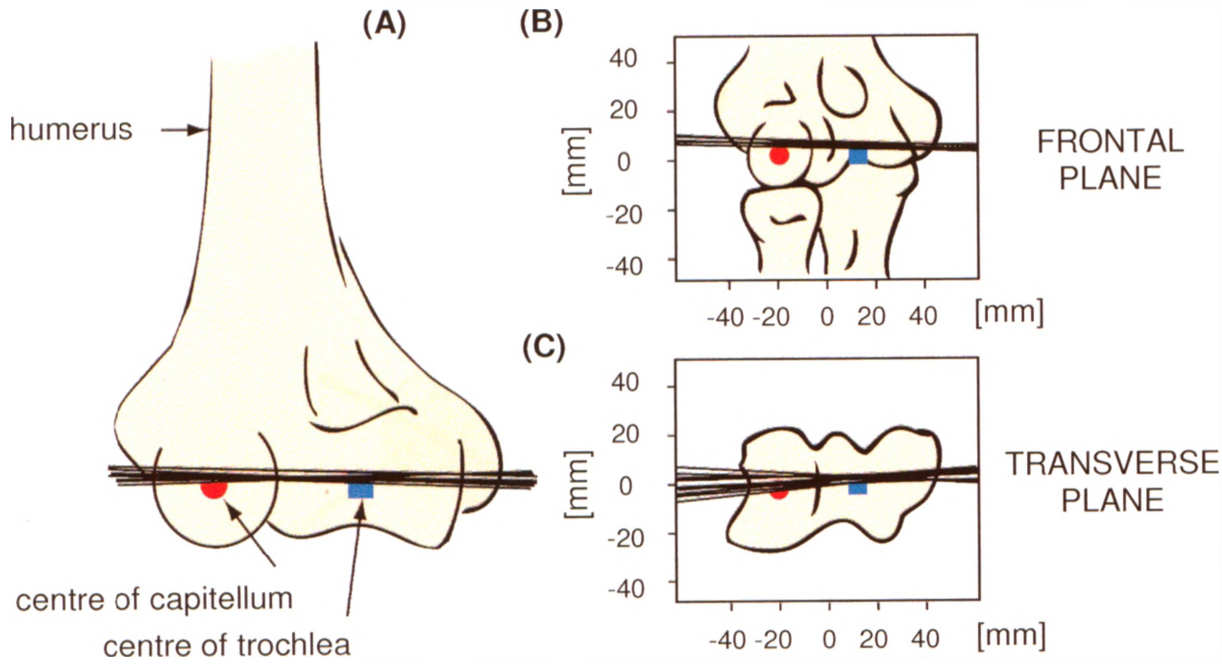

Figure 1.11: Screw displacement axis (SDA)

The SDA is shown for pronated flexion of an intact specimen. The circle and square represent the digitized centres of the capitellum and trochlea, respectively. A frontal view of the distal humerus (A), a frontal view of the elbow joint (B), and an inferior view of the distal humerus (C) are shown. Adapted from Duck et al.[26], 2003.

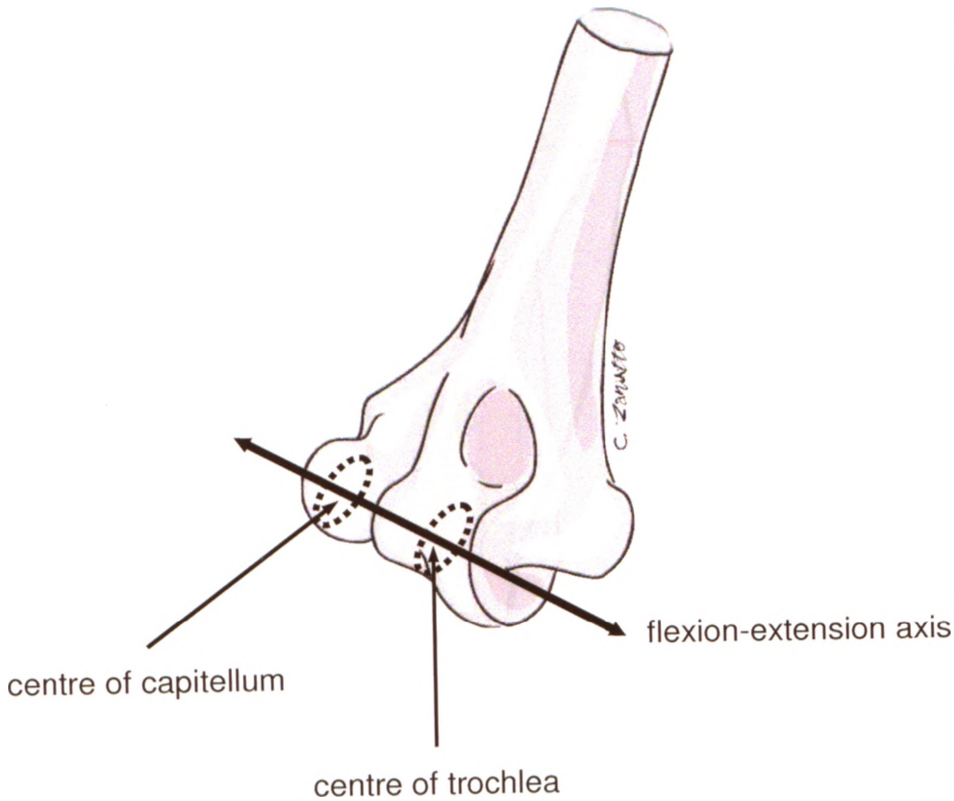

Figure 1.12: Elbow joint axis of motion

An anterior view of a right humerus illustrating the axis of motion of the elbow joint through the centre of the arcs of the trochlea and capitellum.

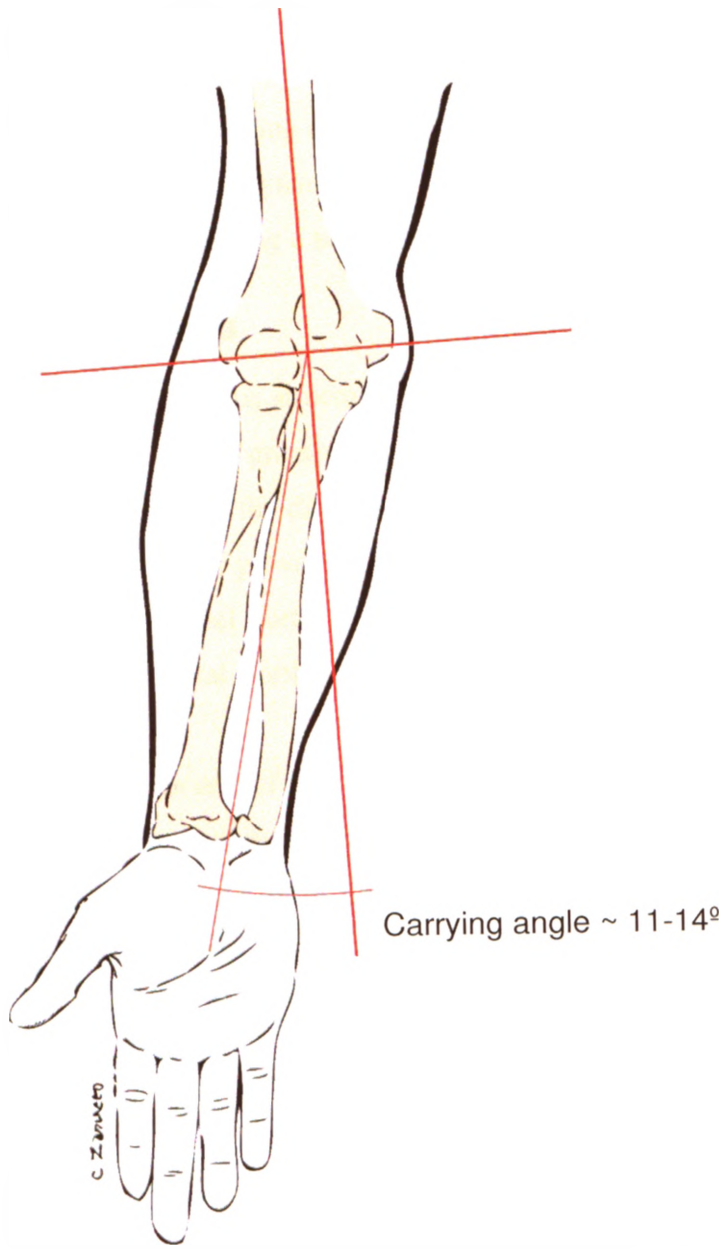

Figure 1.13: The carrying angle of the elbow

The geometry of the articular surfaces of the elbow joint contributes to a valgus angulation known as the carrying angle.

1.3 ELBOW STABILITY

Elbow stability is provided by the osseous articular geometry of the joint itself as well as the soft tissue structures surrounding the joint.[1,4] The passive or static stability of the elbow joint results from the highly congruent articulation between the humerus and the ulna, and the soft tissue constraints, including the medial and lateral collateral ligaments, and the joint capsule.[1-5] The active or dynamic stabilizers of the elbow joint are the muscles that cross the elbow joint, providing a stabilizing joint compressive force.[1,3,4,31-33]

1.3.1 Osseous Contributions

The complementary shapes of the osseous structures of the elbow joint provide stability throughout the range of motion. The greater sigmoid notch (of the proximal ulna) articulates with the trochlear groove (of the distal humerus) to define the arc of flexion.[4] This articular surface geometry helps to prevent medial and lateral translation of the ulna relative to the humerus. The proximal portion of the greater sigmoid notch primarily resists valgus stress, whereas its distal portion (*i.e.* coronoid process) primarily resists varus stress.[1,34]

The tip of the olecranon process (of the posterior-proximal ulna) rests against the posterior-distal humerus to prevent anterior dislocation of the elbow. Furthermore, the olecranon process enhances valgus stability; Kamineni et al.[35] showed that resection of the posterior-medial olecranon increased the strain in the AMCL. The coronoid process (of the anterior-proximal ulna) and the radial head together provide an anterior bony buttress, preventing posterior subluxation or dislocation of the elbow.[36-39] The coronoid process is also a key stabilizer to varus stress and likely contributes more to stability in extension than in flexion.[37,40]

The radiocapitellar joint is an important joint in loading, based on a bench-top static evaluation.[1,42] With extension and axial loading, 60% of the load was transmitted through the radiocapitellar joint and the remaining 40% of the load was transmitted through the ulnohumeral joint.[1,42] The radial head is also a constraint to varus and external rotation in the elbow joint as its presence maintains tension in the LCL.[43]

Morrey et al.[2] quantified the articular and ligamentous contributions to the stability of the elbow in a cadaver-based experiment. When the elbow was extended,

valgus stability was equally divided among the MCL, anterior joint capsule, and joint articulation (31%, 38%, and 31%, respectively); whereas, at 90° of elbow flexion, the MCL, anterior joint capsule, and joint articulation were found to resist approximately 54%, 10%, and 33% of valgus stress, respectively. Furthermore, when the elbow was extended, the MCL, RCL, and anterior joint capsule were found to resist approximately 6%, 5%, and 85% of joint distraction, respectively; whereas, at 90° of elbow flexion, the MCL, RCL, and anterior joint capsule were found to resist approximately 78%, 10%, and 8% of joint distraction, respectively. Thus, this study identified the MCL as an important stabilizer of the elbow joint.

1.3.2 Valgus Stability of the Elbow Joint

Morrey et al.[44] reported that the MCL and the radial head were the primary and secondary valgus and rotatory stabilizers of the ulnohumeral joint, respectively. With radial head excision (intact MCL), little change in the kinematics of the forearm was observed; however, with transection of the MCL (intact radial head), moderate laxity was observed. These observations are in agreement with those made by Hotchkiss et al.[45]. When both structures were removed, gross instability of the elbow resulted (*i.e.* elbow subluxation or dislocation with applied stress). Simulated active muscle activity was observed to reduce valgus laxity, but this had less of an effect on reducing rotatory instability. Muscle activity stabilizes the joint by compressing the articular surfaces together upon activation; contraction of antagonistic muscles increases joint contact area and pressure within the elbow joint.[31-33] Increased elbow joint stability with muscle activation has been further demonstrated by other investigators.[14,46,47]

The AMCL has been reported to be the primary constraint to valgus loads; Hotchkiss et al.[45] reported that the AMCL was the primary stabilizer to valgus stress at 0°, 45°, and 90° of elbow flexion, and similarly, Sojbjerg et al.[5] reported that the AMCL was the primary restraint to valgus instability within 20° and 120° of elbow flexion. Furthermore, the anterior portion of the AMCL (*i.e.* anterior band) has been identified as the primary constraint to valgus loads; Callaway et al.[14] reported that the anterior band was the primary restraint to valgus instability at 30°, 60°, and 90° of elbow flexion, and similarly, Floris et al.[8] reported that this structure was the primary constraint to valgus

loads within 10° and 80° of elbow flexion. While it is clear that the anterior band is the primary constraint to valgus loads in extension and semi-flexion, there is disagreement over the contributing roles of the posterior portion of the AMCL (*i.e.* posterior band), as well as the PMCL, to valgus stability. See Figure 1.9 for an illustration of varus-valgus angulation.

1.3.3 MCL Strain Under Valgus Load

Knowledge of elbow ligament strain and tension allows for a better understanding of the load environment of the tissue. As a result, insight into injury mechanisms would be gained, which in turn, would allow for the development of injury prevention strategies, as well as the design and evaluation of treatment options that optimize healing (*i.e.* bone resection, implant replacement, and ligament repair).

Pribyl et al.[9] quantified the AMCL and PMCL *in situ* strain in response to a valgus load. Localized strain, defined as the change in length divided by the original length, was measured in both the AMCL and PMCL by applying a commercially available differential variable reluctance transducer (DVRT) to each structure. For all flexion angles (20° to 140° of flexion), strain in the AMCL was significantly greater than that in the PMCL, and strain in both bundles increased with more flexion. Strain in the AMCL developed around 30° of flexion, whereas strain in the PMCL developed around 60° of flexion (little strain was seen in the MCL at low flexion angles). For a given flexion angle and forearm position (neutral, pronation, supination), increased valgus load was associated with an increase in AMCL strain and a decrease in PMCL strain. Furthermore, forearm position minimally affected strain in either bundle of the MCL. These findings suggest that the AMCL is a more important valgus stabilizer than the PMCL, particularly in mid-flexion, whereas the importance of the PMCL increases as the elbow approaches full flexion.

Armstrong et al.[48] determined that the AMCL does not contain true isometric fibres (isometric implies a zero length change, or $\Delta L = 0$). However, nearly isometric areas (defined as the smallest ΔL values) were identified in the lateral aspect of the AMCL attachment site on the medial epiconyle of the humerus and near the anatomic axis of rotation of the elbow. This nearly isometric region was obtained with the forearm

in supination, as Armstrong et al.[46] previously reported that the elbow joint is most stable in this forearm position. To elaborate, Armstrong et al.[46] showed that during passive mobilization of the elbow with the arm in the vertical orientation, an MCL-deficient elbow joint was more stable in a fully supinated position than in a fully pronated position; however, active mobilization of the elbow in the vertical position significantly increased the rotational stability with the forearm pronated. Furthermore, they reported that the valgus orientation should be avoided during rehabilitation since forearm position (supination versus pronation) and muscle activation (passive versus active) did not reduce the gross instability observed in the MCL-deficient elbow.

1.3.4 Muscle Contribution to Valgus Stability of the Elbow Joint

Lin et al.[3] investigated the relative contribution of each muscle of the flexor-pronator mass (FPM) and extensor-supinator mass (ESM) on elbow valgus motion and strain on the AMCL at 45° and 90° of flexion. Their aim was to determine the role of the dynamic stabilizers of the elbow in response to valgus stress. Each muscle of the FPM (FCU, FDS, FCR, and PT) and the ESM (ECU, EDC, ECR longus and brevus, and brachioradialis) was loaded individually and during loading, strain in the AMCL was measured via a commercially available differential variable reluctance transducer.

Consistent with the findings of Pribyl et al.[9], Lin et al.[3] found that the AMCL was not tensed until about 20° of flexion and from approximately 20° to 75°-80° of flexion exhibited an almost linear strain response. After about 80° of flexion, less AMCL lengthening was observed as the elbow was flexed further, which is consistent with the findings of Callaway et al.[14] who found that the AMCL tensed less after 90° of elbow flexion.

Individual loading of the FCU, FDS, and FCR significantly decreased AMCL strain at both 45° and 90° of flexion. Significantly greater AMCL strain relief was seen at 90° of flexion than at 45° of flexion for both the FCU and FDS. For all FPM muscles, greater AMCL strain relief was observed at 90° of flexion than at 45° of flexion, and loading of the FCU provided the greatest reduction in AMCL strain at both 45° and 90° of flexion. Furthermore, loading of the ESM muscles increased AMCL strain at both flexion angles, and greater strains were observed at 45° of flexion than at 90° of flexion

for all ESM muscles (however, this was only statistically significant for the ECU at 45° of flexion). At both 45° and 90° of flexion, the greatest increase in AMCL strain was observed upon loading of the ECU.

Loading of the FPM muscles created elbow varus movement, whereas loading of the ESM muscles produced elbow valgus movement. Individual loading of all the FPM muscles produced significant varus motion at both 45° and 90° of flexion. Larger varus movement was observed at 45° of flexion than at 90° of flexion for all FPM muscles (recall that the AMCL was more tensed at 90° of flexion than at 45° of flexion), with the FCU producing the largest varus motion at both 45° and 90° of flexion. Furthermore, the EDC and ECU produced significant elbow valgus movement at both 45° and 90° of flexion. Larger valgus movement was observed at 45° of flexion than at 90° of flexion for all ESM muscles, with the ECU producing the largest valgus motion at both 45° and 90° of flexion.

1.4 MECHANISMS OF MCL INJURY

MCL injuries include elbow dislocations, radial head fractures, and chronic high intensity overuse. Elbow dislocations almost invariably cause MCL rupture; the MCL is most commonly avulsed from its origin at the medial epicondyle.[3,49] Attenuation or rupture of the MCL also commonly occur in association with radial head fractures.[50] Radial head fractures comprise 33% of all elbow fractures and are typically caused by a fall on the outstretched hand.[51] MCL injuries also occur as a result of chronic overuse in high demand athletes such as baseball pitchers, and occasionally in tennis players and javelin throwers.[3,13,52-64] The medial aspect of the elbow joint experiences an abrupt increase in valgus stress during the late cocking and early acceleration phases of the pitching motion.[13,52,58-60,62,63,65] These forces may exceed the tensile strength of the ligament and produce microtears within the tissue.[52,58-60,64] Continued throwing (*i.e.* continued valgus extension overload) can lead to attenuation or rupture of the weakened ligament.[13,52,54,55,57-60,63,64]

1.5 STRAIN AND FORCE MEASUREMENT TECHNIQUES

Fleming et al.[66] and Ravary et al.[67] have elaborately reviewed the invasive and non-invasive techniques used, both *in vivo* and *in vitro*, to measure strains and loads within human and veterinary tendons and ligaments.[68-79] Three types of invasive methods can be defined according to the physical principles on which they function: (1) variation of electrical resistance (liquid metal strain gauge – LMSG, buckle transducer, implantable force transducer – IFT, pressure transducer); (2) variation of magnetic field (Hall effect strain transducer, differential variable reluctance transducer – DVRT); and (3) variation of light flow (optic fibre).[66,67] Non-invasive techniques, or imaging techniques, include ultrasonography (US) and magnetic resonance imaging (MRI).[66,67]

Strains and forces within human tendons and ligaments of the lower extremity have been studied extensively. Much research has evaluated the strain and force within the anterior cruciate ligament (ACL), one of the four main stabilizing ligaments of the knee, as well as the Achilles tendon of the calf.[66-70,75]

In the upper extremity, some recent studies have investigated the strain in the medial collateral ligament of the human elbow. In addition to the aforementioned studies conducted by Pribyl et al.[9] and Kamineni et al.[35], Levin et al.[80] investigated the effect of posterior olecranon resection on strain in the AMCL, whereas Andrews et al.[81] investigated the effect of medial olecranon osteotomy on AMCL strain; both studies quantified strain in the AMCL via a commercially available DVRT. Human tendon and ligament forces of the upper extremity, have not, to our knowledge, been previously studied. While invasive and non-invasive techniques have evolved for quantifying human tendon and ligament forces in the lower extremity, custom developed systems for the upper extremity, particularly the elbow and shoulder, have not been described.

1.6 STUDY RATIONALE

Techniques have evolved for quantifying human tendon and ligament forces in the lower extremity; however, custom developed systems for the upper extremity, particularly the elbow, are not well described. Consequently, ligament forces of the human elbow joint have not been reported. Knowledge of AMCL tension magnitudes would allow for an improved understanding of the load environment of this tissue. As a result, insight into

AMCL injury mechanisms would be gained, which in turn, would allow for the development of injury prevention strategies and rehabilitation techniques that optimize healing. Furthermore, this knowledge should allow for the design and evaluation of improved methods of AMCL repair and reconstruction, and assist in the development of an artificial AMCL and *in vitro* biomechanical models of the elbow.

1.7 OBJECTIVES

The specific objectives of this work were:

1. To quantify the magnitude of AMCL tension in the elbow through the arc of flexion.
2. To determine the effect of wrist flexor muscle loading on the magnitude of AMCL tension through the arc of flexion.
3. To evaluate the effect of radial head excision and arthroplasty on the magnitude of AMCL tension through the arc of flexion.

1.8 HYPOTHESES

The following hypotheses were tested:

1. Tension in the AMCL will increase with elbow flexion, and AMCL loads will be greater for the arms oriented in the valgus gravity-loaded position relative to the dependent (*i.e.* vertical) position.
2. Tension in the AMCL will decrease with increased wrist flexor muscle loads.
3. Tension in the AMCL will increase with radial head excision, and radial head arthroplasty will restore AMCL tension levels similar to that of the native radial head state.

1.9 THESIS OVERVIEW

Chapter 2 describes the design and development of a buckle transducer optimized for use in the AMCL of the elbow. The transducer's calibration equation is also presented in Chapter 2. In Chapter 3, the magnitudes of AMCL tensions through the arc of elbow flexion for different arm orientations are presented and analysed. Studies investigating the effect of wrist flexor muscle loading on AMCL tension levels, and the effect of radial

head excision and arthroplasty on AMCL tension levels, are presented and discussed in Chapters 4 and 5, respectively. Finally, Chapter 6 summarizes the key findings of the studies presented in Chapters 3, 4, and 5, and suggests directions for future work. In addition to these aforementioned studies, functionality testing of the buckle transducer (repeatability, hysteresis, reproducibility, and invasiveness) was performed and the results of these investigations are discussed throughout Chapter 3, Appendix 6, and Appendix 10.

1.10 REFERENCE LIST

1. Fornalski S, Gupta R, Lee TQ. Anatomy and biomechanics of the elbow joint. Tech.Hand Up Extrem.Surg. 2003;7:168-78.

2. Morrey BF, An KN. Articular and ligamentous contributions to the stability of the elbow joint. Am.J.Sports Med. 1983;11:315-9.

3. Lin F, Kohli N, Perlmutter S, Lim D, Nuber GW, Makhsous M. Muscle contribution to elbow joint valgus stability. J.Shoulder.Elbow.Surg. 2007;16:795-802.

4. Stroyan M, Wilk KE. The functional anatomy of the elbow complex. J.Orthop.Sports Phys.Ther. 1993;17:279-88.

5. Sojbjerg JO, Ovesen J, Nielsen S. Experimental elbow instability after transection of the medial collateral ligament. Clin.Orthop.Relat Res. 1987;186-90.

6. Morrey BF. Anatomy of the elbow joint. In: Morrey BF, editor. The elbow and its disorders. Philadelphia: W.B. Saunders Company; 2000. p. 13-42.

7. Morrey BF, An KN. Functional anatomy of the ligaments of the elbow. Clin.Orthop.Relat Res. 1985;84-90.

8. Floris S, Olsen BS, Dalstra M, Sojbjerg JO, Sneppen O. The medial collateral ligament of the elbow joint: anatomy and kinematics. J.Shoulder.Elbow.Surg. 1998;7:345-51.

9. Pribyl CR, Hurley DK, Wascher DC, McNally TP, Firoozbakhsh K, Weiser MW. Elbow ligament strain under valgus load: a biomechanical study. Orthopedics 1999;22:607-12.

10. Olsen BS, Sojbjerg JO, Dalstra M, Sneppen O. Kinematics of the lateral ligamentous constraints of the elbow joint. J.Shoulder.Elbow.Surg. 1996;5:333-41.

11. Marieb EN, Mallat J. Joints. Human anatomy. San Francisco, CA: Benjamin Cummings; 2003. p. 211-42.

12. Dunning CE, Jenkyn TR. Internal Kinetics 1. MME 464a Biomechanics of Human Joint Motion Lecture Notes. London, ON: The University of Western Ontario, Faculty of Engineering; 2006. p. 13-1-13-16.

13. Timmerman LA, Andrews JR. Histology and arthroscopic anatomy of the ulnar collateral ligament of the elbow. Am.J.Sports Med. 1994;22:667-73.

14. Callaway GH, Field LD, Deng XH et al. Biomechanical evaluation of the medial collateral ligament of the elbow. J.Bone Joint Surg.Am. 1997;79:1223-31.

15. Regan WD, Korinek SL, Morrey BF, An KN. Biomechanical study of ligaments around the elbow joint. Clin.Orthop.Relat Res. 1991;170-9.

16. Fuss FK. The ulnar collateral ligament of the human elbow joint. Anatomy, function and biomechanics. J.Anat. 1991;175:203-12.

17. Schwab GH, Bennett JB, Woods GW, Tullos HS. Biomechanics of elbow instability: the role of the medial collateral ligament. Clin.Orthop.Relat Res. 1980;42-52.

18. Dunning CE, Zarzour ZD, Patterson SD, Johnson JA, King GJ. Ligamentous stabilizers against posterolateral rotatory instability of the elbow. J.Bone Joint Surg.Am. 2001;83-A:1823-8.

19. King GJ, Dunning CE, Zarzour ZD, Patterson SD, Johnson JA. Single-strand reconstruction of the lateral ulnar collateral ligament restores varus and posterolateral rotatory stability of the elbow. J.Shoulder.Elbow.Surg. 2002;11:60-4.

20. O'Driscoll SW, Horii E, Morrey BF, Carmichael SW. Anatomy of the Ulnar Part of the Lateral Collateral Ligament of the Elbow. Clinical Anatomy 1992;5:296-303.

21. Berg EE, DeHoll D. The lateral elbow ligaments. A correlative radiographic study. Am.J.Sports Med. 1999;27:796-800.

22. Takigawa N, Ryu J, Kish VL, Kinoshita M, Abe M. Functional anatomy of the lateral collateral ligament complex of the elbow: morphology and strain. J.Hand Surg.[Br.] 2005;30:143-7.

23. Marieb EN, Mallat J. Muscles of the body. Human anatomy. San Francisco: Benjamin Cummings; 2003. p. 265-334.

24. Norkin CC, Levangie PK. Joint structure and function: A comprehensive analysis. Philadelphia: F.A. Davis; 1985. p. 191-210.

25. Basmajian JV, DeLuca CJ. Muscles alive: Their functions revealed by electromyography. Baltimore: Williams & Wilkins; 1895. p. 279-80.

26. Duck TR, Dunning CE, Armstrong AD, Johnson JA, King GJ. Application of screw displacement axes to quantify elbow instability. Clin.Biomech.(Bristol., Avon.) 2003;18:303-10.

27. Morrey BF, Chao EY. Passive motion of the elbow joint. J.Bone Joint Surg.Am. 1976;58:501-8.

28. Amis AA. Mini-symposium: The elbow (iv) Biomechanics of the elbow. Current Orthopaedics 2002;16:349-54.

29. Amis AA, Miller JH. The elbow. Clin.Rheum.Dis. 1982;8:571-93.

30. Morrey BF, Askew LJ, Chao EY. A biomechanical study of normal functional elbow motion. J.Bone Joint Surg.Am. 1981;63:872-7.

31. An KN, Hui FC, Morrey BF, Linscheid RL, Chao EY. Muscles across the elbow joint: a biomechanical analysis. J.Biomech. 1981;14:659-69.

32. Alcid JG, Ahmad CS, Lee TQ. Elbow anatomy and structural biomechanics. Clin.Sports Med. 2004;23:503-17, vii.

33. Seiber K, Gupta R, McGarry MH, Safran MR, Lee TQ. The role of the elbow musculature, forearm rotation, and elbow flexion in elbow stability: an in vitro study. J.Shoulder.Elbow.Surg. 2009;18:260-8.

34. An KN, Morrey BF, Chao EY. The effect of partial removal of proximal ulna on elbow constraint. Clin.Orthop.Relat Res. 1986;270-9.

35. Kamineni S, ElAttrache NS, O'Driscoll SW et al. Medial collateral ligament strain with partial posteromedial olecranon resection. A biomechanical study. J.Bone Joint Surg.Am. 2004;86-A:2424-30.

36. Ring D. Fractures of the coronoid process of the ulna. J.Hand Surg.[Am.] 2006;31:1679-89.

37. Wells J, Ablove RH. Coronoid fractures of the elbow. Clin.Med.Res. 2008;6:40-4.

38. Steinmann SP. Coronoid process fracture. J.Am.Acad.Orthop.Surg. 2008;16:519-29.

39. Schneeberger AG, Sadowski MM, Jacob HA. Coronoid process and radial head as posterolateral rotatory stabilizers of the elbow. J.Bone Joint Surg.Am. 2004;86-A:975-82.

40. Hull JR, Owen JR, Fern SE, Wayne JS, Boardman ND, III. Role of the coronoid process in varus osteoarticular stability of the elbow. J.Shoulder.Elbow.Surg. 2005;14:441-6.

41. Eygendaal D, Olsen BS, Jensen SL, Seki A, Sojbjerg JO. Kinematics of partial and total ruptures of the medial collateral ligament of the elbow. J.Shoulder.Elbow.Surg. 1999;8:612-6.

42. Halls AA, Travill A. Transmission of pressures across the elbow joint. Anat.Rec. 1964;150:243-7.

43. Jensen SL, Olsen BS, Tyrdal S, Sojbjerg JO, Sneppen O. Elbow joint laxity after experimental radial head excision and lateral collateral ligament rupture: efficacy of prosthetic replacement and ligament repair. J.Shoulder.Elbow.Surg. 2005;14:78-84.

44. Morrey BF, Tanaka S, An KN. Valgus stability of the elbow. A definition of primary and secondary constraints. Clin.Orthop.Relat Res. 1991;187-95.

45. Hotchkiss RN, Weiland AJ. Valgus stability of the elbow. J.Orthop.Res. 1987;5:372-7.

46. Armstrong AD, Dunning CE, Faber KJ, Duck TR, Johnson JA, King GJ. Rehabilitation of the medial collateral ligament-deficient elbow: an in vitro biomechanical study. J.Hand Surg.[Am.] 2000;25:1051-7.

47. Dunning CE, Duck TR, King GJ, Johnson JA. Simulated active control produces repeatable motion pathways of the elbow in an in vitro testing system. J.Biomech. 2001;34:1039-48.

48. Armstrong AD, Ferreira LM, Dunning CE, Johnson JA, King GJ. The medial collateral ligament of the elbow is not isometric: an in vitro biomechanical study. Am.J.Sports Med. 2004;32:85-90.

49. Josefsson PO, Johnell O, Wendeberg B. Ligamentous injuries in dislocations of the elbow joint. Clin.Orthop.Relat Res. 1987;221-5.

50. Davidson PA, Moseley JB, Jr., Tullos HS. Radial head fracture. A potentially complex injury. Clin.Orthop.Relat Res. 1993;224-30.

51. Morrey BF. Radial head fracture. In: Morrey BF, editor. The elbow and its disorders. Philadelphia: W.B. Saunders Company; 2000. p. 341-64.

52. Park MC, Ahmad CS. Dynamic contributions of the flexor-pronator mass to elbow valgus stability. J.Bone Joint Surg.Am. 2004;86-A:2268-74.

53. Altchek DW, Andrews JR. Medial collateral ligament injuries. In: Altchek DW, Andrews JR, editors. The athlete's elbow. Philadelphia: Lippincott Williams and Wilkins; 2001. p. 153-73.

54. Cohen MS, Bruno RJ. The collateral ligaments of the elbow: anatomy and clinical correlation. Clin.Orthop.Relat Res. 2001;123-30.

55. Safran MR. Elbow injuries in athletes. A review. Clin.Orthop.Relat Res. 1995;257-77.

56. Pincivero DM, Heinrichs K, Perrin DH. Medial elbow stability. Clinical implications. Sports Med. 1994;18:141-8.

57. Lee ML, Rosenwasser MP. Chronic elbow instability. Orthop.Clin.North Am. 1999;30:81-9.

58. Conway JE, Jobe FW, Glousman RE, Pink M. Medial instability of the elbow in throwing athletes. Treatment by repair or reconstruction of the ulnar collateral ligament. J.Bone Joint Surg.Am. 1992;74:67-83.

59. Miller CD, Savoie FH, III. Valgus Extension Injuries of the Elbow in the Throwing Athlete. J.Am.Acad.Orthop.Surg. 1994;2:261-9.

60. Chen FS, Rokito AS, Jobe FW. Medial elbow problems in the overhead-throwing athlete. J.Am.Acad.Orthop.Surg. 2001;9:99-113.

61. Jobe FW, Stark H, Lombardo SJ. Reconstruction of the ulnar collateral ligament in athletes. J.Bone Joint Surg.Am. 1986;68:1158-63.

62. Nazarian LN, McShane JM, Ciccotti MG, O'Kane PL, Harwood MI. Dynamic US of the anterior band of the ulnar collateral ligament of the elbow in asymptomatic major league baseball pitchers. Radiology 2003;227:149-54.

63. Fleisig GS, Andrews JR, Dillman CJ, Escamilla RF. Kinetics of baseball pitching with implications about injury mechanisms. Am.J.Sports Med. 1995;23:233-9.

64. Popovic N, Ferrara MA, Daenen B, Georis P, Lemaire R. Imaging overuse injury of the elbow in professional team handball players: a bilateral comparison using plain films, stress radiography, ultrasound, and magnetic resonance imaging. Int.J.Sports Med. 2001;22:60-7.

65. Werner SL, Fleisig GS, Dillman CJ, Andrews JR. Biomechanics of the elbow during baseball pitching. J.Orthop.Sports Phys.Ther. 1993;17:274-8.

66. Fleming BC, Beynnon BD. In vivo measurement of ligament/tendon strains and forces: a review. Ann.Biomed.Eng 2004;32:318-28.

67. Ravary B, Pourcelot P, Bortolussi C, Konieczka S, Crevier-Denoix N. Strain and force transducers used in human and veterinary tendon and ligament biomechanical studies. Clin.Biomech.(Bristol., Avon.) 2004;19:433-47.

68. Barry D, Ahmed AM. Design and performance of a modified buckle transducer for the measurement of ligament tension. J.Biomech.Eng 1986;108:149-52.

69. Komi PV, Salonen M, Jarvinen M, Kokko O. In vivo registration of Achilles tendon forces in man. I. Methodological development. Int.J.Sports Med. 1987;8 Suppl 1:3-8.

70. Komi PV. Relevance of in vivo force measurements to human biomechanics. J.Biomech. 1990;23 Suppl 1:23-34.

71. Walmsley B, Hodgson JA, Burke RE. Forces produced by medial gastrocnemius and soleus muscles during locomotion in freely moving cats. J.Neurophysiol. 1978;41:1203-16.

72. Biewener AA, Blickhan R, Perry AK, Heglund NC, Taylor CR. Muscle forces during locomotion in kangaroo rats: force platform and tendon buckle measurements compared. J.Exp.Biol. 1988;137:191-205.

73. Miller JM, Robins D. Extraocular muscle forces in alert monkey. Vision Res. 1992;32:1099-113.

74. Barnes GR, Pinder DN. In vivo tendon tension and bone strain measurement and correlation. J.Biomech. 1974;7:35-42.

75. Lewis JL, Lew WD, Schmidt J. A note on the application and evaluation of the buckle transducer for the knee ligament force measurement. J.Biomech.Eng 1982;104:125-8.

76. Meyer DC, Jacob HA, Nyffeler RW, Gerber C. In vivo tendon force measurement of 2-week duration in sheep. J.Biomech. 2004;37:135-40.

77. Dennerlein JT, Miller JM, Mote CD, Jr., Rempel DM. A low profile human tendon force transducer: the influence of tendon thickness on calibration. J.Biomech. 1997;30:395-7.

78. Platt D, Wilson AM, Timbs A, Wright IM, Goodship AE. Novel force transducer for the measurement of tendon force in vivo. J.Biomech. 1994;27:1489-93.

79. Rupert M, Grood E, Byczkowski T, Levy M. Influence of sensor size on the accuracy of in-vivo ligament and tendon force measurements. J.Biomech.Eng 1998;120:764-9.

80. Levin JS, Zheng N, Dugas J, Cain EL, Andrews JR. Posterior olecranon resection and ulnar collateral ligament strain. J.Shoulder.Elbow.Surg. 2004;13:66-71.

81. Andrews JR, Heggland EJ, Fleisig GS, Zheng N. Relationship of ulnar collateral ligament strain to amount of medial olecranon osteotomy. Am.J.Sports Med. 2001;29:716-21.

CHAPTER 2

Design and Development of a Customized Buckle Transducer for the Medial Collateral Ligament of the Elbow

Overview: A customized buckle transducer was developed using a mathematical modelling and mechanical design process. Basic principles of mechanics of materials were used to analyse the flexural characteristics of the transducer's components, which were the critically loaded and strain gauge instrumented components. Through this analysis, the dimensions of the transducer were optimized to fit the anterior bundle of the medial collateral ligament (AMCL) as well as to sustain the expected loads. The buckle transducer was subsequently calibrated to express the transducer's strain output in units of force.

The emphasis of this chapter is on the mathematical modelling process, and not on the details of the modelling and design process. The dimensions of the transducer are presented along with the explanation of *why* they are optimal. Details of the mathematical modelling process are presented in Appendix 5.

2.1 PHYSICAL PRINCIPLES OF A BUCKLE TRANSDUCER

A buckle transducer is a device used to measure the force that is developed within a tissue by attaching this compliant device to the tissue under investigation. There are many variations in the geometric shapes of buckle transducers, which are referred to as the frame of the device. The geometry and specific dimensions are dictated by the tissue

under study; various frame shapes that have been employed in previous studies include rectangular, oval, and E-form.

The physical principle behind the buckle transducer is the variation of electrical resistance of the strain gauges bonded to the transducer's frame. The tissue under investigation is woven through the frame of the transducer and as tension is applied, it is forced to straighten out from its initial woven position. This straightening action causes the transducer's frame to deflect; the strain gauges mounted on the transducer's frame detect this deflection. Through calibration, an equation is obtained which allows the strain measurements to be converted to force measurements.

Given the anatomical complexity of the anterior bundle of the medial collateral ligament (AMCL), and the constraints of the adjacent bony anatomy, the E-form frame was decided to best fit this ligament. To illustrate the working principles of this transducer, a simplified E-form frame buckle transducer is shown in Figure 2.1. An E-form frame buckle transducer consists of three beams; two outer beams and one centre beam. It was decided that the strain gauge would be mounted to the top surface of the centre beam, as this was the only location where there would be no contact with soft tissue; it was desirable to keep the exposed surface of the strain gauge free to ensure proper functioning of it. The tissue was woven through the beams of the transducer in a fashion similar to that shown in Figure 2.1. In an E-form frame buckle transducer, it is the transducer's three beams that deflect as tension is applied to the tissue. Recalling that the strain gauge was bonded to the transducer's centre beam, deflection of this beam was necessary for a signal to be captured by the strain gauge. Optimization of the centre beam deflection was performed through the design process, as will be discussed in this chapter.

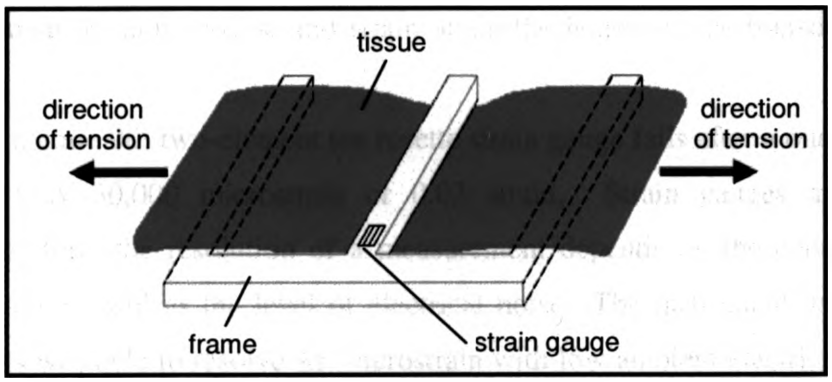

Figure 2.1: Simplified E-form frame buckle transducer

The tissue is woven through the frame of the transducer (*i.e.* through the transducer's three beams).

2.2 STRAIN GAUGE SELECTION

The strain gauge used for this study was a miniature tee rosette strain gauge (Vishay Micro-Measurements, Raleigh, NC – Model Number: EA-06-030TY-120/LE); this strain gauge was designed for the measuring of orthogonal strains as it had two metal foil element patterns, one oriented at an angle of 0° and the other at an angle of 90°. The gauge was bonded to the top surface of the transducer's centre beam such that the 0° element was aligned with the direction of the length-wise axis of the beam, and hence, the 90° element was transverse to the direction of the axial strain (Figure 2.2). The axial strain was of interest as it corresponded to the applied strain due to bending. As the applied strain was known to act in the longitudinal direction of the beam, a two-element tee rosette strain gauge could be used to directly measure the applied bending strain through orienting one of the metal foil elements in the longitudinal direction. Thus, it was crucial for the strain gauge to be aligned accurately in order to properly measure the bending strain; bonding of the strain gauge was done with great care following the manufacturer's procedure (Vishay Micro-Measurements, Instruction Bulletin B-127-12, 2005). The strain gauge was bonded to the base of the centre beam's top surface as this was the location of the largest bending moment, and consequently the location of the largest amount of deformation (*i.e.* strain); thus, this location produced the largest possible signal for the strain gauge. Appendix 5 shows the variation of shear force,

bending moment, bending stress, and strain along the length of the transducer's centre beam.

The miniature 90° two-element tee rosette strain gauge fails after a one-time stretch to approximately 30,000 microstrain or 0.03 strain. Strain gauges are extremely sensitive; therefore, the resolution of a measurement depends on the capability of the instrumentation as well as the level of electrical noise. The instrument used for strain measurements was able to resolve ±1 microstrain with low ambient electrical noise. For full details refer to Appendix 4.

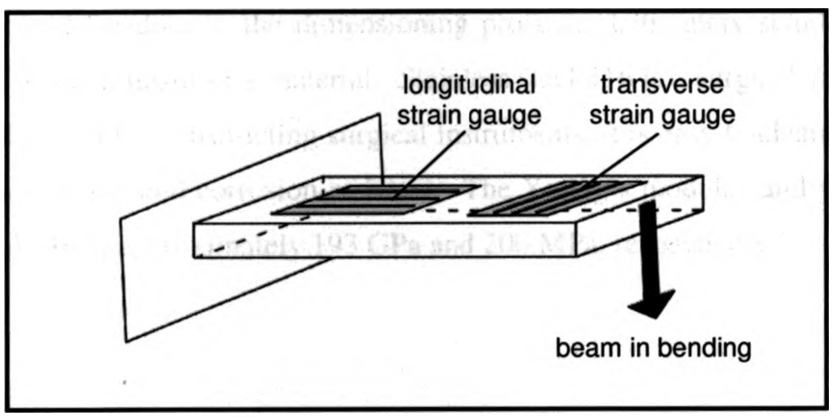

Figure 2.2: Arrangement of two uniaxial strain gauges to detect bending strain

One gauge is aligned along the axis of the applied strain, and other gauge is aligned along the transverse axis to detect the Poisson's effect. A tee rosette strain gauge contains these two uniaxial strain gauges on one backing.

2.3 DESIGN CONSTRAINTS AND REQUIREMENTS

The dimensions of the buckle transducer were markedly influenced by the size of the AMCL. Through a literature review[1-6], the average length, width, and thickness of the AMCL were found to be approximately 27 mm, 5 mm, and 6 mm, respectively. These ligament dimensions served as dimensional constraints for the design of the transducer. In addition to these constraints, the transducer was required to withstand the maximum tension expected to be experienced by the AMCL. From a simplified free body diagram analysis of the forearm in the valgus gravity-loaded orientation – the most aggressive loading scenario for *in vitro* investigations – the maximum tension expected to be

experienced by the AMCL ($F_{AMCL_{max}}$) was calculated to be approximately 110 N (for full details refer to Appendix 5).

The environment of the buckle transducer created constraints for the transducer's material. Since an electromagnetic tracking system would be employed during testing (explained in Chapter 3), the transducer's material needed to exhibit non-magnetic properties. In addition, material biocompatibility required consideration since the transducer could perhaps be employed clinically at a later date. A high material yield stress, taken to be the failure criterion, was also desirable as it allowed the buckle transducer to experience significant bending loads without failing; the result of which was an increased freedom in the dimensioning process. Ultimately stainless steel 316 was selected as the transducer's material. Stainless steel 316 is a surgical grade steel and hence is well-suited for constructing surgical instruments: it is easy to clean and sterilize, non-magnetic, strong, and corrosion-resistant. The Young's modulus and yield stress of stainless steel 316 is approximately 193 GPa and 200 MPa, respectively.[7]

2.4 DESIGN DETAILS

Figure 2.3 illustrates the relevant dimensions of the final buckle transducer design.

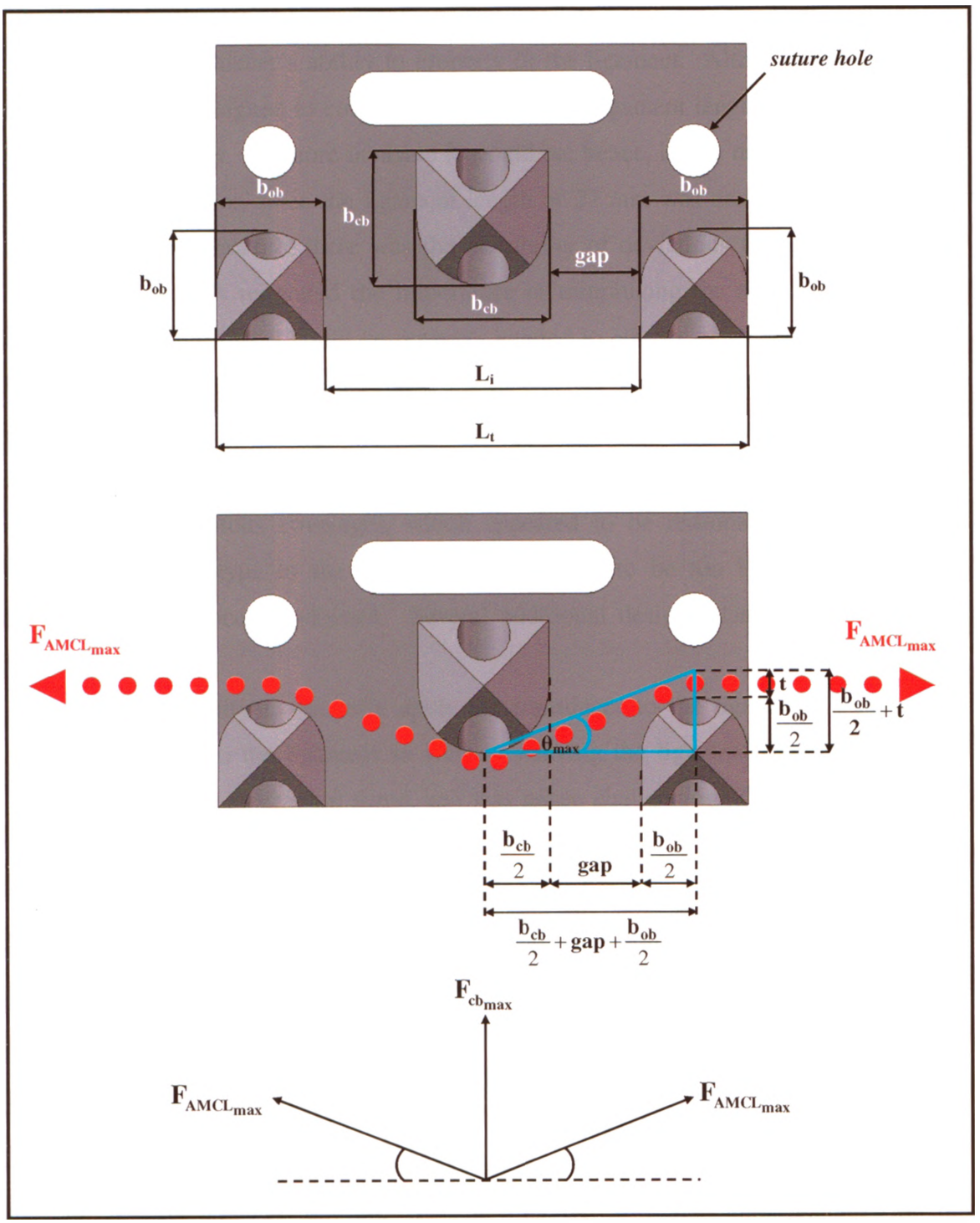

Figure 2.3: Relevant dimensions of the buckle transducer's geometry as viewed from the front

The ligament (represented by the red dots) is woven through the frame of the transducer. In this non-deflected state, the ligament weaving angle is at its maximum (θ_{max}).

2.4.1 Dimensioning Details

2.4.1.1 *Preliminary Considerations*

The overall buckle transducer length (L_t) was of primary concern as this dimension influenced the transducer's ability to properly fit the ligament. Although the transducer could have been designed to cover the total available ligament length (of ~ 27 mm), the larger the transducer, the more invasive it would be; hence, it was desirable to minimize its size. Furthermore, since the ligament length of 27 mm was derived from averaging the results from literature, there was the possibility of deviations from this average in smaller elbows; this reiterated the importance of minimizing the device's ligamentous coverage to ensure that it could be properly applied to elbows of all sizes. However, it was found through trials with prototypes in cadaver specimens that minimizing the device's ligamentous coverage alone did not ensure the successful implementation of the buckle transducer. The initial prototype had an overall transducer length (L_t) of 12.4 mm (or 45.9% ligamentous coverage), which appeared to be reasonable; however, upon applying the prototype to the AMCL, it was found to be too large, and made the implementation process awkward. Several additional design related issues were also found:

1) The inability to properly apply the transducer to the ligament. Pushing the device into the ligament as well as weaving the ligament through the device required a substantial force, and was hence challenging. This was observed to be caused by:
    i) Alignment of the transducer's three beams – the tops of all three beams were aligned with respect to each other; and
    ii) The size of the outer beams (b_{ob}) – the apparent large size of the outer beams (b_{ob}) seemed to forcefully displace a lot of tissue.
2) The transducer did not remain secured to the ligament as it moved through the desired range of motion. This was caused by the *gap* dimension being too large.
3) The ligament did not smoothly slide over the beams of the device during the desired range of motion. This was caused by the ligament catching on the corners of the device's beams.

2.4.1.2 *Transducer Sizing*

The results of the prototype testing were used to refine the design process to address the aforementioned issues. Two dimensions which could immediately be reduced to address the issue of the oversized overall transducer length (L_t) were the dimensions of the centre beam (b_{cb}) and the *gap*. The prototype centre beam width (b_{cb}) of 3 mm, which was based on the size of the strain gauge, was found to be an overestimate of the tolerance required to properly bond the strain gauge and thus was reduced to 2.5 mm. The reduction of the *gap* dimension from 2.2 mm to 1.75 mm was based on inspection during the prototype testing. This combination of the centre beam (b_{cb}) and the *gap* dimensions yielded a reduced inner transducer length (L_i) of 6 mm for the final buckle transducer design. With the inner transducer length (L_i) specified, an appropriate range of overall buckle transducer lengths (L_t) were investigated; the overall transducer length (L_t) was now governed only by the outer beam dimension (b_{ob}). Through mathematical modelling, which examined bending stress and beam deflection, the optimal outer beam dimension (b_{ob}) was found to be 2 mm, which corresponded to an overall transducer length (L_t) of 10 mm (or 37.0% ligamentous coverage). It should be noted that b_{cb} and b_{ob} describe both the width and height of the centre beam and outer beams, respectively; *i.e.* they are equal, as will be explained later.

In the mathematical modelling process, a range of outer beam dimensions (b_{ob}) were investigated, and the results are summarized in Table 2.1. As the outer beam dimension (b_{ob}) was increased, the overall transducer length (L_t), as well as the maximum bending stress ($\sigma_{cb_{\max}}$), the maximum strain ($\varepsilon_{cb_{\max}}$), and the maximum deflection ($\delta_{cb_{\max}}$) of the centre beam increased, whereas the maximum bending stress ($\sigma_{ob_{\max}}$) and the maximum deflection ($\delta_{ob_{\max}}$) of the outer beams decreased. It should be noted that none of the bending stresses ($\sigma_{cb_{\max}}$ and $\sigma_{ob_{\max}}$) were beyond the failure criterion of 200 MPa and that all of the centre beam strain values ($\varepsilon_{cb_{\max}}$) were within the operating range of the strain gauge (recall that the strain gauge fails at approximately 30,000 microstrain or 0.03 strain). Additionally, it can be observed that at an outer beam dimension (b_{ob}) of 2.1 mm, the outer beam deflection ($\delta_{ob_{\max}}$) was approximately equal to the centre beam

deflection ($\delta_{cb_{\max}}$); b_{ob} dimensions less than 2.1 mm resulted in outer beams deflections ($\delta_{ob_{\max}}$) which were greater than the instrumented centre beam deflection ($\delta_{cb_{\max}}$).

Thus, there was a trade off between the size of the transducer (L_t) and the amount of centre beam deflection ($\delta_{cb_{\max}}$); the larger the outer beam dimension (b_{ob}), the less the signal loss of the centre beam due to outer beam deflection ($\delta_{ob_{\max}}$), however, the more invasive the device became. Therefore, the selection of the outer beam dimension (b_{ob}) of 2 mm was a compromise; although some signal was lost since the outer beams deflected approximately 22.1% more than the centre beam, the resulting reduction of the ligamentous coverage to 37.0% was deemed to be more important for the successful implementation of the buckle transducer.

To summarize, the combination of the inner transducer length (L_i) and the outer beam dimension (b_{ob}) yielded an overall transducer length (L_t) of 10 mm.

Table 2.1: Beam analysis results

Results for stress, strain, and deflection for varying outer beam (b_{ob}) dimensions. The maximum values correspond to $F_{AMCL_{max}}$, which was calculated to be approximately 110 N. The highlighted row corresponds to the final buckle transducer design. All column headings are as previously defined; the last column was calculated using $\left(\frac{\left|\delta_{ob_{max}} - \delta_{cb_{max}}\right|}{\delta_{cb_{max}}}\right) \cdot 100\,\%$.

b_{ob} [mm]	L_t [mm]	Ligamentous Coverage [%]	Offset [mm]	θ_{max} [Degrees]	F_{cb} [N]	F_{ob} [N]	I_{ob} [mm^4]	$\sigma_{max,cb}$ [MPa]	$\sigma_{max,ob}$ [MPa]	$\varepsilon_{cb,max}$ [Strain]	$\delta_{max,cb}$ [mm]	$\delta_{max,ob}$ [mm]	$\delta_{max,ob}$ [%]
1.0	8.0	29.6	0.5	23.2	86.7	43.3	0.1	146.6	1145.3	7.6E-04	6.2E-03	1.2E-01	1853.1
1.1	8.2	30.4	0.6	23.6	88.0	44.0	0.1	148.9	874.1	7.7E-04	6.3E-03	8.4E-02	1234.0
1.2	8.4	31.1	0.6	24.0	89.4	44.7	0.1	151.1	683.3	7.8E-04	6.4E-03	6.0E-02	841.9
1.3	8.6	31.9	0.7	24.3	90.6	45.3	0.2	153.3	545.1	7.9E-04	6.5E-03	4.4E-02	583.8
1.4	8.8	32.6	0.7	24.7	91.9	45.9	0.3	155.4	442.4	8.1E-04	6.6E-03	3.3E-02	408.4
1.5	9.0	33.3	0.8	25.0	93.0	46.5	0.3	157.4	364.3	8.2E-04	6.7E-03	2.6E-02	285.8
1.6	9.2	34.1	0.8	25.3	94.2	47.1	0.4	159.3	303.9	8.3E-04	6.7E-03	2.0E-02	198.0
1.7	9.4	34.8	0.9	25.7	95.3	47.6	0.6	161.2	256.3	8.4E-04	6.8E-03	1.6E-02	133.8
1.8	9.6	35.6	0.9	26.0	96.4	48.2	0.7	163.0	218.3	8.4E-04	6.9E-03	1.3E-02	86.1
1.9	9.8	36.3	1.0	26.3	97.4	48.7	0.9	164.7	187.6	8.5E-04	7.0E-03	1.0E-02	49.9
2.0	10.0	37.0	1.0	26.6	98.4	49.2	1.1	166.4	162.5	8.6E-04	7.0E-03	8.6E-03	22.1
2.1	10.2	37.8	1.1	26.8	99.4	49.7	1.3	168.1	141.8	8.7E-04	7.1E-03	7.1E-03	0.4
2.2	10.4	38.5	1.1	27.1	100.3	50.1	1.6	169.7	124.5	8.8E-04	7.2E-03	6.0E-03	-16.6
2.3	10.6	39.3	1.2	27.4	101.2	50.6	1.9	171.2	109.9	8.9E-04	7.2E-03	5.1E-03	-30.2
2.4	10.8	40.0	1.2	27.6	102.1	51.0	2.2	172.7	97.6	8.9E-04	7.3E-03	4.3E-03	-41.1
2.5	11.0	40.7	1.3	27.9	102.9	51.5	2.6	174.1	87.1	9.0E-04	7.4E-03	3.7E-03	-50.0

2.4.2 Beam Analysis

The results of the beam analysis (stress, strain, and deflection) were presented in the process of developing the argument for the selection of the outer beam dimension; however, not all of the transducer parameters required to perform the beam analysis were discussed. The beam analysis will now be discussed in more detail, and in doing so, the remaining relevant transducer parameters will be justified.

2.4.2.1 *Loading Situation*

The transducer's three beams were modelled as cantilever beams in bending subjected to uniform loads distributed along their lengths; these were simplified to resultant loads acting at the mid-length of the beams. Thus for this situation, the bending stress in all of the transducer's beams was given by Equation 2.1 where σ is the bending stress, M is the moment at the neutral axis, y is the perpendicular distance to the neutral axis, and I is the area moment of inertia about the neutral axis.

$$\sigma = \frac{My}{I}$$

Equation 2.1: Calculation of bending stress of the transducer's beams

Considering the moment (M) term, the resultant loads acting on each beam, as well as the appropriate moment arms were required to be determined; in particular, the maximum resultant loads were sought in order to design the transducer for the most extreme loading situation that it may experience. For the centre beam, the maximum resultant load ($F_{cb_{\max}}$) was determined to be the vertical force components of the maximum ligament tension ($F_{AMCL_{\max}}$); mathematically, $F_{cb_{\max}}$ can be expressed as $F_{cb_{\max}} = 2 \cdot F_{AMCL_{\max}} \cdot \sin\theta_{\max}$ (Figure 2.3). $\theta_{\max}$ is the maximum ligament weaving angle and is the angle the ligament makes with the horizontal in the *gap* region after it has been initially woven through the transducer. From Figure 2.3, $\theta_{\max}$ is a function of the outer beam dimension (b_{ob}), and consequently $F_{cb_{\max}}$ is a function of the outer beam dimension (b_{ob}). For the outer beams, the maximum resultant load experienced by each of the two

outer beams ($F_{ob_{max}}$) was determined to be half that of the centre beam (*i.e.* $F_{ob_{max}} = F_{cb_{max}} / 2$).

To determine the moment arm, the length of the transducer's beams was needed. The length of the transducer's centre beam (L) was 8.5 mm, based on the average width of the AMCL (5 mm), the tolerance allotted to properly bond the strain gauge to the centre beam (2 mm), and an additional amount allotted for a hole to be made at the end of the beam for suturing (1.5 mm); the purpose of these suture holes will be discussed later. For simplicity, all of the transducer's beams were made the same length.

Thus, with the maximum resultant loads ($F_{cb_{max}}$ and $F_{ob_{max}}$) and the beam lengths (L) having been identified, the moment (M) term in Equation 2.1 was described in terms of the relevant transducer parameters.

2.4.2.2 *Determination of Beam Cross-Section*

For regular cross-sectioned beams in bending (*i.e.* not I-beams, C-beams, box-beams, etc.), for a given cross-sectional area, it is known that a rectangular beam cross-section, in which the height is greater than the width, is the strongest. Strength was desirable for the outer beams; recall that it was desirable to minimize outer beam deflection in order to reduce signal loss. This cross-sectional shape, however, would have increased the invasiveness of the device. To elaborate, although the overall transducer length (L_t) may have been potentially decreased, the ligament weaving process of this design would have consumed more of the ligament for a given inner transducer length (L_i), making the transducer more invasive in this regard. Furthermore, in order to properly insert the device, taller beams in general would have to displace more tissue; hence, making it more invasive. Similar considerations were examined for a rectangular beam cross-section in which the width was greater than the height. Less tissue would be consumed in the ligament weaving process for a given inner transducer length (L_i); however, the ligamentous coverage of the device would be greater. Additionally, the reduction in outer beam cross-sectional area moment of inertia of this design would cause the outer beams to deflect more, in comparison to the first rectangular beam cross-section orientation. The maximum deflection of the transducer's beams was calculated using Equation 2.2.

$$\delta = \frac{5}{48} \cdot \frac{FL^3}{EI}$$

Equation 2.2: Calculation of deflection of the transducer's beams

In the above equation, δ is the maximum deflection of the beam at its free end, F is the resultant load, L is the effective length of the beam, E is the Young's modulus of the material (stainless steel 316), and I is the area moment of inertia about the neutral axis. It can be observed that for a given resultant load, beam length, and modulus of elasticity, the greater the area moment of inertia, the smaller the deflection (and vice versa). Thus it can be seen that there was an inherent compromise between ligamentous coverage, tissue displacement, and outer beam strength. This compromise was the reason for the height and width of the beams to be the same; *i.e.* square cross-sectioned beams. Ultimately, the final cross-sectional design of all three beams was a rounded-square – a square in which two of the corners were rounded such that they form a semi-circle (Figure 2.4). The rounding was performed to promote a smooth sliding of the ligament through the device.

With the cross-section design of the beams defined, Equation 2.1 was solved for the maximum bending stresses in the beams ($\sigma_{cb_{\max}}$ and $\sigma_{ob_{\max}}$). Moreover, as all of the relevant transducer parameters were defined, the remaining calculations for the beam analysis (strain and deflection) were performed; the maximum deflections of the beams ($\delta_{cb_{\max}}$ and $\delta_{ob_{\max}}$) were determined using Equation 2.2, and the maximum strain in the centre beam ($\varepsilon_{cb_{\max}}$) was calculated via Equation 2.3.

$$\varepsilon = \frac{\sigma}{E}$$

Equation 2.3: Calculation of strain in the transducer's centre beam

In the above equation, ε is the strain, σ is the bending stress, and E is the Young's modulus of the material (stainless steel 316). The details of these calculations are given in Appendix 5.

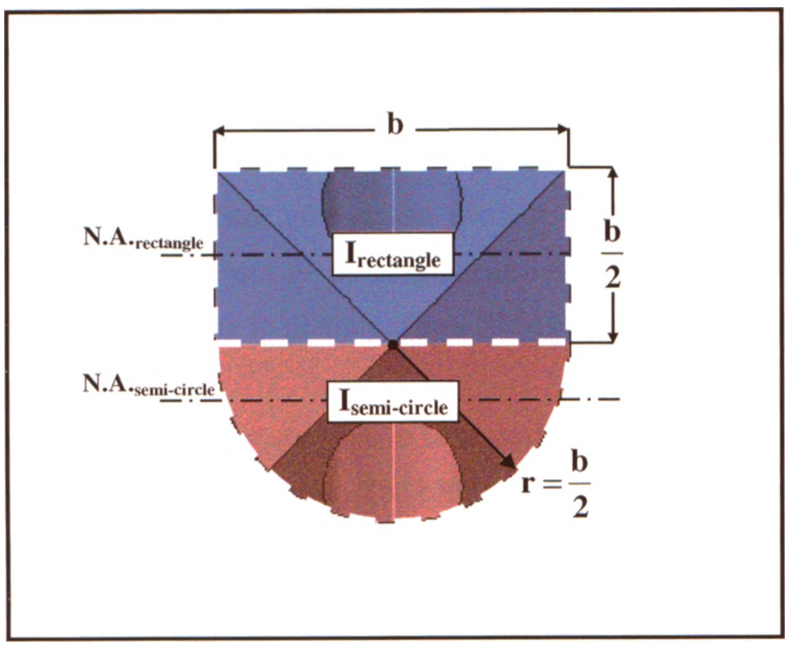

Figure 2.4: Cross-section of the transducer's beams

Note the beams' rounded-square cross-section.

2.5 FINAL TRANSDUCER DESIGN

The above sections have focused on the dimensions of the transducer's design. Additional features of the buckle transducer's design, illustrated in Figure 2.5, include: the offset of the transducer's centre beam, the sharpened beam ends, the base of the transducer, and the suture holes.

The offset of the transducer's centre beam, as well as the sharpened beam ends, were both features to promote the atraumatic insertion of the transducer into the ligament. As indicated in Figure 2.3 and Figure 2.5, the centre beam was shifted upwards so that it was not in the same plane as the two outer beams. The offset was such that the bottom of the centre beam was aligned with the centres of the outer beams (*i.e.* a 1 mm centre beam offset). The effect of this offset was a decrease in the maximum ligament weaving angle (θ_{max}), which reduced the amount of ligament needed for the initial weaving process, which in turn reduced the amount of tissue pre-tensioning. Sharpening the beam tips resulted in the device being able to directly pierce through the tissue, thereby facilitating insertion.

The base of the transducer served two purposes: to support the beams, as well as to allow for easy handling of the device. The base was designed so that the device could be easily manipulated without the need of an insertion tool; in doing so, the thickness of the base was limited. To elaborate, a thick base would have impinged upon the surrounding soft tissue and bony constructs as the arm moved through the desired range of motion, thus altering the transducer's output. The height of the base, however, was not limited as the AMCL would be open to the environment and not covered with soft tissue during testing. Hence, observing Figure 2.5, the resulting cross-section of the base was a rectangle in which the height was greater than the width. The thickness, height, and length of the transducer's base were 1.5 mm, 5.5 mm, and 10 mm, respectively. A horizontal slot was included for routing of the strain gauge's wiring; this protected the wires from excess movement during testing.

To maintain the transducer in the desired orientation on the ligament during testing, suturing the transducer to the adjacent joint capsule was required. Holes were made at the ends of each beam as well as on the base of the transducer to allow sutures to secure the device (Figure 2.3 and Figure 2.5). All suture holes were 1 mm in diameter.

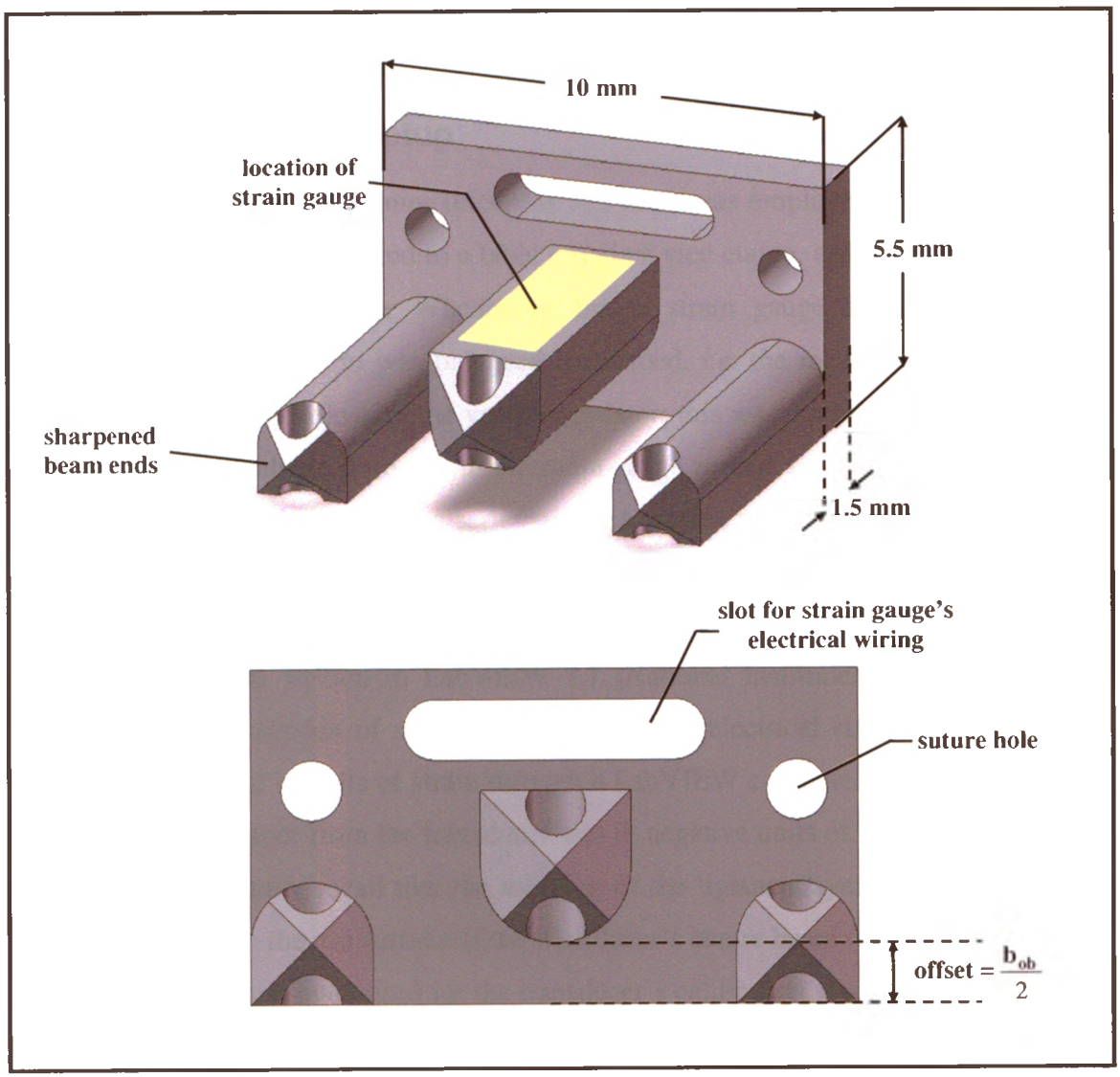

Figure 2.5: Final buckle transducer design as viewed from the front

Note the additional features, including the offset of the transducer's centre beam, the sharpened beam ends, the base of the transducer, and the suture holes.

Detailed drawings of the transducer are given in Appendix 5. For the complete details of the mathematical modelling process, which was used to design the transducer, refer to Appendix 5. The calculations presented in Appendix 5 are complementary to the discussions of this chapter.

2.6 CALIBRATION

2.6.1 Experimental Setup

A synthetic fibre (width = 7 mm; thickness = 2 mm) was employed for the calibration procedure. One end was secured to a table top via a vice clamp, and the other end freely hung off the table top. The Wheatstone bridge strain gauge circuit to which the transducer was connected to was balanced (or zeroed, *i.e.* the measured output voltage was zero) by manually adjusting the variable resistor; this was done prior to applying the transducer to the synthetic fibre. With the strain gauge zeroed, the buckle transducer was applied to the synthetic fibre and a series of brass masses were suspended from the free end of the synthetic fibre one at a time in order to apply specified loads to the transducer. Once the mass(es) had stabilized, the output of the buckle transducer was recorded, using a computer program written in LabVIEW 7.1 (National Instruments, Austin, TX), to obtain at least 10 seconds of strain output data. The electrical signal from the strain gauge was converted to units of strain through a LabVIEW computer program. It should be noted that the output from the transducer was in negative units of voltage, and thereby negative units of strain; recall that the weaving of the ligament/synthetic fibre caused a compressive load on the top surface of the transducer's centre beam (Figure 2.1).

The maximum mass used for the transducer's calibration was selected such that it was approximately equivalent to 100 N of force, as it was anticipated that the AMCL would experience loads up to this value.

For each mass, 10 seconds of strain output data was averaged to obtain the average strain output for the particular mass. This calibration process was repeated six times, and the outputs for each of the six calibration processes were averaged to obtain a final average strain output for each mass. These average strain values were used to obtain the calibration equation.

2.6.2 Development of Calibration Equation

Figure 2.6 shows a plot of the applied loads versus the outputted strain values from the transducer. A linear regression was performed for the data set (Microsoft Office Excel 2002; Microsoft Corporation, Redmond, WA). The equation of the regression and coefficient of determination were $y = -60285x - 7.29$ and $R^2 = 0.97$, respectively. The regression equation was not forced to pass through the origin for two reasons. First, the zero-load – zero-strain condition does not exist; hence, forcing the regression equation through zero-load – zero-strain would be inaccurate. Second, although the regression equation has a y-intercept, only the slope of the line is of interest, as this slope represents the response of the transducer to applied loads; the intercept represents the starting value at the zero-load condition, and this is achieved by manual zeroing prior to testing, as discussed previously. Thus, the calibration equation which was used in all subsequent studies was $y = -60285x$, where y represents the tension experienced by the AMCL, and x represents the strain outputted from the transducer. The equation obtained from the calibration process allowed the strain values to be converted to force values. This conversion was done to directly interpret the results of the subsequent tests. Hysteresis of the transducer was also investigated, the results of which are presented in Appendix 6.

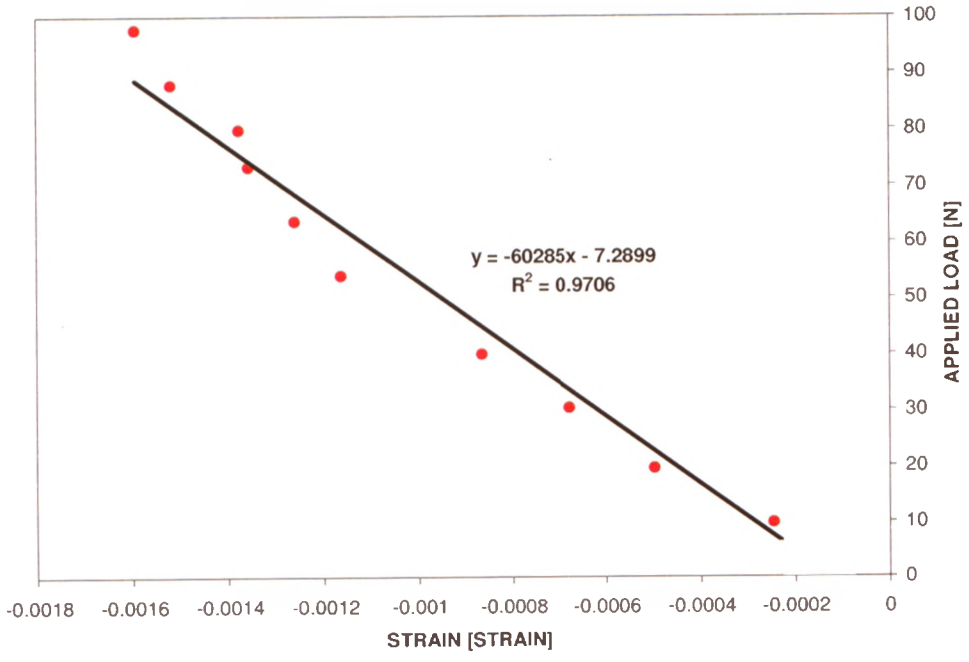

Figure 2.6: Calibration curve of the buckle transducer

The average strain output of the buckle transducer for specified applied loads.

2.7 SUMMARY

The final E-form frame buckle transducer design had an overall transducer length (L_t) of 10 mm, a ligamentous coverage of 37%, a centre beam offset of 1 mm, and rounded-square beam cross-sections. The calibration equation developed (AMCL tension = $-60285 \cdot$ strain) allowed the transducer's strain output to be converted to units of force. In addition, although not discussed here, the efficacy of the buckle transducer was investigated through several functionality investigations. Specific investigations included: hysteresis of the transducer's response (Appendix 6), repeatability of the transducer's response (Chapter 3), reproducibility of the transducer's response (Appendix 10), and tests of the transducer's invasiveness (Appendix 10). The transducer showed good characteristics in all of these investigations.

2.8 REFERENCE LIST

1. Nazarian LN, McShane JM, Ciccotti MG, O'Kane PL, Harwood MI. Dynamic US of the anterior band of the ulnar collateral ligament of the elbow in asymptomatic major league baseball pitchers. Radiology 2003;227:149-54.

2. Floris S, Olsen BS, Dalstra M, Sojbjerg JO, Sneppen O. The medial collateral ligament of the elbow joint: anatomy and kinematics. J.Shoulder.Elbow.Surg. 1998;7:345-51.

3. Timmerman LA, Andrews JR. Histology and arthroscopic anatomy of the ulnar collateral ligament of the elbow. Am.J.Sports Med. 1994;22:667-73.

4. Regan WD, Korinek SL, Morrey BF, An KN. Biomechanical study of ligaments around the elbow joint. Clin.Orthop.Relat Res. 1991;170-9.

5. Morrey BF, An KN. Functional anatomy of the ligaments of the elbow. Clin.Orthop.Relat Res. 1985;84-90.

6. Popovic N, Ferrara MA, Daenen B, Georis P, Lemaire R. Imaging overuse injury of the elbow in professional team handball players: a bilateral comparison using plain films, stress radiography, ultrasound, and magnetic resonance imaging. Int.J.Sports Med. 2001;22:60-7.

7. Callister WDJr. Appendix B: Properties of selected engineering materials. Materials science and engineering. An introduction. New York: John Wiley & Sons, Inc.; 2003. p. 737-64.

CHAPTER 3

Quantification of Medial Collateral Ligament Tension in the Elbow

Overview: This chapter details an *in vitro* cadaveric study examining the magnitude of medial collateral ligament tension in the elbow. Ligament tension was quantified using the custom designed E-form frame buckle transducer described in Chapter 2. Ligament tension and joint kinematics, for both active and passive elbow flexion in the valgus and dependent positions, are presented and analysed.

3.1 INTRODUCTION

Techniques have evolved for quantifying human tendon and ligament forces in the lower extremity; however, custom developed systems for the upper extremity, particularly the elbow, are not well described. Consequently, ligament forces of the human elbow joint have not been reported. Knowledge of the magnitudes of tension of the primary valgus stabilizer, the anterior bundle of the medial collateral ligament (AMCL)[1-10], would allow for an improved understanding of the load environment of this tissue. As a result, insight into AMCL injury mechanisms would be gained, which in turn, would allow for the development of injury prevention strategies and rehabilitation techniques that optimize healing. Furthermore, this knowledge should allow for the design and evaluation of improved methods of AMCL repair and reconstruction, and assist in the development of an artificial AMCL and *in vitro* biomechanical models of the elbow.

The purpose of this *in vitro* study was to quantify the magnitude of tension in the native AMCL through the arc of elbow flexion for different arm orientations. We hypothesized that tension in the AMCL would increase with elbow flexion, and that

AMCL loads would be greater for the arms oriented in the valgus position relative to the dependent (*i.e.* vertical) position.

3.2 MATERIALS AND METHODS

3.2.1 Specimen Preparation

Five fresh-frozen cadaveric upper extremities (mean age 72 ± 10 years; range: 62-82 years; 3 female; 1 right specimen) were amputated at mid-humerus and maintained frozen at -20°C prior to use. The specimens were thawed overnight at room temperature and were prepared for mounting on a specialized testing apparatus (Figure 3.1). All soft tissue and skin were removed from the humerus down to the supracondylar ridges to facilitate fixation in the humeral clamp of the testing apparatus. The brachialis, biceps brachii, and brachioradialis were identified as the principal elbow flexors and the triceps brachii as the principal elbow extensor. A stainless steel cable (0.8 mm diameter) was sutured to the distal tendon of the brachialis, the biceps, and the triceps using 200 lb braided Dacron® (Woodstock Line Co., Putnam, CT) and to the brachioradialis using a #5 Ethibond suture (Johnson & Johnson, Ethicon Inc., Peterborough, ON). The origin of the brachioradialis was simulated using a (Delrin®) pulley attached to the proximal portion of the lateral supracondylar ridge to ensure replication of the muscle's moment arm throughout elbow motion.[11] The lines-of-action of the elbow flexor and extensor muscles were maintained using a tendon alignment unit located within the humeral clamp.

The wrist was stabilized in neutral flexion/extension using a 5 mm Steinman Pin drilled through the long finger metacarpal, across the carpus, and into the distal radius. To prevent forearm rotation (*i.e.* pronation-supination), the forearm was fixed in neutral rotation using a 3.5 mm tap (Synthes Ltd., Mississauga, ON) placed through the distal radius and ulna. All skin incisions were closed with 2-0 Vicryl sutures (Johnson & Johnson, Ethicon Inc., Peterborough, ON) to keep all soft tissues moist during testing.

The humerus was mounted into a specialized testing apparatus in neutral humeral rotation (*i.e.* when the elbow was flexed to 90°, the forearm was perpendicular to the floor) using a clamp that rigidly held the arm while allowing unconstrained elbow motion (Figure 3.1). The humeral mounting clamp was affixed to a base-plate on a two-degree-

of-freedom hinge, which permitted orientation of the arm in the valgus gravity-loaded position, as well as in the dependent (*i.e.* vertical) position (Figure 3.2).

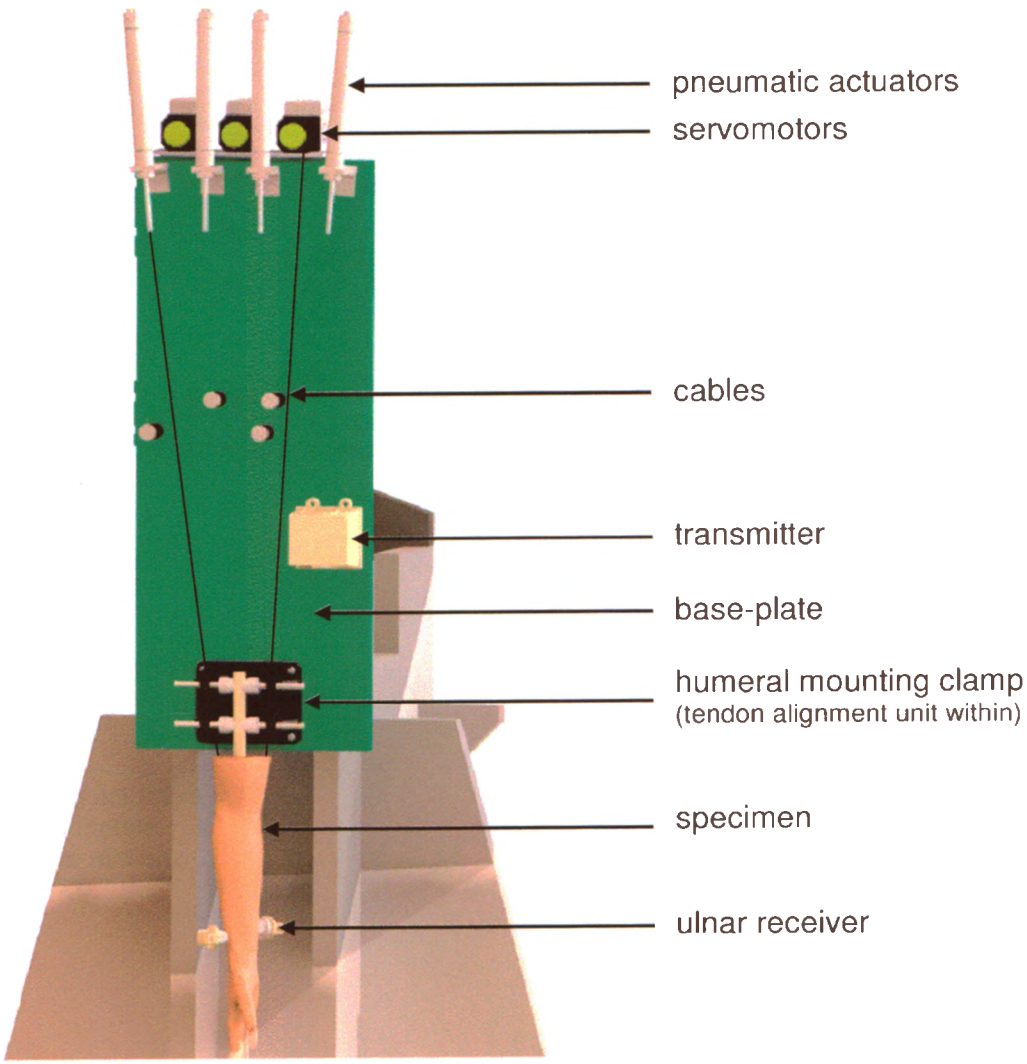

Figure 3.1: Specialized testing apparatus

The humerus was mounted into the specialized testing apparatus in neutral humeral rotation using a clamp that rigidly held the arm while allowing unconstrained elbow motion. Active or passive flexion against gravity with the humerus vertical is shown. For active motion, computer-controlled tendon loading was applied via cables attached to actuators and motors. (For illustrative purposes only two cables are shown; however, for each muscle simulated, a separate cable was connected to either an actuator or motor.) During testing, the position and orientation of the ulnar receiver relative to the transmitter was measured in six-degrees-of-freedom.

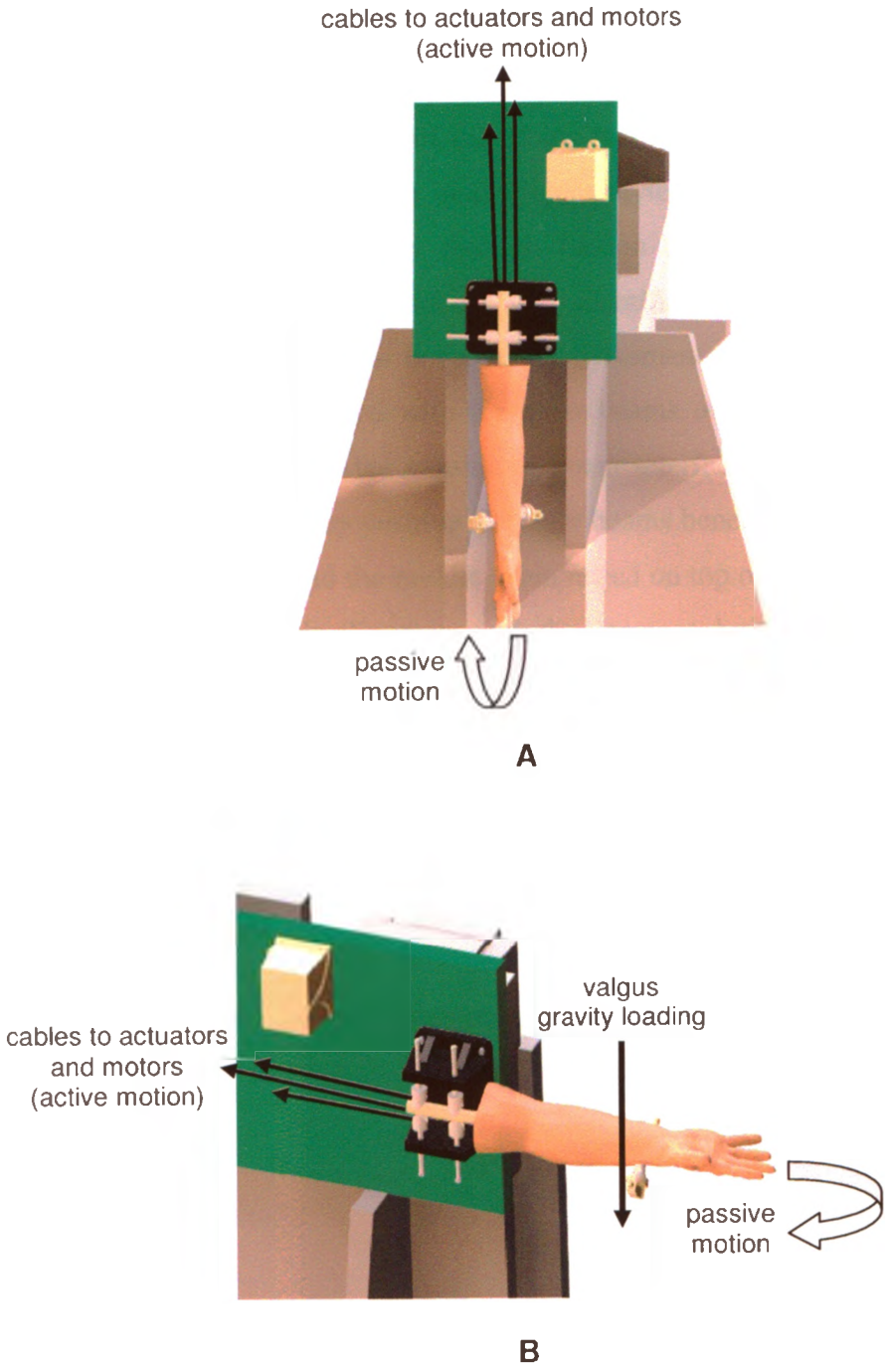

Figure 3.2: Orientation of the apparatus in the dependent (A) and valgus (B) positions

A two-degree-of-freedom hinge allowed placement of the apparatus in the vertical (*i.e.* dependent) position (A) and the valgus gravity-loaded postion (B). For this study, there were four test conditions: (1) passive flexion in the dependent position; (2) active flexion in the dependent position; (3) passive flexion in the valgus position; and (4) active flexion in the valgus position.

3.2.2 Buckle Transducer Implantation

With the specimen mounted in the testing apparatus and oriented in the valgus gravity-loaded position, the medial aspect of the elbow was exposed, and the medial common flexor origin was elevated from the medial epicondyle in order to identify the AMCL. The forearm was cycled passively through flexion and extension until the optimal insertion site for the buckle transducer was identified (*i.e.* the site which avoided impingement of the transducer on bone during movement). Once the insertion site was identified, two incisions, aligned with the outer beams of the buckle transducer, were made beneath the ligament at the capsule-ligament interface. The transducer was then interlaced with the ligament by pushing the outer beams beneath the ligament via the two aforementioned incisions, and the middle beam rested on top of the ligament (Figure 3.3). To maintain the transducer's alignment with the ligament during motion, the device was sutured to the adjacent joint capsule with a #2 FibreWire suture (Arthrex Inc., Naples, FL) through a hole in the middle beam. All skin incisions were closed with 2-0 Vicryl sutures. Data from the buckle transducer were recorded in real time using custom software programmed using LabVIEW 7.1 (National Instruments, Austin, TX). The specimen was kept moist using 0.9% normal saline solution throughout testing.

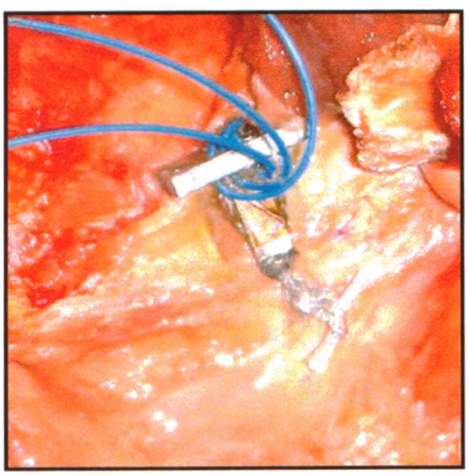

Figure 3.3: Buckle transducer inserted into the AMCL

The transducer was interlaced with the ligament by pushing the outer beams beneath the ligament via two incisions, and the middle beam rested on top of the ligament. To maintain the transducer's alignment with the ligament during motion, the device was sutured to the adjacent joint capsule through a hole in the middle beam.

3.2.3 Active and Passive Simulated Elbow Flexion

To achieve active simulated flexion, each stainless steel cable was attached to an associated computer-controlled pneumatic actuator (brachioradialis) or servomotor (brachialis, biceps, and triceps) of the testing apparatus. The muscles were loaded by the actuators/motors and control of each unit was achieved using custom software (LabVIEW 7.1).

Relative loading among the muscles was derived in accordance with published measurements of quantitative electromyographic (EMG) activity[12] and physiological muscle cross-sectional area (pCSA)[13]. The ratio of muscle loading was determined from the product of the relative EMG activity and pCSA data, as previously validated by our laboratory.[14] Loading of the biceps, brachioradialis, and triceps were determined as a proportion of the load applied by the brachialis, the prime flexor of the elbow (*i.e.* the prime mover). The load applied to the brachialis tendon was such that a controlled rate of elbow flexion was maintained. The brachialis tendon moved at a constant flexion rate of 10 degrees per second, which was achieved by a proportional-integral-derivative control using feedback from the electromagnetic tracking system.

Passive elbow flexion was achieved by an investigator directly guiding the arm through its full range of motion. This involved lightly grasping the specimen at the level of the wrist and guiding the elbow through a full arc of flexion until a definite endpoint of range of motion was reached. Care was taken to avoid applying any additional load to the specimen.

3.2.4 Kinematic Measurements – Electromagnetic Tracking Device

Motion of the ulna relative to the humerus was measured in six-degrees-of-freedom using an electromagnetic tracking device (Flock of Birds; Ascension Technology, Burlington, VT).

The transmitter was rigidly fixed to the base-plate of the testing apparatus, eliminating relative motion between the humerus and the transmitter (Figure 3.1).[15] Two receivers were used in this study: the first receiver was used to digitize the anatomical landmarks, and the second receiver was rigidly attached to the distal third of the medial ulna. During testing, the position and orientation of the ulnar receiver relative to the

transmitter was recorded in six-degrees-of-freedom. Previous research conducted in our laboratory demonstrated that this system has positional and rotational errors of less than 2%, when utilized within its optimal operating range of 22.5-64.0 cm.[16] The device is sensitive enough to read positional and rotational changes of 0.25 mm and 0.1°, respectively, and to be insensitive to commonly used orthopaedic alloys.[16] Care was taken to ensure that the distance between the transmitter and the receiver always remained within the optimum operating range of the tracking system. The testing apparatus was machined from polyethylene (Delrin®) and 316L stainless steel to avoid interference with the electromagnetic tracking device.[16,17]

After completion of testing, the elbow and wrist were disarticulated and anatomical landmarks on the humerus and ulna were digitized using the first receiver. The humeral coordinate system relative to the transmitter frame was established from the centre of the capitellum, the centre of the trochlear groove, and the centre of the humeral shaft. Sphere-fit and circle-fit algorithms were used to find the centre points of the capitellum and trochlear groove, respectively. Similarly, the ulnar coordinate system relative to the ulnar receiver frame was established from the plane and centre of the guiding ridge of the greater sigmoid notch, and the ulnar styloid; a circle-fit algorithm was used to determine the centre point of the greater sigmoid notch. Therefore, the "ulnar receiver with respect to transmitter" data collected during testing could be converted to "ulna with respect to humerus" data using Euler Z-Y-X analyses during *post hoc* data analysis.[15] Hence, clinically relevant coordinate systems could be constructed. Outputted data from the tracking system were recorded in real time using custom software programmed using LabVIEW 7.1. The relative motion of the ulnar coordinate system relative to the humeral coordinate system was analysed using custom software (LabVIEW 7.1). This method has been previously described by our laboratory.[18]

3.2.5 Testing Protocol

Testing was conducted with the arm oriented in the dependent and valgus positions, with the elbow under both passive and active motion. For both orientations, five passive and active flexion cycles (to assess repeatability) were performed with the forearm in neutral rotation.

The AMCL tension measurements corresponding to the five consecutive flexion cycles were used to investigate the repeatability of the buckle transducer; therefore, repeatability of the transducer was investigated in each test condition (*i.e.* active/passive flexion in the dependent position and active/passive flexion in the valgus positions) for each specimen. Repeatability is reported for one specimen (Section 3.3.1). For all subsequent analyses, the AMCL tension and elbow kinematic data from the third flexion cycle of each test condition were analysed.

3.2.6 Data Analysis

One-way and two-way repeated measures analysis of variance (ANOVA) with $\alpha = 0.05$, and *post hoc* paired *t*-tests using the Bonferroni correction for family-wise error were employed. All data were statistically analysed using SPSS software (SPSS V16.0.1, Chicago, IL).

Data from all five specimens tested were analysed for the valgus position (mean age 72 ± 10 years; range: 62-82 years; 3 female; 1 right specimen); however, due to data acquisition difficulties, data from only four specimens were analysed for the dependent position (mean age 74 ± 9 years; range: 65-82 years; 2 female; 1 right specimen). For each test condition (*i.e.* active/passive flexion in the dependent position and active/passive flexion in the valgus position), a one-way repeated ANOVA was performed; *flexion angle* was used as the independent variable. For each forearm orientation (*i.e.* dependent and valgus), a two-way repeated ANOVA was performed; the two independent variables used were *condition* (*i.e.* active motion and passive motion) and *flexion angle*.

During testing, two dependent variables were measured: (1) AMCL tension, which was the output of the buckle transducer; and (2) valgus angulation of the ulna with respect to the humerus. Valgus angulation was calculated, for both the dependent and valgus positions, by measuring the difference in the orientation of the ulna relative to the humerus via the custom software previously described (LabVIEW 7.1). AMCL tension and valgus angulation were measured throughout the arc of elbow flexion but were statistically analysed only at every 10° of elbow flexion from 20°-120° of elbow flexion to

simplify data interpretation; hence, there were eleven levels of the independent variable *flexion angle.*

All kinematic data were analysed using custom software (LabVIEW 7.1), Microsoft Office Excel 2002 (Microsoft Corporation, Redmond, WA), and SPSS. All source tension data were filtered using a program written in Matlab (The MathWorks, Natick, MA), and analysed using Microsoft Office Excel 2002 and SPSS.

3.2.7 Forearm Mass Measurements

To assess whether there was a correlation between AMCL tension and forearm size, the masses of the forearms were quantified. With the arm oriented in the dependent position, the mass of the specimen was measured via a spring sale. With the scale hooked under the wrist of the specimen, three mass readings were taken, while the specimen was kept stationary in the transverse plane. The average of these measurements was taken to be the mass of the specimen. It should be noted that the mass of specimen 1 was not taken, and thus, this specimen is not included in this analysis. A linear regression was performed for each data set, using Microsoft Office Excel 2002, in order to determine the coefficient of determination (R^2 value).

3.3 RESULTS

3.3.1 Repeatability

The results of repeatability testing for one specimen are presented in Figure 3.4, which shows a plot of AMCL tension versus flexion angle for active flexion in the valgus position. (This specimen was arbitrarily chosen to illustrate the results of the repeatability investigation; however, it should be noted that all other specimens were analysed in the same manner. This specimen neither represents the best or worst case repeatability measurements observed in this study; however, the majority of repeatability investigations performed yielded maximum average AMCL tension standard deviations less than that observed for this example.) The curves correspond to the AMCL tension levels of the five consecutive cycles of elbow flexion. All five measurements were similar, hence indicating good repeatability of the buckle transducer; however, in particular, the curves corresponding to flexion cycles 2 through 5 were most equivalent –

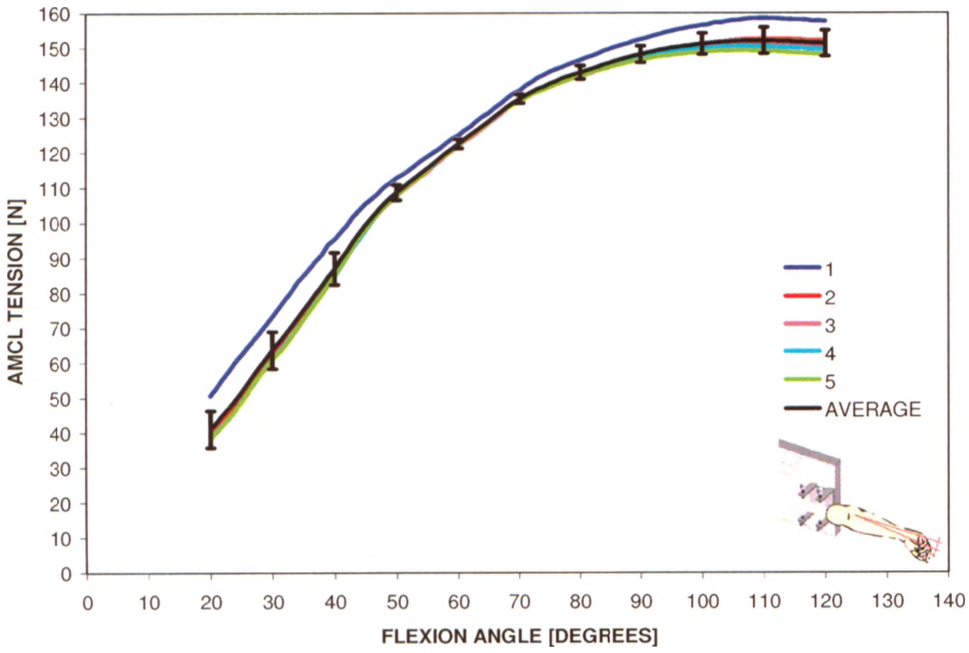

Figure 3.4: AMCL tension measurements of one specimen tested in active flexion in the valgus position for the repeatability investigation

Five consecutive AMCL tension measurements taken throughout the arc of elbow flexion are shown for one specimen (specimen 2). All five measurements were similar, hence indicating good repeatability of the buckle transducer. The average curve shows the standard deviations at every 10° of elbow flexion, which ranged from ±1.2 N to ±6.0 N throughout the arc of elbow flexion.

primarily within mid-range flexion. The net effect of all five AMCL tension measurements is shown by the average curve (± one standard deviation) (Figure 3.4).

The repeatability of the buckle transducer was quantified in terms of the standard deviations. The minimum and maximum magnitudes of standard deviations were approximately ±1.2 N and ±6.0 N, respectively. Expressing the standard deviations as a percentage of the mean AMCL tensions, the minimum and maximum standard deviations as percentages were approximately ± 0.9% (or ±1.2 N / 135.3 N) and ± 13.0% (or ±5.3 N / 41.1 N), respectively. Appendix 7 contains some additional discussion points regarding the repeatability data.

3.3.2 Valgus Position: Active and Passive Elbow Flexion

3.3.2.1 *AMCL Tension*

Figure 3.5 shows the variation of mean AMCL tension with flexion angle for both active and passive flexion in the valgus position (n = 5).

Both the active and passive curves showed an increase in AMCL tension with increasing angles of elbow flexion ($p = 0.05$, for both active and passive motion). For each incremental increase in the flexion angle, the corresponding increase in AMCL tension decreased (*i.e.* the slopes of the curves decreased throughout the range of motion). Both curves showed a greater AMCL tension level at full flexion compared to at full extension. Passive tensions tended to be greater than active tensions at all degrees of elbow flexion; the largest difference between passive and active AMCL tensions was approximately 11.5 N, which occurred at 22° of elbow flexion. There was no statistical difference in the AMCL tension levels between active and passive elbow flexion ($p = 0.2$). For full details refer to Appendix 7.

3.3.2.2 *Kinematics – Valgus Angulation*

Figure 3.6 shows the variation of mean valgus angulation with flexion angle for both active and passive flexion in the valgus position (n = 5).

Both the active and passive curves showed a valgus to varus trend from full extension to mid-range flexion, and thereafter, an approximately constant valgus angulation with increasing angles of flexion; however, there was no statistical difference

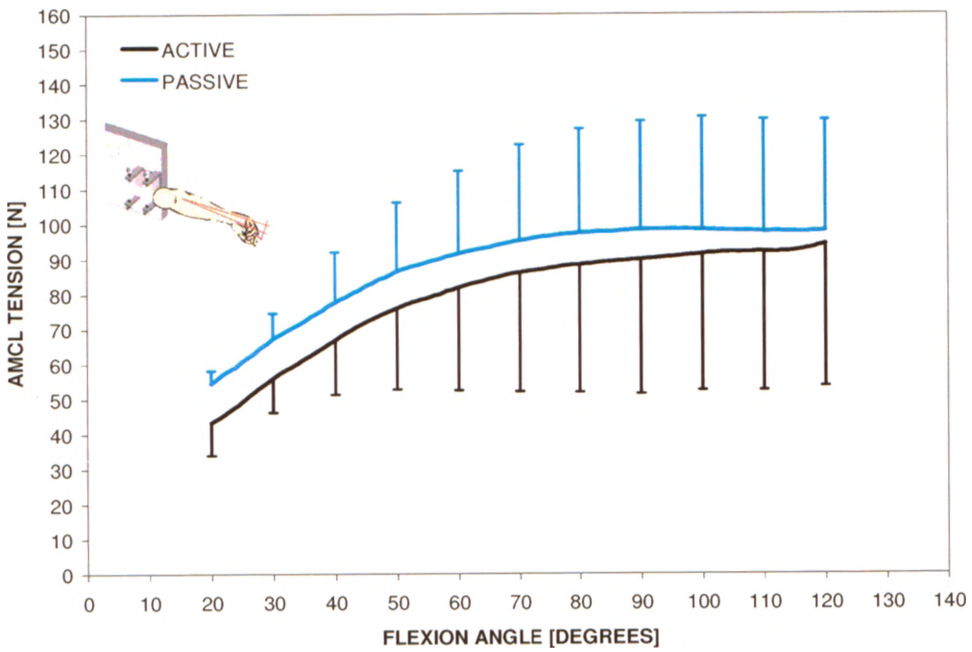

Figure 3.5: Variation of mean AMCL tension with flexion angle for active and passive flexion in the valgus position for the native AMCL

Mean AMCL tension levels throughout the arc of elbow flexion are shown for both active and passive motion (n = 5). Both the active and passive curves showed an increase in AMCL tension with increasing angles of elbow flexion (p = 0.05, for both active and passive motion). There was no statistical difference in the AMCL tension levels between active and passive elbow flexion (p = 0.2). Standard deviations at every 10° of elbow flexion are shown, which ranged from ±8.7 N to ±40.5 N throughout the arc of elbow flexion for the average active curve, and from ±3.4 N to ±32.2 N throughout the arc of elbow flexion for the average passive curve.

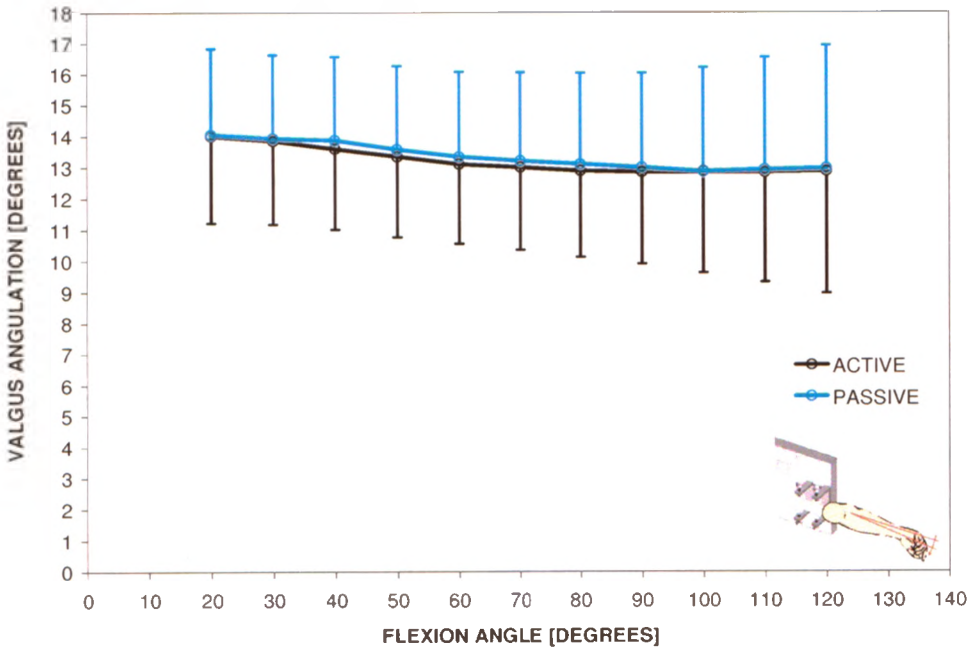

Figure 3.6: Mean elbow kinematic pathways for active and passive flexion in the valgus position for the native AMCL

Mean valgus angulation of the ulna relative to the humerus at every 10° of elbow flexion is shown for active and passive motion (n = 5). There was no statistical difference in elbow kinematics between active and passive elbow flexion (p = 0.4). Standard deviations at every 10° of elbow flexion are shown, which ranged from ±2.5° to ±3.9° for the average active curve, and from ±2.7° to ±4.0° for the average passive curve.

in the valgus angulations between flexion angles for both active and passive motion ($p > 0.3$, for both active and passive motion). Both curves showed a slightly greater valgus angulation at full extension compared to at full flexion. The largest difference between passive and active valgus angulations was approximately 0.3°, which occurred at 40° of elbow flexion. Passive and active elbow kinematics were not statistically different ($p = 0.4$). For full details refer to Appendix 7.

3.3.3 Dependent Position: Active and Passive Elbow Flexion

3.3.3.1 *AMCL Tension*

Figure 3.7 shows the variation of mean AMCL tension with flexion angle for both active and passive flexion in the dependent position ($n = 4$).

Both the active and passive curves showed a gradual increase in AMCL tension with increasing angles of elbow flexion; the slopes of the curves gradually increased throughout the range of motion. There was no statistical difference in the AMCL tension levels between flexion angles for both active and passive motion ($p = 0.06$ and $p = 0.08$, respectively). Both curves showed a greater AMCL tension level at full flexion compared to at full extension. Active and passive tensions were similar within approximately 50° and 110° of elbow flexion, and at both extremes of the range of motion, active tensions were slightly greater; the largest difference between passive and active AMCL tensions was approximately 5.4 N, which occurred at 120° of elbow flexion. There was no statistical difference in the AMCL tension levels between active and passive elbow flexion ($p = 0.7$). For full details refer to Appendix 7.

3.3.3.2 *Kinematics – Valgus Angulation*

Figure 3.8 shows the variation of mean valgus angulation with flexion angle for both active and passive flexion in the dependent position ($n = 4$).

The active and passive motion pathways varied; the active motion pathway had a valgus to varus slope, and the passive motion pathway had a varus to valgus slope. Valgus angulation was greater at full extension than at full flexion for the active curve, whereas valgus angulation was greater at full flexion than at full extension for the passive curve; however, there was no statistical difference in the valgus angulations between

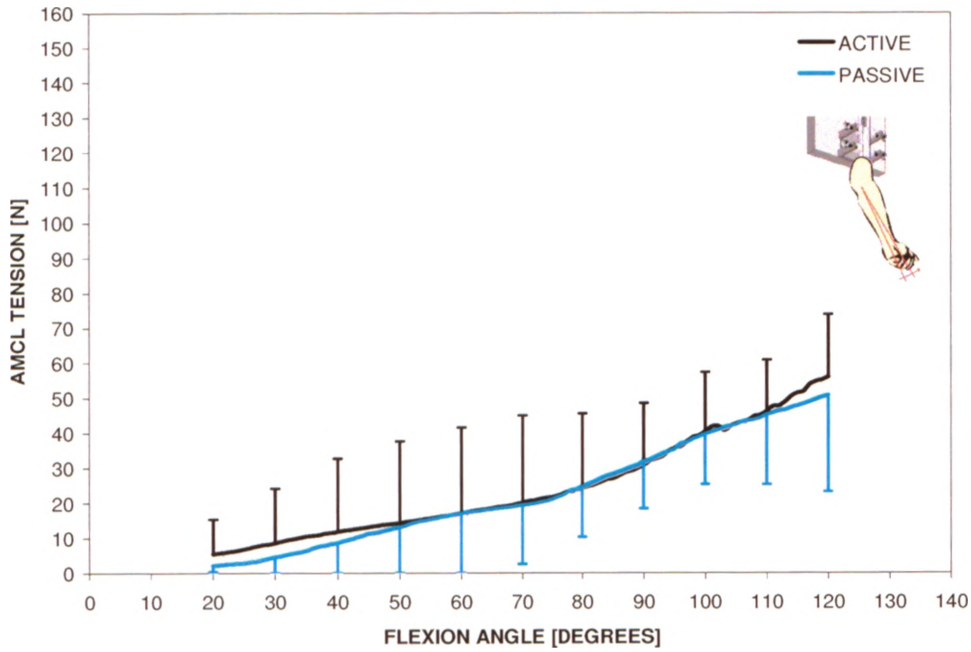

Figure 3.7: Variation of mean AMCL tension with flexion angle for active and passive flexion in the dependent position for the native AMCL

Mean AMCL tension levels throughout the arc of elbow flexion are shown for both active and passive motion (n = 4). Both the active and passive curves showed a gradual increase in AMCL tension with increasing angles of elbow flexion; however, there was no significant difference in the AMCL tension levels between flexion angles for both active and passive motion ($p = 0.06$ and $p = 0.08$, respectively). There was no statistical difference in the AMCL tension levels between active and passive elbow flexion ($p = 0.7$). Standard deviations at every 10° of elbow flexion are shown, which ranged from ±10.0 N to ±25.3 N throughout the arc of elbow flexion for the average active curve, and from ±1.7 N to ±27.5 N throughout the arc of elbow flexion for the average passive curve.

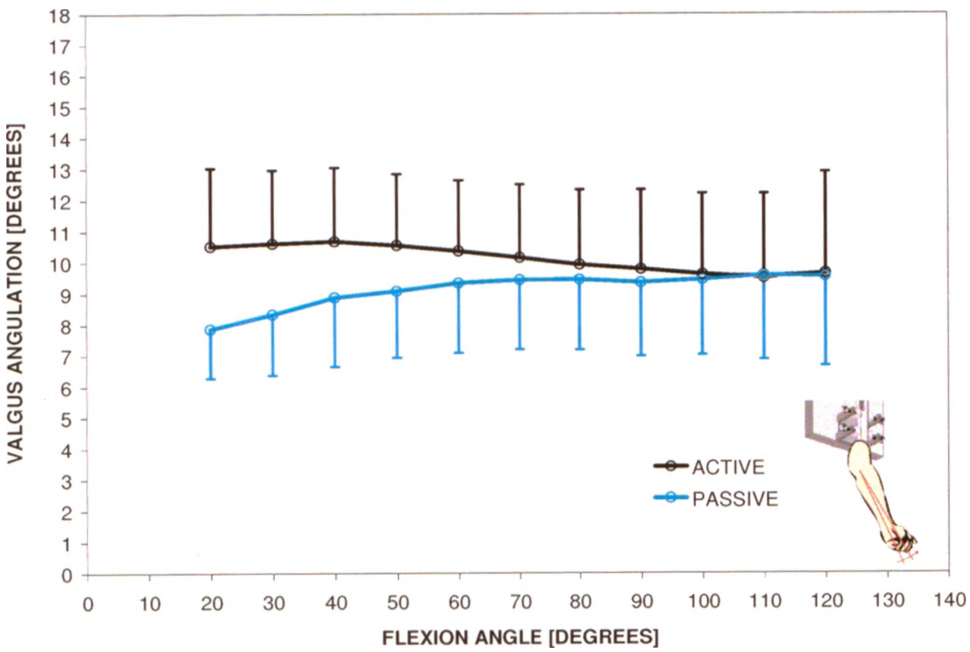

Figure 3.8: Mean elbow kinematic pathways for active and passive flexion in the dependent position for the native AMCL

Mean valgus angulation of the ulna relative to the humerus at every 10° of elbow flexion is shown for active and passive motion (n = 4). There was a statistical difference in elbow kinematics between active and passive elbow flexion ($p = 0.03$). Standard deviations at every 10° of elbow flexion are shown, which ranged from ±2.3° to ±3.2° for the average active curve, and from ±1.6° to ±2.9° for the average passive curve.

flexion angles for both active and passive motion ($p = 0.4$ and $p = 0.06$, respectively). The passive motion pathway tracked in greater varus than the active motion pathway (more prominently at full extension); however, the two curves converged at approximately 110° of elbow flexion. For flexion angles greater than 110°, the passive and active motion pathways effectively coincided. The largest difference between passive and active valgus angulations was approximately 2.7°, which occurred at 20° of elbow flexion. There was a statistical difference in elbow kinematics between active and passive elbow flexion ($p = 0.03$). For full details refer to Appendix 7.

3.3.4 Comparison of Forearm Mass and AMCL Tension

Given the differences in AMCL tension between the specimens, it was of interest to investigate whether arm mass was a factor that affected the magnitudes of AMCL tension. The behaviour at 60° of elbow flexion is presented here.

3.3.4.1 *Valgus Position*

Figure 3.9 shows a plot of AMCL tension (at 60° of elbow flexion) versus forearm mass, for specimens 2 through 5, for both active and passive flexion in the valgus position. For both active and passive flexion, increasing forearm mass corresponded to increasing AMCL tension levels (R^2 values were 0.96 and 0.88 for active and passive flexion, respectively). For full details refer to Appendix 7.

3.3.4.2 *Dependent Position*

Figure 3.10 shows a plot of AMCL tension (at 60° of elbow flexion) versus forearm mass, for specimens 2, 3, and 5, for both active and passive flexion in the dependent position. For both active and passive flexion, no correlation between forearm mass and AMCL tension was observed (R^2 values were 0.02 and 0.00 for active and passive flexion, respectively). For full details refer to Appendix 7.

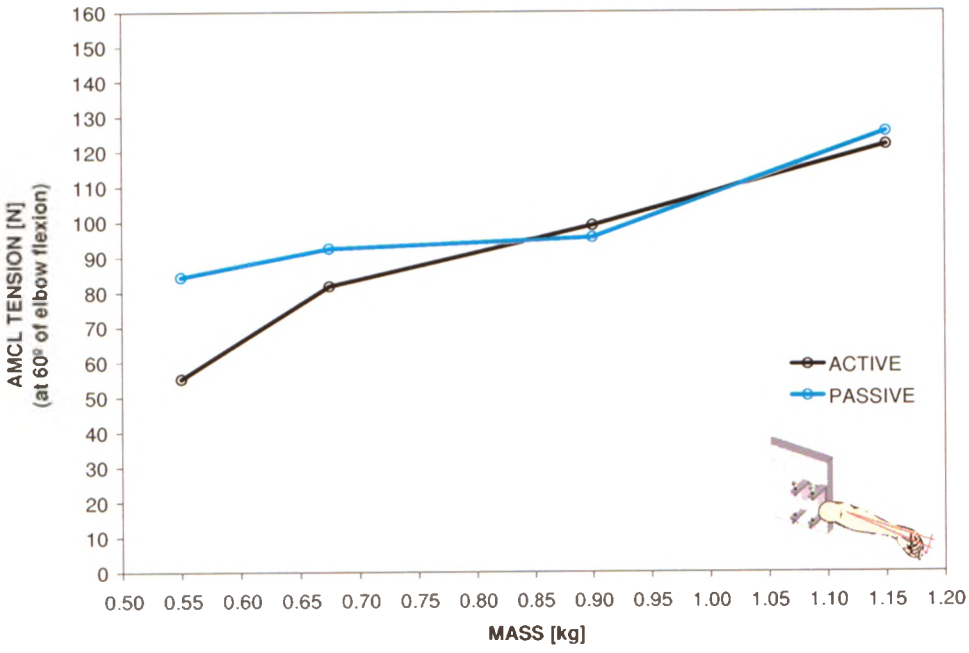

Figure 3.9: AMCL tension (at 60° of elbow flexion) plotted against forearm mass for four specimens tested in active and passive flexion in the valgus position for the native AMCL

For both active and passive flexion, increasing specimen mass corresponded to increasing AMCL tension levels.

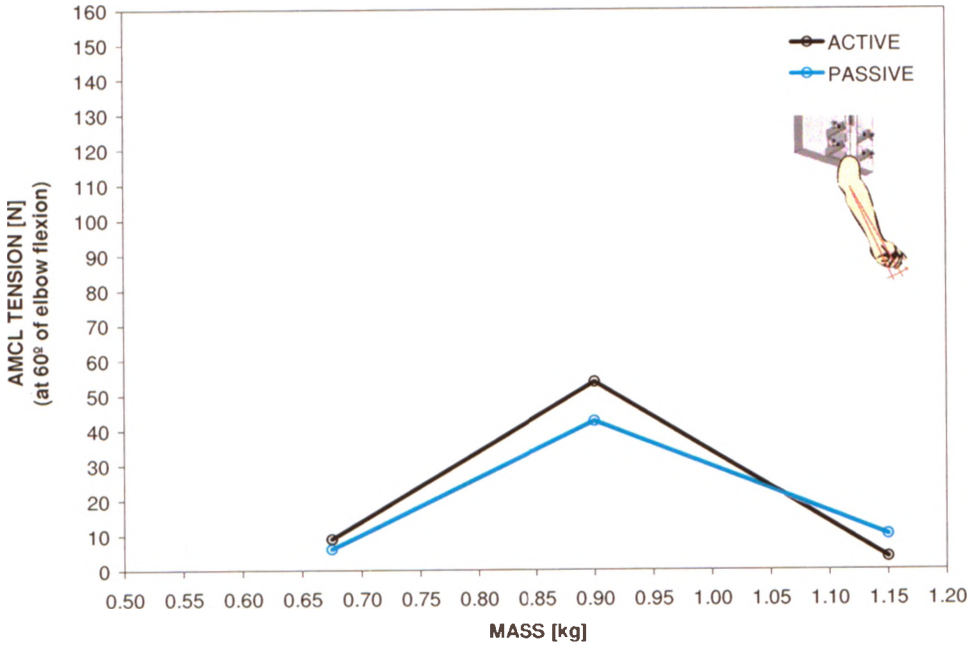

Figure 3.10: AMCL tension (at 60° of elbow flexion) plotted against forearm mass for three specimens tested in active and passive flexion in the dependent position for the native AMCL

For both active and passive flexion, no correlation between specimen mass and AMCL tension was observed.

3.4 DISCUSSION

3.4.1 Repeatability

The results of the repeatability investigation indicated good repeatability of the buckle transducer, as the standard deviations were small both in terms of magnitude, and when expressed as percentages of the mean AMCL tensions. The latter flexion cycles were most equivalent; therefore, the AMCL tension and elbow kinematic data from the third flexion cycle were used for analysis in all subsequent investigations.

3.4.2 Valgus Angulation and AMCL Tension Correlation

It was anticipated that the passive motion pathways would track in greater valgus than their respective active motion pathways at all degrees of elbow flexion, since the dynamic stabilizers (*i.e.* muscular stabilizers) are not activated during passive simulated flexion; muscle activity is thought to stabilize the joint by compressing the articular surfaces together.[19-21] Furthermore, as a result of this greater valgus angulation with passive simulated flexion, it was anticipated that passive AMCL tension levels would be greater than their respective active AMCL tension levels at all degrees of elbow flexion. This valgus angulation – AMCL tension trend was observed when comparing the average active and passive motion pathways and the average active and passive AMCL tension levels in the valgus position (Figure 3.6 and Figure 3.5, respectively).

Although the average curves for the valgus position showed this trend, it was not consistently observed for each specimen tested in the valgus position, nor was it observed for the dependent position. One explanation may be that the investigator may have applied additional forces and moments to the elbow while guiding the forearm through the arc of flexion during passive simulated motion. To elaborate, these additional forces and moments may have forced the forearm in greater valgus or varus either throughout the arc of flexion or within particular regions of elbow flexion, and/or may have altered the loads experienced by the tissue, which would have altered the kinematics and/or the AMCL tension levels. This variability in elbow kinematics with passive motion has previously been reported by Johnson et al.[22] and Dunning et al.[14].

A second explanation for the variability in the anticipated valgus angulation – AMCL tension relationship would be a change in the orientation of the buckle transducer

either *between* consecutive active and passive flexion cycles or *during* a flexion cycle. An example of this would be if the investigator's error was eliminated, but passive AMCL tension levels were less than or equal to the respective active AMCL tension levels. Tension levels that are different *throughout* the arc of flexion or *within* a particular region of elbow flexion may indicate a change in the orientation of the transducer *between* consecutive active and passive flexion cycles or *within* a flexion cycle, respectively. A change in the transducer's orientation may cause the transducer to experience less force from the ligament than it would in its optimal orientation, thereby altering the observed AMCL tension levels and/or trend.

3.4.3 Comparison with Previous Biomechanical Studies

Human tendon and ligament forces of the upper extremity have not, to our knowledge, been studied to date. Previous sectioning studies have demonstrated that the AMCL is the primary restraint to valgus loads and that the radial head is a secondary stabilizer.[1-10] For all test conditions, AMCL tension levels were observed to increase with elbow flexion, indicating that other structures (such as the joint capsule and the shape of the articulation) are likely more responsible for joint stability near full extension, and that the AMCL is recruited at increased angles of elbow flexion.[23] This finding is consistent with previously reported data by Morrey et al.[2], who reported that valgus stability was observed to be equally divided among the MCL, anterior joint capsule, and joint articulation (31%, 38%, and 31%, respectively) when the elbow was extended; whereas, at 90° of elbow flexion, the MCL, anterior joint capsule, and joint articulation were found to resist approximately 54%, 10%, and 33% of valgus stress, respectively. Furthermore, our findings are consistent with previously reported data by Pribyl et al.[23] and Lin et al.[24], who reported that strain in the AMCL increased with elbow flexion. Additionally, Lin et al.[24] found that from approximately 20° to 75°-80° of elbow flexion, the AMCL showed an almost linear strain response, and after about 80° of elbow flexion, less AMCL lengthening was observed as the elbow was flexed further. Furthermore, Callaway et al.[6] found that the AMCL tensed less after 90° of elbow flexion. These data are consistent with our findings for the valgus position, as both active and passive average curves showed an increase in the AMCL tension with increasing angles of elbow flexion;

however, for each incremental increase in flexion angle, the corresponding increase in AMCL tension decreased (*i.e.* the slopes of these curves decreased throughout the range of motion). In contrast, both active and passive average curves for the dependent position showed a gradual increase in the AMCL tension with increasing angles of elbow flexion; the slopes of these curves gradually increased throughout the range of motion. Furthermore, when comparing the elbow kinematics and AMCL tension levels in the valgus position with those of the dependent position, greater valgus angulations and AMCL tension levels were observed in the valgus position. It should be noted that Pribyl et al.[23] and Lin et al.[24] only investigated AMCL strain in the valgus gravity-loaded position and the horizontal position, respectively.

Pribyl et al.[23] observed the maximum AMCL strain to be 30%, which occurred at 130° of elbow flexion. Comparatively, our study found, for both the valgus and dependent positions, greater AMCL tension levels at full flexion compared to at full extension. Similar to Pribyl et al.[23], Regan et al.[4] found the maximum AMCL strain to be 25%, which occurred at the AMCL (bone-ligament-bone preparation) failure load of 261 N. This reported AMCL load to failure was roughly 100 N greater than the maximum AMCL tension level observed in our study, which was approximately 160 N. Conversely, our preliminary AMCL maximum tension calculation was approximately 110 N (see free body diagram analysis, Figure A5.1, in Appendix 5). Furthermore, Armstrong et al.[25] reported a mean peak load to failure of 142.5 ± 39.4 N for the isolated MCL, which is also less than the maximum AMCL load measured in this study. Failure of the AMCL was not observed in the current study, which may be due to differences in specimen size, age, or the method of load application.

Additionally, it has been reported that the MCL is able to withstand a maximum torque of 32 Nm[26]; however, baseball pitchers could experience up to 120 Nm of elbow valgus torque during the pitching motion[27]. Since it is clear that the MCL is not strong enough to withstand this torque by itself, it is believed that the overlying flexor-pronator muscles, which originate on the medial epicondyle, may help to minimize the stress experienced by the MCL by generating varus motion (*i.e.* compressing the joint medially) upon activation.[19,21,24,27-30]

With regard to AMCL isometry, Armstrong et al.[31] reported that true isometric fibres do not exist within the AMCL; they showed that for passive supinated flexion, the smallest mean AMCL length change throughout the arc of elbow flexion was 2.8 ± 1.2 mm (range: 0.7 mm to 5.2 mm). Similarly, Morrey and An[1] showed that the distance between the origin and insertion of the AMCL increased a mean of 4.8 mm from extension to 120° of elbow flexion. Although this study was not designed to investigate AMCL isometry, our findings (*i.e.* increasing AMCL tension levels with elbow flexion) support these previous reports that suggest that the length of the AMCL increases with elbow flexion.

This is the first study that we are aware of that has quantified loads in the AMCL of the elbow. It is interesting to compare this data to loads quantified for soft tissue structures of the lower extremity using similar techniques. Komi et al.[32] reported that the maximum human Achilles tendon force (measured using a buckle transducer) was attained when the subject ran at a speed of 6 ms^{-1} using the ball foot contact technique (*i.e.* ball running), in which case the value was 9 kN, corresponding to 12.5 times the body weight and much larger than the loads measured in the AMCL of the elbow. Griffith et al.[33] used buckle transducers to measure the forces in the posterior oblique ligament and the superficial medial collateral ligament of the knee to applied loads. They reported magnitudes of ligament force similar to those observed in this study; force measurements ranged from approximately 5.4 ± 2.2 N to 103.5 ± 7.9 N. Although these studies suggest wide ranging differences relative to the AMCL of the elbow, it is reasonable to conclude that relative to other joints, elbow ligament loads are not insignificant.

Although the influence of forearm rotation (*i.e.* pronation/supination) was not investigated in this study, Pribyl et al.[23] found that forearm position minimally affected strain in the AMCL. Therefore, the AMCL tension levels quantified in this study with the forearm in neutral rotation may represent the tension levels that would be observed with the forearm in pronation or supination. Furthermore, the observed AMCL tension levels may be an underestimate of the physiological loads experienced by this tissue in younger, larger, or more muscular arms, as it has been shown that the strength of ligaments decreases with age.[34]

AMCL tension levels were observed to increase with increasing specimen mass, for the arms in the valgus position. This correlation was more evident in the valgus position than the dependent position as the AMCL is the primary structure supporting the load of the forearm in the valgus position (*i.e.* it is the primary structure resisting the valgus moment due to the effects of gravity). Conversely, in the dependent position, both the medial and lateral soft tissue structures contribute to supporting the load of the forearm; therefore, as the load of the forearm is supported by both structures, this correlation was less evident in the dependent position.

There are some inherent limitations of buckle transducers in general. For example, installation of the buckle transducer causes some ligament deformation and shortening to occur, potentially altering the distribution of loads in the tissue.[35] During movement, buckle transducers can potentially impinge on bone or be compressed by surrounding soft tissues, thereby producing a false output.[35] In the current study, tissue shortening and impingement with bone was minimized by using a transducer custom designed for the AMCL. While only five specimens were studied, due to the consistent nature of the AMCL tension trends, these data are felt to be representative.

In summary, this *in vitro* cadaveric study demonstrated that tension in the AMCL increases with elbow flexion, and tension levels are greater when the arm is oriented in the valgus position relative to the dependent position; both of these observations are consistent with our hypotheses. Furthermore, for the valgus position, AMCL tension levels were observed to increase with increasing forearm mass. Of particular importance is our new understanding of the magnitudes of AMCL tension through the arc of elbow flexion, as this has important implications with respect to the desired target strength of repair and reconstruction techniques.

3.5 REFERENCE LIST

1. Morrey BF, An KN. Functional anatomy of the ligaments of the elbow. Clin.Orthop.Relat Res. 1985;84-90.

2. Morrey BF, An KN. Articular and ligamentous contributions to the stability of the elbow joint. Am.J.Sports Med. 1983;11:315-9.

3. Morrey BF, Tanaka S, An KN. Valgus stability of the elbow. A definition of primary and secondary constraints. Clin.Orthop.Relat Res. 1991;187-95.

4. Regan WD, Korinek SL, Morrey BF, An KN. Biomechanical study of ligaments around the elbow joint. Clin.Orthop.Relat Res. 1991;170-9.

5. Hotchkiss RN, Weiland AJ. Valgus stability of the elbow. J.Orthop.Res. 1987;5:372-7.

6. Callaway GH, Field LD, Deng XH et al. Biomechanical evaluation of the medial collateral ligament of the elbow. J.Bone Joint Surg.Am. 1997;79:1223-31.

7. Floris S, Olsen BS, Dalstra M, Sojbjerg JO, Sneppen O. The medial collateral ligament of the elbow joint: anatomy and kinematics. J.Shoulder.Elbow.Surg. 1998;7:345-51.

8. Sojbjerg JO, Ovesen J, Nielsen S. Experimental elbow instability after transection of the medial collateral ligament. Clin.Orthop.Relat Res. 1987;186-90.

9. Schwab GH, Bennett JB, Woods GW, Tullos HS. Biomechanics of elbow instability: the role of the medial collateral ligament. Clin.Orthop.Relat Res. 1980;42-52.

10. Fuss FK. The ulnar collateral ligament of the human elbow joint. Anatomy, function and biomechanics. J.Anat. 1991;175:203-12.

11. Armstrong AD, Dunning CE, Faber KJ, Duck TR, Johnson JA, King GJ. Rehabilitation of the medial collateral ligament-deficient elbow: an in vitro biomechanical study. J.Hand Surg.[Am.] 2000;25:1051-7.

12. Funk DA, An KN, Morrey BF, Daube JR. Electromyographic analysis of muscles across the elbow joint. J.Orthop.Res. 1987;5:529-38.

13. Amis AA, Dowson D, Wright V. Muscle strengths and musculo-skeletal geometry of the upper limb. Engineering in Medicine 1979;8:41-8.

14. Dunning CE, Duck TR, King GJ, Johnson JA. Simulated active control produces repeatable motion pathways of the elbow in an in vitro testing system. J.Biomech. 2001;34:1039-48.

15. Dunning CE, Zarzour ZD, Patterson SD, Johnson JA, King GJ. Ligamentous stabilizers against posterolateral rotatory instability of the elbow. J.Bone Joint Surg.Am. 2001;83-A:1823-8.

16. Milne AD, Chess DG, Johnson JA, King GJ. Accuracy of an electromagnetic tracking device: a study of the optimal range and metal interference. J.Biomech. 1996;29:791-3.

17. Dunning CE, Gordon KD, King GJ, Johnson JA. Development of a motion-controlled in vitro elbow testing system. J.Orthop.Res. 2003;21:405-11.

18. King GJ, Zarzour ZD, Rath DA, Dunning CE, Patterson SD, Johnson JA. Metallic radial head arthroplasty improves valgus stability of the elbow. Clin.Orthop.Relat Res. 1999;114-25.

19. An KN, Hui FC, Morrey BF, Linscheid RL, Chao EY. Muscles across the elbow joint: a biomechanical analysis. J.Biomech. 1981;14:659-69.

20. Alcid JG, Ahmad CS, Lee TQ. Elbow anatomy and structural biomechanics. Clin.Sports Med. 2004;23:503-17, vii.

21. Seiber K, Gupta R, McGarry MH, Safran MR, Lee TQ. The role of the elbow musculature, forearm rotation, and elbow flexion in elbow stability: an in vitro study. J.Shoulder.Elbow.Surg. 2009;18:260-8.

22. Johnson JA, Rath DA, Dunning CE, Roth SE, King GJ. Simulation of elbow and forearm motion in vitro using a load controlled testing apparatus. J.Biomech. 2000;33:635-9.

23. Pribyl CR, Hurley DK, Wascher DC, McNally TP, Firoozbakhsh K, Weiser MW. Elbow ligament strain under valgus load: a biomechanical study. Orthopedics 1999;22:607-12.

24. Lin F, Kohli N, Perlmutter S, Lim D, Nuber GW, Makhsous M. Muscle contribution to elbow joint valgus stability. J.Shoulder.Elbow.Surg. 2007;16:795-802.

25. Armstrong AD, Dunning CE, Ferreira LM, Faber KJ, Johnson JA, King GJ. A biomechanical comparison of four reconstruction techniques for the medial collateral ligament-deficient elbow. J.Shoulder.Elbow.Surg. 2005;14:207-15.

26. Dillman, C. J., Smutz, P, and Werner, S. Valgus extension overload in baseball pitching. Med Sci Sports Exerc 23(4), 135. 1991.

27. Werner SL, Fleisig GS, Dillman CJ, Andrews JR. Biomechanics of the elbow during baseball pitching. J.Orthop.Sports Phys.Ther. 1993;17:274-8.

28. Park MC, Ahmad CS. Dynamic contributions of the flexor-pronator mass to elbow valgus stability. J.Bone Joint Surg.Am. 2004;86-A:2268-74.

29. DiGiovine NM, Jobe FW, Pink M, Perry J. An electromyographic analysis of the upper extremity in pitching. J.Shoulder.Elbow.Surg. 1992;1:15-25.

30. Davidson PA, Pink M, Perry J, Jobe FW. Functional anatomy of the flexor pronator muscle group in relation to the medial collateral ligament of the elbow. Am.J.Sports Med. 1995;23:245-50.

31. Armstrong AD, Ferreira LM, Dunning CE, Johnson JA, King GJ. The medial collateral ligament of the elbow is not isometric: an in vitro biomechanical study. Am.J.Sports Med. 2004;32:85-90.

32. Komi PV. Relevance of in vivo force measurements to human biomechanics. J.Biomech. 1990;23 Suppl 1:23-34.

33. Griffith CJ, Wijdicks CA, LaPrade RF, Armitage BM, Johansen S, Engebretsen L. Force measurements on the posterior oblique ligament and superficial medial collateral ligament proximal and distal divisions to applied loads. Am.J.Sports Med. 2009;37:140-8.

34. Woo SL, Hollis JM, Adams DJ, Lyon RM, Takai S. Tensile properties of the human femur-anterior cruciate ligament-tibia complex. The effects of specimen age and orientation. Am.J.Sports Med. 1991;19:217-25.

35. Ravary B, Pourcelot P, Bortolussi C, Konieczka S, Crevier-Denoix N. Strain and force transducers used in human and veterinary tendon and ligament biomechanical studies. Clin.Biomech.(Bristol., Avon.) 2004;19:433-47.

CHAPTER 4

Effect of Wrist Flexor Muscle Loading on Medial Collateral Ligament Tension in the Elbow

Overview: This chapter details an *in vitro* cadaveric study examining the effect of wrist flexor muscle loading on the magnitude of medial collateral ligament tension in the elbow. Ligament tension was quantified using the custom designed E-form frame buckle transducer described in Chapter 2. Ligament tension and joint kinematics, for both active and passive elbow flexion in the valgus and dependent positions, are presented and analysed.

4.1 INTRODUCTION

Medial collateral ligament (MCL) injuries commonly occur as a result of chronic overuse in high demand athletes such as baseball pitchers, and occasionally in javelin throwers and tennis players.[1-15] The medial aspect of the elbow joint experiences a large valgus stress during the late cocking and early acceleration phases of the pitching motion.[1,2,8-10,12,13,16] These forces may exceed the tensile strength of the ligament and produce microtears within the tissue.[2,8-10,15] Continued throwing can lead to attenuation or rupture of the weakened ligament.[1,2,4-6,8-10,13,15] Surgical reconstruction is often required to restore MCL function.[4,6,8-11,14] MCL insufficiency may also occur as a result of acute disruptions from elbow trauma such as dislocations[14,17] and fracture-dislocations[18]. For acute disruption of the MCL, healing usually occurs with non-operative management; however, persistent instability can occur and may require surgical management.[17,18]

Static or passive stability of the elbow joint is provided by the intrinsic constraint of the articulation, the ligaments, and the joint capsule. Active or dynamic stability is

provided by the muscles that cross the elbow joint. The anterior bundle of the MCL (AMCL) and the radial head have been shown to be the primary and secondary valgus stabilizers of the elbow joint, respectively.[19-28] However, little is known about the contributions of dynamic restraints in maintaining valgus stability of the elbow joint.[2,14] The medial elbow musculature, specifically the flexor-pronator muscles, are ideally suited to be important medial stabilizers of the elbow due to their origin on the medial epicondyle of the humerus, and line-of-action which follows a course similar to the MCL.[29] The flexor carpi ulnaris and flexor carpi radialis, two of the flexor-pronator muscles which flex the wrist, have been shown to have increased muscle-firing patterns during the pitching motion and thus have been postulated to dynamically protect the MCL from loading.[16,30] It remains unknown whether increased tension in the wrist flexor (WF) muscles affects the loading borne by the AMCL.

Hence, the purpose of this *in vitro* study was to determine the effect of WF muscle loading on the magnitude of AMCL tension through the arc of elbow flexion. We hypothesized that tension in the AMCL would decrease with increased WF muscle loads.

4.2 MATERIALS AND METHODS

4.2.1 Specimen Preparation and Custom Motion Simulator*

Four fresh-frozen cadaveric upper extremities (mean age 73 ± 11 years; range: 62-82 years; 3 female; 1 right specimen) were prepared for testing as previously described. To simulate active muscle loading, a stainless steel cable (0.8 mm diameter) was affixed to the distal tendon of the brachialis, the biceps brachii, and the triceps brachii using 200 lb braided Dacron® (Woodstock Line Co., Putnam, CT) and to the brachioradialis using a #5 Ethibond suture (Johnson & Johnson, Ethicon Inc., Peterborough, ON). The WF muscles, flexor carpi ulnaris (FCU) and flexor carpi radialis (FCR), were cut just proximal to the extensor retinaculum and sutured together with a #5 Ethibond suture, to which a stainless steel cable was sutured for loading. The origin of the brachioradialis was simulated using a (Delrin®) pulley inserted into the proximal portion of the lateral supracondylar ridge to ensure replication of the muscle's moment arm throughout elbow

* The experimental techniques related to specimen preparation, transducer implantation, simulation trials, and kinematic measurements are identical to those described in Chapter 3, and hence are provided here for completion, but in an abbreviated fashion.

motion.[31] Similarly, the line-of-action of the WF muscles was simulated by passing the cable through a (Delrin®) sleeve implanted at their origin on the medial epicondyle. The lines-of-action of the elbow flexor and extensor muscles were maintained using a tendon alignment unit within the humeral clamp of the testing apparatus (Figure 3.1).

The wrist was maintained in neutral flexion/extension via a 5 mm Steinman Pin drilled through the long finger metacarpal, the carpus, and the distal radius. A 3.5 mm tap (Synthes Ltd., Mississauga, ON) placed through the distal radius and ulna maintained the forearm in neutral rotation. All skin incisions were closed to keep the soft tissues moist during testing.

The humerus was mounted into the testing apparatus in neutral humeral rotation. Both the valgus gravity-loaded position and the dependent (*i.e.* vertical) position were simulated (Figure 3.2). With the specimen oriented in the valgus gravity-loaded position, the buckle transducer was inserted into the AMCL substance as previously described. Data from the buckle transducer were recorded in real time using LabVIEW 7.1 (National Instruments, Austin, TX). The specimen was kept moist using 0.9% normal saline solution throughout testing.

Active simulated flexion was achieved via computer-controlled pneumatic actuation (brachioradialis) and servomotor control (brachialis, biceps, and triceps). Relative loading among the muscles was derived in accordance with published measurements of quantitative electromyographic (EMG) activity[32] and physiological muscle cross-sectional area (pCSA)[33]. The ratio of muscle loading was determined from the product of the relative EMG activity and pCSA data, as previously validated by our laboratory.[34] Loading of the biceps, brachioradialis, and triceps were determined as a proportion of the load applied by the brachialis, the prime flexor of the elbow (*i.e.* the prime mover). The load applied to the brachialis tendon was such that a controlled rate of elbow flexion was maintained. The brachialis tendon moved at a constant flexion rate of 10 degrees per second, which was achieved by a proportional-integral-derivative control using feedback from the electromagnetic tracking system. The WF muscles were loaded using computer-controlled pneumatic actuators to 0, 10, 30, and 50 N, hence yielding four WF load conditions. Passive elbow flexion employed direct guidance by an investigator during which the WF muscles were loaded to 0, 10, 30, and 50 N.

Motion of the ulna relative to the humerus was measured in six-degrees-of-freedom using the electromagnetic tracking device (Flock of Birds; Ascension Technology, Burlington, VT). As the elbow moved through an arc of flexion, the position and orientation of a receiver attached to the distal ulna was recorded relative to a transmitter fixed to the base of the testing apparatus.[34] At the completion of testing, the elbow and wrist were disarticulated and anatomical landmarks on the humerus and ulna were digitized to create anatomic bone coordinate systems, as previously described.[35] This allowed the "ulnar receiver with respect to transmitter" data collected during testing to be converted to "ulna with respect to humerus" data using Euler Z-Y-X analyses during *post hoc* data analysis.[36] Hence, clinically relevant coordinate systems could be constructed. Outputted data from the tracking system were recorded in real time using custom software programmed using LabVIEW 7.1. The relative motion of the ulnar coordinate system relative to the humeral coordinate system was analysed using custom software (LabVIEW 7.1).

4.2.2 Testing Protocol

Testing was conducted with the arm oriented in the dependent and valgus positions, with the elbow under both passive and active motion. Each flexion trial was performed with the forearm in neutral rotation.

Prior to applying the WF loads, five flexion cycles were performed in all four test conditions (*i.e.* active/passive flexion in the dependent position and active/passive flexion in the valgus position). The AMCL tension and elbow kinematic data from the third flexion cycle of each test condition were taken to be the data for the WF 0 N load condition, similar to the protocol of Chapter 3. Once the AMCL tension and valgus angulation measurements for the WF 0 N load condition were obtained, WF loads of 10, 30, and 50 N were sequentially applied and testing was repeated at each load level. For each of these loads, three flexion cycles were performed in all four test conditions. Again, the AMCL tension and elbow kinematic data from the third flexion cycle of each test condition were analysed.

4.2.3 Data Analysis

All data were analysed using two-way repeated measures analysis of variance (ANOVA) with $\alpha = 0.05$, and *post hoc* paired *t*-tests using the Bonferroni correction for family-wise error. All data were statistically analysed using SPSS software (SPSS V16.0.1, Chicago, IL).

Data from all four specimens tested were analysed for the valgus position (mean age 73 ± 11 years; range: 62-82 years; 3 female; 1 right specimen); however, due to data acquisition difficulties, data from only three specimens were analysed for the dependent position (mean age 76 ± 10 years; range: 65-82 years; 2 female; 1 right specimen). For each test condition (*i.e.* active/passive flexion in the dependent position and active/passive flexion in the valgus position), a two-way repeated ANOVA was performed; the two independent variables used were *WF load condition* (*i.e.* no WF load, 10 N WF load, 30 N WF load, and 50 N WF load) and *flexion angle*. For each forearm orientation (*i.e.* dependent and valgus), a two-way repeated ANOVA was performed; the two independent variables used were *motion condition* (*i.e.* active motion and passive motion) and *flexion angle*.

During testing, two dependent variables were measured: (1) AMCL tension, which was the output of the buckle transducer; and (2) valgus angulation of the ulna with respect to the humerus. Valgus angulation was calculated, for both the dependent and valgus positions, by measuring the difference in the orientation of the ulna relative to the humerus via the custom software previously described (LabVIEW 7.1). AMCL tension and valgus angulation were measured throughout the arc of elbow flexion but are reported only at every 10° of elbow flexion from 20°-120° of elbow flexion to simplify data interpretation; hence, there were eleven levels of the independent variable *flexion angle*.

All kinematic data were analysed using custom software (LabVIEW 7.1), Microsoft Office Excel 2002 (Microsoft Corporation, Redmond, WA), and SPSS. All source tension data were filtered using a program written in Matlab (The MathWorks, Natick, MA), and analysed using Microsoft Office Excel 2002 and SPSS.

4.3 RESULTS

The four WF load conditions of the study were: (1) no WF load (WF – 0 N); (2) 10 N WF load (WF – 10 N); (3) 30 N WF load (WF – 30 N); and (4) 50 N WF load (WF – 50 N). The results for the four WF load conditions are presented for both active and passive elbow flexion in the valgus and dependent positions.

4.3.1 Valgus Position: Active Elbow Flexion

4.3.1.1 *AMCL Tension*

With the arm oriented in the valgus position and the elbow under active motion, AMCL tension decreased with increasing WF loads ($p < 0.0001$). All three levels of WF loading produced significantly lower levels of tension compared to that of the unloaded condition; p-values were 0.049, 0.03, and 0.002, for the WF – 10 N, the WF – 30 N, and the WF – 50 N conditions, respectively. (Figure 4.1).

4.3.1.2 *Kinematics – Valgus Angulation*

The elbows tracked in greater varus with increasing WF loads ($p = 0.01$). The motion pathways of the WF – 10 N, the WF – 30 N, and the WF – 50 N conditions were not statistically different from that of the unloaded condition (p-values were 0.09, 0.1, and 0.08, respectively). (Figure 4.2).

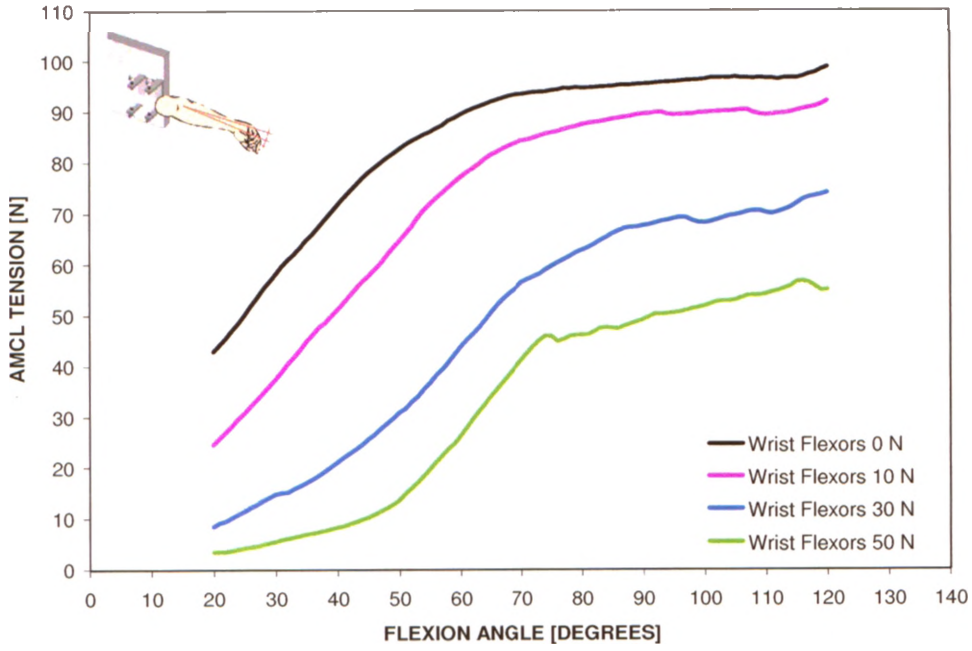

Figure 4.1: Variation of mean AMCL tension with flexion angle for active flexion in the valgus position for WF loading

Mean AMCL tension levels throughout the arc of elbow flexion are shown for the four WF load conditions (n = 4). AMCL tension decreased with increasing WF loads ($p < 0.0001$). All three levels of WF loading produced significantly lower levels of tension compared to that of the WF – 0 N condition; p-values were 0.049, 0.03, and 0.002, for the WF – 10 N, the WF – 30 N, and the WF – 50 N conditions, respectively. Standard deviations are omitted for clarity but ranged from ±3.4 N to ±57.9 N.

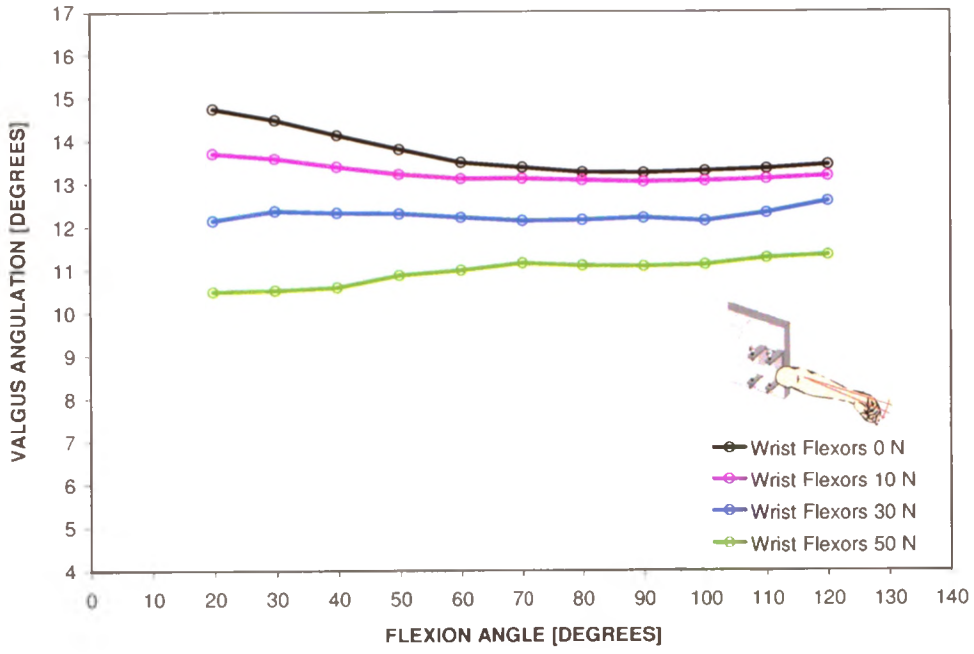

Figure 4.2: Mean elbow kinematic pathways for active flexion in the valgus position for WF loading

Mean valgus angulation of the ulna relative to the humerus at every 10° of elbow flexion is shown for the four WF load conditions (n = 4). The elbows tracked in greater varus with increasing WF loads (p = 0.01); however, there was no statistical difference in the motion pathways between the four WF load conditions. Standard deviations are omitted for clarity but ranged from ±2.2° to ±4.3°.

4.3.2 Valgus Position: Passive Elbow Flexion

4.3.2.1 *AMCL Tension*

With the arm oriented in the valgus position and the elbow under passive motion, AMCL tension decreased with increasing WF loads ($p = 0.003$). WF loading of 30 N and 50 N produced significantly lower levels of tension compared to that of the unloaded condition ($p = 0.047$ and $p < 0.0001$, respectively), whereas differences in AMCL tension levels between the WF – 10 N and the unloaded conditions were not significant ($p = 0.3$). (Figure 4.3).

4.3.2.2 *Kinematics – Valgus Angulation*

The elbows tracked in greater varus with increasing WF loads ($p = 0.02$). The motion pathways of the WF – 10 N, the WF – 30 N, and the WF – 50 N conditions were not statistically different from that of the unloaded condition (p-values were 0.7, 0.1, and 0.1, respectively). (Figure 4.4).

4.3.3 Valgus Position: Active versus Passive Elbow Flexion

For the valgus position, there were no statistical differences in the AMCL tension levels between active and passive motion for any of the WF load conditions ($p > 0.05$, for all WF load conditions). Furthermore, there were no statistical differences in the motion pathways between active and passive motion for any of the WF load conditions ($p > 0.05$, for all WF load conditions). For full details refer to Appendix 8.

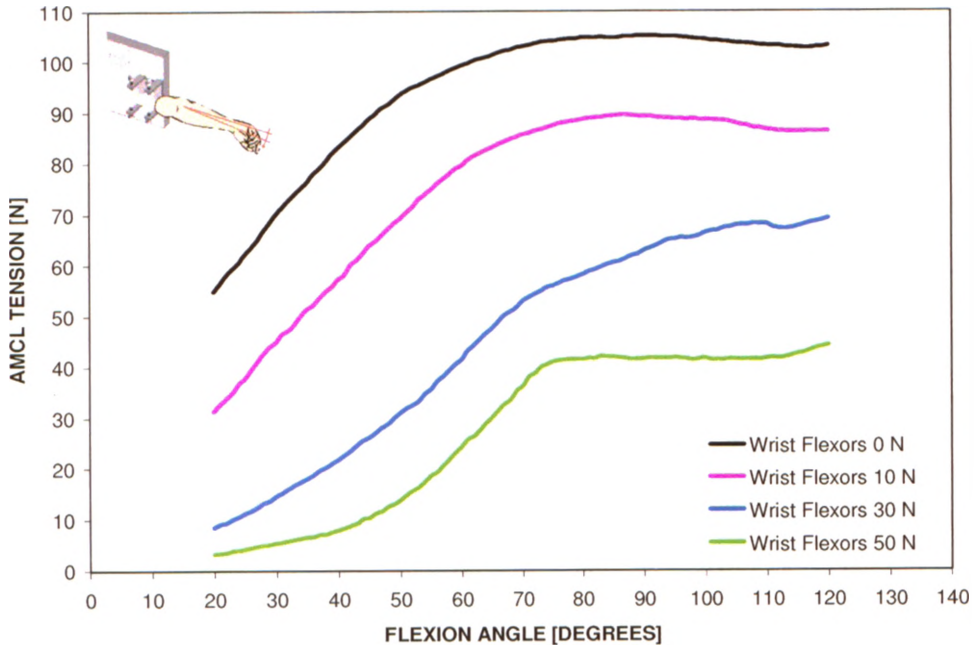

Figure 4.3: Variation of mean AMCL tension with flexion angle for passive flexion in the valgus position for WF loading

Mean AMCL tension levels throughout the arc of elbow flexion are shown for the four WF load conditions (n = 4). AMCL tension decreased with increasing WF loads ($p = 0.003$). WF loading of 30 N and 50 N produced significantly lower levels of tension compared to that of the WF – 0 N condition ($p = 0.047$ and $p < 0.0001$, respectively), whereas differences in AMCL tension levels between the WF – 10 N and the WF – 0 N conditions were not significant ($p = 0.3$). Standard deviations are omitted for clarity but ranged from ±2.6 N to ±56.8 N.

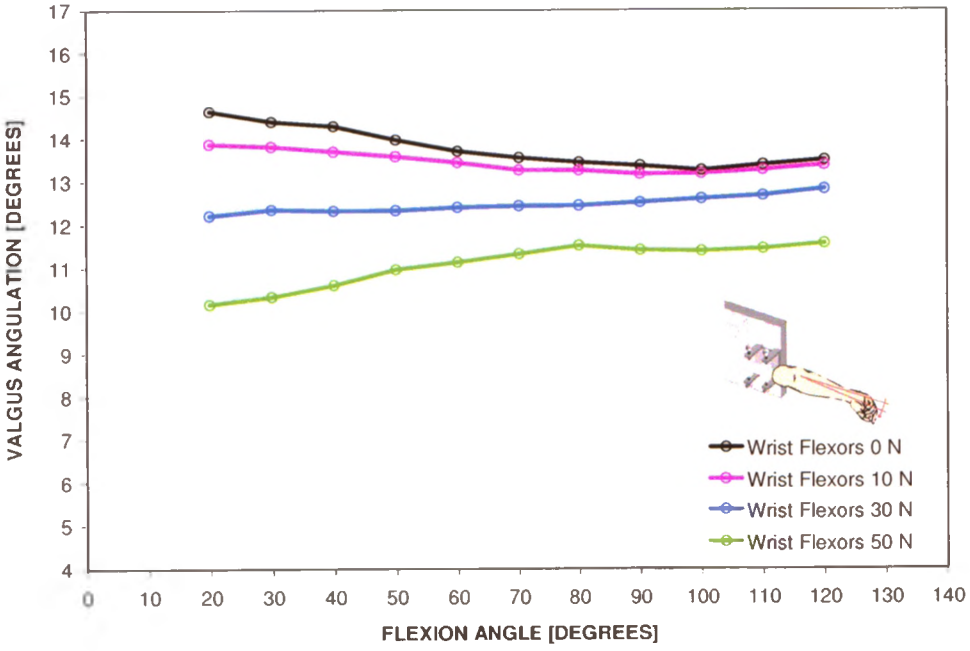

Figure 4.4: Mean elbow kinematic pathways for passive flexion in the valgus position for WF loading

Mean valgus angulation of the ulna relative to the humerus at every 10° of elbow flexion is shown for the four WF load conditions (n = 4). The elbows tracked in greater varus with increasing WF loads ($p = 0.02$); however, there was no statistical difference in the motion pathways between the four WF load conditions. Standard deviations are omitted for clarity but ranged from ±2.4° to ±4.5°.

4.3.4 Dependent Position: Active Elbow Flexion

4.3.4.1 *AMCL Tension*

With the arm oriented in the dependent position and the elbow under active motion, there was no significant effect of WF loading on AMCL tension, despite a trend of decreasing AMCL tension with increasing WF loads ($p = 0.2$). (Figure 4.5).

4.3.4.2 *Kinematics – Valgus Angulation*

The elbows tracked in greater varus with increasing WF loads; however, this trend was not statistically significant ($p = 0.07$). (Figure 4.6).

4.3.5 Dependent Position: Passive Elbow Flexion

4.3.5.1 *AMCL Tension*

With the arm oriented in the dependent position and the elbow under passive motion, there was no significant effect of WF loading on AMCL tension ($p = 0.08$). (Figure 4.7).

4.3.5.2 *Kinematics – Valgus Angulation*

The elbows tracked in greater varus with increasing WF loads ($p = 0.04$). The motion pathways of the WF – 10 N, the WF – 30 N, and the WF – 50 N conditions were not statistically different from that of the unloaded condition (p-values were 0.4, 0.3, and 0.3, respectively). (Figure 4.8).

4.3.6 Dependent Position: Active versus Passive Elbow Flexion

For the dependent position, there were no statistical differences in the AMCL tension levels between active and passive motion for any of the WF load conditions ($p > 0.05$, for all WF load conditions). Furthermore, the passive motion pathway of each WF load condition tracked in greater varus than its respective active motion pathway, with the passive motion pathways having varus to valgus slopes and the active motion pathways having valgus to varus slopes. Statistical differences were found between the active and passive motion pathways for the WF – 0 N, the WF – 10 N, the WF – 30 N, and the WF – 50 N conditions (p-values were 0.006, 0.04, 0.04, and 0.045, respectively). For full details refer to Appendix 8.

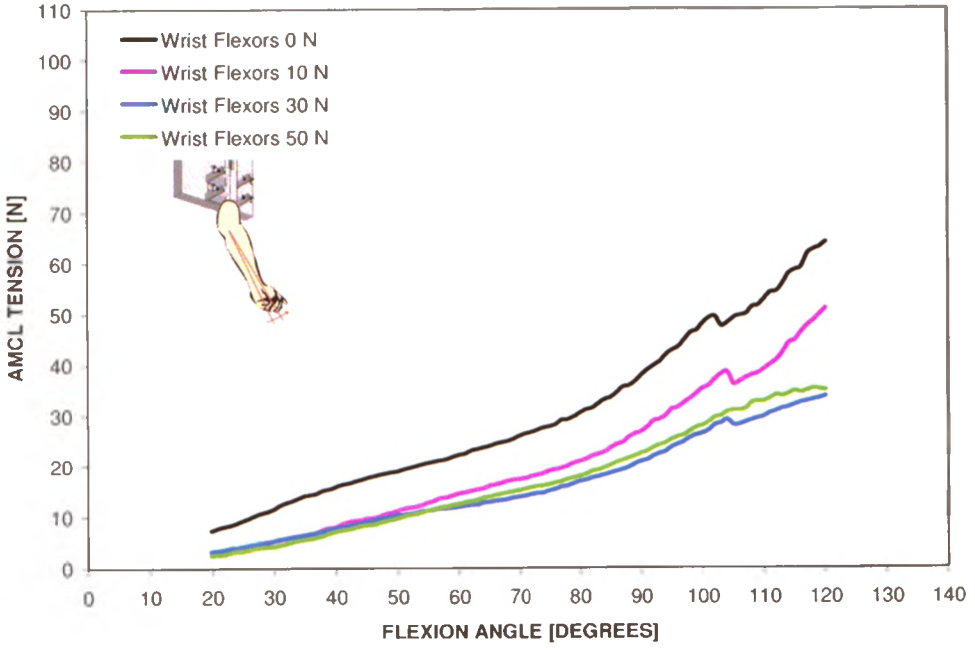

Figure 4.5: Variation of mean AMCL tension with flexion angle for active flexion in the dependent position for WF loading

Mean AMCL tension levels throughout the arc of elbow flexion are shown for the four WF load conditions (n = 3). There was no significant effect of WF loading on AMCL tension ($p = 0.2$). Standard deviations are omitted for clarity but ranged from ±1.9 N to ±28.0 N.

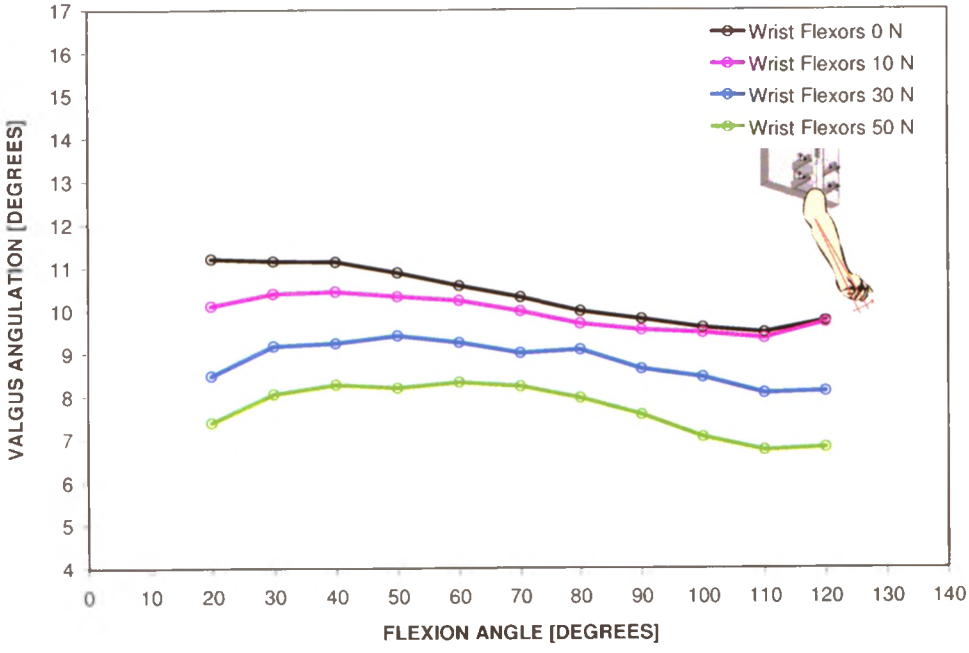

Figure 4.6: Mean elbow kinematic pathways for active flexion in the dependent position for WF loading

Mean valgus angulation of the ulna relative to the humerus at every 10° of elbow flexion is shown for the four WF load conditions (n = 3). The elbows tracked in greater varus with increasing WF loads; however this trend was not statistically significance (p = 0.07). Standard deviations are omitted for clarity but ranged from ±2.4° to ±4.1°.

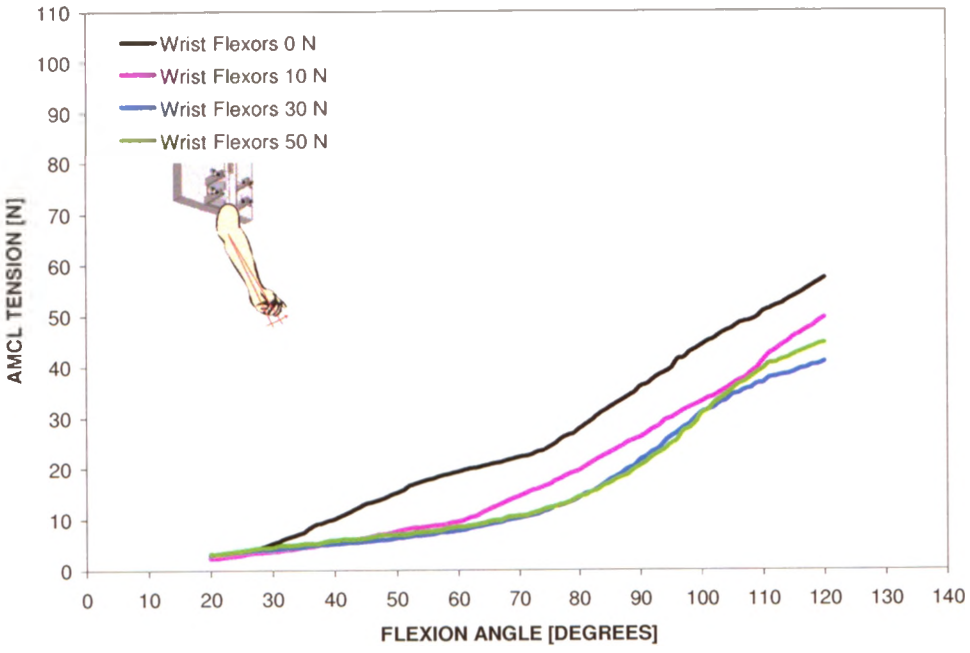

Figure 4.7: Variation of mean AMCL tension with flexion angle for passive flexion in the dependent position for WF loading

Mean AMCL tension levels throughout the arc of elbow flexion are shown for the four WF load conditions (n = 3). There was no significant effect of WF loading on AMCL tension ($p = 0.08$). Standard deviations are omitted for clarity but ranged from ±0.3 N to ±29.4 N.

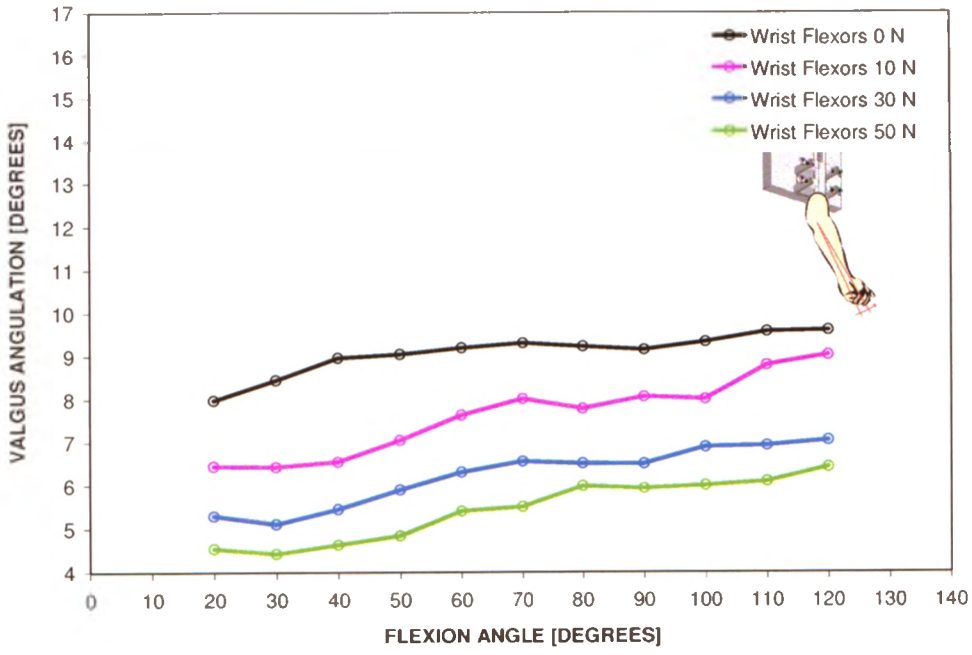

Figure 4.8: Mean elbow kinematic pathways for passive flexion in the dependent position for WF loading

Mean valgus angulation of the ulna relative to the humerus at every 10° of elbow flexion is shown for the four WF load conditions (n = 3). The elbows tracked in greater varus with increasing WF loads ($p = 0.04$); however, there was no statistical difference in the motion pathways between the four WF load conditions. Standard deviations are omitted for clarity but ranged from ±1.0° to ±3.5°.

4.4 DISCUSSION

We are not aware of any previous studies that have examined the effect of WF muscle loading on AMCL tension levels. Sectioning studies have demonstrated that the AMCL is the primary restraint to valgus loads and that the radial head is a secondary stabilizer.[19-28] Furthermore, it has been reported that MCL is able to withstand a maximum torque of 32 Nm[37]; however, baseball pitchers could experience up to 120 Nm of elbow valgus torque during the pitching motion[16]. Since it is clear that the MCL is not strong enough to withstand this torque by itself, it is believed that the overlying flexor-pronator muscles, which originate on the medial epicondyle, may help to minimize the stress experienced by the MCL by generating varus motion (*i.e.* compressing the joint medially) upon activation.[2,14,16,29,30,38,39] Furthermore, Davidson et al.[29] determined that of the flexor-pronator muscles, the flexor carpi ulnaris (FCU) was best suited to provide medial elbow support, especially at 120° of elbow flexion, as this muscle is positioned directly over the MCL at all degrees of elbow flexion and is the only muscle positioned over the MCL at 120° of elbow flexion. Consistent with the findings of Davidson et al.[29], Park et al.[2] demonstrated that simulated contraction of the FCU (at both 30° and 90° of elbow flexion) provided the greatest stability to the MCL-insufficient elbows when compared with the loading of other individual flexor-pronator muscles. It is unclear whether MCL injury results from inadequate protection provided by the flexor-pronator muscles due to impaired muscle firing prior to injury, or from alterations in the kinematic chain.[2,8-10,14,40,41]

For both active and passive flexion in the valgus position, the elbows tracked in greater varus, and the AMCL tension levels decreased, with increasing WF loads. This varus angulation – AMCL tension relationship was similar but less evident for both active and passive motion in the dependent position. These findings are consistent with previously reported data by Lin et al.[14]. These investigators found that individual loading of the FCU, flexor carpi radialis (FCR), and flexor digitorum superficialis (FDS) significantly decreased AMCL strain at both 45° and 90° of elbow flexion (the only two flexion angles tested). Furthermore, individual loading of the flexor-pronator muscles (FCU, FCR, FDS, and pronator teres) produced significant varus motion at both 45° and 90° of elbow flexion.[14] We also observed elbow varus movement, as well as decreased

AMCL tension levels, with WF loading at all angles of elbow flexion in our unconstrained testing system. Therefore, strengthening of the overlying flexor-pronator muscles may prevent MCL injury, as this may result, in part, from impaired flexor-pronator muscle activation.[2,6,8-10,29,40,41] Furthermore, activation of the flexor-pronator muscles should also be considered in the rehabilitation of MCL injuries to offload the ligament during healing.[2,14,39]

It is interesting to examine the AMCL tension results in light of the kinematic findings. In particular, does tension increase due to elongation of the tissue that would arise with greater valgus angulation, or is it a response due to load balance and the maintenance of a quasi-static equilibrium? In order to provide some insight, AMCL tension versus valgus angulation at 30°, 60°, and 90° of elbow flexion was plotted for active flexion in the valgus and dependent positions (Figure 4.9 and Figure 4.10, respectively). A linear regression was performed for each data set, using Microsoft Office Excel 2002, in order to determine the coefficient of determination (R^2 value). A quasi-linear AMCL tension – valgus angulation response was observed, to some extent, at all three degrees of elbow flexion for the valgus position (R^2 values were 0.90, 0.95, and 0.99 for 30°, 60°, and 90° of elbow flexion, respectively – Figure 4.9). This suggests that AMCL tension may well be influenced by the valgus position of the ulna. In other words, as the elbow moved through the arc of flexion, the observed change in AMCL tension levels was strongly correlated with a change in valgus angulation. Had elbow kinematics not affected the load response of the AMCL, a constant AMCL tension – valgus angulation response would have been observed. In comparison to the valgus position, a somewhat non-linear AMCL tension – valgus angulation response was observed for the dependent position (R^2 values were 0.63, 0.58, and 0.56 for 30°, 60°, and 90° of elbow flexion, respectively – Figure 4.10). Relatively small changes in AMCL tension levels were observed despite changes in valgus angulation, suggesting that AMCL tension was not as strongly influenced by the valgus position of the ulna in the dependent position. This is likely related to the greater effects of gravity on AMCL loading with the arm in the valgus orientation, and the smaller sample size of our study for the dependent position.

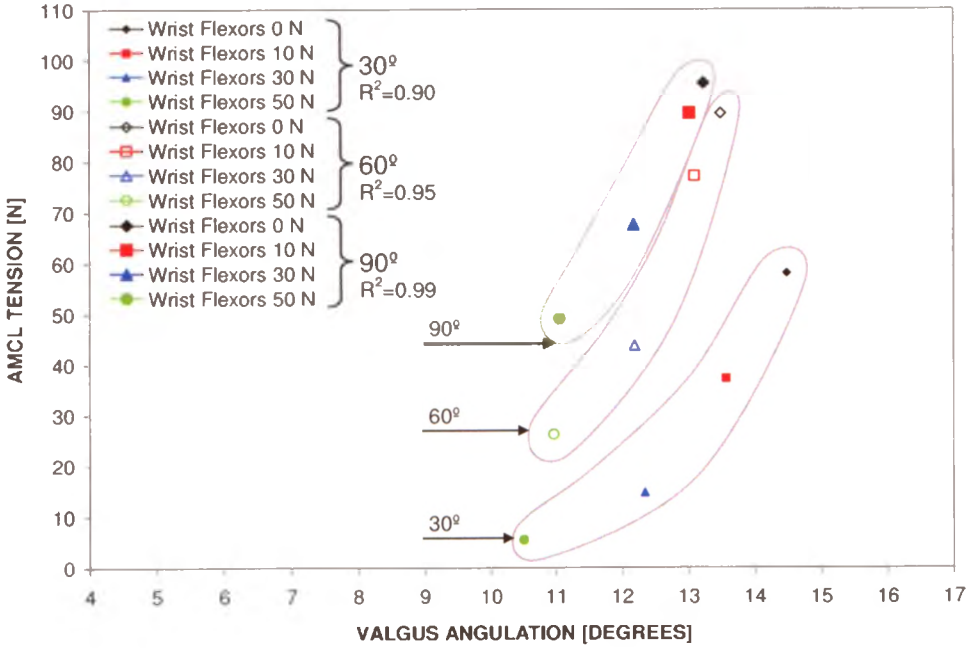

Figure 4.9: AMCL tension versus valgus angulation at 30°, 60°, and 90° of elbow flexion for active flexion in the valgus position for WF loading

A quasi-linear AMCL tension – valgus angulation response was observed, to some extent, at all three degrees of elbow flexion (R^2 values were 0.90, 0.95, and 0.99 for 30°, 60°, and 90° of elbow flexion, respectively). The data set for each flexion angle is circled for clarity. Standard deviations are omitted for clarity but ranged from ±5.8 N to ±57.1 N and ±2.4° to ±3.5°.

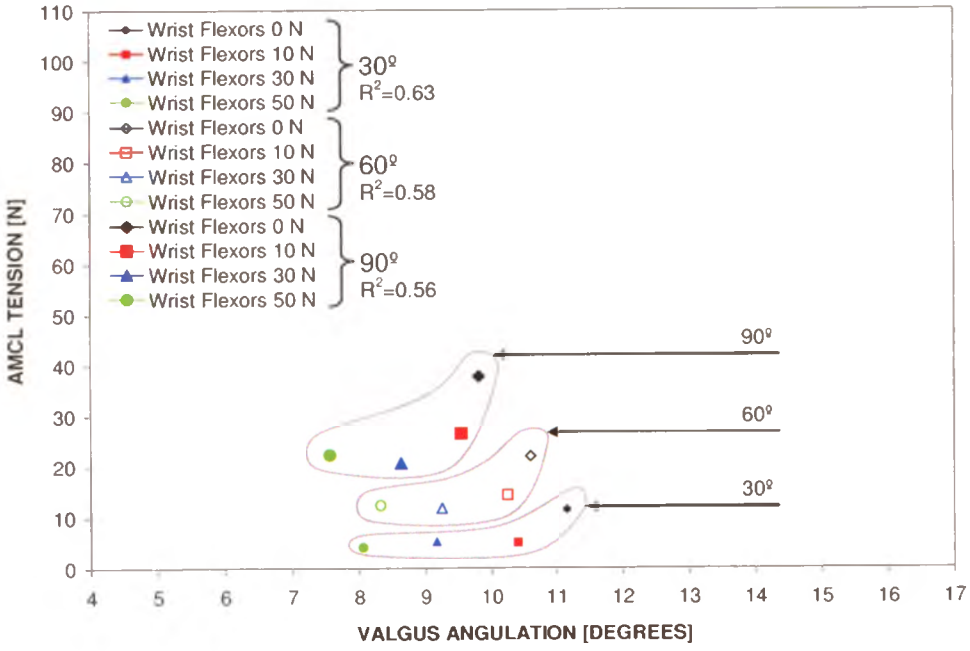

Figure 4.10: AMCL tension versus valgus angulation at 30°, 60°, and 90° of elbow flexion for active flexion in the dependent position for WF loading

A non-linear AMCL tension – valgus angulation response was observed at all three degrees of elbow flexion (R^2 values were 0.63, 0.58, and 0.56 for 30°, 60°, and 90° of elbow flexion, respectively). The data set for each flexion angle is circled for clarity. Standard deviations are omitted for clarity but ranged from ±3.0 N to ±27.5 N and ±2.5° to ±3.3°.

For the valgus position, we observed slightly smaller valgus angulations during active motion as compared with passive motion, for all WF load conditions. Additionally, when comparing the elbow kinematics and AMCL tension levels in the valgus position with those of the dependent position, greater valgus angulations and AMCL tension levels were observed in the valgus position. This observation was anticipated – with the arm oriented in the dependent position, both medial and lateral soft tissue structures contribute to supporting the load of the forearm, whereas with the arm oriented in the valgus gravity-loaded position, the AMCL is the primary structure supporting the load of the forearm (*i.e.* it is the primary structure resisting the valgus moment due to the effects of gravity). Based on these observations, we are in agreement with Armstrong et al.[31] with regard to avoiding the valgus orientation during rehabilitation to minimize both valgus instability and AMCL tension; hence, allowing optimal AMCL healing. Furthermore, active mobilization of the elbow joint in the dependent position should further minimize valgus instability and AMCL tension, as active mobilization of the elbow has been shown to improve joint stability by several previous investigators.[21,24,31,34] Dynamic structures that cross the elbow joint provide compressive joint force and thereby convey greater stability to the elbow.[38,39,42] The effect of forearm rotation on AMCL tension levels was not studied in the current investigation (recall that the forearms were fixed in neutral rotation); the influence of forearm rotation should be investigated in a future study.

The differences in motion pathways and AMCL tension levels with WF loading were consistent across the four specimens employed in the current investigation; however, our relatively small sample size may have precluded our ability to detect differences between WF load conditions, particularly with the arm in the dependent position (*i.e.* as statistical power increases, the chances of a Type II error decreases). Additionally, the WF loads studied (10, 30, and 50 N) were arbitrarily chosen and it is unclear whether these loads are clinically relevant – these loads are likely higher in throwing athletes, in particular. Finally, to reduce specimen preparation time, only the WF muscles (and not the wrist extensors muscles) were modelled in this investigation. Other flexor-pronator muscles, like the FDS and pronator teres, were not studied.

Therefore, it is unclear whether our experiment represents what occurs under physiological circumstances.

In summary, this *in vitro* cadaveric study demonstrated that AMCL tension levels and elbow kinematics are altered with simulated WF muscle loading. Increased WF muscle loading caused the elbows to track in greater varus and the AMCL tension levels to decrease, which is consistent with our hypothesis. Strengthening and activation of the flexor-pronator muscles should be considered to prevent MCL injury, and to assist in rehabilitation. The valgus orientation of the arm should be avoided during rehabilitation to minimize AMCL loading.

4.5 REFERENCE LIST

1. Timmerman LA, Andrews JR. Histology and arthroscopic anatomy of the ulnar collateral ligament of the elbow. Am.J.Sports Med. 1994;22:667-73.

2. Park MC, Ahmad CS. Dynamic contributions of the flexor-pronator mass to elbow valgus stability. J.Bone Joint Surg.Am. 2004;86-A:2268-74.

3. Altchek DW, Andrews JR. Medial collateral ligament injuries. In: Altchek DW, Andrews JR, editors. The athlete's elbow. Philadelphia: Lippincott Williams and Wilkins; 2001. p. 153-73.

4. Lee ML, Rosenwasser MP. Chronic elbow instability. Orthop.Clin.North Am. 1999;30:81-9.

5. Safran MR. Elbow injuries in athletes. A review. Clin.Orthop.Relat Res. 1995;257-77.

6. Cohen MS, Bruno RJ. The collateral ligaments of the elbow: anatomy and clinical correlation. Clin.Orthop.Relat Res. 2001;123-30.

7. Pincivero DM, Heinrichs K, Perrin DH. Medial elbow stability. Clinical implications. Sports Med. 1994;18:141-8.

8. Conway JE, Jobe FW, Glousman RE, Pink M. Medial instability of the elbow in throwing athletes. Treatment by repair or reconstruction of the ulnar collateral ligament. J.Bone Joint Surg.Am. 1992;74:67-83.

9. Miller CD, Savoie FH, III. Valgus Extension Injuries of the Elbow in the Throwing Athlete. J.Am.Acad.Orthop.Surg. 1994;2:261-9.

10. Chen FS, Rokito AS, Jobe FW. Medial elbow problems in the overhead-throwing athlete. J.Am.Acad.Orthop.Surg. 2001;9:99-113.

11. Jobe FW, Stark H, Lombardo SJ. Reconstruction of the ulnar collateral ligament in athletes. J.Bone Joint Surg.Am. 1986;68:1158-63.

12. Nazarian LN, McShane JM, Ciccotti MG, O'Kane PL, Harwood MI. Dynamic US of the anterior band of the ulnar collateral ligament of the elbow in asymptomatic major league baseball pitchers. Radiology 2003;227:149-54.

13. Fleisig GS, Andrews JR, Dillman CJ, Escamilla RF. Kinetics of baseball pitching with implications about injury mechanisms. Am.J.Sports Med. 1995;23:233-9.

14. Lin F, Kohli N, Perlmutter S, Lim D, Nuber GW, Makhsous M. Muscle contribution to elbow joint valgus stability. J.Shoulder.Elbow.Surg. 2007;16:795-802.

15. Popovic N, Ferrara MA, Daenen B, Georis P, Lemaire R. Imaging overuse injury of the elbow in professional team handball players: a bilateral comparison using plain films, stress radiography, ultrasound, and magnetic resonance imaging. Int.J.Sports Med. 2001;22:60-7.

16. Werner SL, Fleisig GS, Dillman CJ, Andrews JR. Biomechanics of the elbow during baseball pitching. J.Orthop.Sports Phys.Ther. 1993;17:274-8.

17. Josefsson PO, Johnell O, Wendeberg B. Ligamentous injuries in dislocations of the elbow joint. Clin.Orthop.Relat Res. 1987;221-5.

18. Davidson PA, Moseley JB, Jr., Tullos HS. Radial head fracture. A potentially complex injury. Clin.Orthop.Relat Res. 1993;224-30.

19. Morrey BF, An KN. Functional anatomy of the ligaments of the elbow. Clin.Orthop.Relat Res. 1985;84-90.

20. Morrey BF, An KN. Articular and ligamentous contributions to the stability of the elbow joint. Am.J.Sports Med. 1983;11:315-9.

21. Morrey BF, Tanaka S, An KN. Valgus stability of the elbow. A definition of primary and secondary constraints. Clin.Orthop.Relat Res. 1991;187-95.

22. Regan WD, Korinek SL, Morrey BF, An KN. Biomechanical study of ligaments around the elbow joint. Clin.Orthop.Relat Res. 1991;170-9.

23. Hotchkiss RN, Weiland AJ. Valgus stability of the elbow. J.Orthop.Res. 1987;5:372-7.

24. Callaway GH, Field LD, Deng XH et al. Biomechanical evaluation of the medial collateral ligament of the elbow. J.Bone Joint Surg.Am. 1997;79:1223-31.

25. Floris S, Olsen BS, Dalstra M, Sojbjerg JO, Sneppen O. The medial collateral ligament of the elbow joint: anatomy and kinematics. J.Shoulder.Elbow.Surg. 1998;7:345-51.

26. Sojbjerg JO, Ovesen J, Nielsen S. Experimental elbow instability after transection of the medial collateral ligament. Clin.Orthop.Relat Res. 1987;186-90.

27. Schwab GH, Bennett JB, Woods GW, Tullos HS. Biomechanics of elbow instability: the role of the medial collateral ligament. Clin.Orthop.Relat Res. 1980;42-52.

28. Fuss FK. The ulnar collateral ligament of the human elbow joint. Anatomy, function and biomechanics. J.Anat. 1991;175:203-12.

29. Davidson PA, Pink M, Perry J, Jobe FW. Functional anatomy of the flexor pronator muscle group in relation to the medial collateral ligament of the elbow. Am.J.Sports Med. 1995;23:245-50.

30. DiGiovine NM, Jobe FW, Pink M, Perry J. An electromyographic analysis of the upper extremity in pitching. J.Shoulder.Elbow.Surg. 1992;1:15-25.

31. Armstrong AD, Dunning CE, Faber KJ, Duck TR, Johnson JA, King GJ. Rehabilitation of the medial collateral ligament-deficient elbow: an in vitro biomechanical study. J.Hand Surg.[Am.] 2000;25:1051-7.

32. Funk DA, An KN, Morrey BF, Daube JR. Electromyographic analysis of muscles across the elbow joint. J.Orthop.Res. 1987;5:529-38.

33. Amis AA, Dowson D, Wright V. Muscle strengths and musculo-skeletal geometry of the upper limb. Engineering in Medicine 1979;8:41-8.

34. Dunning CE, Duck TR, King GJ, Johnson JA. Simulated active control produces repeatable motion pathways of the elbow in an in vitro testing system. J.Biomech. 2001;34:1039-48.

35. King GJ, Zarzour ZD, Rath DA, Dunning CE, Patterson SD, Johnson JA. Metallic radial head arthroplasty improves valgus stability of the elbow. Clin.Orthop.Relat Res. 1999;114-25.

36. Dunning CE, Zarzour ZD, Patterson SD, Johnson JA, King GJ. Ligamentous stabilizers against posterolateral rotatory instability of the elbow. J.Bone Joint Surg.Am. 2001;83-A:1823-8.

37. Dillman, C. J., Smutz, P, and Werner, S. Valgus extension overload in baseball pitching. Med Sci Sports Exerc 23(4), 135. 1991.

38. Seiber K, Gupta R, McGarry MH, Safran MR, Lee TQ. The role of the elbow musculature, forearm rotation, and elbow flexion in elbow stability: an in vitro study. J.Shoulder.Elbow.Surg. 2009;18:260-8.

39. An KN, Hui FC, Morrey BF, Linscheid RL, Chao EY. Muscles across the elbow joint: a biomechanical analysis. J.Biomech. 1981;14:659-69.

40. Hamilton CD, Glousman RE, Jobe FW, Brault J, Pink M, Perry J. Dynamic stability of the elbow: electromyographic analysis of the flexor pronator group

and the extensor group in pitchers with valgus instability. J.Shoulder.Elbow.Surg. 1996;5:347-54.

41. Glousman RE, Barron J, Jobe FW, Perry J, Pink M. An electromyographic analysis of the elbow in normal and injured pitchers with medial collateral ligament insufficiency. Am.J.Sports Med. 1992;20:311-7.

42. Alcid JG, Ahmad CS, Lee TQ. Elbow anatomy and structural biomechanics. Clin.Sports Med. 2004;23:503-17, vii.

CHAPTER 5

Effect of Radial Head Excision and Arthroplasty on Medial Collateral Ligament Tension in the Elbow

Overview: This chapter details an *in vitro* cadaveric study examining the effect of radial head excision and arthroplasty on the magnitude of medial collateral ligament tension in the elbow. Ligament tension was quantified using the custom designed E-form frame buckle transducer described in Chapter 2. Ligament tension and elbow kinematics, for active elbow flexion in the valgus and dependent positions, are presented and analysed.

5.1 INTRODUCTION

Displaced comminuted radial head (RH) fractures, primary and post-traumatic osteoarthritis, and rheumatoid arthritis are often treated with RH excision and/or prosthetic replacement. An increased carrying angle due to attenuation of the medial collateral ligament of the elbow is commonly reported as a late sequela of RH excision.[1-7] An increase in tension in the anterior bundle of the medial collateral ligament (AMCL), due to the absence of the RH, has been predicted in biomechanical studies[8-10]; however, the effect of RH excision and replacement on the load environment of the AMCL has not been quantified experimentally.

The purpose of this *in vitro* study was to determine the effect of RH excision and arthroplasty on the magnitude of AMCL tension through the arc of elbow flexion. We hypothesized that tension in the AMCL would increase with RH excision, and that RH arthroplasty would restore AMCL tension levels similar to that of the native RH state.

5.2 MATERIALS AND METHODS

5.2.1 Specimen Preparation and Custom Motion Simulator*

Five fresh-frozen cadaveric upper extremities (mean age 72 ± 10 years; range: 62-82 years; 3 female; 1 right specimen) were prepared for testing as previously described. To simulate active muscle loading, a stainless steel cable (0.8 mm diameter) was sutured to the distal tendon of the brachialis, the biceps brachii, and the triceps brachii using 200 lb braided Dacron® (Woodstock Line Co., Putnam, CT) and to the brachioradialis using a #5 Ethibond suture (Johnson & Johnson, Ethicon Inc., Peterborough, ON). The origin of the brachioradialis was simulated using a (Delrin®) pulley inserted into the proximal portion of the lateral supracondylar ridge to ensure replication of the muscle's moment arm throughout elbow motion.[11] The lines-of-action of the elbow flexor and extensor muscles were maintained using a tendon alignment unit located within the humeral clamp of the testing apparatus (Figure 3.1).

The wrist was fixed in neutral flexion/extension using a 5 mm Steinman Pin drilled through the long finger metacarpal, across the carpus, and into the distal radius. To prevent forearm rotation, the distal radius was fixed to the ulna in neutral rotation using a 3.5 mm tap (Synthes Ltd., Mississauga, ON). All skin incisions were closed to keep the soft tissues moist during testing.

The humerus was mounted into the testing apparatus in neutral humeral rotation using a clamp that rigidly held the arm while allowing unconstrained elbow motion. The humeral mounting clamp was affixed to a base-plate on a two-degree-of-freedom hinge, which permitted orientation of the arm in the valgus gravity-loaded position, as well as the dependent (*i.e.* vertical) position (Figure 3.2). With the specimen oriented in the valgus gravity-loaded position, the buckle transducer was inserted into the AMCL substance as previously described. Data from the buckle transducer were recorded in real time using LabVIEW 7.1 (National Instruments, Austin, TX). The specimen was kept moist using 0.9% normal saline solution throughout testing.

---

* The experimental techniques related to specimen preparation, transducer implantation, simulation trials, and kinematic measurements are identical to those described in Chapter 3, and hence are provided here for completion, but in an abbreviated fashion.

To achieve active simulated flexion, each stainless steel cable was attached to an associated computer-controlled pneumatic actuator (brachioradialis) or servomotor (brachialis, biceps, and triceps) of the testing apparatus. The muscles were loaded by the actuators/motors and control of each unit was achieved using custom software (LabVIEW 7.1). Relative loading among the muscles was derived in accordance with published measurements of quantitative electromyographic (EMG) activity[12] and physiological muscle cross-sectional area (pCSA)[13]. The ratio of muscle loading was determined from the product of the relative EMG activity and pCSA data, as previously validated by our laboratory.[14] Loading of the biceps, brachioradialis, and triceps were determined as a proportion of the load applied by the brachialis, the prime flexor of the elbow (*i.e.* the prime mover). The load applied to the brachialis tendon was such that a controlled rate of elbow flexion was maintained. The brachialis tendon moved at a constant flexion rate of 10 degrees per second, which was achieved by a proportional-integral-derivative control using feedback from the electromagnetic tracking system.

Motion of the ulna relative to the humerus was measured in six-degrees-of-freedom using an electromagnetic tracking device (Flock of Birds; Ascension Technology, Burlington, VT). As the elbow moved through an arc of flexion, the position and orientation of a receiver attached to the distal ulna was recorded relative to a transmitter fixed to the base of the testing apparatus.[14] At the completion of testing, the elbow and wrist were disarticulated and anatomical landmarks on the humerus and ulna were digitized to create anatomic bone coordinate systems, as previously described.[15] This allowed the "ulnar receiver with respect to transmitter" data collected during testing to be converted to "ulna with respect to humerus" data using Euler Z-Y-X analyses during *post hoc* data analysis.[16] Hence, clinically relevant coordinate systems could be constructed. Outputted data from the tracking system were recorded in real time using custom software programmed using LabVIEW 7.1. The relative motion of the ulnar coordinate system relative to the humeral coordinate system was analysed using custom software (LabVIEW 7.1).

5.2.2 Testing Protocol

Testing was conducted with the arm oriented in the dependent and valgus positions, with the elbow under active motion. Each flexion trial was performed with the forearm in neutral rotation.

Testing of the intact elbow was performed first. Five flexion cycles were performed in the two test conditions (*i.e.* active flexion in the dependent position and active flexion in the valgus position). The AMCL tension and elbow kinematic data from the third flexion cycle of each test condition were analysed, similar to the protocol of Chapters 3 and 4. Once the AMCL tension and valgus angulation measurements for the intact condition were obtained, a direct anterior surgical approach was used to allow access to the RH while preserving the integrity of the radial collateral ligament (RCL) and the lateral ulnar collateral ligament (LUCL). After sectioning, the annular ligament (AL) and anterior joint capsule were repaired with a #2 Ethibond suture (Johnson & Johnson, Ethicon Inc., Peterborough, ON) and the motion protocol was performed. This condition was tested as a control in order to determine whether the surgical approach used to excise and replace the RH had an effect on elbow kinematics and AMCL tension levels. After motion testing, the AL and joint capsule sutures were removed and the RH was excised at the junction of the head and neck. The AL and joint capsule were then repaired and the motion protocol was repeated. Finally, the AL and joint capsule sutures were removed and a RH implant was inserted, closely matching the diameter and thickness of the articular surface to that of the resected RH (EVOLVE; Wright Medical Technology Inc., Arlington, TN). The AL and joint capsule were repaired and the motion protocol was repeated. For each of the aforementioned stages (*i.e.* the AL repaired, the RH excised, and the RH arthroplasty conditions), three active flexion cycles were performed in the dependent and valgus positions. Again, the AMCL tension and elbow kinematic data from the third flexion cycle of each test condition were analysed, similar to the protocol of Chapters 3 and 4.

5.2.3 Data Analysis

For each test condition (*i.e.* active flexion in the dependent position and active flexion in the valgus position), differences in the RH conditions were statistically analysed using SPSS software (SPSS V16.0.1, Chicago, IL). All data were analysed using two-way repeated measures analysis of variance (ANOVA) with $\alpha = 0.05$, and *post hoc* paired *t*-tests using the Bonferroni correction for family-wise error.

Data from all five specimens tested were analysed for the valgus position (mean age 72 ± 10 years; range: 62-82 years; 3 female; 1 right specimen); however, due to data acquisition difficulties, data from only four specimens were analysed for the dependent position (mean age 74 ± 9 years; range: 65-82 years; 2 female; 1 right specimen). For the two-way repeated ANOVAs, the two independent variables used were *RH condition* and *flexion angle*. There were four RH conditions: (1) intact; (2) AL repaired; (3) RH excised; and (4) RH arthroplasty.

During testing, two dependent variables were measured: (1) AMCL tension, which was the output of the buckle transducer; and (2) valgus angulation of the ulna with respect to the humerus. Valgus angulation was calculated, for both the dependent and valgus positions, by measuring the difference in the orientation of the ulna relative to the humerus via the custom software previously described (LabVIEW 7.1). AMCL tension and valgus angulation were measured throughout the arc of elbow flexion but are reported only at every 10° of elbow flexion from 20°-120° of elbow flexion to simplify data interpretation; hence, there were eleven levels of the independent variable *flexion angle*.

All kinematic data were analysed using custom software (LabVIEW 7.1), Microsoft Office Excel 2002 (Microsoft Corporation, Redmond, WA), and SPSS. All source tension data were filtered using a program written in Matlab (The MathWorks, Natick, MA), and analysed using Microsoft Office Excel 2002 and SPSS.

5.3 RESULTS

The four RH conditions of the study were: (1) intact; (2) AL repaired; (3) RH excised; and (4) RH arthroplasty. The results for the four RH conditions are presented for active elbow flexion in the valgus and dependent positions.

5.3.1 Valgus Position: Active Elbow Flexion

5.3.1.1 *AMCL Tension*

With the arm oriented in the valgus position and the elbow under active motion, there was a significant effect of RH condition on AMCL tension ($p = 0.003$). There was a statistical difference in the AMCL tension levels between the intact and the RH excised elbows ($p = 0.006$). Differences in the AMCL tension levels between the intact and the AL repaired elbows, as well as the intact and the RH arthroplasty elbows, were not statistically significant ($p = 0.4$ and $p = 0.1$, respectively). (Figure 5.1).

5.3.1.2 *Kinematics – Valgus Angulation*

There was a significant effect of RH condition on valgus angulation ($p = 0.02$). The motion pathways of the intact and AL repaired elbows were significantly different from the RH excised elbows ($p = 0.05$, for both pairwise comparisons). There was no statistical difference in the motion pathways between the intact and the AL repaired elbows ($p = 0.8$), as well as the intact and the RH arthroplasty elbows ($p = 1.0$). (Figure 5.2).

5.3.2 Dependent Position: Active Elbow Flexion

5.3.2.1 *AMCL Tension*

With the arm oriented in the dependent position and the elbow under active motion, there was no significant effect of RH condition on AMCL tension ($p = 0.06$). (Figure 5.3).

5.3.2.2 *Kinematics – Valgus Angulation*

There was no significant effect of RH condition on valgus angulation ($p = 0.09$). (Figure 5.4).

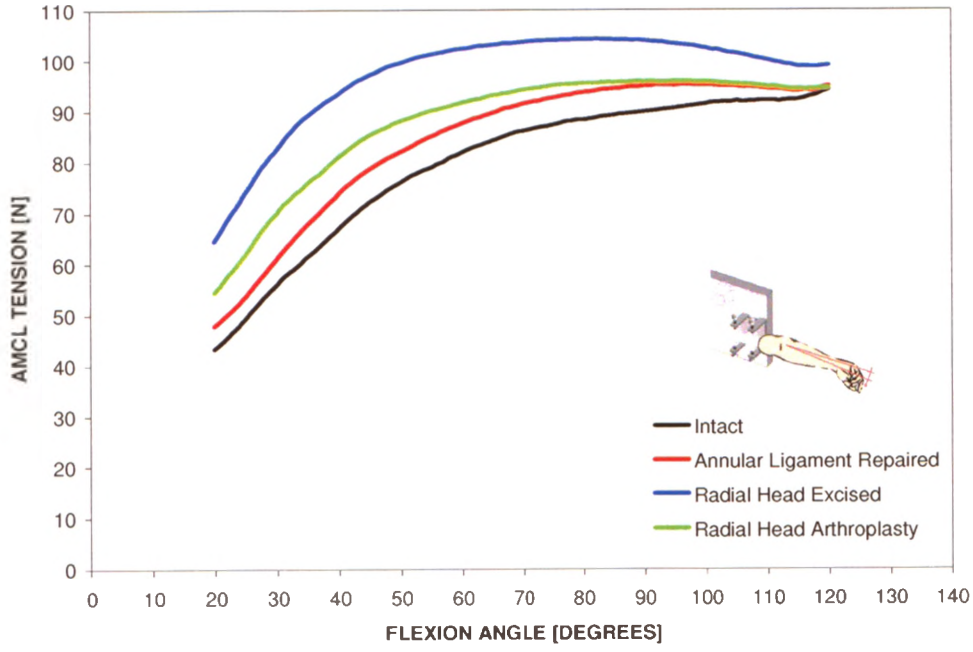

Figure 5.1: Variation of mean AMCL tension with flexion angle for active flexion in the valgus position for RH excision and arthroplasty

Mean AMCL tension levels throughout the arc of elbow flexion are shown for the four RH conditions (n = 5). There was a significant difference between the intact and the RH excised elbows (p = 0.006); however, there was no statistical difference between the intact and AL repaired elbows (p = 0.4), and the intact and the RH arthroplasty elbows (p = 0.1). Standard deviations are omitted for clarity but ranged from ±8.7 N to ±40.5 N.

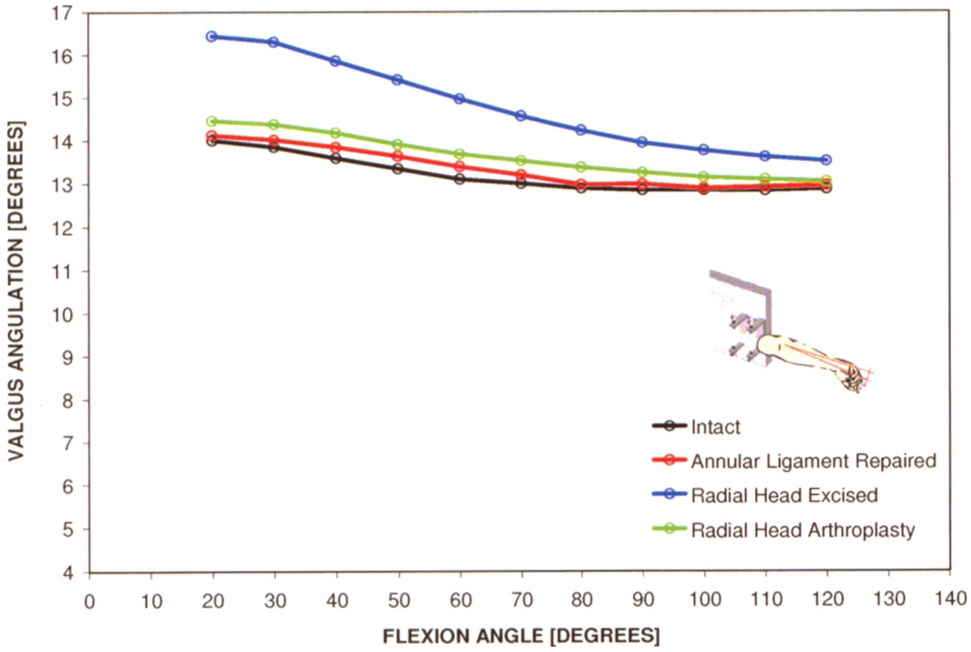

Figure 5.2: Mean elbow kinematic pathways for active flexion in the valgus position for RH excision and arthroplasty

Mean valgus angulation of the ulna relative to the humerus at every 10° of elbow flexion is shown for the four RH conditions (n = 5). The intact and AL repaired elbows were statistically different from the RH excised elbows ($p = 0.05$, for both pairwise comparisons). The intact elbows were not statistically different from the AL repaired and the RH arthroplasty elbows ($p = 0.8$ and $p = 1.0$, respectively). Standard deviations are omitted for clarity but ranged from ±2.5° to ±4.1°.

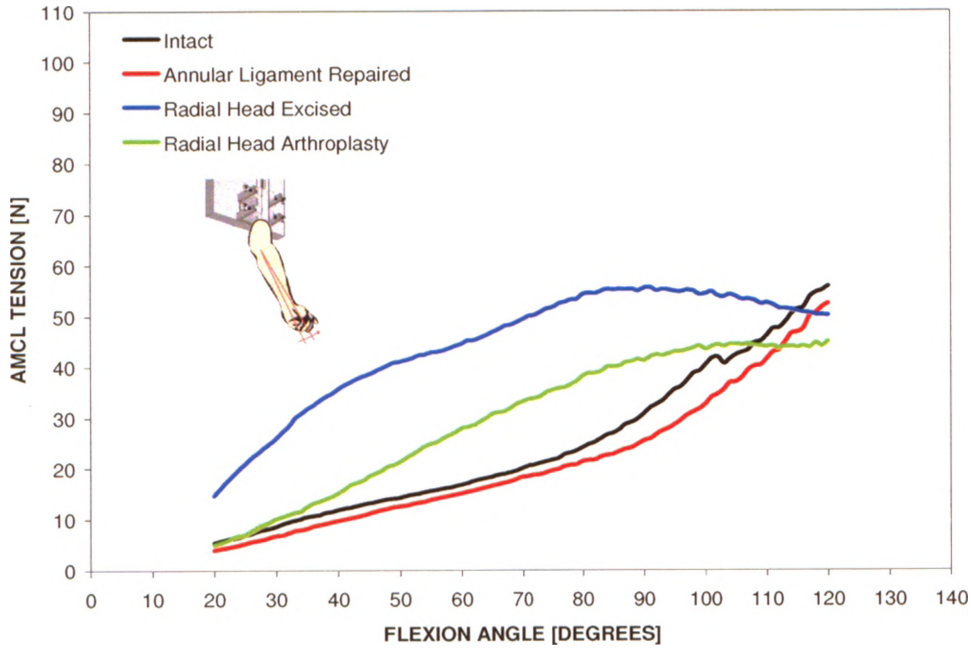

Figure 5.3: Variation of mean AMCL tension with flexion angle for active flexion in the dependent position for RH excision and arthroplasty

Mean AMCL tension levels throughout the arc of elbow flexion are shown for the four RH conditions (n = 4). There was no significant effect of RH condition on AMCL tension ($p = 0.06$). Standard deviations are omitted for clarity but ranged from ±6.7 N to ±36.0 N.

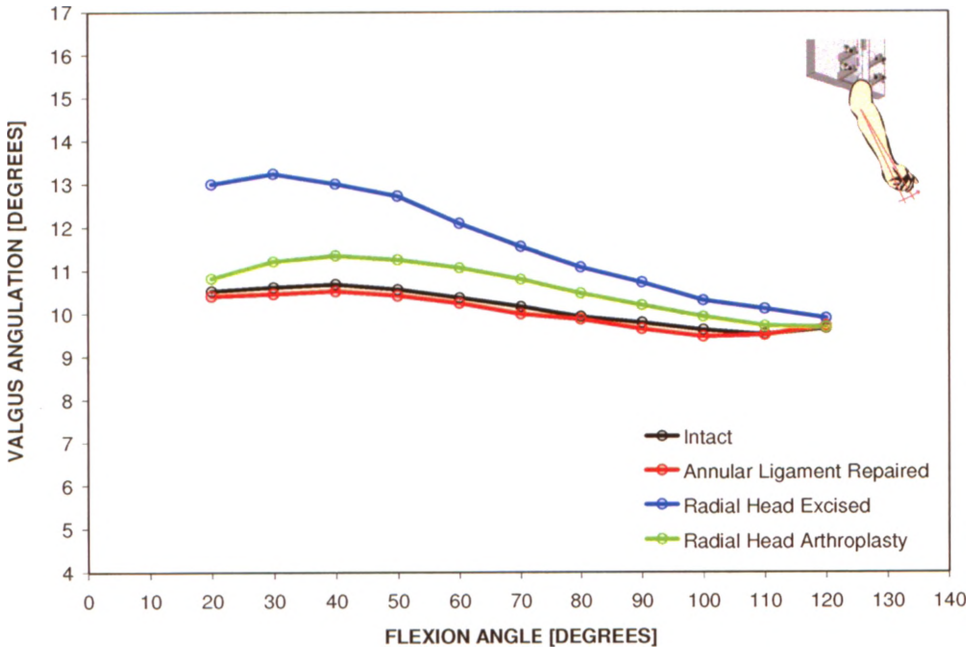

Figure 5.4: Mean elbow kinematic pathways for active flexion in the dependent position for RH excision and arthroplasty

Mean valgus angulation of the ulna relative to the humerus at every 10° of elbow flexion is shown for the four RH conditions (n = 4). There was no significant effect of RH condition on valgus angulation ($p = 0.09$). Standard deviations are omitted for clarity but ranged from ±2.0° to ±3.9°.

5.4 DISCUSSION

We are not aware of any previous studies that have examined the effect of RH excision and arthroplasty on AMCL tension levels. Sectioning studies have demonstrated that the AMCL is the primary restraint to valgus loads and that the RH is a secondary stabilizer.[10,17-25] The surgical approach used to excise and replace the RH, while not typically employed clinically, was chosen in this *in vitro* study to preserve the integrity of the radial collateral ligament (RCL) and the lateral ulnar collateral ligament (LUCL), thereby minimizing the soft tissue disruption to the elbow. For active elbow flexion in the valgus position, the elbows were observed to track in slightly greater valgus, and to experience slightly greater AMCL tension levels, following sectioning and repair of the AL, when compared to the intact elbows. While not statistically significant, these data suggest that the surgical approach used to excise and replace the RH had a small effect on the behaviour of the elbows, presumably due to an inability of the sutured anterior capsule and AL to precisely restore the soft tissue integrity.

As has been reported by other investigators, RH excision shifted the motion pathways of the elbows into greater valgus.[21,26] Concomitant with this increase in valgus tracking, we observed a 22.1% increase in AMCL tension following RH excision (see Table A9.8 in Appendix 9), confirming the importance of the RH in resisting valgus angulation and offloading the medial soft tissue structures. RH arthroplasty restored near-normal elbow kinematics and AMCL tension levels; valgus stability and AMCL tension levels were similar to those quantified after sectioning and repair of the AL with the native RH. Small differences in elbow kinematics and AMCL tension levels between the native RH and the RH arthroplasty may have been a consequence of errors in surgical implantation, incorrect implant sizing, differences in the articular shape of the axisymmetric metallic implant from that of the native RH, or soft tissue tensioning.

Similar effects of RH excision and arthroplasty on elbow kinematics and AMCL tension levels were observed for active elbow flexion in the dependent position. Relative to the observations with the arm in the valgus position, these differences were smaller and not statistically significant. Furthermore, when comparing the elbow kinematics and AMCL tension levels in the valgus position with those of the dependent position, greater valgus angulations and AMCL tension levels were observed in the valgus position. This

suggests that following RH excision, rehabilitation of the elbow with the arm adjacent to the side of the body, and avoiding valgus positioning, should optimize healing of a concomitant AMCL injury.

Similar to the studies of Morrey et al.[21], Jensen et al.[27], and Beingessner et al.[26], a change in valgus elbow stability was observed following RH excision. Contrary to the findings of Beingessner et al.[26], a significant increase in valgus angulation after RH excision was not found for active flexion in the dependent position; however, the trends were similar. Statistical significance in our study was likely not achieved due to our smaller sample size, which limited our statistical power. We observed that the valgus angulation after RH arthroplasty was similar to that seen with the native RH intact, for active flexion in the dependent position, which is consistent with the findings of Beingessner et al.[26].

In the absence of a RH, the axial load on the radius is shifted medially to the ulna.[8-10] The net effect is an increase in MCL tension to prevent valgus deformity from occurring and increased ulnohumeral joint loading concentrated on the lateral portion of the ulnohumeral joint.[8-10] The prolonged absence of a RH has been associated with the development of osteoarthritis, which may be due to this altered loading on the ulnohumeral joint.[1,8] An increased carrying angle of the elbow has also been reported due to attenuation of the MCL, which likely results from chronic MCL overloading.[1-7] In contrast, RH arthroplasty restores the load balance across the elbow, thereby protecting the MCL from overload and possibly preventing degeneration of the ulnohumeral joint. Our data confirmed the importance of the RH in offloading the AMCL and restoring near-normal elbow kinematics. Long-term comparative studies of metallic RH arthroplasty verses RH excision are currently unavailable. Whether the biomechanical benefits of RH arthroplasty observed in this study will reduce the incidence of arthritis and attenuation of the AMCL over time, requires further clinical study.

It is interesting to examine the AMCL tension results in light of the kinematic findings. In particular, does tension increase due to elongation of the tissue that would arise with greater valgus angulation, or is it a response due to load balance and the maintenance of a quasi-static equilibrium? In order to provide some insight, AMCL tension versus valgus angulation at 30°, 60°, and 90° of elbow flexion was plotted for

active flexion in the valgus and dependent positions (Figure 5.5 and Figure 5.6, respectively). A linear regression was performed for each data set, using Microsoft Office Excel 2002, in order to determine the coefficient of determination (R^2 value). A quasi-linear AMCL tension – valgus angulation response was observed, to some extent, at all three degrees of elbow flexion for the valgus position (R^2 values were 0.90, 0.96, and 0.93 for 30°, 60°, and 90° of elbow flexion, respectively – Figure 5.5) and most prominently at 60° and 90° of elbow flexion for the dependent position (R^2 values were 0.98, 1.00, and 1.00 for 30°, 60°, and 90° of elbow flexion, respectively – Figure 5.6). This suggests that AMCL tension may well be influenced by the valgus position of the ulna. Had elbow kinematics not affected the load response of the AMCL, a constant AMCL tension – valgus angulation response would have been observed. Deviations from linearity may be explained by the change in AMCL tissue biomechanics as a result of AL repair, RH excision, and RH arthroplasty.

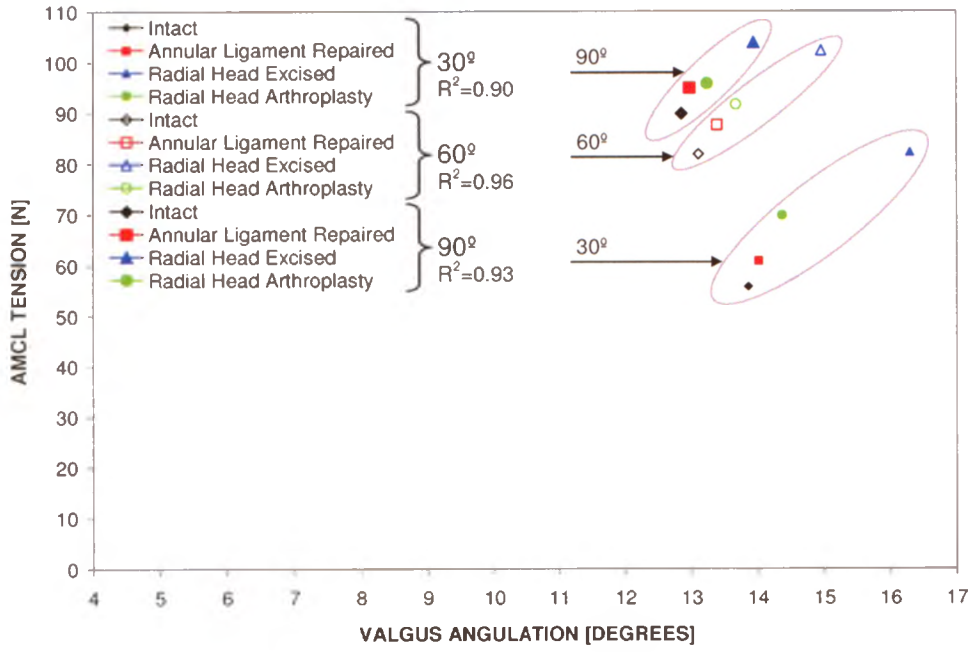

Figure 5.5: AMCL tension versus valgus angulation at 30°, 60°, and 90° of elbow flexion for active flexion in the valgus position for RH excision and arthroplasty

A linear AMCL tension – valgus angulation response was observed, to some extent, at all three degrees of elbow flexion (R^2 values were 0.90, 0.96, and 0.93 for 30°, 60°, and 90° of elbow flexion, respectively). The data set for each flexion angle is circled for clarity. Standard deviations are omitted for clarity but ranged from ±9.7 N to ±38.6 N and ±2.5° to ±3.6°.

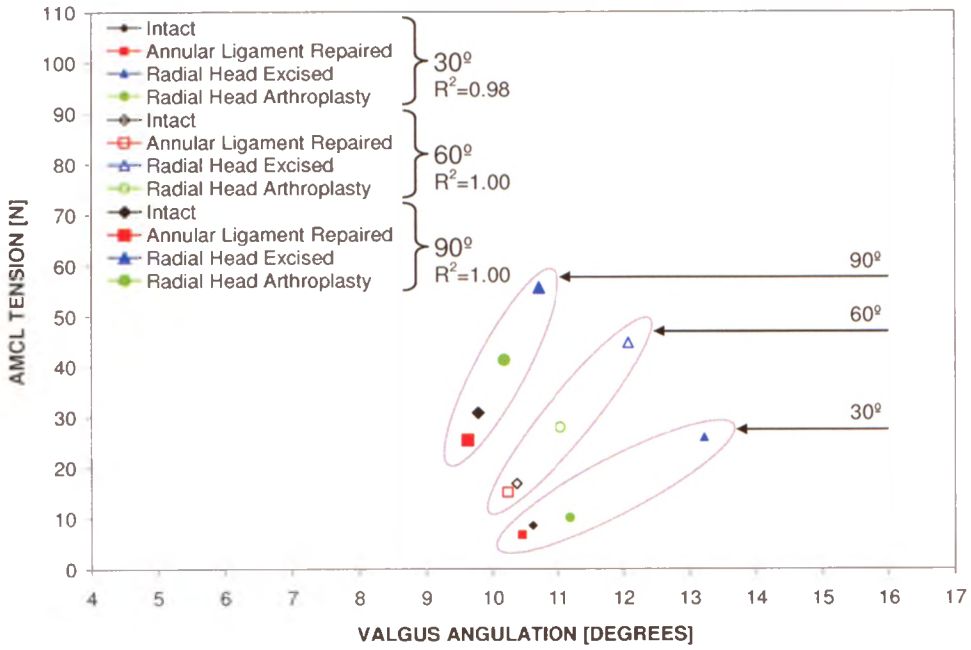

Figure 5.6: AMCL tension versus valgus angulation at 30°, 60°, and 90° of elbow flexion for active flexion in the dependent position for RH excision and arthroplasty

A linear AMCL tension – valgus angulation response was observed at all three degrees of elbow flexion (R^2 values were 0.98, 1.00, and 1.00 for 30°, 60°, and 90° of elbow flexion, respectively). The data set for each flexion angle is circled for clarity. Standard deviations are omitted for clarity but ranged from ±11.1 N to ±32.4 N and ±2.0° to ±3.8°.

The differences in motion pathways and AMCL tension levels following RH excision and arthroplasty were consistent across the five specimens employed in the current investigation; however, our relatively small sample size may have precluded our ability to detect differences between interventions, particularly with the arm in the dependent position (*i.e.* as statistical power increases, the chances of a Type II error decreases). Finally, the chosen surgical approach had a small effect on elbow kinematics and AMCL tension levels, which further limited our ability to isolate the effects of RH excision and arthroplasty.

In summary, this *in vitro* cadaveric study demonstrated that AMCL tension levels and elbow kinematics are altered following RH excision, and metallic RH arthroplasty restores near-normal AMCL tension levels and elbow kinematics. These observations are consistent with our hypotheses.

5.5 REFERENCE LIST

1. Ikeda M, Sugiyama K, Kang C, Takagaki T, Oka Y. Comminuted fractures of the radial head. Comparison of resection and internal fixation. J.Bone Joint Surg.Am. 2005;87:76-84.

2. Janssen RP, Vegter J. Resection of the radial head after Mason type-III fractures of the elbow: follow-up at 16 to 30 years. J.Bone Joint Surg.Br. 1998;80:231-3.

3. Goldberg I, Peylan J, Yosipovitch Z. Late results of excision of the radial head for an isolated closed fracture. J.Bone Joint Surg.Am. 1986;68:675-9.

4. Mikic ZD, Vukadinovic SM. Late results in fractures of the radial head treated by excision. Clin.Orthop.Relat Res. 1983;220-8.

5. Sutro CJ, Sutro WH. Fractures of the radial head in adults with the complication "cubitus valgus". Bull.Hosp.Jt.Dis.Orthop.Inst. 1985;45:65-73.

6. Coleman DA, Blair WF, Shurr D. Resection of the radial head for fracture of the radial head. Long-term follow-up of seventeen cases. J.Bone Joint Surg.Am. 1987;69:385-92.

7. Sanchez-Sotelo J, Romanillos O, Garay EG. Results of acute excision of the radial head in elbow radial head fracture-dislocations. J.Orthop.Trauma 2000;14:354-8.

8. Bano KY, Kahlon RS. Radial head fractures--advanced techniques in surgical management and rehabilitation. J.Hand Ther. 2006;19:114-35.

9. Amis AA, Miller JH, Dowson D, Wright V. Biomechanical aspects of the elbow: joint forces related to prosthesis design. Engineering in Medicine 1981;10:65-8.

10. Hotchkiss RN, Weiland AJ. Valgus stability of the elbow. J.Orthop.Res. 1987;5:372-7.

11. Armstrong AD, Dunning CE, Faber KJ, Duck TR, Johnson JA, King GJ. Rehabilitation of the medial collateral ligament-deficient elbow: an in vitro biomechanical study. J.Hand Surg.[Am.] 2000;25:1051-7.

12. Funk DA, An KN, Morrey BF, Daube JR. Electromyographic analysis of muscles across the elbow joint. J.Orthop.Res. 1987;5:529-38.

13. Amis AA, Dowson D, Wright V. Muscle strengths and musculo-skeletal geometry of the upper limb. Engineering in Medicine 1979;8:41-8.

14. Dunning CE, Duck TR, King GJ, Johnson JA. Simulated active control produces repeatable motion pathways of the elbow in an in vitro testing system. J.Biomech. 2001;34:1039-48.

15. King GJ, Zarzour ZD, Rath DA, Dunning CE, Patterson SD, Johnson JA. Metallic radial head arthroplasty improves valgus stability of the elbow. Clin.Orthop.Relat Res. 1999;114-25.

16. Dunning CE, Zarzour ZD, Patterson SD, Johnson JA, King GJ. Ligamentous stabilizers against posterolateral rotatory instability of the elbow. J.Bone Joint Surg.Am. 2001;83-A:1823-8.

17. Schwab GH, Bennett JB, Woods GW, Tullos HS. Biomechanics of elbow instability: the role of the medial collateral ligament. Clin.Orthop.Relat Res. 1980;42-52.

18. Regan WD, Korinek SL, Morrey BF, An KN. Biomechanical study of ligaments around the elbow joint. Clin.Orthop.Relat Res. 1991;170-9.

19. Morrey BF, An KN. Articular and ligamentous contributions to the stability of the elbow joint. Am.J.Sports Med. 1983;11:315-9.

20. Morrey BF, An KN. Functional anatomy of the ligaments of the elbow. Clin.Orthop.Relat Res. 1985;84-90.

21. Morrey BF, Tanaka S, An KN. Valgus stability of the elbow. A definition of primary and secondary constraints. Clin.Orthop.Relat Res. 1991;187-95.

22. Sojbjerg JO, Ovesen J, Nielsen S. Experimental elbow instability after transection of the medial collateral ligament. Clin.Orthop.Relat Res. 1987;186-90.

23. Callaway GH, Field LD, Deng XH et al. Biomechanical evaluation of the medial collateral ligament of the elbow. J.Bone Joint Surg.Am. 1997;79:1223-31.

24. Floris S, Olsen BS, Dalstra M, Sojbjerg JO, Sneppen O. The medial collateral ligament of the elbow joint: anatomy and kinematics. J.Shoulder.Elbow.Surg. 1998;7:345-51.

25. Fuss FK. The ulnar collateral ligament of the human elbow joint. Anatomy, function and biomechanics. J.Anat. 1991;175:203-12.

26. Beingessner DM, Dunning CE, Gordon KD, Johnson JA, King GJ. The effect of radial head excision and arthroplasty on elbow kinematics and stability. J.Bone Joint Surg.Am. 2004;86-A:1730-9.

27. Jensen SL, Olsen BS, Sojbjerg JO. Elbow joint kinematics after excision of the radial head. J.Shoulder.Elbow.Surg. 1999;8:238-41.

CHAPTER 6

Conclusions and Future Directions

Overview: This chapter is a summary of the key findings in Chapters 3, 4, and 5. Future directions for research are also outlined.

6.1 OVERVIEW OF KEY FINDINGS

6.1.1 Quantification of Medial Collateral Ligament Tension in the Elbow (Chapter 3)

Human tendon and ligament forces of the upper extremity have not, to our knowledge, been studied to date. An understanding of the magnitudes of AMCL tension through the arc of elbow flexion has important implications with respect to the desired target strength of repair and reconstruction techniques. In Chapter 3, it was shown that, for both the valgus and dependent positions, AMCL tension increased with increasing angles of elbow flexion (*i.e.* AMCL tension was greater at full flexion than at full extension). Comparing valgus and dependent position AMCL tensions, the AMCL tension curves in the valgus position had a decreasing slope throughout the arc of elbow flexion, whereas the AMCL tension curves in the dependent position had an increasing slope. When comparing the elbow kinematics and AMCL tension levels in the valgus position to those of the dependent position, greater valgus angulations and AMCL tension levels were observed in the valgus position. Furthermore, for the valgus position, AMCL tension levels were observed to increase with increasing specimen mass.

The buckle transducer was found to have good repeatability, as the results of the repeatability investigation yielded standard deviations which were small both in terms of magnitude, and when expressed as percentages of the mean AMCL tensions.

6.1.2 Effect of Wrist Flexor Muscle Loading on Medial Collateral Ligament Tension in the Elbow (Chapter 4)

This investigation showed that AMCL tension levels and elbow kinematics are altered with simulated wrist flexor muscle loading. For both the valgus and dependent positions, increased wrist flexor muscle loading caused the elbows to track in greater varus and the AMCL tension levels to decrease. When comparing the elbow kinematics and AMCL tension levels in the valgus position to those of the dependent position, greater valgus angulations and AMCL tension levels were observed in the valgus position. Additionally, a quasi-linear AMCL tension – valgus angulation response was observed for the valgus position, suggesting that the change in AMCL tension levels was strongly correlated with a change in the valgus position of the ulna. In contrast, for the dependent position, a somewhat non-linear AMCL tension – valgus angulation response was observed.

Therefore, strengthening and activation of the wrist flexor muscles should be considered to prevent MCL injury, and to assist in rehabilitation. Furthermore, the valgus orientation of the arm should be avoided during rehabilitation to minimize AMCL loading.

6.1.3 Effect of Radial Head Excision and Arthroplasty on Medial Collateral Ligament Tension in the Elbow (Chapter 5)

This study demonstrated that AMCL tension levels and elbow kinematics are altered following radial head excision, and that metallic radial head arthroplasty restores near-normal AMCL tension levels and elbow kinematics. For both the valgus and dependent positions, radial head excision increased AMCL tension levels and shifted the motion pathways of the elbow into greater valgus. Radial head arthroplasty restored valgus stability and AMCL tension levels similar to those quantified after sectioning and repair of the annular ligament with the native radial head. When comparing the elbow kinematics and AMCL tension levels in the valgus position to those of the dependent position, greater valgus angulations and AMCL tension levels were observed in the valgus position. Additionally, a quasi-linear AMCL tension – valgus angulation response was observed for both the valgus and dependent positions, suggesting that the change in

AMCL tension levels was strongly correlated with a change in the valgus position of the ulna.

Therefore, these findings confirmed the importance of the radial head in resisting valgus angulation and offloading the medial soft tissue structures.

6.2 FUTURE WORK

All AMCL tension and valgus angulation measurements presented in this thesis were obtained with the forearm maintained in neutral rotation; therefore, future investigations into the effect of forearm rotation (*i.e.* pronation and supination) on AMCL tension levels would provide further insight into the biomechanics of this tissue. While only five specimens were studied, due to the consistent nature of the AMCL tension trends, these data are felt to be representative. However, our relatively small sample size may have precluded our ability to detect differences between conditions and therefore, more specimens need to be tested (*i.e.* as statistical power increases, the chances of a Type II error decreases).

It is our hope that this improved knowledge of AMCL tissue biomechanics will allow for the design and evaluation of improved methods of AMCL repair/reconstruction and rehabilitation, and assist in the development of an artificial AMCL and *in vitro* biomechanical models of the elbow. Furthermore, this device will permit numerous additional projects to be explored that will investigate the ligament and soft tissue loading at the elbow, shoulder, and wrist.

LIST OF TABLES FOR APPENDICES

Appendix 3

Appendix 4

Appendix 5

Appendix 7

Appendix 8

Appendix 9

Appendix 10

LIST OF FIGURES FOR APPENDICES

Appendix 2

Appendix 4

Appendix 5

Appendix 6

Appendix 7

Appendix 10

APPENDIX 1

Glossary

Active Motion — Muscle forces used to move the joint.

Algorithm — A sequence of finite instructions, often used for calculation and data processing; a precise step-by-step plan for a computational procedure that begins with an input value and yields an output value in a finite number of steps.

Anatomical Position — Body upright, with the head, gaze (eyes), and toes directed anteriorly (forward), the lower limbs close together with the feet parallel and the toes directed anteriorly, and the arms adjacent to the sides with the palms facing anteriorly.

Anconeus — A muscle originating from a broad site on the posterior aspect of the lateral epicondyle of the humerus and from the lateral triceps fascia, and inserts into the lateral dorsal surface of the proximal ulna; its primary role is that of a joint stabilizer.

Antagonist — A muscle that counteracts the action of another muscle, its agonist.

Anterior — Situated at or directed toward the front; opposite of posterior; refers to the front surface of the human body.

Anthropometry — A branch of science studying the measurement of size, weight and proportions of the human body.

Attrition — A reduction or decrease in strength.

Arthritis — Inflammation of a joint characterized by pain and swelling.

Arthroplasty — Surgical repair or replacement of a joint; the operative formation or restoration of a joint.

Articular Surface	The end of the bone that forms a synovial joint.
Articulate	To unite by forming a joint or joints; consisting of segments united by joints.
Biceps Brachii	The large muscle of the upper arm on the anterior surface of the humerus, arising from two separate origins from the scapula, and whose action flexes the elbow and supinates the forearm.
Brachialis	The largest of the muscles that act to flex the elbow.
Brachioradialis	A muscle that originates near the lateral epicondyle of the humerus and inserts at the base of the styloid process of the radius; a strong elbow flexor.
Cadaver	Of, or pertaining to, a dead body preserved for anatomical study.
Cancellous Bone	Also known as trabecular bone, this osseous tissue is normally present in the interior of many bones, where the spaces are usually filled with marrow; of a reticular, spongy, or lattice-like structure.
Capitellum	A small eminence on the distal end of the humerus that articulates with the radius.
Comminuted	Broken or crushed into small pieces.
Common Extensors	A group of muscles that originate from the lateral epicondyle of the humerus and act to extend the wrist and digits.
Common Flexors	A group of muscles that originate from the medial epicondyle of the humerus and act to flex the wrist and digits.
Compression	The act of pressing upon or together; the state of being pressed together.
Coronoid	The anterior-most aspect of the proximal ulna forming part of the greater sigmoid notch.
Cortical Bone	Also known as compact bone, this osseous tissue is dense and forms the surface of bones; the hard, rigid osseous tissue.

Distal	Anatomically located far from a point of reference, such as an origin or a point of attachment; used to describe structures in limbs.
Dislocation	Displacement of a bone from its normal articulation with a joint.
Dorsal	Of, toward, on, in or near the back; opposite of volar.
Electromyography	The recording and study of the electrical properties of skeletal muscle.
Epicondyle	A rounded projection close to the knuckle-shaped surface (*i.e.* condyle), usually serving as a point of attachment for ligaments and tendons.
Excision	To remove by cutting.
Extension	The movement by which the two ends of any jointed part are drawn away from each other; a movement bringing the members of a limb into or toward a straight condition.
Extensor	Any muscle that extends a joint.
External (Lateral) Rotation	The act of rotating away from the mid-line of the body; supination.
Flexion	The act of bending a joint or limb in the body; the resulting condition of being bent.
Flexor	Any muscle that flexes a joint.
Force	The tension developed in a ligament/tendon during motion.
Fossa	In anatomy, a hollow or depressed area.
Greater Sigmoid Notch	An aspect of the proximal ulna that articulates with the trochlea of the humerus.
Inferior	In anatomy, used in reference to the lower surface of a structure, or to the lower of two (or more) similar structures.

Internal (Medial) Rotation	The act of rotating toward the mid-line of the body; pronation.
In Situ	In place; localized and confined to one area.
In Vitro	In an artificial environment outside the living organism.
In Vivo	Within the living organism.
Joint Capsule	A sheet of fibrous connective tissue enclosing a synovial joint and lined with a synovial membrane.
Kinematics	The branch of mechanics dealing with the study of the motion of a body or a system of bodies without consideration given to its mass or the forces acting on it; the study of motion of one body with respect to another.
Lateral	Denoting a position farther from the mid-line of the body or a structure.
Lesser Sigmoid Notch	An aspect of the proximal, lateral ulna that articulates with the proximal end of the radius (*i.e.* radial head).
Ligament	A band of fibrous tissue connecting bones or cartilages, serving to support and strengthen the joints.
Medial	Situated toward the mid-line of the body or a structure.
Olecranon	The large process on the upper end of the ulna that projects behind the elbow joint and forms the point of the elbow; the bony projection of the ulna at the elbow.
Osseous	Composed of, containing, or resembling bone; bony.
Orthopaedics	The branch of surgery dealing with the preservation and restoration of the function of the skeletal system, its articulations, and associated structures.
Osteoarthritis	A non-inflammatory, degenerative joint disease marked by degeneration of the articular cartilage and bone at joint margins, and changes in the synovial

	membrane, accompanied by pain and stiffness; also know as osteoarthrosis, degenerative arthritis, degenerative joint disease; is the most common form of arthritis.
Osteotomy	A surgical operation whereby a bone is cut to shorten, lengthen, or change its alignment.
Passive Motion	External object or being moves the joint with no muscle activation.
Physiological	In accordance with or characteristic of the normal functioning of a living organism.
Posterior	Directed toward or situated at the back; opposite of anterior; refers to the back surface of the human body.
Pronation	Applied to the hand, the act of turning the palm backward (posteriorly) or downward, performed by medial rotation of the forearm; the rotation of the forearm so that the palm of the hand faces downward or backward.
Proximal	Anatomically located close to a point of reference, such as an origin or a point of attachment; used to describe structures in limbs.
Radial Head	An anatomical structure resembling a cylinder that forms the proximal end of the radius, which articulates with the capitellum of the humerus and the lesser sigmoid notch of the ulna.
Radiohumeral	Pertaining to the radius and humerus.
Radioulnar	Pertaining to the radius and ulna.
Radius	A long, slightly curved bone that lies to the lateral side of the forearm when in the anatomical position; the shorter and thicker of the two forearm bones.
Range of Motion	The range, measured in degrees of a circle, through which a joint can be extended and flexed.
Rheumatoid Arthritis	An autoimmune disorder where the body attacks itself such that there is inflammation of the lining of

	the joint (synovium) which progresses to joint damage and in few cases, deformity; a form of arthritis that causes pain, swelling, stiffness and loss of function in your joints.
Strain	Ratio of the change in length due to application of a stress to the initial unstressed length; the elongation undergone by a tendon and ligament during motion.
Subluxation	Incomplete or partial dislocation.
Superior	Situated above, or directed upward.
Supination	Applied to the hand, the act of turning the palm forward (anteriorly) or upward, performed by lateral rotation of the forearm; the rotation of the forearm so that the palm of the hand faces upward.
Suture	A stitch or series of stitches made to secure tissues or close wounds; a material used in closing a wound with stitches.
Ulnar Styloid Process	A bony protrusion on the distal ulna used in defining the ulnar coordinate system at the elbow.
Tension	The act of pulling or straining until taut.
Transection	A cross-section; division by cutting transversely.
Triceps Brachii	A three-headed muscle of the upper arm on the posterior surface of the humerus, and whose action extends the forearm.
Ulnohumeral	Pertaining to the ulna and humerus.
Valgus	Bent outward; denoting angulation away from the mid-line of the body.
Varus	Bent inward; denoting angulation toward the mid-line of the body.
Volar	Pertaining to the sole or palm; indicating the flexor surface of the forearm, wrist, or hand; opposite of dorsal.

APPENDIX 2

Anatomical Planes of the Body

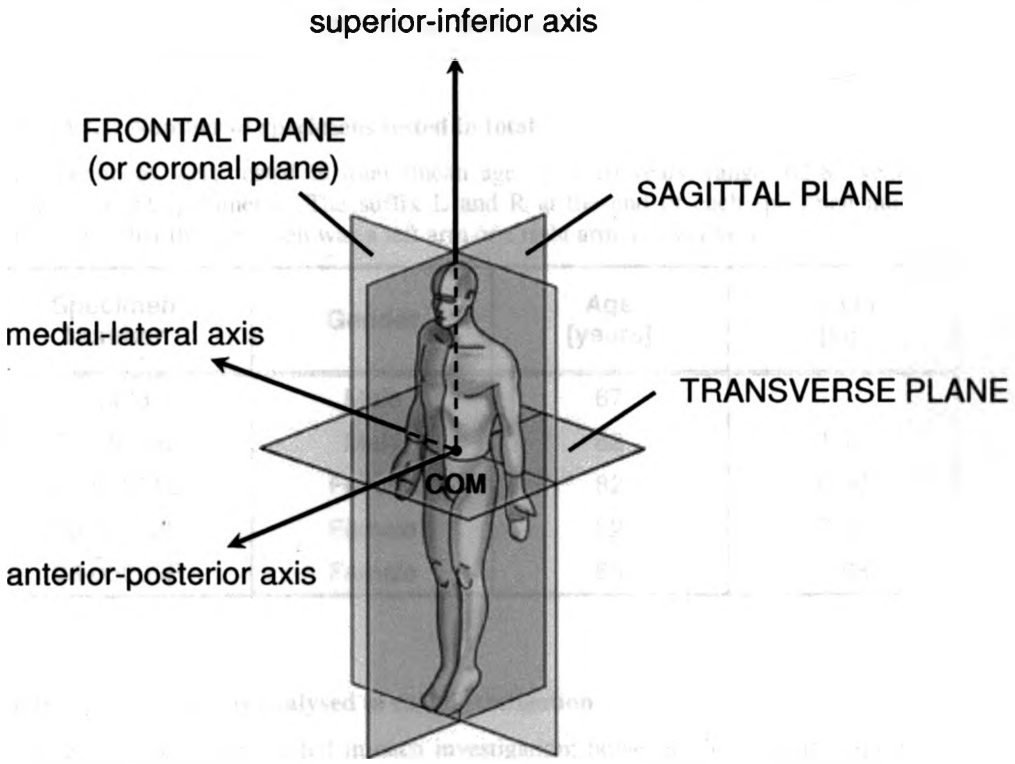

Figure A2.1: Anatomical planes of the body*

The position of the body can be described in relation to a three-dimensional coordinate system. The three-dimensional coordinate system for the body has its origin at the centre of mass (COM) and forms three planes which are at right angles to one another; the sagittal plane divides the body into left and right halves, the transverse plane divides the body into upper and lower halves, and the frontal (or coronal) plane divides the body into front and back halves.

* Rendition of the figure obtained from
<http://training.seer.cancer.gov/anatomy/body/terminology.html#planes>

APPENDIX 3

Specimen Information

Specimens were procured following the guidelines of our institution (The University of Western Ontario) and the government regulatory agencies.

Table A3.1: Number of specimens tested in total

Five specimens were tested in total (mean age 72 ± 10 years; range: 62-82 years; 3 female; 1 right specimen). The suffix L and R at the end of each specimen number denotes whether the specimen was a left arm or a right arm, respectively.

Specimen Number	Gender	Age [years]	Mass [kg]
(1) 08-04082L	Male	67	—
(2) 08-05088L	Male	82	1.15
(3) 08-04051L	Female	82	0.90
(4) 08-04052L	Female	62	0.55
(5) 08-05009R	Female	65	0.68

Table A3.2: Specimens analysed in each investigation

All five specimens were tested in each investigation; however, due to data acquisition difficulties, only select data was used for analysis. Summarized below are the specimens analysed for each investigation.

Investigation	Position	Specimens	Mean Age [years]
Chapter 3 *Native AMCL*	Valgus	1 – 5	72 ± 10
	Dependent	1 – 3, 5	74 ± 9
Chapter 4 *WF Muscle Loading*	Valgus	2 – 5	73 ± 11
	Dependent	2 – 3, 5	76 ± 10
Chapter 5 *RH Excision & Arthroplasty*	Valgus	1 – 5	72 ± 10
	Dependent	1 – 3, 5	74 ± 9

APPENDIX 4

Appendix to Chapter 2 (Part I)
Strain Gauge Physical Principles and Specifications

A4.1 PHYSICAL PRINCIPLES OF THE STRAIN GAUGE

The strain gauge used was of resistive type. Resistive type strain gauges consist of one or more metal foil element(s) arranged in various patterns, which are supported on an insulated flexible backing. These types of strain gauges are bonded to the object in which the strain is to be measured from, using a suitable adhesive; recall that the strain gauge was bonded to the top surface of the transducer's centre beam.

As the object to which the strain gauge is bonded to is deformed or strained, the metal foil element(s) of the strain gauge are deformed. This deformation of the metal foil element(s) causes the electrical resistance (R) of the strain gauge to change; this change in resistance (ΔR) is measured using a Wheatstone bridge. The equation for electrical resistance is defined by Equation A4.1.

$$R = \frac{\rho L}{A}$$

Equation A4.1: Calculation of electrical resistance

In the above equation, R is the electrical resistance, L is the length of the conductive metal wire, A is the cross-sectional area of the conductive metal wire, and ρ is the resistivity of the conductive metal wire material. The change in resistance (ΔR) across the strain gauge, measured by the Wheatstone bridge, can be related to the strain (ε) by the quantity known as the gauge factor (GF). Therefore, the strain can be calculated using Equation A4.2.

$$\varepsilon = \frac{1}{GF} \cdot \frac{\Delta R}{R}$$

Equation A4.2: Calculation of strain

In the above equation, ε is the strain, GF is the gauge factor, ΔR is the change in resistance across the strain gauge, and R is the nominal gauge resistance or the resistance of the undeformed strain gauge. Nominal resistance, which is supplied by the manufacturer, is the intended resistance of the strain gauge as designed; the actual resistance may vary due to manufacturing tolerances and effects of installation.* Gauge factor is a measure of the sensitivity of the strain gauge; it is the ratio of the fractional change in resistance to the fractional change in length (*i.e.* strain) along the axis of the gauge.† A larger gauge factor implies a larger change in resistance for a given strain, which is advantageous as a larger change in resistance is easier to measure accurately. Gauge factor is a dimensionless quantity and is supplied by the manufacturer. Gauge factor is defined by Equation A4.3.

$$GF = \frac{\left(\frac{\Delta R}{R}\right)}{\left(\frac{\Delta L}{L}\right)} = \frac{\left(\frac{\Delta R}{R}\right)}{\varepsilon}$$

Equation A4.3: Calculation of gauge factor

In the above equation, strain (ε) is defined as the change in length (ΔL) of the conductive material per unit of the original length (L) of the conductive material (*i.e.* it is the fractional change in length of the conductive material); all other parameters are as previously defined.

A4.1.1 Wheatstone Bridge Configuration: Half-Bridge Type I

The particular type of Wheatstone bridge configuration used for the strain gauge in this study was a half-bridge type I configuration (also known as a half Poisson bridge configuration). The half-bridge type I configuration is used to measure either axial or bending strain; however, their electrical circuit arrangements are identical. This circuit consists of two uniaxial active strain gauges that are perpendicular to each other; one gauge is aligned along the axis of the applied strain, and the other gauge is aligned along the transverse axis to detect the Poisson's effect (Figure 2.2). In order to further discuss

---

* *Interactive Guide to Strain Gauge Technology, Glossary (Technical Terms)*, Vishay Micro-Measurements, 2001 <www.vishay.com/company/brands/measurements-group/guide/index.htm>

† *Practical Strain Gauge Measurements*, Agilent Technologies, 1999 <http://www.omega.com/techref/pdf/StrainGage_Measurement.pdf>

the advantages of this type of Wheatstone configuration for the buckle transducer, an understanding of some practical considerations of using strain gauges is first required.

All resistive strain gauges are designed to be sensitive to the strain in the direction parallel to the metal foil element and insensitive to the strain perpendicular to the metal foil element; however, these gauges still detect very small levels of transverse strain. Furthermore, temperature effects require consideration for these types of gauges, as thermal expansion/contraction of the specimen (*i.e.* the material the strain gauge is bonded to) and changes in gauge resistance occur with changes in temperature (*i.e.* resistivity is a function of temperature). Thus, if a single uniaxial gauge aligned in the direction of the applied strain was to be used to detect the applied strain in the buckle transducer (via a quarter-bridge type I configuration), the strain measurement obtained would be an inaccurate measurement of purely the applied strain, as its signal would include the effects of the small sensitivity to the transverse strain, as well as the temperature effects.

Conversely, perpendicularly mounting two individual uniaxial active gauges to the centre beam of the buckle transducer (*i.e.* the half-bridge type I configuration), the effects of the transverse strain and temperature on the strain gauge aligned in the direction of the applied strain can be compensated. To elaborate, as this configuration has a transversely oriented strain gauge which measures the strain due to the Poisson's effect of the transducer material, this strain measurement can be used to nullify the transverse strain effects on the applied strain measurement. Additionally, as both strain gauges experience the same temperature effects, the temperature effects on the applied strain measurement can be nullified. The net effect is a more accurate representation of purely the applied strain as both the transverse strain and temperature effects on the strain gauge in the direction of the applied strain can be nullified through the use of the signal of the transversely oriented gauge.

To construct the Wheatstone half-bridge type I configuration for the buckle transducer, instead of using two individual uniaxial strain gauges as discussed above, a tee rosette strain gauge was used, as this was a more compact alternative; the size of the transducer was required to be small. The half-bridge type I circuit diagram is shown in Figure A4.1.

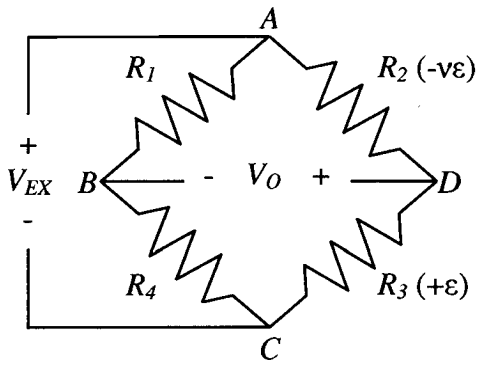

Figure A4.1: Half-bridge type I circuit diagram

In this circuit diagram, a primary gauge (R_3) is paired with a transverse gauge (R_2) to measure Poisson's strain and provide temperature compensation. The components of the circuit diagram are defined below.

The components of the half-bridge type I circuit diagram (Figure A4.1) are defined as follows:

- R_1 and R_4 are half-bridge completion resistors
- R_2 is the active strain gauge element measuring the transverse strain due to the effects of the Poisson's ratio of the transducer material (–νε)
- R_3 is the active strain gauge element measuring the applied strain (+ε)
- V_{EX} is the excitation voltage; excitation voltage is the nominal voltage required for excitation of a circuit
- V_O is the measured signal's voltage or output voltage

Using Ohm's and Kirchhoff's law, the current that flows through branches *ABC* and *ADC* in Figure A4.1 (I_{ABC} and I_{ADC}, respectively) are defined by Equation A4.4 and Equation A4.5, respectively.

$$I_{ABC} = \frac{V_{EX}}{R_1 + R_4}$$

Equation A4.4: Calculation of the current through branch ABC

$$I_{ADC} = \frac{V_{EX}}{R_2 + R_3}$$

Equation A4.5: Calculation of the current through branch ADC

Seeking the output voltage (V_O), which is defined as $V_O = V_D - V_B$, expressions for the voltage drops across R_4 and R_3 are necessary. Using Ohm's law again, the voltage drop across R_4 is $V_B - V_C$, which equals $I_{ABC}R_4$, and the voltage drop across R_3 is $V_D - V_C$, which equals $I_{ADC}R_3$. Thus, the output voltage (V_O) can be expressed by Equation A4.6.

$$V_O = (V_D - V_C) - (V_B - V_C)$$
$$= I_{ADC} R_3 - I_{ABC} R_4$$

Equation A4.6: Calculation of the output voltage

Substituting the expressions for the currents (I_{ABC} and I_{ADC}) and simplifying, the simplified expression for the output voltage (V_O) is defined by Equation A4.7.

$$V_O = \frac{R_3 V_{EX}}{R_2 + R_3} + \frac{R_4 V_{EX}}{R_1 + R_4}$$
$$= V_{EX} \frac{R_3 R_1 + R_3 R_4 - R_4 R_2 + R_3 R_4}{(R_2 + R_3)(R_1 + R_4)}$$
$$= V_{EX} \frac{R_3 R_1 - R_4 R_2}{(R_2 + R_3)(R_1 + R_4)}$$

Equation A4.7: Simplified calculation of the output voltage

When the transducer's centre beam deflects, the strain gauge metal foil elements become strained, which changes the resistance of the axially and transversely oriented metal foil elements by ΔR_3 and ΔR_2, respectively. These resistance changes consequently cause the output voltage (V_O) to change. Therefore, the Wheatstone bridge circuit converts a resistance change to a voltage change. This change in the output voltage (*i.e.* strained versus unstrained) is used to determine the strain measurement via a LabVIEW program (National Instruments, Austin, TX). This LabVIEW program requires prior definition of various parameters pertaining to the strain gauge and the Wheatstone bridge circuitry in order to perform the voltage to strain conversion; some of these parameters include: the gauge factor (GF), the nominal strain gauge resistance (R), and the Poisson's ratio of the specimen material.

A4.2 STRAIN GAUGE SELECTION

The minimum dimensions (*i.e.* length and width) of the transducer's centre beam were dictated by the size of the strain gauge used for monitoring the bending beam. Referring to Figure A4.2, which shows a single element strain gauge, the overall pattern length and width correspond to the dimensions of the metal foil element, excluding the backing. The matrix width and length are the dimensions of the flexible backing of the strain gauge. Trimming away the excess backing of the strain gauge reduces the size of the strain

gauge, which was desirable in order to reduce the dimensions of the transducer's centre beam. The backing of the strain gauge could be trimmed on all sides to within 0.005 inches or 0.127 mm of the overall pattern dimensions without altering the performance of the strain gauge. Therefore, the trimmed dimensions are obtained by adding 0.010 inches or 0.254 mm to the overall pattern length and width dimensions; these dimensions included the solder tabs. The trimmed length and width of the miniature 90° two-element tee rosette strain gauge are presented in Table A4.1. Additionally, a summary of the technical data of the strain gauge is presented in Table A4.2.

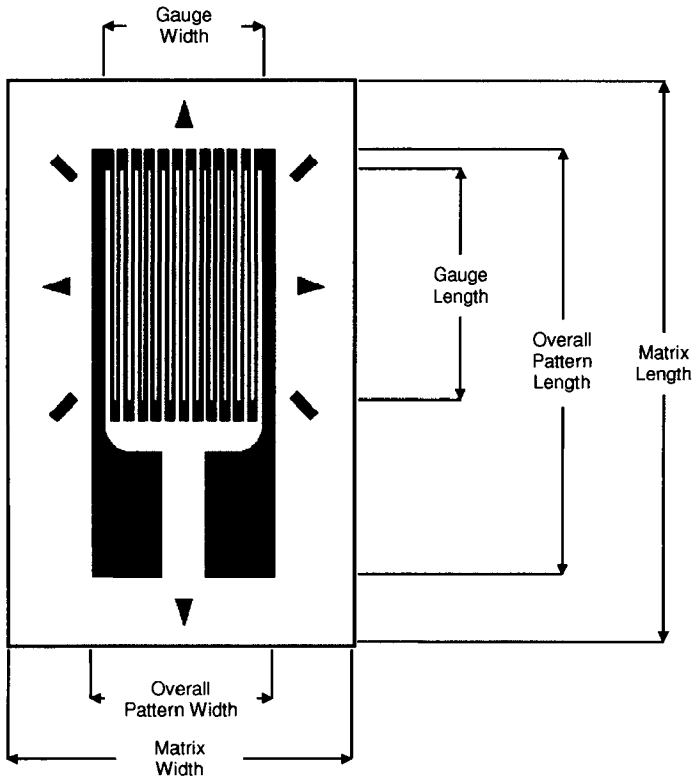

Figure A4.2: Diagram of a single-element resistive strain gauge showing relevant dimensions*

The strain gauge is more sensitive to strain in the direction parallel to the metal foil element than to strain perpendicular to the metal foil element. The markings outside the active area help to align the gauge during installation.

* Rendition of a figure found in *Interactive Guide to Strain Gauge Technology, Glossary (Technical Terms)*, Vishay Micro-Measurements, 2001 <www.vishay.com/company/brands/measurements-group/guide/index.htm>

Table A4.1: Trimmed length and width of the miniature 90° two-element tee rosette strain gauge

Overall Pattern Length	0.19 in × 25.4 mm·in^{-1} = 4.83 mm
Trimmed Length	(0.19 in + 0.01 in) × 25.4 mm·in^{-1} = **5.08 mm**
Overall Pattern Width	0.06 in × 25.4 mm·in^{-1} = 1.52 mm
Trimmed Width	(0.06 in + 0.01 in) × 25.4 mm·in^{-1} = **1.78 mm**

Table A4.2: Summary of the technical data of the miniature 90° two-element tee rosette strain gauge

Nominal Gauge Resistance at 24ºC (in ohms)		120.0 ± 0.8%
Temperature Coefficient of gauge factor (%/100ºC)		+1.2 ± 0.2
Tee rosette metal foil element	**Gauge Factor at 24ºC**	**Transverse Sensitivity at 24ºC**
Axially oriented metal foil element	2.04 ± 1.0%	(+0.7 ± 0.2)%
Transversely oriented metal foil element	1.99 ± 1.0%	(+1.2 ± 0.2)%
Nominal	2.02 ± 2.5%	—

Where: ·Temperature coefficient* of the gauge factor is the ratio of the unit variation of the gauge factor to the temperature variation

·Transverse sensitivity† factor (K_t) is defined as $K_t = \frac{GF(transverse)}{GF(longitudinal)}$

* *Interactive Guide to Strain Gauge Technology, Glossary (Technical Terms)*, Vishay Micro-Measurements, 2001 <www.vishay.com/company/brands/measurements-group/guide/index.htm>

† *Practical Strain Gauge Measurements*, Agilent Technologies, 1999 <http://www.omega.com/techref/pdf/StrainGage_Measurement.pdf>

APPENDIX 5

Appendix to Chapter 2 (Part II)
Details of the Buckle Transducer Design Process

A5.1 PRELIMINARY DESIGN CONSIDERATIONS

A5.1.1 Free Body Diagram Analysis

A free body diagram (FBD) analysis of the forearm oriented in the valgus gravity-loaded position (Figure A5.1) was performed to determine the maximum tension expected to be experienced by the anterior bundle of the medial collateral ligament (AMCL).

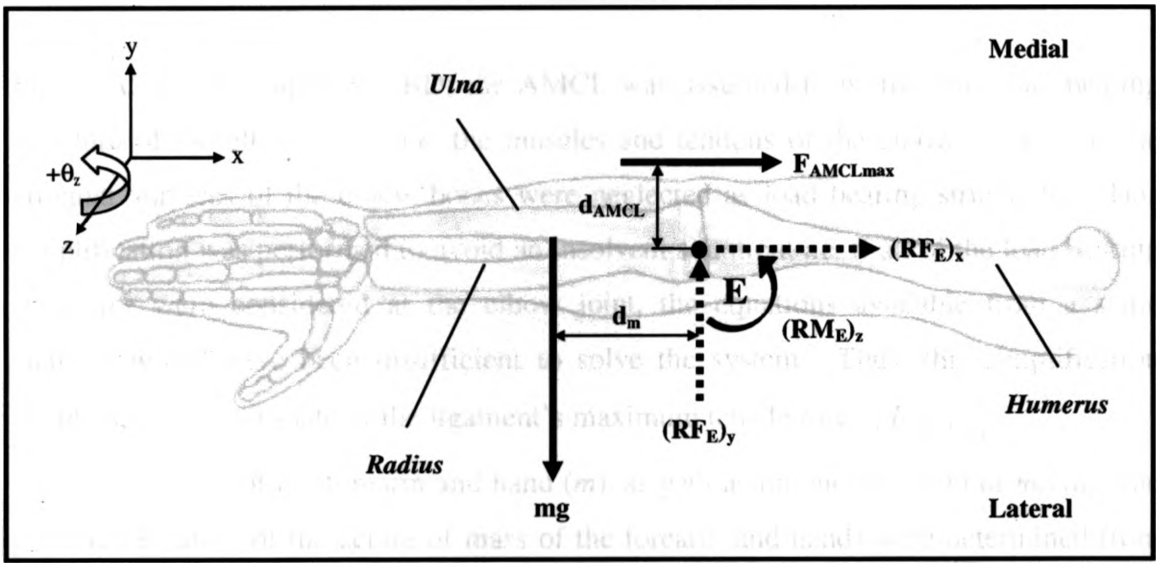

Figure A5.1: Free body diagram of the forearm oriented in the valgus gravity-loaded position

The AMCL was assumed to be the only load bearing structure of the elbow joint. Furthermore, it was assumed to be parallel to the long axis of the forearm and perpendicular to the direction of gravity. The variables of the free body diagram are defined below.

The variables of the free body diagram (Figure A5.1) are defined as follows:

Where:

m	mass of the forearm and hand
g	acceleration due to gravity
d_m	moment arm of mg (or the proximal location of the centre of mass of the forearm and hand)
$F_{AMCL_{\max}}$	maximum tension expected to be experienced by the AMCL
d_{AMCL}	moment arm of the AMCL force $F_{AMCL_{\max}}$
$(RE_E)_x$ $(RE_E)_y$ $(RM_E)_z$	resultant forces and moment acting at the elbow joint

Note: The fulcrum was taken to be the centre of the elbow joint.

Figure A5.1 is a simplified FBD; the AMCL was assumed to be the only load bearing structure of the elbow joint (*i.e.* the muscles and tendons of the elbow, as well as the articular surfaces of the elbow bones were neglected as load bearing structures). This simplification was performed to avoid an insolvent situation; *i.e.* if all of the load bearing structures were considered at the elbow joint, the equations available from a static analysis would have been insufficient to solve the system. Thus, this simplification results in an overestimate of the ligament's maximum tensile force ($F_{AMCL_{\max}}$).

The mass of the forearm and hand (m), as well as the moment arm of mg (d_m, the proximal location of the centre of mass of the forearm and hand) were determined from anthropometric measurements.[1] To perform these calculations, the average mass (M) and height (H) of a Canadian male (42 ± 22 years) were used: 83.2 kg and 1.78 m, respectively.[2]

Mass of the forearm and hand,

$$m = 0.022 \cdot M = 0.022 \cdot (83.2\,\text{kg}) = 1.830\,\text{kg}$$

Length of the forearm and hand,

$$L_{forearm+hand} = (0.630 - 0.377) \cdot H = (0.630 - 0.377) \cdot (1.78\,\text{m}) = 0.4503\,\text{m}$$

Proximal location of the centre of mass of the forearm and hand,

$$d_m = 0.682 \cdot L_{forearm+hand} = 0.682 \cdot (0.4503\,\text{m}) = 0.3071\,\text{m}$$

To calculate the maximum tension expected to be experienced by the AMCL ($F_{AMCL_{\max}}$), the lever arm for the AMCL (d_{AMCL}, the distance between the AMCL and the centre of the elbow joint) was directly measured from a cadaveric upper extremity, and was found to be 50 mm (0.05 m).

Using the above information, an external analysis was performed to calculate the resultant forces and moments acting at the elbow joint. Balancing the forces and taking the moment about the centre of the elbow joint, the resultant forces and moment were determined as follows:

$$0 = Internal - External$$

$$\sum F_x = 0 = RF_{x_{proximal}} - \sum F_{x_{external}}$$
$$\sum F_x = 0 = RF_{E_x} - 0$$

$$\sum F_y = 0 = RF_{y_{proximal}} - \sum F_{y_{external}}$$
$$\sum F_y = 0 = RF_{E_y} - mg$$
$$\sum F_y = 0 = RF_{E_y} - (1.830\,\text{kg})(9.81\,\text{m/s}^2)$$
$$\sum F_y = 0 = RF_{E_y} - (17.9523\,\text{N})$$

$$\sum M_z = 0 = RM_{z_{proximal}} - \sum M_{z_{external}}$$
$$\sum M_z = 0 = RM_{E_z} - mg \cdot d_m$$
$$\sum M_z = 0 = RM_{E_z} - (17.9523\,\text{N})(0.3071\,\text{m})$$
$$\sum M_z = 0 = RM_{E_z} - (5.5132\,\text{Nm})$$

Resultant forces and moment,

$$RF_{E_x} = 0$$
$$RF_{E_y} = 17.9523\,\text{N}$$
$$RM_{E_z} = 5.5132\,\text{Nm}$$

These resultant loads (forces and moment) are the loads that are produced by the internal structures of the elbow joint; these resultant loads at the proximal joint can be referred to as the internal forces and moment.

$$RM_{E_z} = F_{AMCL_{\max}} \cdot d_{AMCL}$$
$$F_{AMCL_{\max}} \cdot d_{AMCL} = 5.5132 \text{ Nm}$$
$$F_{AMCL_{\max}} = \frac{5.5132 \text{ Nm}}{d_{AMCL}} = \frac{5.5132 \text{ Nm}}{0.05 \text{ m}} = 110.2640 \text{ N} \approx 110 \text{ N}$$

Thus, the maximum tension expected to be experienced by the AMCL ($F_{AMCL_{\max}}$) was approximately 110 N. Having quantified $F_{AMCL_{\max}}$, the focus was now on the ligament parameters as well as the transducer geometry.

A5.1.2 Ligament Parameters

The first step was to define the dimensions of the relevant ligament parameters. Through literature review, the average length, width, and thickness of the AMCL were determined.[3-8]

Length of ligament, $L_{AMCL} = 27$ mm

Width of ligament, $W_{AMCL} = 5$ mm

Thickness of ligament, $T_{AMCL} = 6$ mm

Additionally, a dimension of 1 mm was approximated as the available tissue thickness to be woven through the device in all test specimens.

Tissue thickness available for weaving, $t = 1$ mm

A5.2 MATHEMATICAL MODELLING OF THE BUCKLE TRANSDUCER

A5.2.1 Transducer Geometry

From Figure A5.2, it can be observed that the maximum force acting on the centre beam ($F_{cb\max}$) is the vertical force components of the previously calculated maximum expected AMCL tension ($F_{AMCL_{\max}}$) of 110 N.

Thus, the maximum force that acts on the centre beam is:

$$F_{cb_{\max}} = 2 \cdot F_{AMCL_{\max}} \cdot \sin\theta_{\max}$$

The maximum force that acts on each outer beam is half that of the centre beam:

$$F_{ob_{\max}} = \frac{F_{cb_{\max}}}{2} = \frac{2 \cdot F_{AMCL_{\max}} \cdot \sin\theta_{\max}}{2} = F_{AMCL_{\max}} \cdot \sin\theta_{\max}$$

It can be observed that the above calculations for the maximum forces that act on the centre beam and the outer beams ($F_{cb\max}$ and $F_{ob\max}$, respectively) are dependent on the maximum ligament weaving angle (θ_{max}, the maximum angle the ligament makes with the horizontal in the *gap* region due to the ligament weaving process). To elaborate, the angle the ligament makes within the *gap* region after it has been initially woven through the transducer's frame is the maximum possible ligament weaving angle (θ_{max}), as shown in Figure A5.2. Furthermore, the expressions for the maximum forces that act on the centre beam and the outer beams ($F_{cb\max}$ and $F_{ob\max}$, respectively) assume that the maximum expected AMCL tension ($F_{AMCL\max}$) and the maximum ligament weaving angle (θ_{max}) occur simultaneously; however, this is not possible – as ligament tension is increased towards its maximum value, the beams will deflect causing the ligament weaving angle to decrease. Therefore, recalling that the value of $F_{AMCL_{\max}}$ was concluded to be an overestimate, this aforementioned assumption causes further overestimation of $F_{cb\max}$ and $F_{ob\max}$; hence, the reader should keep these points in mind when interpreting the results of the mathematical modelling process.

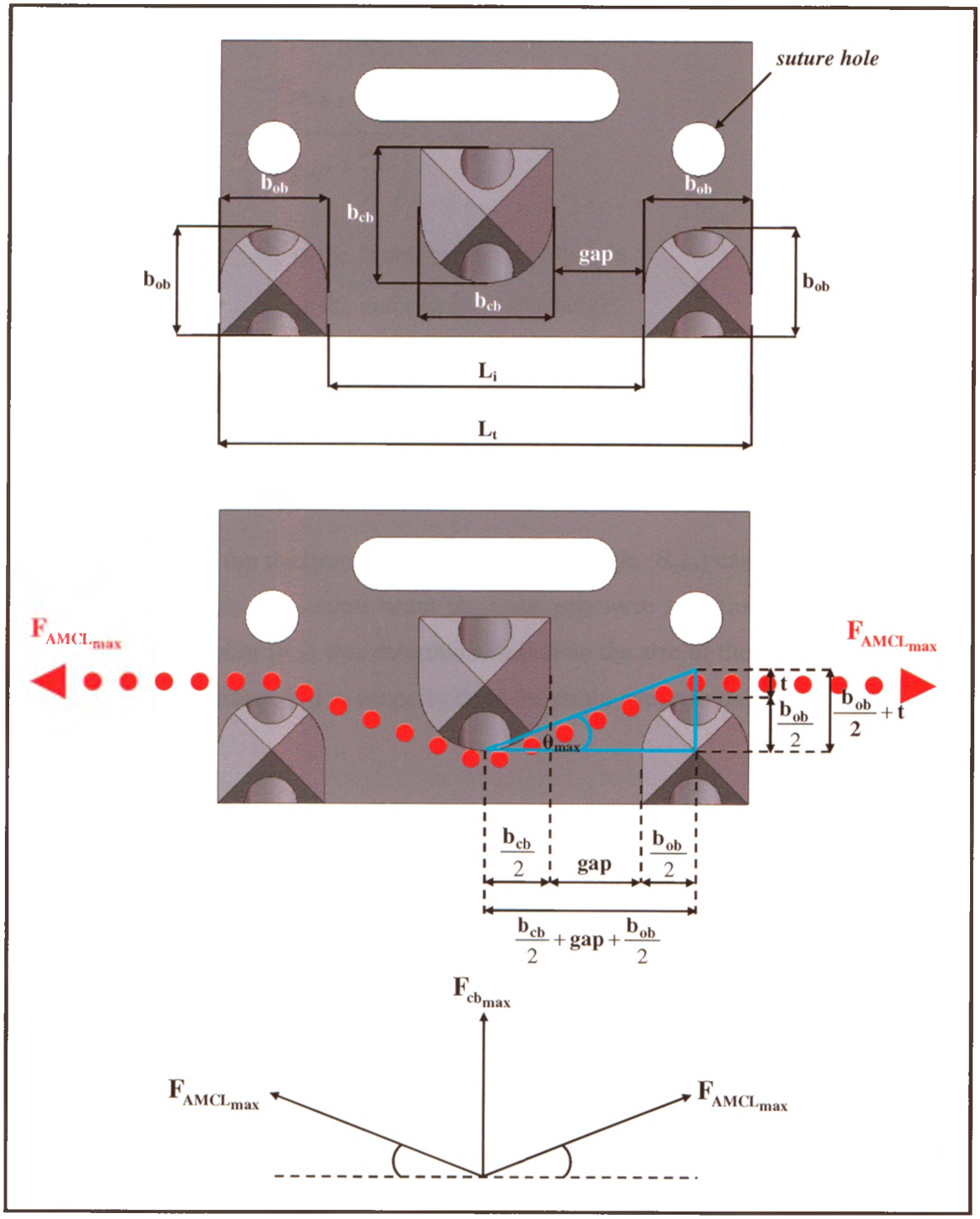

Figure A5.2: Relevant dimensions of the buckle transducer's geometry as viewed from the front

The ligament (represented by the red dots) is woven through the frame of the transducer. In this non-deflected state, the ligament weaving angle is at its maximum (θ_{max}). This figure is the same as Figure 2.3.

Through geometric relations (Figure A5.2), the maximum ligament weaving angle (θ_{max}) can be described by the following expression:

$$\theta_{\max} = \tan^{-1}\left(\frac{\frac{b_{ob}}{2} + t}{\frac{b_{cb}}{2} + gap + \frac{b_{ob}}{2}}\right)$$

Where:
- b_{cb} is the centre beam width/height
- b_{ob} is the outer beam width/height
- gap is the distance between the centre beam and the outer beams

Note: b_{cb} and b_{ob} describe both the widths and heights of the centre beam and outer beams, respectively; *i.e.* the width and height are equal, as will be discussed later.

The expression for the maximum ligament weaving angle (θ_{max}) can be further specified as the dimensions for the centre beam (b_{cb}) and gap were specified at this point. The centre beam dimension (b_{cb}) was determined based on the size of the strain gauge and the amount of tolerance required to properly bond the strain gauge to the centre beam (Figure A5.3):

Trimmed width of strain gauge, $W_{SG} = 1.78$ mm

Tolerance allotted to properly bond the strain gauge to the centre beam,

$2 \times \delta_W = 0.72$ mm

Hence, the centre beam dimension $b_{cb} = W_{SG} + 2 \cdot \delta_W = 2.5$ mm

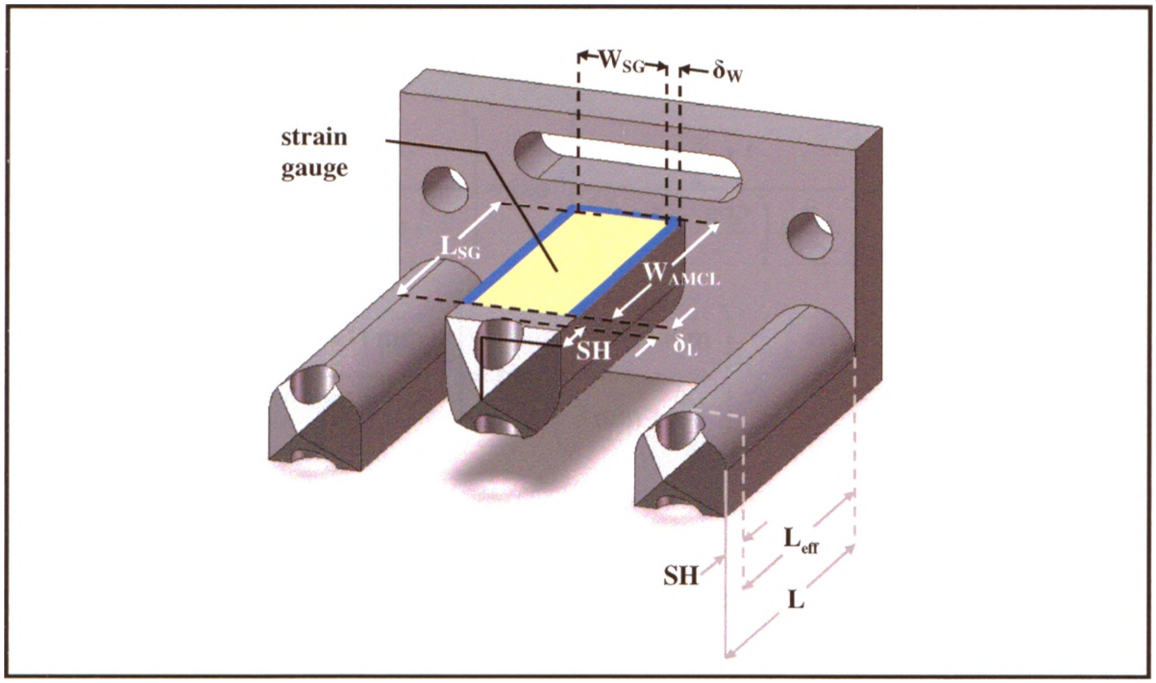

Figure A5.3: Relevant dimensions of the transducer's beams

Geometry of the transducer's beams showing the centre beam and outer beam lengths, and the centre beam width.

The *gap* dimension was determined based on visual inspection during prototype testing:

Distance between the centre beam and the outer beams, $gap = 1.75$ mm

The combination of the centre beam (b_{cb}) and *gap* dimensions composed the inner transducer length dimension (L_i), as shown in Figure A5.2:

Inner transducer length, $L_i = b_{cb} + 2 \cdot gap = 2.5\text{ mm} + 2 \cdot (1.75\text{ mm}) = 6\text{ mm}$

Hence, the maximum ligament weaving angle (θ_{max}) becomes:

$$\theta_{\max} = \tan^{-1}\left(\frac{\frac{b_{ob}}{2}+t}{\frac{b_{cb}}{2}+gap+\frac{b_{ob}}{2}}\right) = \tan^{-1}\left(\frac{\frac{b_{ob}}{2}+t}{\left(\frac{b_{cb}+2\cdot gap}{2}\right)+\frac{b_{ob}}{2}}\right) = \tan^{-1}\left(\frac{\frac{b_{ob}}{2}+t}{\left(\frac{L_i}{2}\right)+\frac{b_{ob}}{2}}\right)$$

$$= \tan^{-1}\left(\frac{\frac{b_{ob}}{2}+(1\text{ mm})}{\left(\frac{6\text{ mm}}{2}\right)+\frac{b_{ob}}{2}}\right) = \tan^{-1}\left(\frac{\frac{b_{ob}}{2}+1\text{ mm}}{3\text{ mm}+\frac{b_{ob}}{2}}\right)$$

It can be observed that the maximum ligament weaving angle (θ_{max}) is a function of the outer beam dimension (b_{ob}), and consequently the maximum forces that act on the centre beam and the outer beams ($F_{cb\max}$ and $F_{ob\max}$, respectively) also become functions of the outer beam dimension (b_{ob}). The overall transducer length (L_t) was determined as follows (Figure A5.2):

Overall transducer length dimension,

$$L_t = (b_{cb} + 2\cdot gap) + 2\cdot b_{ob} = L_i + 2\cdot b_{ob} = 6\text{ mm} + 2\cdot b_{ob}$$

From the above expression, it can be observed that the overall transducer length (L_t) was also governed by the outer beam dimension (b_{ob}).

A5.2.2 Beam Analysis

Next, the maximum stress ($\sigma_{cb\max}$), maximum strain ($\varepsilon_{cb\max}$), and maximum deflection ($\delta_{cb\max}$) experienced by the centre beam, as well as the maximum stress ($\sigma_{ob\max}$) and maximum deflection ($\delta_{ob_{\max}}$) experienced by the outer beams, due to $F_{cb\max}$ and $F_{ob\max}$, respectively, were quantified.

The transducer's three beams were modelled as cantilever beams in bending subjected to uniform loads distributed along their lengths; these were simplified to resultant loads ($F_{cb\max}$ and $F_{ob\max}$) acting at the mid-length of the beams (Figure A5.4). The lengths of the beams (L) were composed of the average width of the AMCL (W_{AMCL}),

the tolerance allotted to properly bond the strain gauge to the centre beam (δ_L), and an additional amount allotted for holes to be made at the ends of each beam for suturing (SH) (Figure A5.3):

Length of transducer's beams, $L = W_{AMCL} + \delta_L + SH$

Where:
- $W_{AMCL} = 5$ mm
- $\delta_L = 2$ mm
- $SH = 1.5$ mm

Thus, $L = 8.5$ mm

However, it was deemed undesirable for the ligament to spread over the area of the suture hole (SH); hence, the effective length over which the ligament's force would act (L_{eff}) was the total ligament length (L) less the amount allotted for the suture hole (SH) (Figure A5.4):

$$L_{eff} = L - SH = 7 \text{ mm}$$

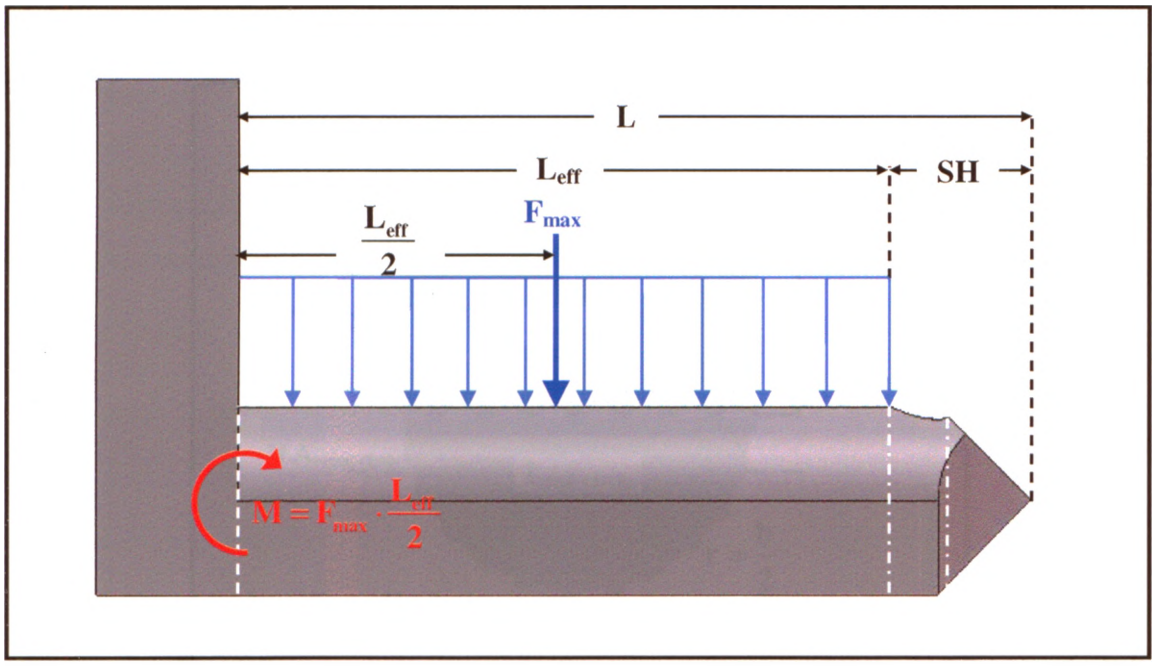

Figure A5.4: Load modelling of the transducer's beams

Side view of the transducer illustrating the load modelling of the transducer's beams.

A5.2.3 Calculation of Bending Stress

The bending stress experienced by the transducer's beams was given by Equation A5.1:

$$\text{Bending stress, } \sigma = \frac{My}{I} \qquad \textbf{Equation A5.1}$$

Where:
- M is the moment at the neutral axis
- y is the perpendicular distance to the neutral axis
- I is the area moment of inertia about the neutral axis

The moment M, can be found by: $M = F_{\max} \cdot \left(\frac{L_{eff}}{2}\right)$

Where:
- $F_{\max} = F_{cb\max}$ or $F_{ob\max}$ (*i.e.* $F_{cb\max}$ corresponds to the maximum force acting on the centre beam and $F_{ob\max}$ corresponds to the maximum force acting on the outer beams)
- L_{eff} is the effective length over which the ligament's force acts

The values for y and I are dependent upon the cross-section design of the beams. Recall that rounded-square beam cross-sections were chosen (a square in which two of the corners were rounded such that they form a semi-circle) (Figure A5.5).

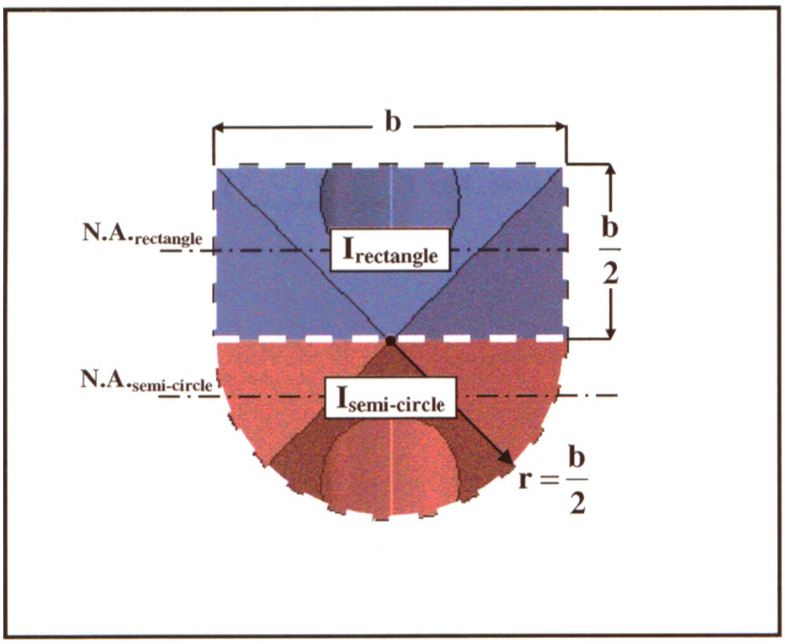

Figure A5.5: Cross-section of the transducer's beams

Note the beams' rounded-square cross-sections. This figure is the same as Figure 2.4.

A5.2.4 Rounded-Square Beam Cross-Section

For the centre beam and the outer beams, their respective area moments of inertia ($I_{cb_{rounded-square}}$ and $I_{ob_{rounded-square}}$, respectively) were calculated using the parallel-axis theorem as follows:

$$I_{rounded-square} = \sum \bar{I}_{x'} + Ad_y^2$$

$$= \left(\bar{I}_{x'} + Ad_y^2\right)_{\text{semi-circle}} + \left(\bar{I}_{x'} + Ad_y^2\right)_{\text{rectangle}}$$

$$= \left[\left(\frac{\pi}{8} - \frac{8}{9\pi}\right)\cdot r^4 + \left(\frac{\pi \cdot r^2}{2}\right)\left(\frac{4\cdot r}{3\pi}\right)^2\right] + \left[\frac{1}{12}(b)\left(\frac{b}{2}\right)^3 + (b)\left(\frac{b}{2}\right)\left(\frac{b}{4}\right)^2\right]$$

$$= \left[\left(\frac{\pi}{8} - \frac{8}{9\pi}\right)\cdot\left(\frac{b}{2}\right)^4 + \frac{\pi}{2}\left(\frac{b}{2}\right)^2\cdot\left(\frac{4}{3\pi}\left(\frac{b}{2}\right)\right)^2\right] + \left[\frac{1}{12}(b)\left(\frac{b}{2}\right)^3 + (b)\left(\frac{b}{2}\right)\left(\frac{b}{4}\right)^2\right]$$

Note: r describes the radius of the semi-circular portion of the beam (r is equal to $b/2$) whereas b and $b/2$ describe the width and height of the rectangular portion of the beam, respectively (Figure A5.5).

Furthermore, the perpendicular distance to the neutral axis for a rounded-square cross-section is $y_{rounded-square} = \frac{b}{2}$, where b corresponds to the dimension of the beam being analysed.

Substituting the dimension of the centre beam (b_{cb}), the corresponding centre beam area moment of inertia ($I_{cb_{rounded-square}}$) and neutral axis distance ($y_{cb_{rounded-square}}$) could be quantified:

Centre beam area moment of inertia,

$$I_{cb_{rounded-square}} = \left[\left(\frac{\pi}{8}-\frac{8}{9\pi}\right)\cdot r_{cb}{}^{4} + \left(\frac{\pi\cdot r_{cb}{}^{2}}{2}\right)\left(\frac{4\cdot r_{cb}}{3\pi}\right)^{2}\right] + \left[\frac{1}{12}(b_{cb})\left(\frac{b_{cb}}{2}\right)^{3} + (b_{cb})\left(\frac{b_{cb}}{2}\right)\left(\frac{b_{cb}}{4}\right)^{2}\right]$$

$$= \left[\left(\frac{\pi}{8}-\frac{8}{9\pi}\right)(1.25\,\text{mm})^{4} + \left(\frac{\pi\cdot(1.25\,\text{mm})^{2}}{2}\right)\left(\frac{4\cdot(1.25\,\text{mm})}{3\pi}\right)^{2}\right] + \left[\frac{1}{12}(2.5\,\text{mm})(1.25\,\text{mm})^{3} + (2.5\,\text{mm})(1.25\,\text{mm})(0.625\,\text{mm})^{2}\right]$$

$$= 0.9587\,\text{mm}^{4} + 1.6276\,\text{mm}^{4}$$

$$= 2.5863\,\text{mm}^{4}$$

Centre beam distance to the neutral axis,

$$y_{ob_{rounded-square}} = \frac{b_{cb}}{2} = \frac{2.5\,\text{mm}}{2} = 1.25\,\text{mm}$$

The area moment of inertia of the outer beams ($I_{ob_{rounded-square}}$) and the corresponding distance to the neutral axis ($y_{ob_{rounded-square}}$) could not be determined at this point, since the outer beam dimension (b_{ob}) was yet to be defined.

Outer beam area moment of inertia, $I_{ob_{rounded-square}}$

$$= \left[\left(\frac{\pi}{8}-\frac{8}{9\pi}\right)\cdot r_{ob}{}^{4} + \left(\frac{\pi\cdot r_{ob}{}^{2}}{2}\right)\left(\frac{4\cdot r_{ob}}{3\pi}\right)^{2}\right] + \left[\frac{1}{12}(b_{ob})\left(\frac{b_{ob}}{2}\right)^{3} + (b_{ob})\left(\frac{b_{ob}}{2}\right)\left(\frac{b_{ob}}{4}\right)^{2}\right]$$

Outer beam distance to the neutral axis, $y_{ob_{rounded-square}} = \frac{b_{ob}}{2}$

Substituting the expressions for M, $y_{rounded-square}$, and $I_{rounded-square}$ into the equation for bending stress (σ) (Equation A5.1), the respective equations for the maximum bending stress in the centre beam ($\sigma_{cb_{\max}}$) and the outer beams ($\sigma_{ob_{\max}}$) now become:

Maximum bending stress experienced by the centre beam,

$$\sigma_{cb_{\max}} = \frac{M_{cb} \cdot y_{cb_{rounded-square}}}{I_{cb_{rounded-square}}}$$

$$= \frac{\left[F_{cb} \cdot \left(\frac{L_{eff}}{2}\right)\right] \cdot y_{cb_{rounded-square}}}{I_{cb_{rounded-square}}}$$

$$= \frac{\left[2 \cdot F_{AMCL_{\max}} \cdot \sin\theta_{\max} \cdot \left(\frac{L_{eff}}{2}\right)\right] \cdot \left(\frac{b_{cb}}{2}\right)}{I_{cb_{rounded-square}}}$$

$$= \frac{\left[2 \cdot (110\,\text{N}) \cdot \sin\theta \cdot \left(\frac{7\,\text{mm}}{2}\right)\right] \cdot (1.25\,\text{mm})}{2.5863\,\text{mm}^4}$$

Where:

$$\theta_{\max} = \tan^{-1}\left(\frac{\frac{b_{ob}}{2} + 1\,\text{mm}}{3\,\text{mm} + \frac{b_{ob}}{2}}\right)$$

Maximum bending stress experienced by the outer beams,

$$\sigma_{ob_{\max}} = \frac{M_{ob} \cdot y_{ob_{rounded-square}}}{I_{ob_{rounded-square}}}$$

$$= \frac{\left[F_{ob} \cdot \left(\frac{L_{eff}}{2}\right)\right] \cdot y_{ob_{rounded-square}}}{I_{ob_{rounded-square}}}$$

$$= \frac{\left[F_{AMCL_{\max}} \cdot \sin\theta \cdot \left(\frac{L_{eff}}{2}\right)\right] \cdot \left(\frac{b_{ob}}{2}\right)}{I_{ob_{rounded-square}}}$$

$$= \frac{\left[(110\,\text{N}) \cdot \sin\theta \cdot \left(\frac{7\,\text{mm}}{2}\right)\right] \cdot \left(\frac{b_{ob}}{2}\right)}{I_{ob_{rounded-square}}}$$

Where:

- $\theta_{\max} = \tan^{-1}\left(\dfrac{\frac{b_{ob}}{2} + 1\,\text{mm}}{3\,\text{mm} + \frac{b_{ob}}{2}}\right)$

- $I_{ob_{rounded-square}} = \left[\left(\frac{\pi}{8} - \frac{8}{9\pi}\right) \cdot r_{ob}^{\,4} + \left(\frac{\pi \cdot r_{ob}^{\,2}}{2}\right)\left(\frac{4 \cdot r_{ob}}{3\pi}\right)^2\right] + \left[\frac{1}{12}(b_{ob})\left(\frac{b_{ob}}{2}\right)^3 + (b_{ob})\left(\frac{b_{ob}}{2}\right)\left(\frac{b_{ob}}{4}\right)^2\right]$

$$= \left[\left(\frac{\pi}{8} - \frac{8}{9\pi}\right) \cdot \left(\frac{b_{ob}}{2}\right)^4 + \frac{\pi}{2}\left(\frac{b_{ob}}{2}\right)^2 \cdot \left(\frac{4}{3\pi}\left(\frac{b_{ob}}{2}\right)\right)^2\right] + \left[\frac{1}{12}(b_{ob})\left(\frac{b_{ob}}{2}\right)^3 + (b_{ob})\left(\frac{b_{ob}}{2}\right)\left(\frac{b_{ob}}{4}\right)^2\right]$$

Thus, it can be observed that $\sigma_{cb_{\max}}$ and $\sigma_{ob_{\max}}$ were functions of the outer beam dimension (b_{ob}).

A5.2.5 Calculation of Strain

The centre beam strain ($\varepsilon_{cb_{max}}$) required investigation as the strain gauge had an allowable one-time stretch to approximately 0.03 strain. From Hooke's law (Equation A5.2), the maximum strain in the centre beam ($\varepsilon_{cb_{max}}$) due to the maximum bending stress ($\sigma_{cb_{max}}$) was determined as follows:

Hooke's law, $\sigma = E\varepsilon$ **Equation A5.2**

Maximum strain in centre beam, $\varepsilon_{cb_{max}} = \dfrac{\sigma_{cb_{max}}}{E_{316}} = \dfrac{\sigma_{cb_{max}}}{193\times10^3 \text{ MPa}}$

Where:

- $\sigma_{cb_{max}} = \dfrac{\left[2\cdot(110\text{ N})\cdot\sin\theta_{max}\cdot\left(\dfrac{7\text{ mm}}{2}\right)\right]\cdot(1.25\text{ mm})}{2.5863\text{ mm}^4}$
- $\theta_{max} = \tan^{-1}\left(\dfrac{\dfrac{b_{ob}}{2}+1\text{ mm}}{3\text{ mm}+\dfrac{b_{ob}}{2}}\right)$
- E_{316} is the Young's modulus of stainless steel 316, which is approximately 193 GPa (193×10^3 MPa)[9]

It can be observed that the maximum strain in the centre beam ($\varepsilon_{cb_{max}}$) was a function of the maximum bending stress ($\sigma_{cb_{max}}$), and since the maximum bending stress ($\sigma_{cb_{max}}$) was a function of the outer beam dimension (b_{ob}), consequently the maximum strain experienced by the centre beam ($\varepsilon_{cb_{max}}$) was a function of the outer beam dimension (b_{ob}).

A5.2.6 Calculation of Deflection

The deflection of a cantilever beam with a resultant load acting at its mid-length (as shown in Figure A5.4) is given by Equation A5.3:

$$\delta = \frac{5 \cdot F_{\max} \cdot \left(\frac{L_{eff}}{2}\right)^3}{6 \cdot E_{316} \cdot I_{cb_{rounded\text{-}square}}} \qquad \textbf{Equation A5.3}$$

Where:

- $F_{\max} = F_{cb\max}$ or $F_{ob\max}$ (*i.e.* $F_{cb\max}$ corresponds to the maximum force acting on the centre beam and $F_{ob\max}$ corresponds to the maximum force acting on the outer beams)
- L_{eff} effective length over which the ligament's force acts
- E_{316} is the Young's modulus of stainless steel 316, which is approximately 193 GPa (193×10^3 MPa)[9]

Performing the appropriate variable substitutions into Equation A5.3, the expressions for the maximum deflections (*i.e.* maximum deflection at the free end of the beam) of the centre beam ($\delta_{cb_{\max}}$) and outer beams ($\delta_{ob_{\max}}$) were found to be as follows:

Maximum deflection of the centre beam,

$$\delta_{cb_{\max}} = \frac{5 \cdot F_{cb_{\max}} \cdot \left(\frac{L_{eff}}{2}\right)^3}{6 \cdot E_{316} \cdot I_{cb_{rounded-square}}}$$

$$= \frac{5 \cdot \left(2 \cdot F_{AMCL_{\max}} \cdot \sin\theta_{\max}\right) \cdot \left(\frac{L_{eff}}{2}\right)^3}{6 \cdot E_{316} \cdot I_{cb_{rounded-square}}}$$

$$= \frac{5 \cdot \left[2 \cdot (110\,\text{N}) \cdot \sin\theta_{\max}\right] \cdot \left(\frac{7\,\text{mm}}{2}\right)^3}{6 \cdot \left(193\times10^3\,\text{MPa}\right) \cdot \left(2.5863\,\text{mm}^4\right)}$$

Where:

- $\theta_{\max} = \tan^{-1}\left(\dfrac{\frac{b_{ob}}{2}+1\,\text{mm}}{3\,\text{mm}+\frac{b_{ob}}{2}}\right)$
- E_{316} is the Young's modulus of stainless steel 316, which is approximately 193 GPa (193×10^3 MPa)[9]

Maximum deflection of the outer beams,

$$\delta_{ob_{\max}} = \frac{5\cdot F_{ob_{\max}}\cdot\left(\frac{L_{eff}}{2}\right)^3}{6\cdot E_{316}\cdot I_{ob_{rounded-square}}}$$

$$= \frac{5\cdot\left(F_{AMCL_{\max}}\cdot\sin\theta_{\max}\right)\cdot\left(\frac{L_{eff}}{2}\right)^3}{6\cdot E_{316}\cdot I_{ob_{rounded-square}}}$$

$$= \frac{5\cdot\left[(110\text{ N})\cdot\sin\theta_{\max}\right]\cdot\left(\frac{7\text{ mm}}{2}\right)^3}{6\cdot(193\times10^3\text{ MPa})\cdot I_{ob_{rounded-square}}}$$

Where:

- $\theta_{\max} = \tan^{-1}\left(\dfrac{\frac{b_{ob}}{2}+1\,\text{mm}}{3\,\text{mm}+\frac{b_{ob}}{2}}\right)$
- E_{316} is the Young's modulus of stainless steel 316, which is approximately 193 GPa (193×10^3 MPa)[9]
- $I_{ob_{rounded-square}} = \left[\left(\frac{\pi}{8}-\frac{8}{9\pi}\right)\cdot {r_{ob}}^4+\left(\frac{\pi\cdot {r_{ob}}^2}{2}\right)\left(\frac{4\cdot r_{ob}}{3\pi}\right)^2\right]$
$$+\left[\frac{1}{12}(b_{ob})\left(\frac{b_{ob}}{2}\right)^3+(b_{ob})\left(\frac{b_{ob}}{2}\right)\left(\frac{b_{ob}}{4}\right)^2\right]$$
$$= \left[\left(\frac{\pi}{8}-\frac{8}{9\pi}\right)\cdot\left(\frac{b_{ob}}{2}\right)^4+\left(\frac{\pi\cdot\left(\frac{b_{ob}}{2}\right)^2}{2}\right)\left(\frac{4\cdot\left(\frac{b_{ob}}{2}\right)}{3\pi}\right)^2\right]$$
$$+\left[\frac{1}{12}(b_{ob})\left(\frac{b_{ob}}{2}\right)^3+(b_{ob})\left(\frac{b_{ob}}{2}\right)\left(\frac{b_{ob}}{4}\right)^2\right]$$

Thus, it can be observed that $\delta_{cb_{\max}}$ and $\delta_{ob_{\max}}$ were functions of the outer beam dimension (b_{ob}).

A5.2.7 Final Buckle Transducer Design

As expressions for the maximum bending stress experienced by the centre beam ($\sigma_{cb_{\max}}$), the maximum bending stress experienced by the outer beams ($\sigma_{ob_{\max}}$), the maximum strain experienced by the centre beam ($\varepsilon_{cb_{\max}}$), and the maximum deflections of the centre beam ($\delta_{cb_{\max}}$) and outer beams ($\delta_{ob_{\max}}$), were functions of the outer beam dimension (b_{ob}), these calculations were performed for a range of outer beam dimensions (b_{ob}); the results are summarized in Table A5.1. Additionally, the last column of Table A5.1 shows the outer beam deflection as a percentage of the centre beam deflection (*e.g.* at an outer beam dimension of 1.7 mm, the percentage of 133.8 can be read as an outer beam deflection of approximately 133.8 times that of the centre beam).

Referring to the discussions in the Chapter 2, an outer beam dimension (b_{ob}) of 2 mm was selected. The highlighted row in Table A5.1 corresponds to the final transducer design. The detailed drawings of the final buckle transducer design are shown in Figure A5.6.

For the completed transducer design (Figure A5.2), the amount of ligament needed for the initial weaving process was approximately:

$$= 2 \cdot \left[\left(\frac{b_{ob}}{2} + t \right)^2 + \left(\frac{b_{cb}}{2} + gap + \frac{b_{ob}}{2} \right)^2 \right]^{\frac{1}{2}}$$

$$= 2 \cdot \left[(1\,\text{mm} + 1\,\text{mm})^2 + (1.25\,\text{mm} + 1.75\,\text{mm} + 1\,\text{mm})^2 \right]^{\frac{1}{2}} = 2 \cdot \left[(2\,\text{mm})^2 + (4\,\text{mm})^2 \right]^{\frac{1}{2}}$$

$$= 2 \cdot \left(20\,\text{mm}^2 \right)^{\frac{1}{2}}$$

$$= 2 \cdot (4.4721\,\text{mm})$$

$$= 8.9443\,\text{mm}$$

Therefore, the amount of tissue consumed by the device was approximately:

$$
\begin{aligned}
&= 8.9443\,\text{mm} - L_i \\
&= 8.9443\,\text{mm} - 2 \cdot \left(\frac{b_{cb}}{2} + gap + \frac{b_{ob}}{2} \right) \\
&= 8.9443\,\text{mm} - 2 \cdot (1.25\,\text{mm} + 1.75\,\text{mm} + 1\,\text{mm}) \\
&= 8.9443\,\text{mm} - 2 \cdot (4\,\text{mm}) \\
&= 8.9443\,\text{mm} - 8\,\text{mm} \\
&= 0.9443\,\text{mm}
\end{aligned}
$$

Table A5.1: Beam analysis results

Results for stress, strain, and deflection for varying outer beam (b_{ob}) dimensions. The maximum values correspond to $F_{AMCL_{max}}$, which was calculated to be approximately 110 N. The highlighted row corresponds to the final buckle transducer design. All column headings are as previously defined; the last column was calculated using $\left(\frac{|\delta_{ob_{max}} - \delta_{cb_{max}}|}{\delta_{cb_{max}}}\right) \cdot 100\,\%$. This table is the same as Table 2.1.

b_{ob} [mm]	L_t [mm]	Ligamentous Coverage [%]	Offset [mm]	θ_{max} [Degrees]	F_{cb} [N]	F_{ob} [N]	I_{ob} [mm^4]	$\sigma_{max,cb}$ [MPa]	$\sigma_{max,ob}$ [MPa]	$\varepsilon_{cb,max}$ [Strain]	$\delta_{max,cb}$ [mm]	$\delta_{max,ob}$ [mm]	$\delta_{max,ob}$ [%]
1.0	8.0	29.6	0.5	23.2	86.7	43.3	0.1	146.6	1145.3	7.6E-04	6.2E-03	1.2E-01	1853.1
1.1	8.2	30.4	0.6	23.6	88.0	44.0	0.1	148.9	874.1	7.7E-04	6.3E-03	8.4E-02	1234.0
1.2	8.4	31.1	0.6	24.0	89.4	44.7	0.1	151.1	683.3	7.8E-04	6.4E-03	6.0E-02	841.9
1.3	8.6	31.9	0.7	24.3	90.6	45.3	0.2	153.3	545.1	7.9E-04	6.5E-03	4.4E-02	583.8
1.4	8.8	32.6	0.7	24.7	91.9	45.9	0.3	155.4	442.4	8.1E-04	6.6E-03	3.3E-02	408.4
1.5	9.0	33.3	0.8	25.0	93.0	46.5	0.3	157.4	364.3	8.2E-04	6.7E-03	2.6E-02	285.8
1.6	9.2	34.1	0.8	25.3	94.2	47.1	0.4	159.3	303.9	8.3E-04	6.7E-03	2.0E-02	198.0
1.7	9.4	34.8	0.9	25.7	95.3	47.6	0.6	161.2	256.3	8.4E-04	6.8E-03	1.6E-02	133.8
1.8	9.6	35.6	0.9	26.0	96.4	48.2	0.7	163.0	218.3	8.4E-04	6.9E-03	1.3E-02	86.1
1.9	9.8	36.3	1.0	26.3	97.4	48.7	0.9	164.7	187.6	8.5E-04	7.0E-03	1.0E-02	49.9
2.0	10.0	37.0	1.0	26.6	98.4	49.2	1.1	166.4	162.5	8.6E-04	7.0E-03	8.6E-03	22.1
2.1	10.2	37.8	1.1	26.8	99.4	49.7	1.3	168.1	141.8	8.7E-04	7.1E-03	7.1E-03	0.4
2.2	10.4	38.5	1.1	27.1	100.3	50.1	1.6	169.7	124.5	8.8E-04	7.2E-03	6.0E-03	-16.6
2.3	10.6	39.3	1.2	27.4	101.2	50.6	1.9	171.2	109.9	8.9E-04	7.2E-03	5.1E-03	-30.2
2.4	10.8	40.0	1.2	27.6	102.1	51.0	2.2	172.7	97.6	8.9E-04	7.3E-03	4.3E-03	-41.1
2.5	11.0	40.7	1.3	27.9	102.9	51.5	2.6	174.1	87.1	9.0E-04	7.4E-03	3.7E-03	-50.0

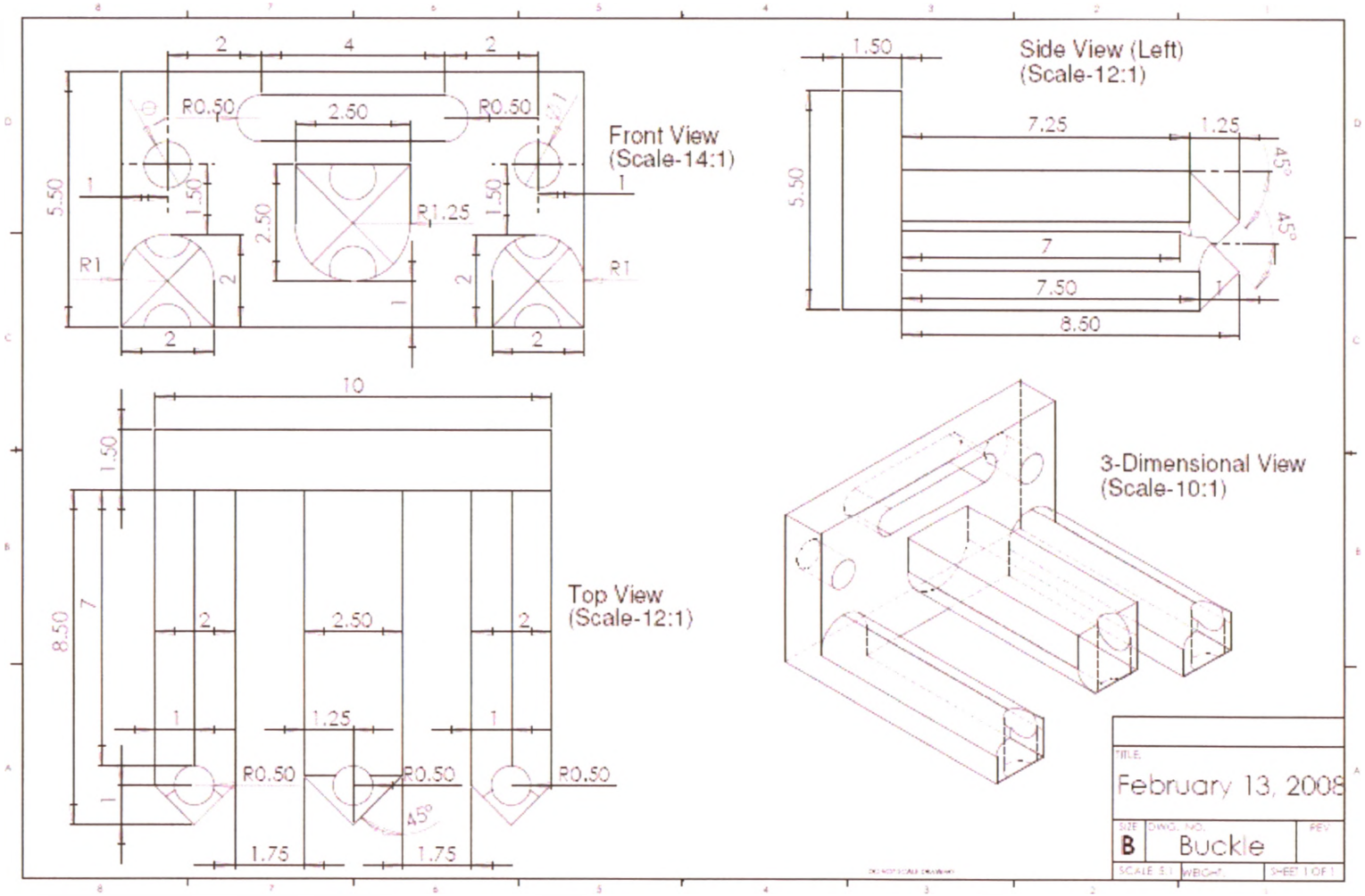

Figure A5.6: Detailed drawings of the final buckle transducer design

A5.3 SHEAR, MOMENT, STRESS, AND STRAIN DIAGRAMS

A5.3.1 Shear and Moment Diagrams

The loading situation for the transducer's centre beam is shown in Figure A5.7.

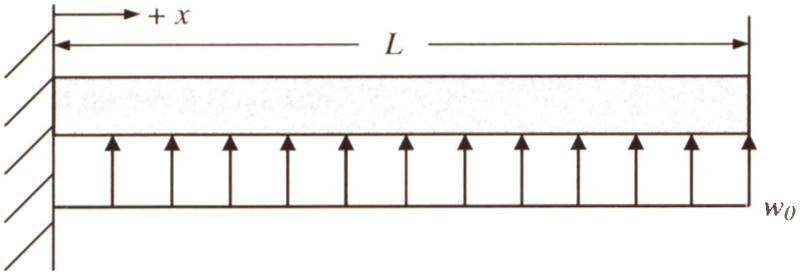

Figure A5.7: Load modelling of the transducer's centre beam

The reactions at the fixed support are shown on the free body diagram below, Figure A5.8.

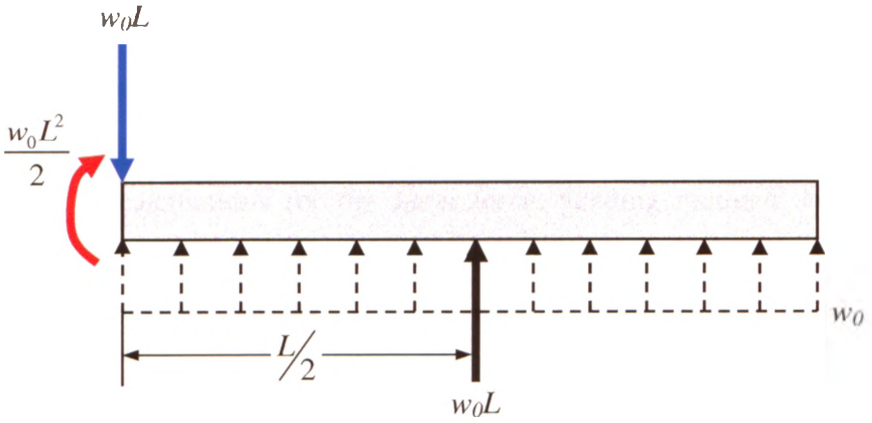

Figure A5.8: The vertical wall reaction force and the wall reaction moment

For a beam subjected to a distributed load $w = w(x)$, the variation in the internal shear force along the length of the beam $V(x)$ can be found by integrating the distributed loading function:[10]

$$V(x) = -\int w(x)dx$$

Similarly, the variation in the internal bending moment along the beam $M(x)$ can be found by integrating the shear force function:[10]

$$M(x) = \int V(x)dx$$

Recall that the maximum force that acts on the centre beam ($F_{cb_{\max}}$), as well as the effective length of the beam (L_{eff}), are:

$$F_{cb_{\max}} = 98.4 \text{ N}$$
$$L_{eff} = L = 7 \text{ mm}$$

Therefore, the uniform distributed load over the effective length of the beam (w_0) is:

$$w_0 = \frac{98.4 \text{ N}}{7 \text{ mm}} = 14.057 \frac{\text{N}}{\text{mm}}$$

It should be noted that since the maximum force that acts on the centre beam ($F_{cb_{\max}}$) was used to calculate the uniform distributed load (w_0), this w_0 corresponds to the maximum possible distributed load that the transducer's centre beam may experience; consequently, the subsequent calculations for the shear force, bending moment, bending stress, and strain distributions along the length of the transducer's centre beam all correspond to the maximum possible distributions.

A5.3.1.1 *Shear Force Diagram*

Since the distributed load acts upwards on the beam, by the beam sign convention, it is in the negative direction.

$$\begin{aligned} V(x) &= -\int w(x)dx \\ &= -\int (-w_0)dx \\ &= w_0 \cdot x + c \end{aligned}$$

The constant of the integral (c) can be found by using the initial condition; at the base of the beam, the shear force is the vertical wall reaction force:

$$V(x=0) = -w_0 \cdot L = w_0 \cdot (0) + c$$
$$\therefore c = -w_0 \cdot L$$

Therefore, the shear force at any point (x) along the length of the beam is defined by:

$$V(x) = w_0 \cdot x - w_0 \cdot L$$
$$V(x) = \left(14.057 \frac{\text{N}}{\text{mm}}\right) \cdot x - \left(14.057 \frac{\text{N}}{\text{mm}}\right) \cdot (7\text{mm})$$
$$= \left(14.057 \frac{\text{N}}{\text{mm}}\right) \cdot x - 98.4\ \text{N}$$

Solving the above expression for the shear force at the base, the midpoint, and the free end of the beam:

The shear force at the base of the beam ($x = 0$) is

$$V(x=0) = w_0 \cdot (0) - w_0 \cdot L = -w_0 \cdot L$$
$$V(x=0) = \left(14.057 \frac{\text{N}}{\text{mm}}\right) \cdot (0) - 98.4\ \text{N} = -98.4\ \text{N}$$

The shear force at the midpoint of the beam ($x = L/2$) is

$$V\left(x = \frac{L}{2}\right) = w_0 \cdot \left(\frac{L}{2}\right) - w_0 \cdot L = -\frac{w_0 L}{2}$$
$$V\left(x = \frac{L}{2}\right) = \left(14.057 \frac{\text{N}}{\text{mm}}\right) \cdot \left(\frac{7\ \text{mm}}{2}\right) - 98.4\ \text{N} = 49.2\ \text{N} - 98.4\ \text{N} = -49.2\ \text{N}$$

The shear force at the free end of the beam ($x = L$) is

$$V(x = L) = w_0 \cdot (L) - w_0 \cdot L = 0$$
$$V(x = L) = \left(14.057 \frac{\text{N}}{\text{mm}}\right) \cdot (7\ \text{mm}) - 98.4\ \text{N} = 98.4\ \text{N} - 98.4\ \text{N} = 0$$

The shear force diagram for the centre beam is shown in Figure A5.9.

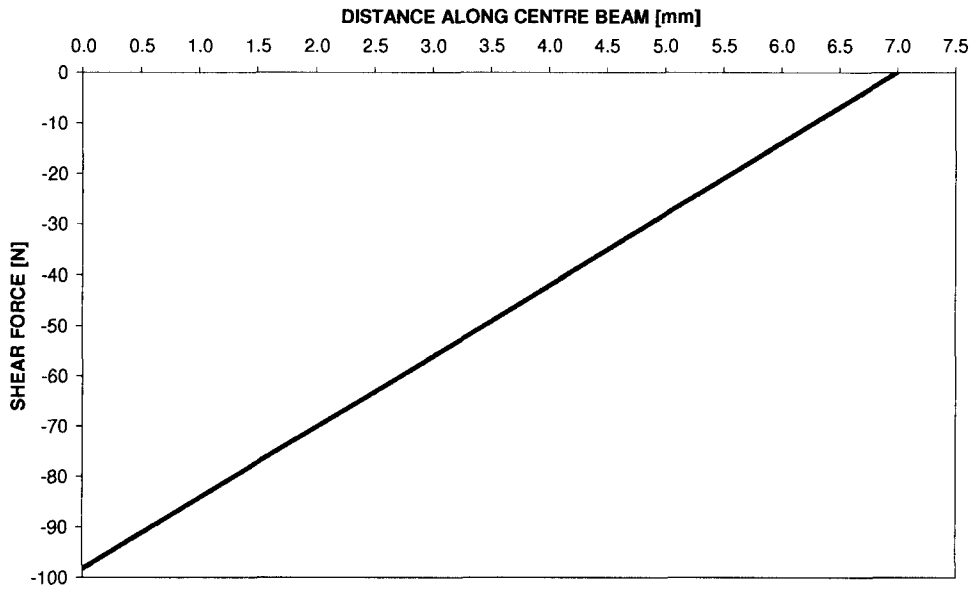

Figure A5.9: Shear force diagram

The maximum possible variation of shear force along the length of the transducer's centre beam.

A5.3.1.2 *Bending Moment Diagram*

Integrating the shear force function yields:

$$\begin{aligned} M(x) &= \int V(x)dx \\ &= \int (w_0 \cdot x - w_0 \cdot L)dx \\ &= \frac{w_0 \cdot x^2}{2} - w_0 \cdot L \cdot x + d \end{aligned}$$

The constant of the integral (d) can be found by using the initial condition; at the base of the beam, the bending moment is the wall reaction moment:

$$M(x=0) = w_0 \cdot L \cdot \frac{L}{2} = \frac{w_0 \cdot (0)^2}{2} - w_0 \cdot L \cdot (0) + d$$

$$\therefore d = \frac{w_0 L^2}{2}$$

Therefore, the bending moment at any point (x) along the length of the beam is defined by:

$$M(x) = \frac{w_0 \cdot x^2}{2} - w_0 \cdot L \cdot x + \frac{w_0 L^2}{2}$$

$$M(x) = \frac{\left(14.057 \frac{\text{N}}{\text{mm}}\right) \cdot x^2}{2} - \left(14.057 \frac{\text{N}}{\text{mm}}\right) \cdot (7\ \text{mm}) \cdot x + \frac{\left(14.057 \frac{\text{N}}{\text{mm}}\right) \cdot (7\ \text{mm})^2}{2}$$

$$= \frac{\left(14.057 \frac{\text{N}}{\text{mm}}\right) \cdot x^2}{2} - (98.4\ \text{N}) \cdot x + 344.4\ \text{Nmm}$$

Solving the above expression for the bending moment at the base, the midpoint, and the free end of the beam:

The bending moment at the base of the beam ($x = 0$) is

$$M(x=0) = \frac{w_0 \cdot (0)^2}{2} - w_0 \cdot L \cdot (0) + \frac{w_0 L^2}{2} = \frac{w_0 L^2}{2}$$

$$M(x=0) = \frac{\left(14.057 \frac{\text{N}}{\text{mm}}\right) \cdot (0)^2}{2} - (98.4\ \text{N}) \cdot (0) + 344.4\ \text{Nmm} = 344.4\ \text{Nmm}$$

The bending moment at the midpoint of the beam ($x = L/2$) is

$$M\left(x = \frac{L}{2}\right) = \frac{w_0 \cdot \left(\frac{L}{2}\right)^2}{2} - w_0 \cdot L \cdot \left(\frac{L}{2}\right) + \frac{w_0 L^2}{2} = \frac{w_0 L^2}{8} - \frac{w_0 L^2}{2} + \frac{w_0 L^2}{2} = \frac{w_0 L^2}{8}$$

$$M\left(x = \frac{L}{2}\right) = \frac{\left(14.057 \frac{\text{N}}{\text{mm}}\right) \cdot \left(\frac{7\ \text{mm}}{2}\right)^2}{2} - (98.4\ \text{N}) \cdot \left(\frac{7\ \text{mm}}{2}\right) + 344.4\ \text{Nmm} = 86.1\ \text{Nmm}$$

The bending moment at the free end of the beam ($x = L$) is

$$M(x=L) = \frac{w_0 \cdot (L)^2}{2} - w_0 \cdot L \cdot (L) + \frac{w_0 L^2}{2} = 0$$

$$M(x=L) = \frac{\left(14.057 \frac{\text{N}}{\text{mm}}\right) \cdot (7\ \text{mm})^2}{2} - (98.4\ \text{N}) \cdot (7\ \text{mm}) + 344.4\ \text{Nmm} = 0$$

The bending moment diagram for the centre beam is shown in Figure A5.10.

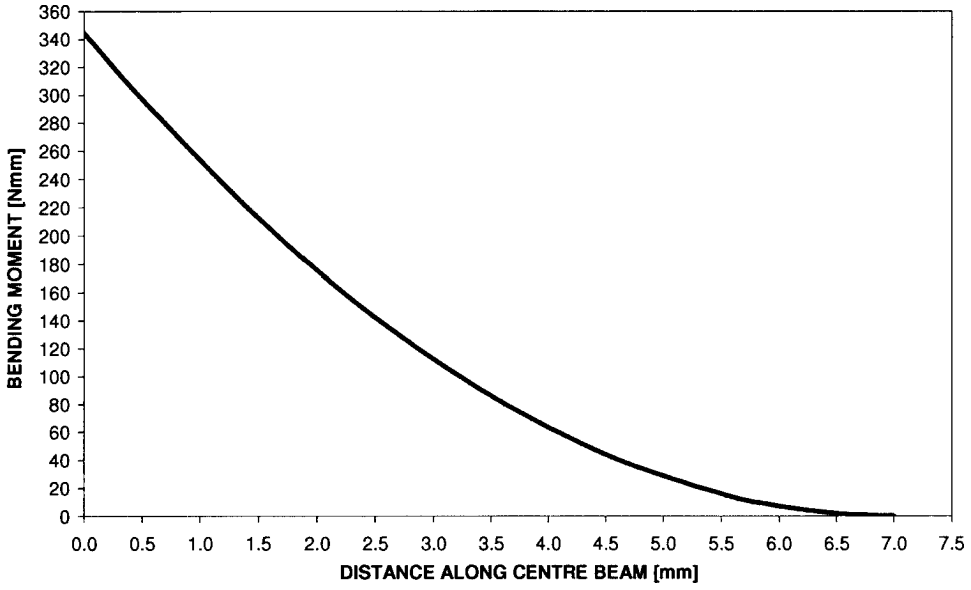

Figure A5.10: Bending moment diagram

The maximum possible variation of bending moment along the length of the transducer's centre beam.

A5.3.2 Bending Stress and Strain Diagrams

For completeness, the bending stress distribution and the corresponding strain distribution along the length of the transducer's centre beam (at the top surface) were calculated and are shown in Figure A5.11 and Figure A5.12, respectively. These stress and strain distributions were determined using Equation A5.1 and Equation A5.2, respectively.

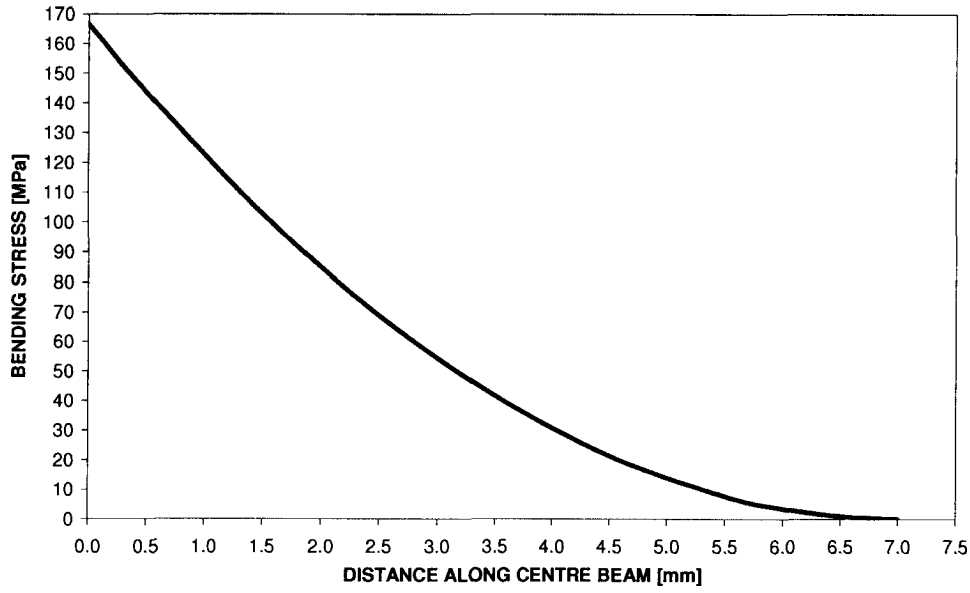

Figure A5.11: Bending stress diagram

The maximum possible variation of bending stress along the length of the transducer's centre beam (at the top surface).

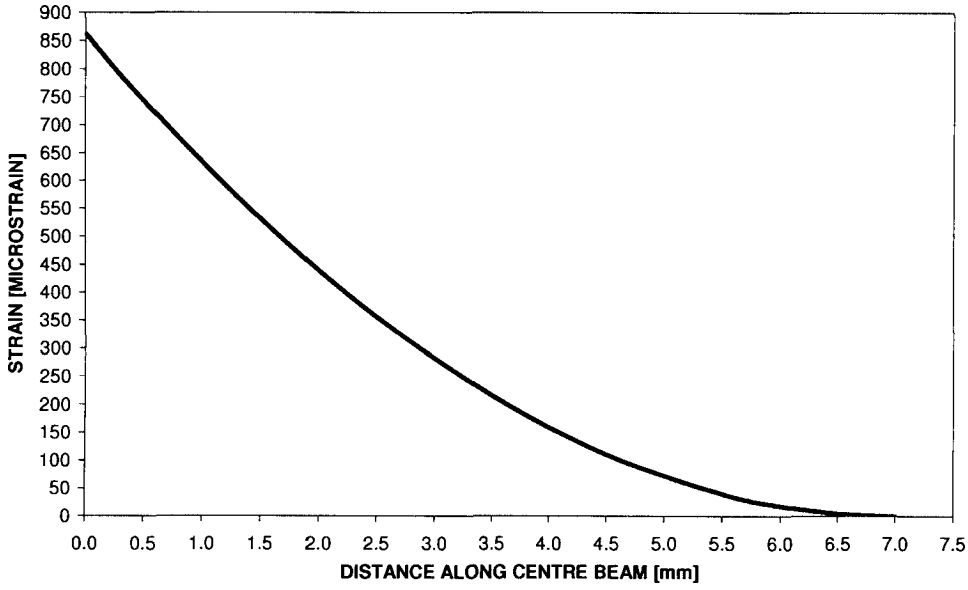

Figure A5.12: Strain diagram

The maximum possible variation of strain along the length of the transducer's centre beam (at the top surface).

A5.4 REFERENCE LIST

1. Dunning CE, Jenkyn TR. Kinetics 1. MME 464a Biomechanics of Human Joint Motion Lecture Notes. London, ON: The University of Western Ontario, Faculty of Engineering; 2006. p. 8-1-8-15.

2. Expert Panel of the National Institutes of Health. Clinical guidelines on the identification, evaluation and treatment of overweight and obesity in adults: Executive Summary. The American Journal of Clinical Nutrition 1998;68:899-917.

3. Nazarian LN, McShane JM, Ciccotti MG, O'Kane PL, Harwood MI. Dynamic US of the anterior band of the ulnar collateral ligament of the elbow in asymptomatic major league baseball pitchers. Radiology 2003;227:149-54.

4. Floris S, Olsen BS, Dalstra M, Sojbjerg JO, Sneppen O. The medial collateral ligament of the elbow joint: anatomy and kinematics. J.Shoulder.Elbow.Surg. 1998;7:345-51.

5. Timmerman LA, Andrews JR. Histology and arthroscopic anatomy of the ulnar collateral ligament of the elbow. Am.J.Sports Med. 1994;22:667-73.

6. Regan WD, Korinek SL, Morrey BF, An KN. Biomechanical study of ligaments around the elbow joint. Clin.Orthop.Relat Res. 1991;170-9.

7. Morrey BF, An KN. Functional anatomy of the ligaments of the elbow. Clin.Orthop.Relat Res. 1985;84-90.

8. Popovic N, Ferrara MA, Daenen B, Georis P, Lemaire R. Imaging overuse injury of the elbow in professional team handball players: a bilateral comparison using plain films, stress radiography, ultrasound, and magnetic resonance imaging. Int.J.Sports Med. 2001;22:60-7.

9. Callister WDJr. Appendix B: Properties of selected engineering materials. Materials science and engineering. An introduction. New York: John Wiley & Sons, Inc.; 2003. p. 737-64.

10. Hibbeler RC. Bending. Mechanics of Materials. New Jersey: Pearson Education, Inc.; 2003. p. 255-75.

APPENDIX 6

Appendix to Chapter 2 (Part III)
Investigation of Hysteresis in the Buckle Transducer

The experimental setup described for the transducer's calibration in Chapter 2 (Section 2.6) was also applied to the transducer's hysteresis investigation. Figure A6.1 shows a plot of the applied loads versus the outputted strain values from the transducer. It can be observed that hysteresis was present in this test setup; the loading curve for increasing and decreasing force values did not coincide. The greatest degree of hysteresis was assessed by finding the largest difference in strain values for the two loading curves; this occurred at a force value of approximately 10 N (or 1 kg). When 10 N was approached from an increasing direction of force, the strain was -2.5×10^{-4} strain; conversely, when approached from a decreasing direction, the strain was -4.9×10^{-4} strain. The percentage difference between these two strain values was approximately 63.2%.

The hysteresis present in this system is largely due to the recruitment of the synthetic fibres and not due to the inherent design of the buckle transducer itself. To elaborate, due to the woven nature of the synthetic fibre, when the synthetic fibre was loaded, the individual strands of fibre were recruited such that the synthetic fibre as a whole was tensioned; however, when unloaded, the fibre did not fully return to its pre-tensioned state (*i.e.* the state before the load had been applied) instantaneously. Thus, for each applied load measurement, the states of the fibre strands on the unloading cycle were all slightly stretched beyond their corresponding states of the loading-up cycle, as the fibre strands did not fully return to their pre-tensioned states. This is apparent in the trend seen in Figure A6.1; the curve corresponding to the increasing force direction experienced lower strains than the curve corresponding to the decreasing force direction, for any given force value.

Hysteresis due to the stainless steel of the transducer was minimal as the maximum applied load of 100 N lies within the linear region of the material's stress-

strain curve. Furthermore, in hindsight, the use of a synthetic woven fibre was not the ideal material to quantify hysteresis for the device; and hence, the hysteresis reported here for the buckle transducer may be a gross overestimate. The optimal set-up for quantifying the hysteresis of the *system* would have been to use the AMCL; however, as previously stated, this ligament is not easily harvested.

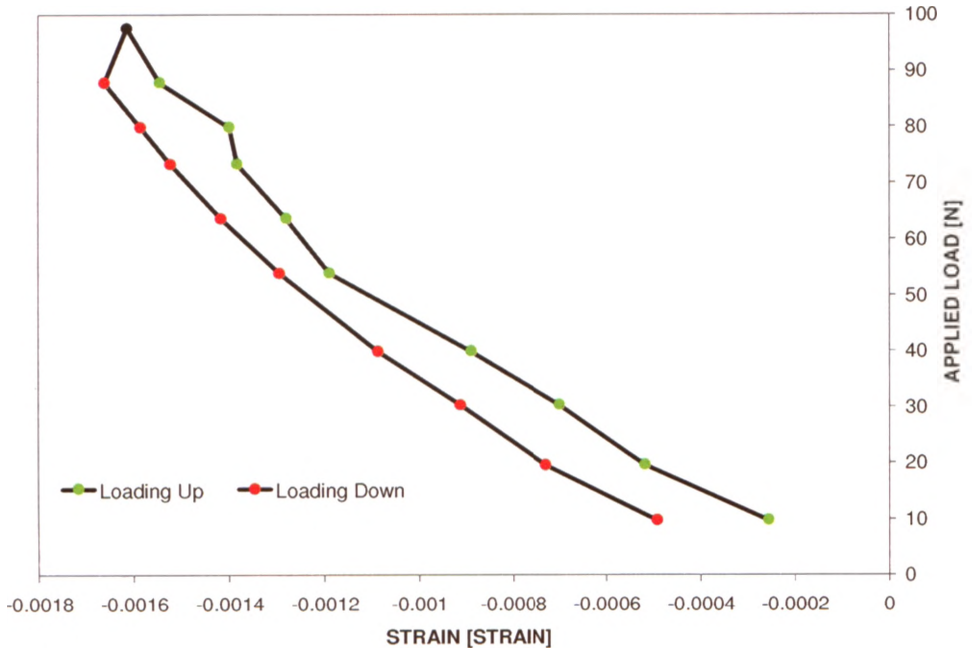

Figure A6.1: Hysteresis of the buckle transducer

The average strain output of the buckle transducer for specified loads applied upwards (green) and downwards (red). Note that the loading-up strain values are greater than the loading-down strain values.

APPENDIX 7

Appendix to Chapter 3
Quantification of Medial Collateral Ligament Tension in the Elbow

A7.1 MATERIALS AND METHODS

A7.1.1 Specimen Preparation

Table A7.1: Number of specimens analysed for the valgus and dependent positions for the native AMCL study

Five specimens were tested for both the valgus and dependent positions; however, due to data acquisition difficulties, data from only four of the five specimens were analysed for the dependent position.

Valgus Position	5 specimens (mean age 72 ± 10 years; range: 62-82 years; 3 female; 1 right specimen)
Dependent Position	4 specimens (mean age 74 ± 9 years; range: 65-82 years; 2 female; 1 right specimen)

A7.1.2 Testing Protocol

Table A7.2: Motion protocol for the native AMCL study

There were four test conditions: (1) passive flexion in the dependent position; (2) active flexion in the dependent position; (3) passive flexion in the valgus position; and (4) active flexion in the valgus position. For the repeatability investigation of the buckle transducer, AMCL tension data from all five flexion cycles were analysed. For all subsequent tests, AMCL tension and valgus angulation data from only the third flexion cycle (of five) were analysed. Extension data were not analysed.

DEPENDENT POSITION				VALGUS POSITION			
Test Condition				Test Condition			
Passive Motion		Active Motion		Passive Motion		Active Motion	
Extension (×5)	Flexion (×5)	Extension (×5)	Flexion (×5)	Extension (×5)	Flexion (×5)	Extension (×5)	Flexion (×5)

A7.2 RESULTS

A7.2.1 Repeatability

Observing the plot of the AMCL tension measurements of each flexion cycle (Figure 3.4), it can be observed that each flexion cycle's measurement was less than the previous flexion cycle's measurement. Observing the corresponding prime mover loads of each flexion cycle, these were also observed to decrease with each flexion cycle (Figure A7.1), and furthermore, the corresponding valgus angulations tracked in greater valgus with each flexion cycle (Figure A7.2). These differences in prime mover load and valgus angulation for each flexion cycle indicated that each consecutive flexion cycle's test condition was slightly different. Thus, it is fair to conclude that a portion of the variation observed in the repeatability investigation can be attributed to the change in test conditions between each consecutive flexion cycle; hence, had the tests conditions been identical, it is anticipated that the buckle transducer would have produced higher levels of repeatability.

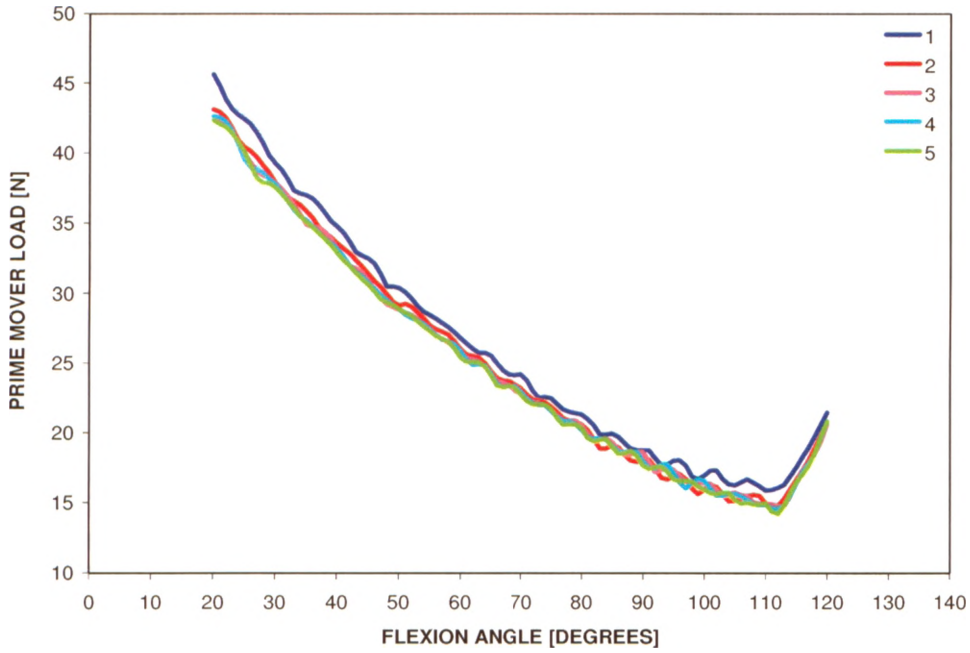

Figure A7.1: Prime mover load measurements of one specimen tested in active flexion in the valgus position for the repeatability investigation

Five consecutive prime mover load measurements taken throughout the arc of elbow flexion are shown for one specimen. These plots correspond to the measurements taken for specimen 2, which is also the specimen discussed in the repeatability section of Chapter 3 (Section 3.3.1). Note the variation in prime mover load between each consecutive flexion cycle.

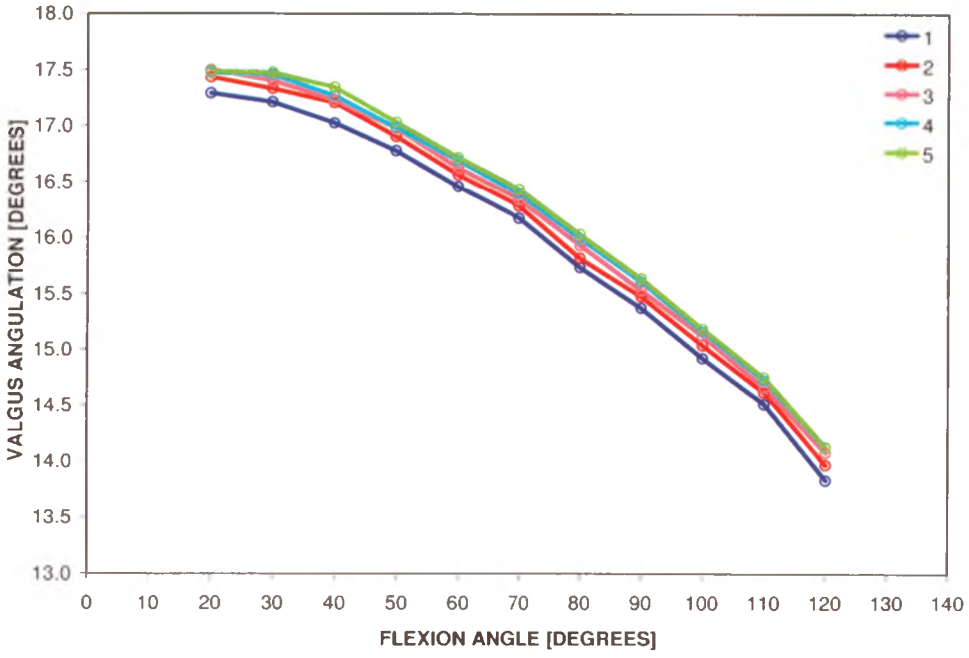

Figure A7.2: Valgus angulation measurements of one specimen tested in active flexion in the valgus position for the repeatability investigation

Five consecutive valgus angulation measurements taken at every 10° of elbow flexion are shown for one specimen. These plots correspond to the measurements taken for specimen 2, which is also the specimen discussed in the repeatability section of Chapter 3 (Section 3.3.1). Note the variation in the motion pathways between each consecutive flexion cycle.

A7.2.2 Repeatability Results for all Four Test Conditions

Table A7.3: Minimum and maximum standard deviations of the average AMCL tension for each specimen tested in active valgus neutral flexion for the repeatability investigation

Specimen No.	Standard Deviation [N]		Standard Deviation Expressed as a Percentage of the Average AMCL Tension [%]	
	minimum	maximum	minimum	maximum
1	± 0.03	± 0.89	± 0.07 (± 0.0348 N / 46.7161 N) (± 0.0348 N / 46.9371 N)	± 1.20 (± 0.8948 N / 74.8089 N)
2	± 1.23	± 5.99	± 0.91 (± 1.2294 N / 135.3047 N)	± 12.97 (± 5.3315 N / 41.0990 N)
3	± 0.80	± 4.13	± 1.21 (± 0.8024 N / 66.4972 N)	± 4.15 (± 4.1279 N / 99.4746 N)
4	± 0.32	± 2.91	± 0.76 (± 0.3220 N / 42.5267 N)	± 5.93 (± 2.8395 N / 47.8926 N)
5	± 0.81	± 3.32	± 1.45 (± 0.8206 N / 56.5827 N)	± 3.63 (± 2.3463 N / 64.5498 N)

Table A7.4: Minimum and maximum standard deviations of the average AMCL tension for each specimen tested in passive valgus neutral flexion for the repeatability investigation

Specimen No.	Standard Deviation [N]		Standard Deviation Expressed as a Percentage of the Average Tension [%]	
	minimum	maximum	minimum	maximum
1	± 0.18	± 1.75	± 0.28 (± 0.1838 N / 66.1721 N)	± 3.08 (± 1.7526 N / 56.8158 N)
2	± 0.76	± 3.28	± 0.50 (± 0.7611 N / 152.0960 N)	± 4.15 (± 2.1390 N / 51.5978 N)
3	± 4.94	± 10.08	± 5.73 (± 4.9375 N / 86.1138 N)	± 10.37 (± 10.0780 N / 97.1774 N)
4	± 1.06	± 6.15	± 1.74 (± 1.2532 N / 71.8339 N)	± 8.90 (± 6.1470 N / 69.0841 N)
5	± 0.48	± 4.59	± 0.77 (± 0.4801 N / 62.6138 N)	± 4.48 (± 4.4211 N / 98.7932 N) (± 4.4315 N / 98.8434 N) (± 4.4369 N / 99.0010 N)

Table A7.5: Minimum and maximum standard deviations of the average AMCL tension for each specimen tested in active dependent neutral flexion for the repeatability investigation

Specimen No.	Standard Deviation [N]		Standard Deviation Expressed as a Percentage of the Average Tension [%]	
	minimum	maximum	minimum	maximum
1	± 0.34	± 1.62	± 0.24 (± 0.0731 N / 30.4084 N)	± 108.25 (± 0.1296 N / 0.1197 N)
2	± 0.51	± 4.15	± 2.33 (± 1.5940 N / 68.4576 N)	± 36.74 (± 0.6763 N / 1.8405 N)
3	± 2.47	± 6.06	± 6.68 (± 3.3489 N / 50.1100 N)	± 15.86 (± 4.3243 N / 27.2653 N)
5	± 0.32	± 5.91	± 5.62 (± 0.0234 N / 0.4165 N)	± 223.61 (± 0.0080 N / 0.0036 N)

TableA7.6: Minimum and maximum standard deviations of the average AMCL tension for each specimen tested in passive dependent neutral flexion for the repeatability investigation

Specimen No.	Standard Deviation [N]		Standard Deviation Expressed as a Percentage of the Average Tension [%]	
	minimum	maximum	minimum	maximum
1	± 0.14	± 2.97	± 1.95 (± 0.0259 N / 1.3316 N)	± 91.12 (± 0.3818 N / 0.4189 N)
2	± 0.23	± 8.53	± 7.97 (± 0.2350 N / 2.9464 N)	± 25.30 (± 2.0581 N / 8.1342 N)
3	± 3.96	± 11.44	± 15.08 (± 4.5496 N / 30.1681 N)	± 51.42 (± 5.0834 N / 9.8868 N)
5	± 1.05	± 3.88	± 3.91 (± 2.4990 N / 63.9428 N)	± 223.61 (± 0.0562 N / 0.0251 N)

A7.2.3 Valgus Position: Active Elbow Flexion

A7.2.3.1 *Specimen Specific AMCL Tension Trends*

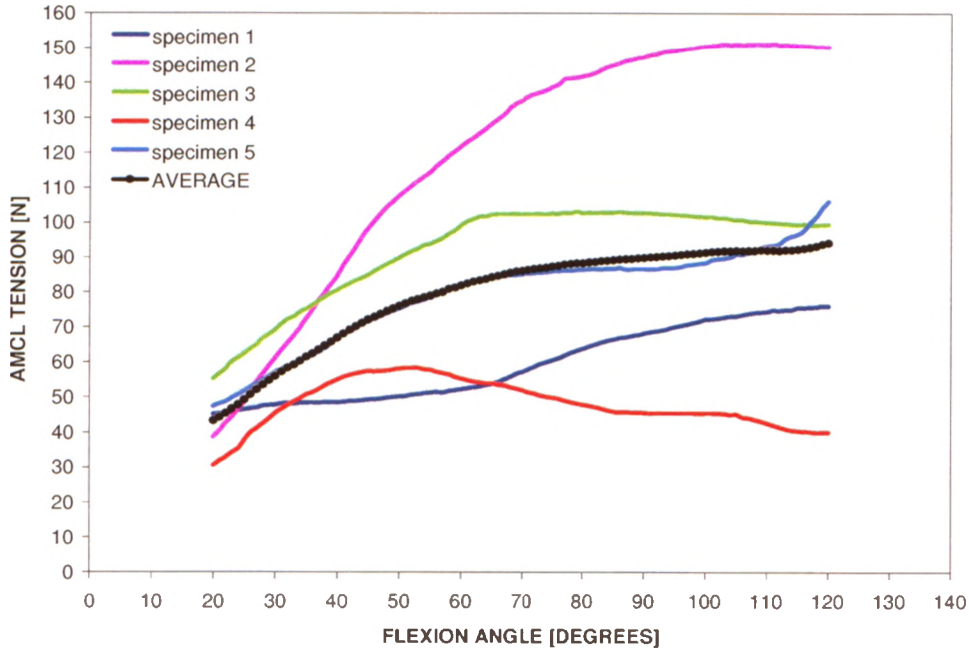

Figure A7.3: Variation of AMCL tension with flexion angle for active flexion in the valgus position for the native AMCL study

Each curve corresponds to the AMCL tension levels of the third flexion cycle for each specimen tested (n = 5); the average AMCL tension levels for these five specimen curves are also shown. Standard deviations are omitted for clarity but ranged from ±8.7 N to ±40.5 N for the average curve.

Table A7.7: Minimum and maximum AMCL tension magnitudes for active valgus neutral flexion for the native AMCL study

Ranges of AMCL tension magnitudes (considering all degrees of elbow flexion) for specimens 1 through 5, as well as for the average.

Specimen 1	
minimum:	45.2 N at both 20º and 21º of flexion
maximum:	76.0 N at 119º of flexion
Specimen 2	
minimum:	38.7 N at 20º of flexion
maximum:	151.1 N at 111º of flexion
Specimen 3	
minimum:	55.2 N at 20º of flexion
maximum:	103.0 N at 79º of flexion
Specimen 4	
minimum:	30.6 N at 20º of flexion
maximum:	58.3 N at 51º, 52º, and 53º of flexion
Specimen 5	
minimum:	47.3 N at 20º of flexion
maximum:	106.0 N at 120º of flexion
Average	
minimum:	43.4 ± 9.3 N at 20º of flexion
maximum:	94.3 ± 40.5 N at 120º of flexion

Table A7.8: AMCL tension at every 10° of elbow flexion for each specimen tested in active valgus neutral flexion for the native AMCL study

Flexion Angle [Degrees]	Specimen 1	Specimen 2	Specimen 3	Specimen 4	Specimen 5	Average	
	AMCL Tension [N]	AMCL Tension [N]	AMCL Tension [N]	AMCL Tension [N]	AMCL Tension [N]	AMCL Tension [N]	Standard Deviation [N]
20	45.2	38.7	55.2	30.6	47.3	43.4	± 9.3
30	47.8	61.0	69.0	45.4	56.9	56.0	± 9.7
40	48.4	84.4	80.4	55.0	66.7	67.0	± 15.6
50	50.1	107.5	89.7	58.1	75.1	76.1	± 23.3
60	52.2	121.8	99.0	55.3	81.8	82.0	± 29.5
70	57.1	134.8	102.2	51.9	84.9	86.2	± 34.0
80	63.7	141.7	102.6	47.9	86.4	88.4	± 36.4
90	68.0	147.2	102.5	45.6	86.5	90.0	± 38.4
100	72.1	150.3	101.4	45.4	88.3	91.5	± 39.0
110	74.3	150.9	99.8	42.6	93.0	92.1	± 39.6
120	75.9	150.1	99.3	40.0	106.0	94.3	± 40.5

Table A7.9: AMCL tension one-way repeated measures ANOVA statistical analysis results (p-value) for active valgus neutral flexion for the native AMCL study

Main effect of flexion angle on AMCL tension	p = 0.052

A7.2.3.2 *Specimen Specific Motion Pathways*

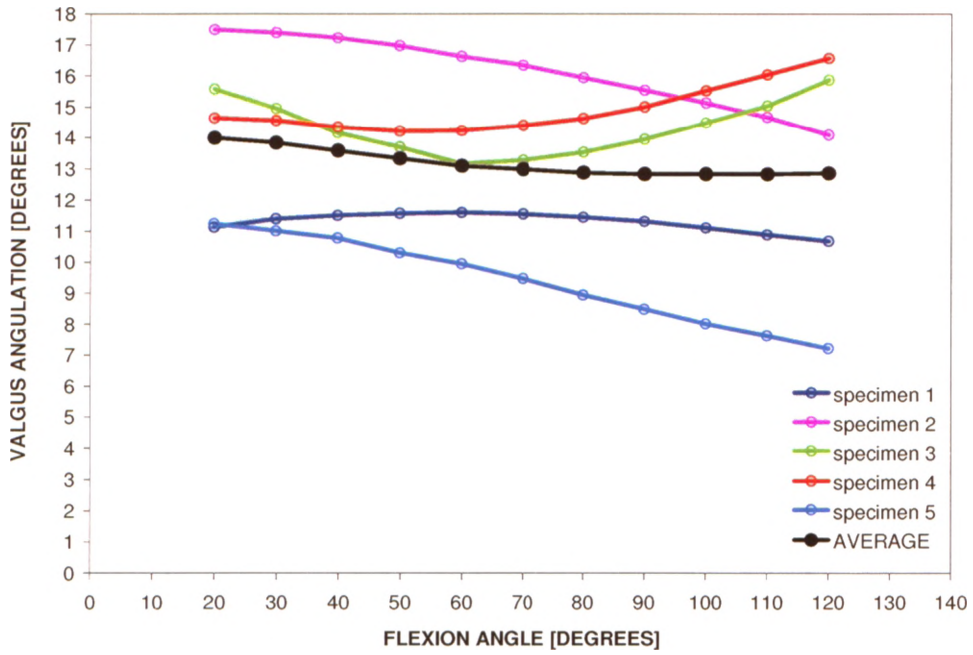

Figure A7.4: Elbow kinematic pathways for active flexion in the valgus position for the native AMCL study

Each curve corresponds to the valgus angulations (at every 10° of elbow flexion) of the third flexion cycle for each specimen tested (n = 5); the average valgus angulations for these five specimen curves are also shown. Standard deviations are omitted for clarity but ranged from ±2.5° to ±3.9° for the average curve.

Table A7.10: Minimum and maximum valgus angulations for active valgus neutral flexion for the native AMCL study

Ranges of valgus angulations (considering all degrees of elbow flexion) for specimens 1 through 5, as well as for the average.

Specimen 1	
maximum:	11.6º at both 50º and 60º of flexion
minimum:	10.7º at 120º of flexion
Specimen 2	
maximum:	17.5º at 20º of flexion
minimum:	14.1º at 120º of flexion
Specimen 3	
maximum:	15.9º at 120º of flexion
minimum:	13.2º at 60º of flexion
Specimen 4	
maximum:	16.6º at 120º of flexion
minimum:	14.2º at both 50º and 60º of flexion
Specimen 5	
maximum:	11.2º at 20º of flexion
minimum:	7.2º at 120º of flexion
Average	
maximum:	14.0 ± 2.8º at 20º of flexion
minimum:	12.8 ± 2.9º, 12.8 ± 3.2º, and 12.8 ± 3.5º at 90º, 100º and 110º of flexion, respectively

Table A7.11: Valgus angulation at every 10º of elbow flexion for each specimen tested in active valgus neutral flexion for the native AMCL study

Flexion Angle [Degrees]	Specimen 1	Specimen 2	Specimen 3	Specimen 4	Specimen 5	Average	
	Valgus Angulation [Degrees]	Valgus Angulation [Degrees]	Valgus Angulation [Degrees]	Valgus Angulation [Degrees]	Valgus Angulation [Degrees]	Valgus Angulation [Degrees]	Standard Deviation [Degrees]
20	11.1	17.5	15.6	14.6	11.2	14.0	± 2.8
30	11.4	17.4	14.9	14.6	11.0	13.9	± 2.7
40	11.5	17.2	14.1	14.4	10.8	13.6	± 2.6
50	11.6	17.0	13.7	14.2	10.3	13.3	± 2.6
60	11.6	16.6	13.2	14.2	9.9	13.1	± 2.5
70	11.5	16.3	13.3	14.4	9.5	13.0	± 2.6
80	11.4	15.9	13.5	14.6	8.9	12.9	± 2.8
90	11.3	15.5	13.9	15.0	8.5	12.8	± 2.9
100	11.1	15.1	14.5	15.5	8.0	12.8	± 3.2
110	10.9	14.7	15.0	16.0	7.6	12.8	± 3.5
120	10.7	14.1	15.9	16.6	7.2	12.9	± 3.9

Table A7.12: Valgus angulation one-way repeated measures ANOVA statistical analysis results (p-value) for active valgus neutral flexion for the native AMCL study

Main effect of flexion angle on valgus angulation	p = 0.396

A7.2.4 Valgus Position: Passive Elbow Flexion

A7.2.4.1 *Specimen Specific AMCL Tension Trends*

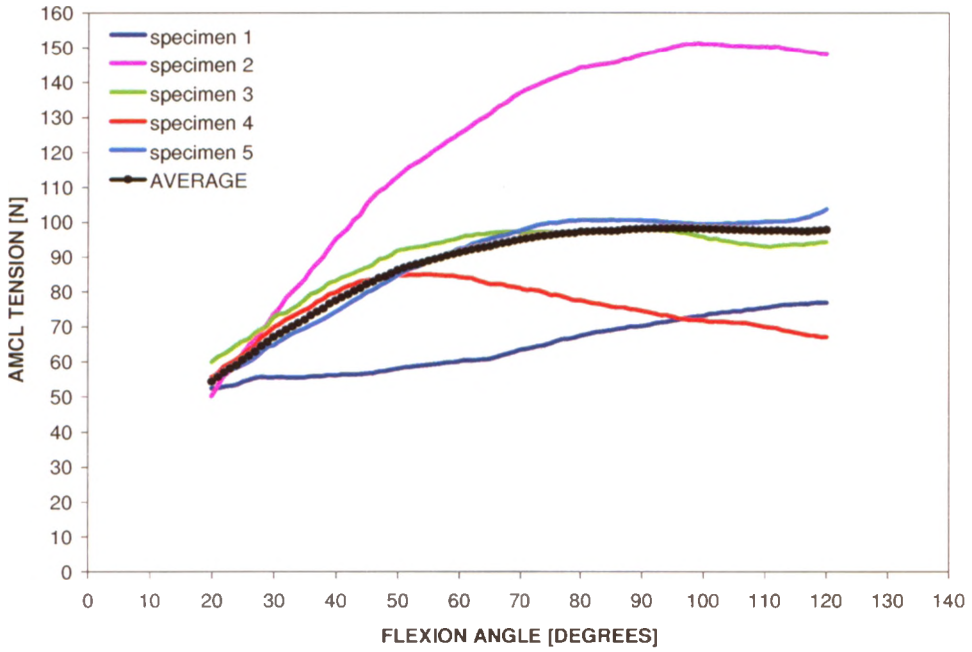

Figure A7.5: Variation of AMCL tension with flexion angle for passive flexion in the valgus position for the native AMCL study

Each curve corresponds to the AMCL tension levels of the third flexion cycle for each specimen tested (n = 5); the average AMCL tension levels for these five specimen curves are also shown. Standard deviations are omitted for clarity but ranged from ±3.4 N to ±32.2 N for the average curve.

Table A7.13: Minimum and maximum AMCL tension magnitudes for passive valgus neutral flexion for the native AMCL study

Ranges of AMCL tension magnitudes (considering all degrees of elbow flexion) for specimens 1 through 5, as well as for the average.

Specimen 1	
minimum:	52.3 N at 20º of flexion
maximum:	76.8 N at both 119º and 120º of flexion
Specimen 2	
minimum:	50.1 N at 20º of flexion
maximum:	151.1 N at 99º of flexion
Specimen 3	
minimum:	59.8 N at 20º of flexion
maximum:	98.0 N at 89º, 90º, and 91º of flexion
Specimen 4	
minimum:	55.6 N at both 20º and 21º of flexion
maximum:	85.0 N at 55º of flexion
Specimen 5	
minimum:	54.3 N at 20º of flexion
maximum:	103.5 N at 120º of flexion
Average	
minimum:	54.4 ± 3.6 N at 20º of flexion
maximum:	98.4 ± 31.8 N at 95º of flexion

Table A7.14: AMCL tension at every 10º of elbow flexion for each specimen tested in passive valgus neutral flexion for the native AMCL study

Flexion Angle [Degrees]	Specimen 1	Specimen 2	Specimen 3	Specimen 4	Specimen 5	Average	
	AMCL Tension [N]	AMCL Tension [N]	AMCL Tension [N]	AMCL Tension [N]	AMCL Tension [N]	AMCL Tension [N]	Standard Deviation [N]
20	52.3	50.1	59.8	55.6	54.3	54.4	± 3.6
30	55.5	73.4	72.5	69.7	64.5	67.1	± 7.4
40	56.0	94.9	83.0	79.8	74.1	77.6	± 14.2
50	57.9	112.9	91.7	84.7	84.6	86.4	± 19.6
60	60.0	125.3	95.3	84.2	92.3	91.4	± 23.5
70	63.3	136.9	97.0	81.0	97.4	95.1	± 27.2
80	67.4	144.1	97.2	77.5	100.4	97.3	± 29.5
90	70.1	147.9	98.0	74.5	100.3	98.2	± 30.9
100	73.0	151.0	95.6	71.7	99.4	98.1	± 32.1
110	75.3	150.2	92.9	69.9	99.9	97.6	± 31.9
120	76.8	148.0	94.2	66.9	103.5	97.9	± 31.5

Table A7.15: AMCL tension one-way repeated measures ANOVA statistical analysis results (p-value) for passive valgus neutral flexion for the native AMCL study

Main effect of flexion angle on AMCL tension	p = 0.048

A7.2.4.2 *Specimen Specific Motion Pathways*

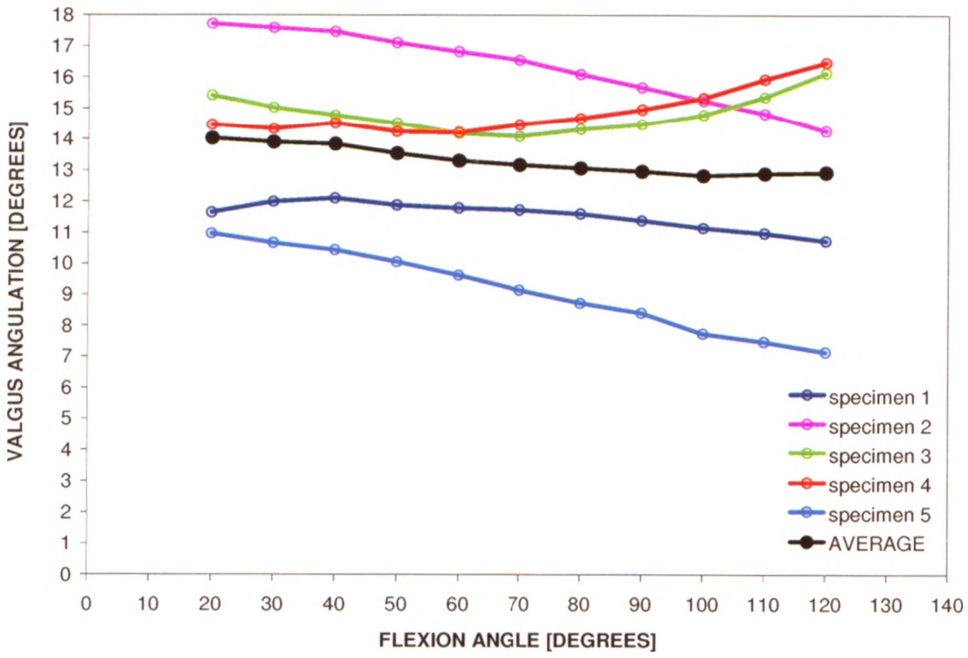

Figure A7.6: Elbow kinematic pathways for passive flexion in the valgus position for the native AMCL study

Each curve corresponds to the valgus angulations (at every 10° of elbow flexion) of the third flexion cycle for each specimen tested (n = 5); the average valgus angulations for these five specimen curves are also shown. Standard deviations are omitted for clarity but ranged from ±2.7° to ±4.0° for the average curve.

Table A7.16: Minimum and maximum valgus angulations for passive valgus neutral flexion for the native AMCL study

Ranges of valgus angulations (considering all degrees of elbow flexion) for specimens 1 through 5, as well as for the average.

Specimen 1	
maximum:	12.1º at 40º of flexion
minimum:	10.7º at 120º of flexion
Specimen 2	
maximum:	17.7º at 20º of flexion
minimum:	14.3º at 120º of flexion
Specimen 3	
maximum:	16.1º at 120º of flexion
minimum:	14.1º at 70º of flexion
Specimen 4	
maximum:	16.5º at 120º of flexion
minimum:	14.2º at both 50º and 60º of flexion
Specimen 5	
maximum:	11.0º at 20º of flexion
minimum:	7.1º at 120º of flexion
Average	
maximum:	14.0 ± 2.8º at 20º of flexion
minimum:	12.8 ± 3.3º at 100º of flexion

Table A7.17: Valgus angulation at every 10° of elbow flexion for each specimen tested in passive valgus neutral flexion for the native AMCL study

Flexion Angle [Degrees]	Specimen 1	Specimen 2	Specimen 3	Specimen 4	Specimen 5	Average	
	Valgus Angulation [Degrees]	Valgus Angulation [Degrees]	Valgus Angulation [Degrees]	Valgus Angulation [Degrees]	Valgus Angulation [Degrees]	Valgus Angulation [Degrees]	Standard Deviation [Degrees]
20	11.6	17.7	15.4	14.5	11.0	14.0	± 2.8
30	12.0	17.6	15.0	14.3	10.7	13.9	± 2.7
40	12.1	17.5	14.8	14.5	10.4	13.9	± 2.7
50	11.9	17.1	14.5	14.2	10.0	13.6	± 2.7
60	11.8	16.8	14.2	14.2	9.6	13.3	± 2.7
70	11.7	16.5	14.1	14.5	9.1	13.2	± 2.8
80	11.6	16.1	14.3	14.7	8.7	13.1	± 2.9
90	11.4	15.7	14.5	15.0	8.4	13.0	± 3.0
100	11.1	15.2	14.8	15.3	7.7	12.8	± 3.3
110	11.0	14.8	15.3	15.9	7.5	12.9	± 3.6
120	10.7	14.3	16.1	16.5	7.1	12.9	± 4.0

Table A7.18: Valgus angulation one-way repeated measures ANOVA statistical analysis results (p-value) for passive valgus neutral flexion for the native AMCL study

Main effect of flexion angle on valgus angulation	p = 0.344

A7.2.5 Valgus Position: Active versus Passive Elbow Flexion

A7.2.5.1 *Comparison of Active and Passive AMCL Tensions*

Comparing the passive AMCL tension levels (Figure A7.5) with their respective active AMCL tension levels (Figure A7.3), for the valgus position, the following observations were made:

(1) For specimen 1, passive and active tension trends were similar. Passive tensions were greater than active tensions at all degrees of elbow flexion (more prominently within beginning and mid-range flexion); the largest difference between passive and active AMCL tensions was approximately **8.3 N**, which occurred at **27°** of elbow flexion.

(2) For specimen 2, passive and active tension trends were similar. Passive tensions were greater than active tensions within approximately 20° and 100° of elbow flexion (more prominently within beginning and mid-range flexion), and for flexion angles greater than approximately 100°, passive tensions were slightly less than active tensions; the largest difference between passive and active AMCL tensions was approximately **13.6 N**, which occurred at **25°** of elbow flexion.

(3) For specimen 3, passive and active tension trends were similar. Passive tensions were greater than active tensions up to approximately 55° of elbow flexion, and for flexion angles greater than approximately 55°, passive tensions were less than active tensions; the largest difference between passive and active AMCL tensions was approximately **7.0 N**, which occurred at **106°** of elbow flexion.

(4) For specimen 4, passive and active tension trends were similar. Passive tensions were greater than active tensions at all degrees of elbow flexion; the largest difference between passive and active AMCL tensions was approximately **29.9 N**, which occurred at **84°** of elbow flexion.

(5) For specimen 5, passive and active tension trends were similar. Passive tensions were greater than active tensions at all degrees of elbow flexion except at full flexion, where passive tensions were slightly less than active tensions; the largest difference between passive and active AMCL tensions was approximately **14.2 N**, which occurred at **78°** of elbow flexion.

(6) For the average curves (Figure 3.5), passive and active tension trends were similar. Passive tensions were greater than active tensions at all degrees of elbow flexion; the largest difference between passive and active AMCL tensions was approximately **11.5 N**, which occurred at **22°** of elbow flexion. There was no statistical difference in the average AMCL tensions between active and passive elbow flexion, for the valgus position ($p = 0.159$).

A7.2.5.2 *Comparison of Active and Passive Motion Pathways*

Comparing the passive motion pathways (Figure A7.6) with their respective active motion pathways (Figure A7.4), for the valgus position, the following observations were made when closely comparing the motion pathways:

(1) For specimen 1, passive and active motion pathways were similar. The passive motion pathway tracked in greater valgus than the active motion pathway at all degrees of elbow flexion (more prominently within 20° and 90° of elbow flexion); however, the largest difference between passive and active valgus angulations was only approximately **0.6°**, which occurred at both **30°** and **40°** degrees of elbow flexion.

(2) For specimen 2, passive and active motion pathways were similar. The passive motion pathway tracked in greater valgus than the active motion pathway at all degrees of elbow flexion; however, the largest difference between passive and active valgus angulations was only approximately **0.2°**, which occurred at all angles of elbow flexion except at **50°**, **90°**, and **100°** of elbow flexion.

(3) For specimen 3, passive and active motion pathways were similar. The passive motion pathway tracked in greater valgus after approximately 30° of elbow flexion (more prominently within mid-range flexion); however, the largest difference between passive and active valgus angulations was only approximately **1.0°**, which occurred at **60°** of elbow flexion.

(4) For specimen 4, passive and active motion pathways were similar. The active motion pathway tracked in greater valgus than the passive motion pathway within approximately 20°-35° and 85°-120° of elbow flexion; however, the largest

difference between passive and active valgus angulations was only approximately **0.2°**, which occurred at **20°**, **30°**, **40°**, and **100°** of elbow flexion.

(5) For specimen 5, passive and active motion pathways were similar. The active motion pathway tracked in greater valgus than the passive motion pathway at all degrees of elbow flexion; however, the largest difference between passive and active valgus angulations was only approximately **0.3°**, which occurred at all angles of elbow flexion except at **80°**, **90°**, **110°**, and **120°** of elbow flexion.

(6) For the average curves (Figure 3.6), passive and active motion pathways were similar. The passive motion pathway tracked in greater valgus than the active motion pathway at all degrees of elbow flexion (more prominently within 30° and 100° of elbow flexion); however, the largest difference between passive and active valgus angulations was only approximately **0.3°**, which occurred at **40°** of elbow flexion. There was no statistical difference in the average motion pathways between active and passive elbow flexion, for the valgus position ($p = 0.375$).

A7.2.6 Dependent Position: Active Elbow Flexion

A7.2.6.1 *Specimen Specific AMCL Tension Trends*

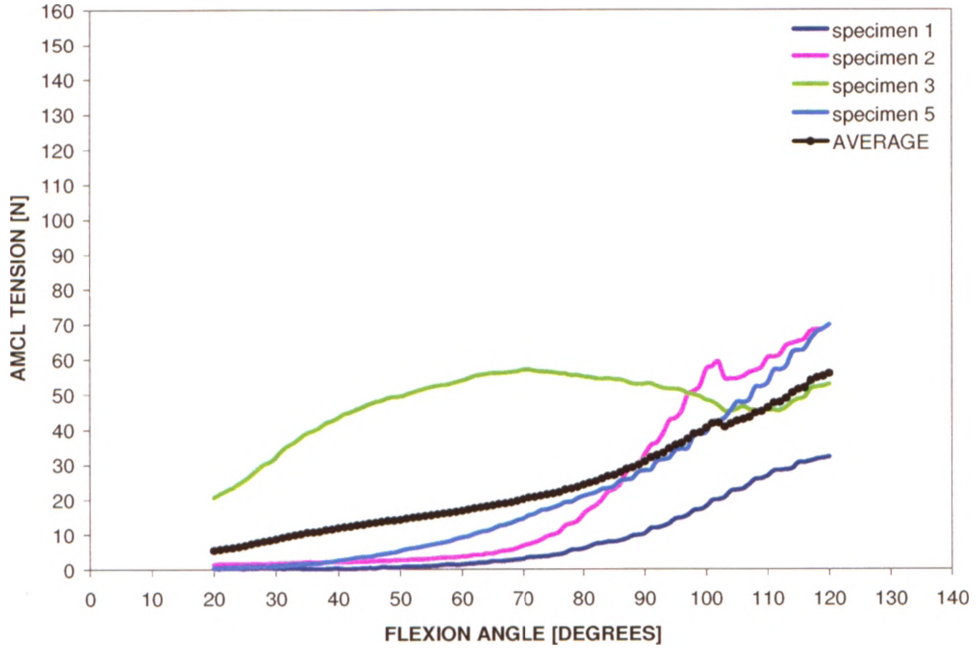

Figure A7.7: Variation of AMCL tension with flexion angle for active flexion in the dependent position for the native AMCL study

Each curve corresponds to the AMCL tension levels of the third flexion cycle for each specimen tested (n = 4); the average AMCL tension levels for these four specimen curves are also shown. Standard deviations are omitted for clarity but ranged from ±10.0 N to ±25.3 N for the average curve. It should be noted that the "bumps" in the AMCL tension curves, including the average curve, correspond to forearm "shaking" during active simulated flexion in this orientation; the simulator was unable to smoothly move the forearm through the arc of elbow flexion in the dependent position.

Table A7.19: Minimum and maximum AMCL tension magnitudes for active dependent neutral flexion for the native AMCL study

Ranges of AMCL tension magnitudes (considering all degrees of elbow flexion) for specimens 1, 2, 3, and 5, as well as for the average.

Specimen 1	
minimum:	0 N at both 20º and 40º of flexion
maximum:	31.9 N at 120º of flexion
Specimen 2	
minimum:	1.3 N at 20º of flexion
maximum:	69.6 N at 120º of flexion
Specimen 3	
minimum:	20.4 N at 20º of flexion
maximum:	56.9 N at 71º of flexion
Specimen 5	
minimum:	0.3 N at 20º of flexion
maximum:	69.6 N at 120º of flexion
Average	
minimum:	5.5 ± 10.0 N at 20º of flexion
maximum:	56.0 ± 17.9 N at 120º of flexion

Table A7.20: AMCL tension at every 10° of elbow flexion for each specimen tested in active dependent neutral flexion for the native AMCL study

Flexion Angle [Degrees]	Specimen 1	Specimen 2	Specimen 3	Specimen 5	Average	
	AMCL Tension [N]	AMCL Tension [N]	AMCL Tension [N]	AMCL Tension [N]	AMCL Tension [N]	Standard Deviation [N]
20	0.0	1.3	20.4	0.3	5.5	± 10.0
30	0.1	1.6	31.9	1.0	8.7	± 15.5
40	0.0	2.1	43.2	2.4	11.9	± 20.9
50	0.3	2.5	49.3	5.2	14.3	± 23.4
60	1.1	3.6	53.8	9.0	16.9	± 24.8
70	2.7	6.7	56.8	14.4	20.2	± 24.9
80	5.6	15.7	54.9	20.8	24.2	± 21.4
90	9.9	32.6	52.8	28.1	30.9	± 17.6
100	17.7	57.0	48.2	39.0	40.5	± 16.9
110	26.5	60.3	45.4	53.0	46.3	± 14.6
120	31.9	69.6	52.7	69.6	56.0	± 17.9

Table A7.21: AMCL tension one-way repeated measures ANOVA statistical analysis results (p-value) for active dependent neutral flexion for the native AMCL study

Main effect of flexion angle on AMCL tension	p = 0.055

A7.2.6.2 *Specimen Specific Motion Pathways*

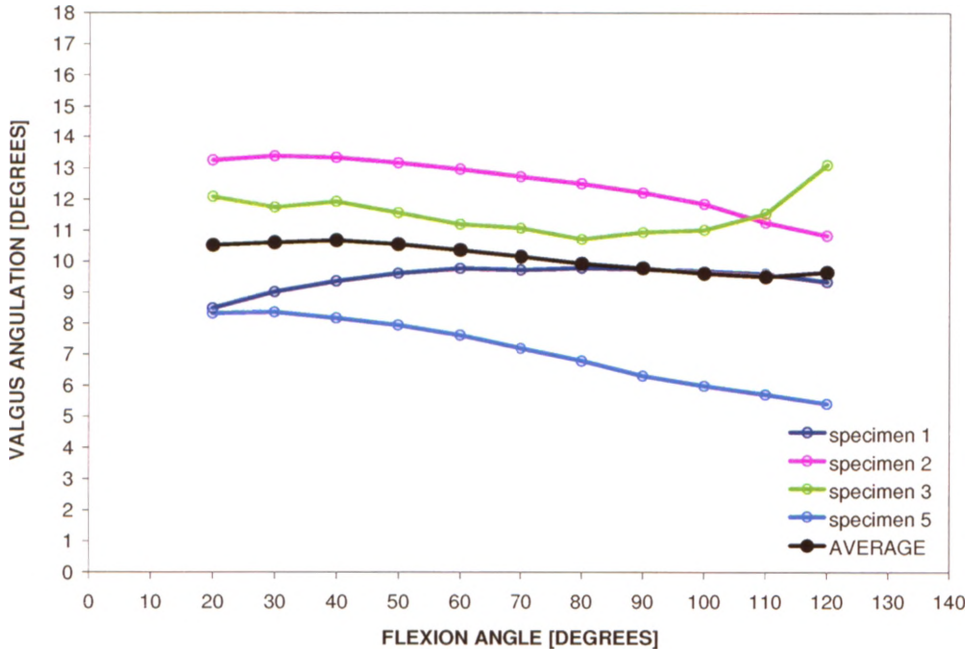

Figure A7.8: Elbow kinematic pathways for active flexion in the dependent position for the native AMCL study

Each curve corresponds to the valgus angulations (at every 10° of elbow flexion) of the third flexion cycle for each specimen tested (n = 4); the average valgus angulations for these four specimen curves are also shown. Standard deviations are omitted for clarity but ranged from ±2.3° to ±3.2° for the average curve.

Table A7.22: Minimum and maximum valgus angulations for active dependent neutral flexion for the native AMCL study

Ranges of valgus angulations (considering all degrees of elbow flexion) for specimens 1, 2, 3, and 5, as well as for the average.

Specimen 1	
maximum:	9.8º at both 60º and 80º of flexion
minimum:	8.5º at 20º of flexion
Specimen 2	
maximum:	13.4º at 30º of flexion
minimum:	10.8º at 120º of flexion
Specimen 3	
maximum:	13.1º at 120º of flexion
minimum:	10.7º at 80º of flexion
Specimen 5	
maximum:	8.3º at both 20º and 30º of flexion
minimum:	5.4º at 120º of flexion
Average	
maximum:	10.7 ± 2.4º at 40º of flexion
minimum:	9.5 ± 2.7º at 110º of flexion

Table A7.23: Valgus angulation at every 10° of elbow flexion for each specimen tested in active dependent neutral flexion for the native AMCL study

Flexion Angle [Degrees]	Specimen 1	Specimen 2	Specimen 3	Specimen 5	Average	
	Valgus Angulation [Degrees]	Valgus Angulation [Degrees]	Valgus Angulation [Degrees]	Valgus Angulation [Degrees]	Valgus Angulation [Degrees]	Standard Deviation [Degrees]
20	8.5	13.2	12.1	8.3	10.5	± 2.5
30	9.0	13.4	11.7	8.3	10.6	± 2.4
40	9.3	13.3	11.9	8.2	10.7	± 2.4
50	9.6	13.2	11.6	7.9	10.6	± 2.3
60	9.8	13.0	11.2	7.6	10.4	± 2.3
70	9.7	12.7	11.1	7.2	10.2	± 2.3
80	9.8	12.5	10.7	6.8	9.9	± 2.4
90	9.7	12.2	10.9	6.3	9.8	± 2.5
100	9.7	11.8	11.0	6.0	9.6	± 2.6
110	9.6	11.2	11.5	5.7	9.5	± 2.7
120	9.3	10.8	13.1	5.4	9.7	± 3.2

Table 7.24: Valgus angulation one-way repeated measures ANOVA statistical analysis results (p-value) for active dependent neutral flexion for the native AMCL study

Main effect of flexion angle on valgus angulation	p = 0.355

A7.2.7 Dependent Position: Passive Elbow Flexion

A7.2.7.1 *Specimen Specific AMCL Tension Trends*

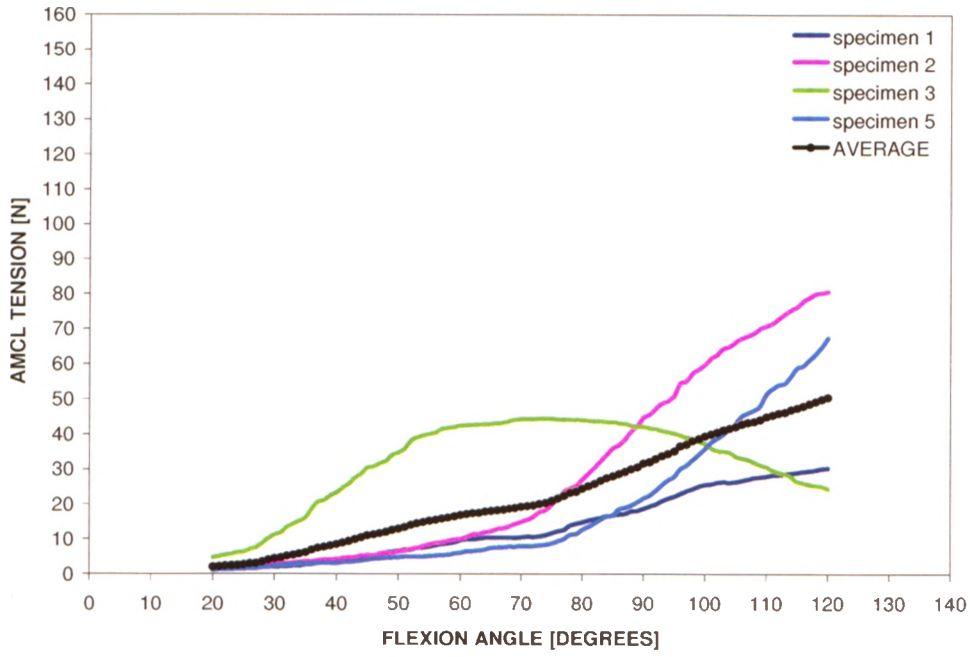

Figure A7.9: Variation of AMCL tension with flexion angle for passive flexion in the dependent position for the native AMCL study

Each curve corresponds to the AMCL tension levels of the third flexion cycle for each specimen tested (n = 4); the average AMCL tension levels for these four specimen curves are also shown. Standard deviations are omitted for clarity but ranged from ±1.7 N to ±27.5 N for the average curve.

Table A7.25: Minimum and maximum AMCL tension magnitudes for passive dependent neutral flexion for the native AMCL study

Ranges of AMCL tensions magnitudes (considering all degrees of elbow flexion) for specimens 1, 2, 3, and 5, as well as for the average.

Specimen 1	
minimum:	1.0 N at 20º of flexion
maximum:	30.2 N at 120º of flexion
Specimen 2	
minimum:	1.6 N at 20º of flexion
maximum:	80.5 N at 120º of flexion
Specimen 3	
minimum:	4.6 N at 20º of flexion
maximum:	44.2 N at 70º, 71º, 72º, 73º, 74º, and 75º of flexion
Specimen 5	
minimum:	1.0 N at 20º of flexion
maximum:	67.2 N at 120º of flexion
Average	
minimum:	2.0 ± 1.7 N at 20º of flexion
maximum:	50.6 ± 27.5 N at 120º of flexion

Table A7.26: AMCL tension at every 10º of elbow flexion for each specimen tested in passive dependent neutral flexion for the native AMCL study

Flexion Angle [Degrees]	Specimen 1	Specimen 2	Specimen 3	Specimen 5	Average	
	AMCL Tension [N]	AMCL Tension [N]	AMCL Tension [N]	AMCL Tension [N]	AMCL Tension [N]	Standard Deviation [N]
20	1.0	1.6	4.6	1.0	2.0	± 1.7
30	1.8	2.7	11.1	2.2	4.5	± 4.4
40	3.7	4.2	23.2	2.9	8.5	± 9.8
50	6.4	6.3	34.7	4.7	13.0	± 14.5
60	9.6	9.9	42.3	5.9	16.9	± 17.0
70	10.4	14.8	44.2	7.8	19.3	± 16.8
80	14.7	26.9	43.9	12.5	24.5	± 14.4
90	18.7	44.7	42.1	21.6	31.8	± 13.5
100	25.5	59.6	37.2	35.7	39.5	± 14.4
110	27.9	70.8	30.5	51.2	45.1	± 20.0
120	30.2	80.5	24.3	67.2	50.6	± 27.5

Table A7.27: AMCL tension one-way repeated measures ANOVA statistical analysis results (p-value) for passive dependent neutral flexion for the native AMCL study

Main effect of flexion angle on AMCL tension	p = 0.081

A7.2.7.2 *Specimen Specific Motion Pathways*

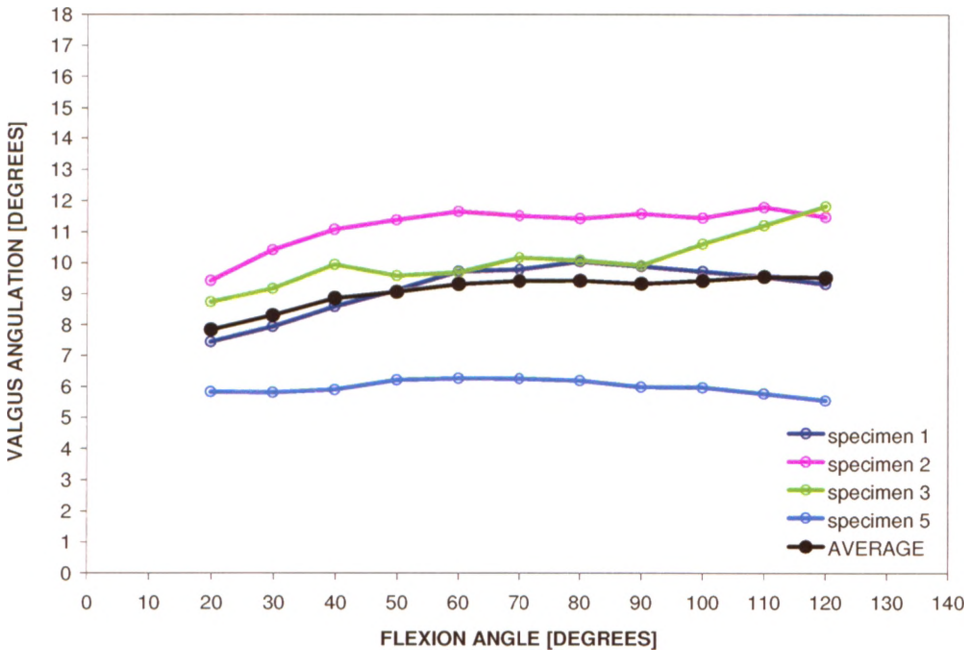

Figure A7.10: Elbow kinematic pathways for passive flexion in the dependent position for the native AMCL study

Each curve corresponds to the valgus angulations (at every 10° of elbow flexion) of the third flexion cycle for each specimen tested (n = 4); the average valgus angulations for these four specimen curves are also shown. Standard deviations are omitted for clarity but ranged from ±1.6° to ±2.9° for the average curve.

Table A7.28: Minimun and maximum valgus angulations for passive dependent neutral flexion for the native AMCL study

Ranges of valgus angulations (considering all degrees of elbow flexion) for specimens 1, 2, 3, and 5, as well as for the average.

Specimen 1	
maximum:	10.0º at 80º of flexion
minimum:	7.4º at 20º of flexion
Specimen 2	
maximum:	11.8º at 110º of flexion
minimum:	9.4º at 20º of flexion
Specimen 3	
maximum:	11.8º at 120º of flexion
minimum:	8.7º at 20º of flexion
Specimen 5	
maximum:	6.3º at 60º of flexion
minimum:	5.5º at 120º of flexion
Average	
maximum:	9.6 ± 2.7º at 110º of flexion
minimum:	7.8 ± 1.6º at 20º of flexion

Table A7.29: Valgus angulation at every 10° of elbow flexion for each specimen tested in passive dependent neutral flexion for the native AMCL study

Flexion Angle [Degrees]	Specimen 1	Specimen 2	Specimen 3	Specimen 5	Average	
	Valgus Angulation [Degrees]	Valgus Angulation [Degrees]	Valgus Angulation [Degrees]	Valgus Angulation [Degrees]	Valgus Angulation [Degrees]	Standard Deviation [Degrees]
20	7.4	9.4	8.7	5.8	7.8	± 1.6
30	7.9	10.4	9.1	5.8	8.3	± 2.0
40	8.6	11.1	9.9	5.9	8.9	± 2.2
50	9.1	11.4	9.6	6.2	9.1	± 2.1
60	9.7	11.6	9.7	6.3	9.3	± 2.2
70	9.8	11.5	10.2	6.2	9.4	± 2.3
80	10.0	11.4	10.1	6.2	9.4	± 2.3
90	9.9	11.6	9.9	6.0	9.3	± 2.4
100	9.7	11.4	10.6	6.0	9.4	± 2.4
110	9.5	11.8	11.2	5.8	9.6	± 2.7
120	9.3	11.5	11.8	5.5	9.5	± 2.9

Table A7.30: Valgus angulation one-way repeated measures ANOVA statistical analysis results (p-value) for passive dependent neutral flexion for the native AMCL study

Main effect of flexion angle on valgus angulation	p = 0.061

A7.2.8 Dependent Position: Active versus Passive Elbow Flexion

A7.2.8.1 *Comparison of Active and Passive AMCL Tensions*

When comparing the passive AMCL tension levels (Figure A7.9) with their respective active AMCL tension levels (Figure A7.7), for the dependent position, the following observations were made:

(1) For specimen 1, passive and active tension trends were similar. Passive tensions were greater than active tensions within approximately 20° and 110° of elbow flexion (more prominently within 40° and 100° of elbow flexion), and for flexion angles greater than approximately 110°, passive tensions were slightly less than active tensions; the largest difference between passive and active AMCL tensions was approximately **9.1 N**, which occurred at **80°** and **86°** of elbow flexion.

(2) For specimen 2, passive and active tension trends were similar. Passive tensions were greater than active tensions at all degrees of flexion; the largest difference between passive and active AMCL tensions was approximately **13.0 N**, which occurred at **85°** of elbow flexion.

(3) For specimen 3, passive and active tension trends were similar within approximately 20° and 110° of elbow flexion. Passive tensions were less than active tensions at all degrees of elbow flexion; the largest difference between passive and active AMCL tensions was approximately **28.4 N**, which occurred at **120°** of elbow flexion.

(4) For specimen 5, passive and active tension trends were similar. Passive tensions were slightly greater than, if not equal to, active tensions within approximately 20° and 50° of elbow flexion, and for flexion angles greater than approximately 50°, active tensions were slightly greater than passive tension; the largest difference between passive and active AMCL tensions was approximately **9.2 N**, which occurred at **77°** of elbow flexion.

(5) For the average curve (Figure 3.7), passive and active tension trends and levels were similar. Active tensions were slightly greater than passive tensions within approximately 20° and 50° of elbow flexion, as well as at flexion angles greater than approximately 110°; the largest difference between passive and active AMCL tensions was approximately **5.4 N**, which occurred at **120°** of elbow flexion. There was no statistical difference in the average AMCL tensions between active and passive elbow motion, for the dependent position ($p = 0.745$).

A7.2.8.2 *Comparison of Active and Passive Motion Pathways*

When comparing the passive motion pathways (Figure A7.10) with their respective active motion pathways (Figure A7.8), for the dependent position, the following observations were made:

(1) For specimen 1, passive and active motion pathways varied. The passive motion pathway tracked in greater valgus than the active motion pathway within approximately 65° and 105° of elbow flexion (most prominently at 80° of elbow flexion), and for flexion angles greater than approximately 105°, the passive and active motion pathways effectively coincided; however, the largest difference between passive and active valgus angulations was approximately **1.1°**, which occurred at **30°** of elbow flexion.

(2) For specimen 2, passive and active motion pathways varied. The passive motion pathway tracked in greater varus than the active motion pathway within approximately 20° and 105° of elbow flexion (more prominently at the beginning of flexion), and for flexion angles greater than approximately 105°, the passive motion pathway tracked in greater valgus than the active motion pathway; the largest difference between passive and active valgus angulations was approximately **3.8°**, which occurred at **20°** of elbow flexion.

(3) For specimen 3, passive and active motion pathways varied. The passive motion pathway tracked in greater varus than the active motion pathway at all degrees of flexion (more prominently at the beginning of flexion); the largest difference between passive and active valgus angulations was approximately **3.3°**, which occurred at **20°** of elbow flexion.

(4) For specimen 5, passive and active motion pathways varied. The passive motion pathway tracked in greater varus than the active motion pathway within approximately 20° and 100° of elbow flexion (more prominently at the beginning of flexion), and for flexion angles greater than approximately 100°, the passive and active motion pathways effectively coincided; the largest difference between passive and active valgus angulations was approximately **2.6°**, which occurred at **30°** of elbow flexion.

(5) For the average curve (Figure 3.8), passive and active motion pathways varied. The passive motion pathway tracked in greater varus than the active motion pathway within approximately 20° and 110° of elbow flexion (more prominently at the beginning of flexion), and for flexion angles greater than approximately 110°, the passive and active motion pathways effectively coincided; the largest difference between passive and active valgus angulations was approximately **2.7°**, which occurred at **20°** of elbow flexion. There was a statistical difference in the average motion pathways between active and passive elbow flexion, for the dependent position ($p = 0.030$).

A7.2.9 Comparison of Forearm Mass and AMCL Tension

A7.2.9.1 *Valgus Position: Active Elbow Flexion*

The load required to move the forearm through the arc of elbow flexion (*i.e.* the prime mover load) was approximately the same for all specimens, regardless of forearm mass (Figure A7.11); the variation in prime mover load at 60° of elbow flexion for specimens 2 through 5 was approximately 5.1 N (Figure A7.12). *Recall that the muscle that supplies the largest percentage of the total applied load responsible for producing the desired motion is designated as the prime mover; for elbow flexion, the brachialis is designated the prime mover.*

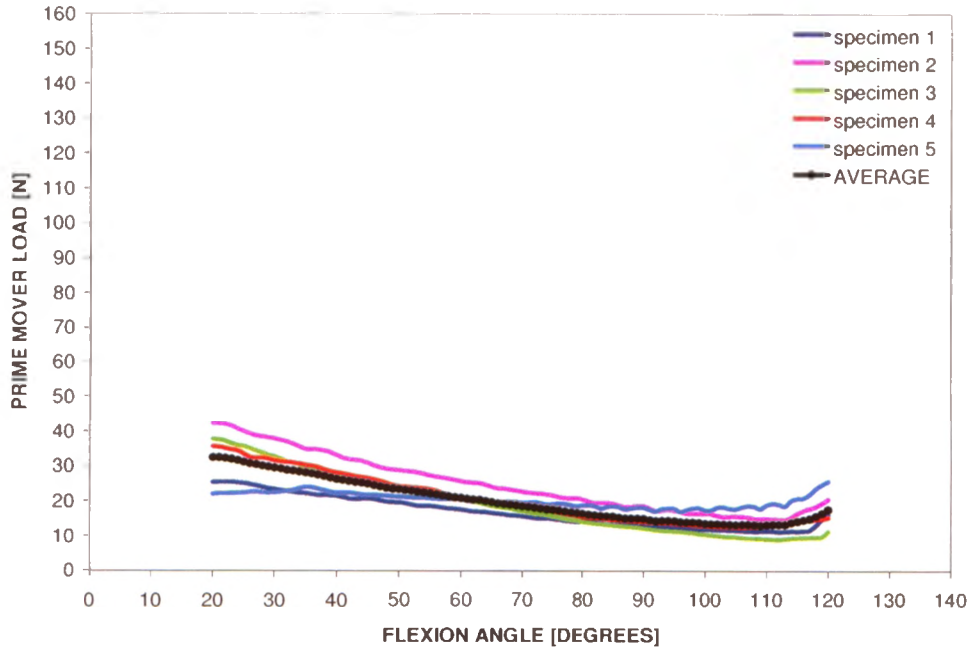

Figure A7.11: Prime mover load measurements for active flexion in the valgus position for the native AMCL study

Each curve corresponds to the prime mover loads of the third flexion cycle for each specimen tested (n = 5); the average prime mover loads for these five specimen curves are also shown. Standard deviations are omitted for clarity but ranged from ±2.5 N to ±8.6 N for the average curve.

Table A7.31: Prime mover load at every 10° of elbow flexion for each specimen tested in active valgus neutral flexion for the native AMCL study

Flexion Angle [Degrees]	Specimen 1	Specimen 2	Specimen 3	Specimen 4	Specimen 5	Average	
	Prime Mover Load [N]	Prime Mover Load [N]	Prime Mover Load [N]	Prime Mover Load [N]	Prime Mover Load [N]	Prime Mover Load [N]	Standard Deviation [N]
20	25.3	42.3	37.6	35.7	21.9	32.6	± 8.7
30	23.4	37.8	32.6	31.6	22.4	29.6	± 8.8
40	21.5	33.1	27.0	28.1	22.3	26.4	± 8.8
50	19.6	28.8	23.9	24.2	21.2	23.5	± 8.8
60	17.6	25.6	20.5	21.2	20.5	21.1	± 8.8
70	15.7	22.7	17.1	18.4	19.5	18.7	± 8.9
80	14.1	20.5	14.0	15.5	18.7	16.6	± 9.1
90	12.7	18.6	12.1	14.1	18.1	15.1	± 9.4
100	11.9	16.4	10.3	12.9	17.3	13.8	± 9.6
110	11.4	14.9	9.1	12.8	18.8	13.4	± 9.9
120	16.1	20.6	11.3	15.3	25.6	17.8	± 9.9

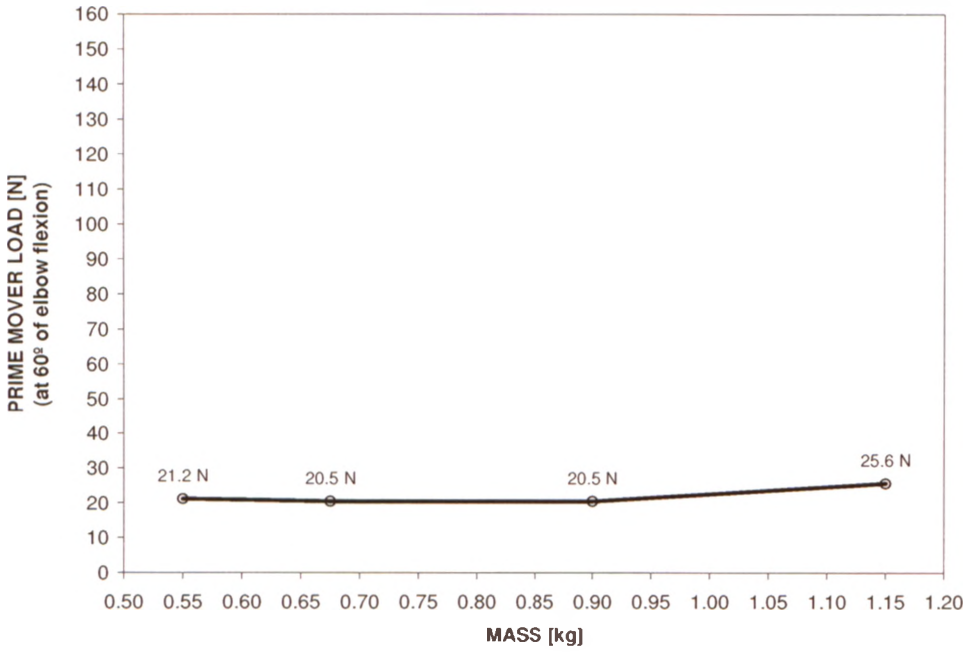

Figure A7.12: Prime mover load (at 60° of elbow flexion) plotted against forearm mass for four specimens tested in active flexion in the valgus position for the native AMCL study

The variation in prime mover load at 60° of elbow flexion for specimens 2 through 5 was approximately 5.1 N.

A7.2.9.2 *Dependent Position: Active Elbow Flexion*

The load required to move the forearm through the arc of elbow flexion (*i.e.* the prime mover load) varied for each specimen (Figure A7.13); however, prime load was not observed to increase with increasing forearm mass (Figure A7.14). The variation in prime mover load at 60° of elbow flexion for specimens 2, 3, and 5 was approximately 26.3 N (Figure A7.14), and, as anticipated, prime mover loads were greater in the dependent position than in the valgus position for all forearm masses (Figure A7.14 versus Figure A7.12); in order to move the forearm through the arc of elbow flexion in the dependent position, the prime mover load needs to overcome the force of gravity. Additionally, prime mover load was not observed to increase with increasing valgus angulation (Figure A7.15).

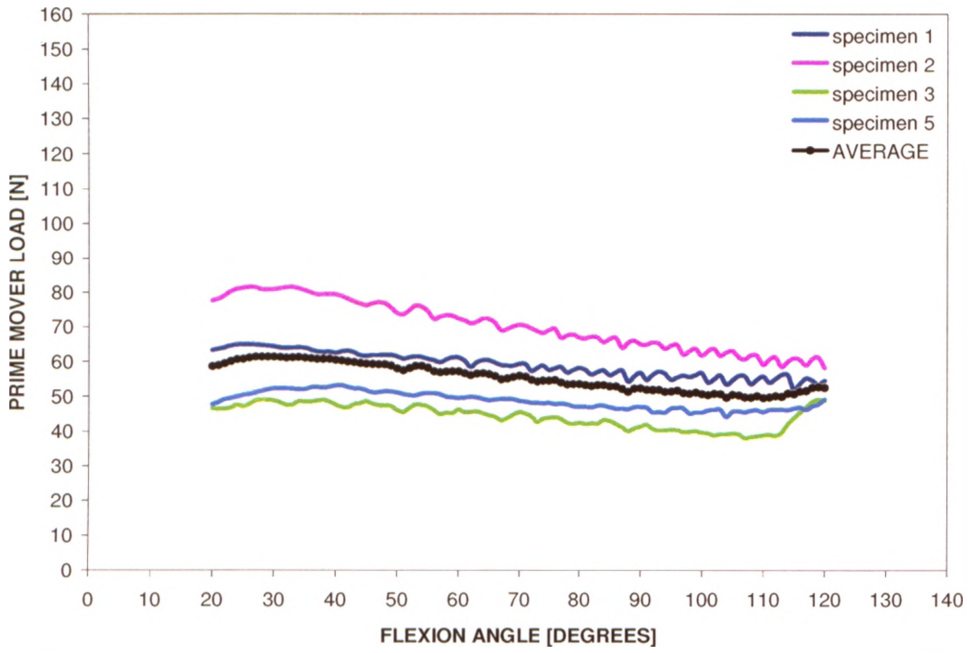

Figure A7.13: Prime mover load measurements for active flexion in the dependent position for the native AMCL study

Each curve corresponds to the prime mover loads of the third flexion cycle for each specimen (n = 4); the average prime mover loads for these four specimen curves are also shown. Standard deviations are omitted for clarity but ranged from ±4.5 N to ±15.6 N for the average curve.

Table A7.32: Prime mover load at every 10° of elbow flexion for each specimen tested in active dependent neutral flexion for the native AMCL study

Flexion Angle [Degrees]	Specimen 1	Specimen 2	Specimen 3	Specimen 5	Average	
	Prime Mover Load [N]	Prime Mover Load [N]	Prime Mover Load [N]	Prime Mover Load [N]	Prime Mover Load [N]	Standard Deviation [N]
20	63.2	77.6	46.4	47.7	58.7	± 14.7
30	64.3	80.8	48.7	52.1	61.5	± 14.5
40	62.5	79.3	47.5	53.0	60.6	± 13.9
50	61.4	73.9	45.9	50.9	58.0	± 12.4
60	61.1	72.4	46.1	49.4	57.3	± 12.0
70	59.3	70.5	45.4	48.6	56.0	± 11.4
80	58.0	66.9	42.3	47.0	53.6	± 11.1
90	56.7	64.9	41.2	46.9	52.4	± 10.5
100	56.7	61.6	39.5	45.3	50.8	± 10.2
110	55.6	59.0	38.7	45.4	49.7	± 9.3
120	54.5	58.1	48.7	49.0	52.6	± 4.5

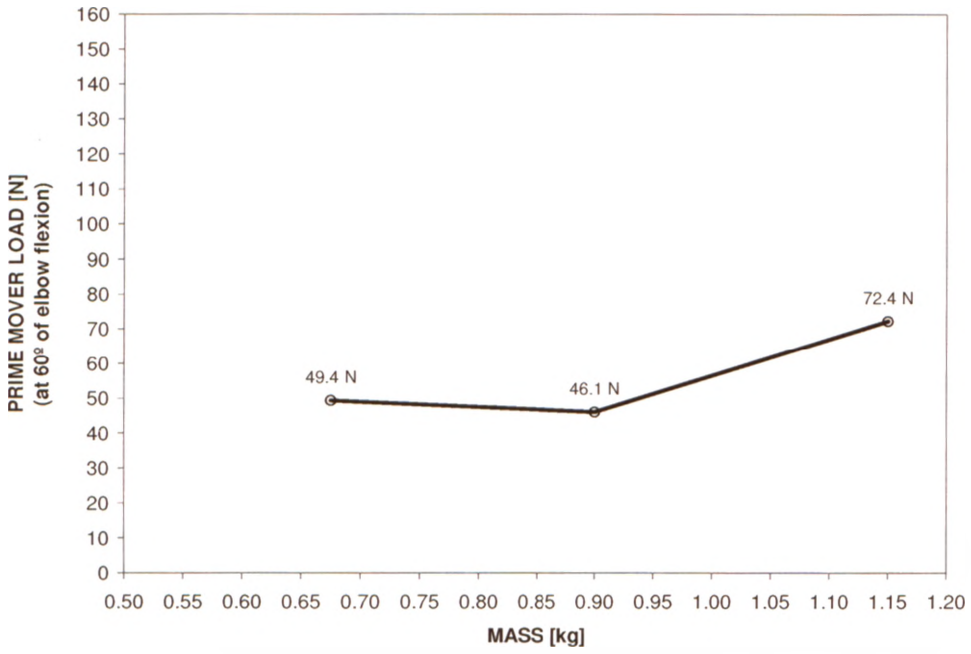

Figure A7.14: Prime mover load (at 60° of elbow flexion) plotted against forearm mass for three specimens tested in active flexion in the dependent position for the native AMCL study

The variation in prime mover load at 60° of elbow flexion for specimens 2, 3, and 5 was approximately 26.3 N.

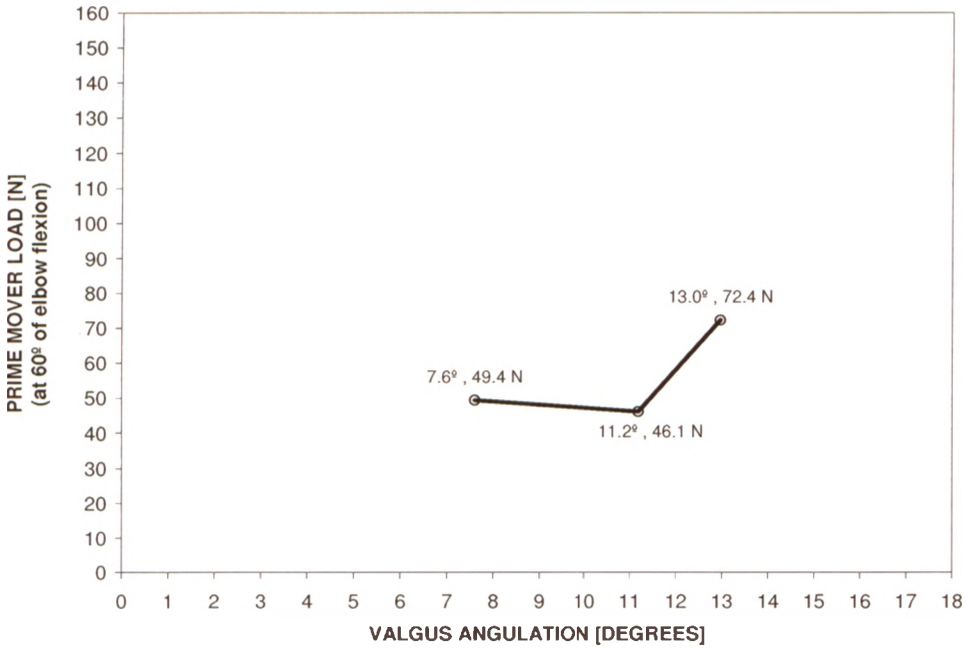

Figure A7.15: Prime mover load (at 60° of elbow flexion) plotted against valgus angulation for three specimens tested in active flexion in the dependent position for the native AMCL study

Prime mover load was not observed to increase with increasing valgus angulation, for specimens 2, 3, and 5.

APPENDIX 8

Appendix to Chapter 4
Effect of Wrist Flexor Muscle Loading on Medial Collateral Ligament Tension in the Elbow

A8.1 MATERIALS AND METHODS

A8.1.1 Specimen Preparation

Table A8.1: Number of specimens analysed for the valgus and dependent positions for the WF study

Four specimens were tested for both the valgus and dependent positions; however, due to data acquisition difficulties, data from only three of the four specimens were analysed for the dependent position.

Valgus Position	4 specimens (mean age 73 ± 11 years; range: 62-82 years; 3 female; 1 right specimen)
Dependent Position	3 specimens (mean age 76 ± 10 years; range: 65-82 years; 2 female; 1 right specimen)

A8.1.2 Testing Protocol

Table A8.2: Motion protocol for the WF study

There were four test conditions: (1) passive flexion in the dependent position; (2) active flexion in the dependent position; (3) passive flexion in the valgus position; and (4) active flexion in the valgus position. For each WF load condition, AMCL tension and elbow kinematic data from only the third flexion (Flex) cycle were analysed. Extension (Ext) data were not analysed.

WF Load Condition	Dependent Position				Valgus Position			
	Test Condition				Test Condition			
	Passive Motion		Active Motion		Passive Motion		Active Motion	
	Ext	Flex	Ext	Flex	Ext	Flex	Ext	Flex
0 N	×5	×5	×5	×5	×5	×5	×5	×5
10 N	×3	×3	×3	×3	×3	×3	×3	×3
30 N	×3	×3	×3	×3	×3	×3	×3	×3
50 N	×3	×3	×3	×3	×3	×3	×3	×3

A8.2 RESULTS

A8.2.1 Valgus Position: Active Elbow Flexion

A8.2.1.1 *AMCL Tension (Figure 4.1)*

Table A8.3: AMCL tension two-way repeated measures ANOVA statistical analysis results (p-values) for active valgus neutral flexion for the WF study

Main effect of WF load condition on AMCL tension			$p < 0.0001$
Pairwise Comparison Results			
WF 0 N	vs.	WF 10 N	$p = 0.049$
	vs.	WF 30 N	$p = 0.031$
	vs.	WF 50 N	$p = 0.002$
WF 10 N	vs.	WF 50 N	$p = 0.018$
All other combinations of the WF load conditions			$p > 0.050$

Table A8.4: Minimum and maximum AMCL tension magnitudes for active valgus neutral flexion for the WF study

Ranges of AMCL tension magnitudes (considering all degrees of elbow flexion) for the WF – 0 N, the WF – 10 N, the WF – 30 N, and the WF – 50 N conditions.

WF – 0 N	
minimum:	43.0 ± 10.6 N at 20º of flexion
maximum:	98.9 ± 45.2 N at 120º of flexion
WF – 10 N	
minimum:	24.5 ± 7.5 N at 20º of flexion
maximum:	91.9 ± 47.1 N at 120º of flexion
WF – 30 N	
minimum:	8.4 ± 6.0 N at 20º of flexion
maximum:	73.9 ± 51.1 N at 120º of flexion
WF – 50 N	
minimum:	3.3 ± 3.4 N at 20º of flexion
maximum:	56.6 ± 48.3 N at 116º of flexion

Table A8.5: AMCL tension at every 10° of elbow flexion for each WF load condition for active valgus neutral flexion

Flexion Angle [Degrees]	WF 0 N		WF 10 N		WF 30 N		WF 50 N	
	Mean AMCL Tension [N]	Standard Deviation [N]	Mean AMCL Tension [N]	Standard Deviation [N]	Mean AMCL Tension [N]	Standard Deviation [N]	Mean AMCL Tension [N]	Standard Deviation [N]
20	43.0	± 10.6	24.5	± 7.5	8.4	± 6.0	3.3	± 3.4
30	58.1	± 9.8	37.3	± 11.5	14.7	± 13.1	5.4	± 5.8
40	71.6	± 13.4	51.0	± 16.0	20.9	± 14.3	8.1	± 8.5
50	82.6	± 21.0	64.5	± 24.6	30.7	± 24.2	13.5	± 11.0
60	89.5	± 28.0	77.0	± 34.0	43.7	± 39.3	26.2	± 22.7
70	93.5	± 34.5	84.2	± 41.1	56.4	± 50.6	41.1	± 40.1
80	94.6	± 38.9	87.3	± 45.3	62.7	± 55.7	46.0	± 43.0
90	95.4	± 42.0	89.4	± 47.9	67.5	± 57.1	49.0	± 43.5
100	96.4	± 43.2	89.7	± 47.9	68.0	± 55.7	51.8	± 44.4
110	96.6	± 44.3	89.3	± 47.4	70.0	± 54.0	54.1	± 46.9
120	98.9	± 45.2	91.9	± 47.1	73.9	± 51.1	54.9	± 49.1

Table A8.6: Minimum and maximum AMCL tension standard deviations for active valgus neutral flexion for the WF study

Ranges of AMCL tension standard deviations (considering all degrees of elbow flexion) for the WF – 0 N, the WF – 10 N, the WF – 30 N, and the WF – 50 N conditions.

WF Load Condition	Range of Standard Deviations
WF – 0 N	±9.7 N – ±45.2 N
WF – 10 N	±7.5 N – ±48.3 N
WF – 30 N	±6.0 N – ±57.9 N
WF – 50 N	±3.4 N – ±49.1 N

Table A8.7: The average AMCL tension level (considering all degrees of elbow flexion) for each WF load condition for active valgus neutral flexion

	WF 0 N	WF 10 N	WF 30 N	WF 50 N
Average AMCL tension throughout elbow flexion [N]	84.8 ± 30.3	72.7 ± 34.3	47.5 ± 39.2	32.6 ± 29.3

A8.2.1.2 *Kinematics – Valgus Angulation (Figure 4.2)*

Table A8.8: Valgus angulation two-way repeated measures ANOVA statistical analysis results (p-values) for active valgus neutral flexion for the WF study

Main effect of WF load condition on valgus angulation			p = 0.010
Pairwise Comparison Results *(no statistically significant differences)*			
WF 0 N	vs.	WF 10 N	p = 0.087
	vs.	WF 30 N	p = 0.114
	vs.	WF 50 N	p = 0.076
All other combinations of the WF load conditions			p > 0.050

Table A8.9: Minimum and maximum valgus angulations for active valgus neutral flexion for the WF study

Ranges of valgus angulations (considering all degrees of elbow flexion) for the WF – 0 N, the WF – 10 N, the WF – 30 N, and the WF – 50 N conditions.

WF – 0 N	
maximum:	14.7 ± 2.6º at 20º of flexion
minimum:	13.2 ± 3.2º at 90º of flexion
WF – 10 N	
maximum:	13.7 ± 2.5º at 20º of flexion
minimum:	13.0 ± 3.3º and 13.0 ± 3.6º at 90º and 100º of flexion, respectively
WF – 30 N	
maximum:	12.6 ± 4.1º at 120º of flexion
minimum:	12.1 ± 2.2º, 12.1 ± 3.2º, 12.1 ± 3.3º, and 12.1 ± 3.6º at 20º, 70º, 80º, and 100º of flexion, respectively
WF – 50 N	
maximum:	11.3 ± 3.8º at 120º of flexion
minimum:	10.5 ± 2.2º and 10.5 ± 2.4º at 20º and 30º of flexion, respectively

Table A8.10: Valgus angulation at every 10° of elbow flexion for each WF load condition for active valgus neutral flexion

Flexion Angle [Degrees]	WF 0 N		WF 10 N		WF 30 N		WF 50 N	
	Mean Valgus Angulation [Degrees]	Standard Deviation [Degrees]	Mean Valgus Angulation [Degrees]	Standard Deviation [Degrees]	Mean Valgus Angulation [Degrees]	Standard Deviation [Degrees]	Mean Valgus Angulation [Degrees]	Standard Deviation [Degrees]
20	14.7	± 2.6	13.7	± 2.5	12.1	± 2.2	10.5	± 2.2
30	14.5	± 2.6	13.6	± 2.5	12.3	± 2.4	10.5	± 2.4
40	14.1	± 2.6	13.4	± 2.7	12.3	± 2.7	10.6	± 2.7
50	13.8	± 2.7	13.2	± 2.7	12.3	± 2.8	10.9	± 3.0
60	13.5	± 2.8	13.1	± 2.8	12.2	± 3.0	11.0	± 3.2
70	13.4	± 2.9	13.1	± 3.0	12.1	± 3.2	11.1	± 3.3
80	13.3	± 3.0	13.1	± 3.2	12.1	± 3.3	11.1	± 3.4
90	13.2	± 3.2	13.0	± 3.3	12.2	± 3.4	11.1	± 3.5
100	13.3	± 3.5	13.0	± 3.6	12.1	± 3.6	11.1	± 3.6
110	13.3	± 3.9	13.1	± 3.9	12.3	± 3.8	11.2	± 3.7
120	13.4	± 4.3	13.2	± 4.3	12.6	± 4.1	11.3	± 3.8

Table A8.11: Minimum and maximum valgus angulation standard deviations for active valgus neutral flexion for the WF study

Ranges of valgus angulation standard deviations (considering all degrees of elbow flexion) for the WF – 0 N, the WF – 10 N, the WF – 30 N, and the WF – 50 N conditions.

WF Load Condition	Range of Standard Deviations
WF – 0 N	±2.6º – ±4.3º
WF – 10 N	±2.5º – ±4.3º
WF – 30 N	±2.2º – ±4.1º
WF – 50 N	±2.2º – ±3.8º

Table A8.12: The average valgus angulation (considering all degrees of elbow flexion) for each WF load condition for active valgus neutral flexion

	WF 0 N	WF 10 N	WF 30 N	WF 50 N
Average valgus angulation throughout elbow flexion [Degrees]	13.7 ± 3.1	13.2 ± 3.1	12.2 ± 3.1	10.9 ± 3.2

A8.2.2 Valgus Position: Passive Elbow Flexion

A8.2.2.1 *AMCL Tension (Figure 4.3)*

Table A8.13: AMCL tension two-way repeated measures ANOVA statistical analysis results (p-values) for passive valgus neutral flexion for the WF study

Main effect of WF load condition on AMCL tension			p = 0.003
Pairwise Comparison Results			
WF 0 N	vs.	WF 10 N	p = 0.322
	vs.	WF 30 N	p = 0.047
	vs.	WF 50 N	p < 0.0001
WF 10 N	vs.	WF 30 N	p = 0.009
WF 10 N	vs.	WF 50 N	p = 0.013
All other combinations of the WF load conditions			p > 0.050

Table A8.14: Minimum and maximum AMCL tension magnitudes for passive valgus neutral flexion for the WF study

Ranges of AMCL tension magnitudes (considering all degrees of elbow flexion) for the WF – 0 N, the WF – 10 N, the WF – 30 N, and the WF – 50 N conditions.

WF – 0 N	
minimum:	54.9 ± 4.0 N at 20º of flexion
maximum:	105.2 ± 30.8 N at 90º of flexion
WF – 10 N	
minimum:	31.2 ± 9.6 N at 20º of flexion
maximum:	89.4 ± 45.8 N at 87º of flexion
WF – 30 N	
minimum:	8.4 ± 6.3 N at 20º of flexion
maximum:	69.1 ± 47.1 N at 120º of flexion
WF – 50 N	
minimum:	3.2 ± 2.6 N at 20º of flexion
maximum:	44.1 ± 43.6 N at 120º of flexion

Table A8.15: AMCL tension at every 10° of elbow flexion for each WF load condition for passive valgus neutral flexion

Flexion Angle [Degrees]	WF 0 N		WF 10 N		WF 30 N		WF 50 N	
	Mean AMCL Tension [N]	Standard Deviation [N]	Mean AMCL Tension [N]	Standard Deviation [N]	Mean AMCL Tension [N]	Standard Deviation [N]	Mean AMCL Tension [N]	Standard Deviation [N]
20	54.9	± 4.0	31.2	± 9.6	8.4	± 6.3	3.2	± 2.6
30	70.0	± 4.0	44.8	± 12.0	14.5	± 11.6	5.3	± 4.7
40	83.0	± 8.8	57.1	± 17.1	21.7	± 16.0	7.8	± 7.3
50	93.5	± 13.4	69.0	± 24.8	30.9	± 22.3	13.7	± 9.9
60	99.3	± 18.0	79.4	± 32.9	41.4	± 32.6	24.2	± 20.7
70	103.1	± 23.8	85.6	± 40.3	52.9	± 45.4	36.1	± 36.1
80	104.8	± 28.1	88.5	± 44.3	58.1	± 52.5	41.3	± 39.6
90	105.2	± 30.8	89.1	± 45.2	62.8	± 56.3	41.5	± 41.4
100	104.4	± 33.4	88.5	± 45.0	66.3	± 53.8	41.6	± 42.4
110	103.2	± 33.8	86.5	± 44.8	67.9	± 49.7	41.6	± 43.5
120	103.2	± 33.7	86.2	± 43.5	69.1	± 47.1	44.1	± 43.6

Table A8.16: Minimum and maximum AMCL tension standard deviations for passive valgus neutral flexion for the WF study

Ranges of AMCL tension standard deviations (considering all degrees of elbow flexion) for the WF – 0 N, the WF – 10 N, the WF – 30 N, and the WF – 50 N conditions.

WF Load Condition	Range of Standard Deviations
WF – 0 N	±2.7 N – ±33.9 N
WF – 10 N	±9.6 N – ±45.8 N
WF – 30 N	±6.3 N – ±56.8 N
WF – 50 N	±2.6 N – ±43.6 N

Table A8.17: The average AMCL tension level (considering all degrees of elbow flexion) for each WF load condition for passive valgus neutral flexion

	WF 0 N	WF 10 N	WF 30 N	WF 50 N
Average AMCL tension throughout elbow flexion [N]	94.4 ± 21.1	74.4 ± 33.4	45.4 ± 36.7	27.7 ± 26.9

A8.2.2.2 *Kinematics – Valgus Angulation (Figure 4.4)*

Table A8.18: Valgus angulation two-way repeated measures ANOVA statistical analysis results (p-values) for passive valgus neutral flexion for the WF study

Main effect of WF load condition on valgus angulation			p = 0.019
Pairwise Comparison Results *(no statistically significant differences)*			
WF 0 N	vs.	WF 10 N	p = 0.681
	vs.	WF 30 N	p = 0.148
	vs.	WF 50 N	p = 0.135
All other combinations of the WF load conditions			p > 0.050

Table A8.19: Minimum and maximum valgus angulations for passive valgus neutral flexion for the WF study

Ranges of valgus angulations (considering all degrees of elbow flexion) for the WF – 0 N, the WF – 10 N, the WF – 30 N, and the WF – 50 N conditions.

WF – 0 N	
maximum:	14.6 ± 2.8º at 20º of flexion
minimum:	13.3 ± 3.7º at 100º of flexion
WF – 10 N	
maximum:	13.9 ± 2.6º at 20º of flexion
minimum:	13.2 ± 3.4º, 13.2 ± 3.6º, and 13.2 ± 3.7º at 80º, 90º, and 100º of flexion, respectively
WF – 30 N	
maximum:	12.8 ± 4.4º at 120º of flexion
minimum:	12.2 ± 2.6º at 20º of flexion
WF – 50 N	
maximum:	11.5 ± 3.2º and 11.5 ± 3.9º at 80º and 120º of flexion, respectively
minimum:	10.2 ± 2.4º at 20º of flexion

Table A8.20: Valgus angulation at every 10° of elbow flexion for each WF load condition for passive valgus neutral flexion

Flexion Angle [Degrees]	WF 0 N		WF 10 N		WF 30 N		WF 50 N	
	Mean Valgus Angulation [Degrees]	Standard Deviation [Degrees]	Mean Valgus Angulation [Degrees]	Standard Deviation [Degrees]	Mean Valgus Angulation [Degrees]	Standard Deviation [Degrees]	Mean Valgus Angulation [Degrees]	Standard Deviation [Degrees]
20	14.6	± 2.8	13.9	± 2.6	12.2	± 2.6	10.2	± 2.4
30	14.4	± 2.9	13.8	± 2.7	12.3	± 2.6	10.3	± 2.5
40	14.3	± 2.9	13.7	± 2.7	12.3	± 2.8	10.6	± 2.9
50	14.0	± 2.9	13.6	± 2.9	12.3	± 2.8	11.0	± 3.1
60	13.7	± 3.0	13.4	± 3.0	12.4	± 3.0	11.1	± 3.3
70	13.5	± 3.1	13.3	± 3.2	12.4	± 3.0	11.3	± 3.4
80	13.4	± 3.2	13.2	± 3.4	12.4	± 3.3	11.5	± 3.2
90	13.4	± 3.4	13.2	± 3.6	12.5	± 3.6	11.4	± 3.4
100	13.3	± 3.7	13.2	± 3.7	12.6	± 3.8	11.4	± 3.5
110	13.4	± 4.0	13.3	± 4.1	12.7	± 4.2	11.4	± 3.6
120	13.5	± 4.4	13.4	± 4.5	12.8	± 4.4	11.5	± 3.9

Table A8.21: Minimum and maximum valgus angulation standard deviations for passive valgus neutral flexion for the WF study

Ranges of valgus angulation standard deviations (considering all degrees of elbow flexion) for the WF – 0 N, the WF – 10 N, the WF – 30 N, and the WF – 50 N conditions.

WF Load Condition	Range of Standard Deviations
WF – 0 N	±2.8º – ±4.4º
WF – 10 N	±2.6º – ±4.5º
WF – 30 N	±2.6º – ±4.4º
WF – 50 N	±2.4º – ±3.9º

Table A8.22: The average valgus angulation (considering all degrees of elbow flexion) for each WF load condition for passive valgus neutral flexion

	WF 0 N	WF 10 N	WF 30 N	WF 50 N
Average valgus angulation throughout elbow flexion [Degrees]	13.8 ± 3.3	13.4 ± 3.3	12.5 ± 3.3	11.1 ± 3.2

A8.2.3 Valgus Position: Active versus Passive Elbow Flexion

A8.2.3.1 *Comparison of Active and Passive AMCL Tensions*

Comparing the passive AMCL tension levels (Figure 4.3) with their respective active AMCL tension levels (Figure 4.1), for the valgus position, the following observations were made:

(1) For the WF – 0 N condition, passive and active tension trends were similar. Passive tensions were greater than active tensions at all degrees of elbow flexion; the largest difference between passive and active AMCL tensions was approximately **12.6 N**, which occurred at **22°** of elbow flexion. There was no statistical difference in the AMCL tension levels between active and passive elbow flexion for the WF – 0 N condition, for the valgus position ($p = 0.228$).

(2) For the WF – 10 N condition, passive and active tension trends were similar. Passive tensions were greater than active tensions within approximately 20° and 85° of elbow flexion, and for flexion angles greater than approximately 85°, passive tensions were less than active tensions; the largest difference between passive and active AMCL tensions was approximately **8.0 N**, which occurred at **28°** of elbow flexion. There was no statistical difference in the AMCL tension levels between active and passive elbow flexion for the WF – 10 N condition, for the valgus position ($p = 0.669$).

(3) For the WF – 30 N condition, passive and active tension trends were similar. Passive tensions were approximately equal to active tensions within approximately 20° and 50° of elbow flexion, and for flexion angles greater than approximately 50°, passive tensions were less than active tensions; the largest

difference between passive and active AMCL tensions was approximately **5.8 N**, which occurred at **87°** of elbow flexion. There was no statistical difference in the AMCL tension levels between active and passive elbow flexion for the WF – 30 N condition, for the valgus position ($p = 0.270$).

(4) For the WF – 50 N condition, passive and active tension trends were similar. Passive tensions were approximately equal to active tensions within approximately 20° and 50° of elbow flexion, and for flexion angles greater than approximately 50°, passive tensions were less than active tensions; the largest difference between passive and active AMCL tensions was approximately **14.1 N**, which occurred at **115°** of elbow flexion. There was no statistical difference in the AMCL tension levels between active and passive elbow flexion for the WF – 50 N condition, for the valgus position ($p = 0.146$).

A8.2.3.2 *Comparison of Active and Passive Motion Pathways*

Comparing the passive motion pathways (Figure 4.4) with their respective active motion pathways (Figure 4.2), for the valgus position, the following observations were made when closely comparing the motion pathways:

(1) For the WF – 0 N condition, the passive motion pathway tracked in greater valgus than the active motion pathway at all degrees of flexion after approximately 35° of elbow flexion (except at 100° of elbow flexion where active and passive valgus angulations were approximately equal); however, the largest difference between passive and active valgus angulations was only approximately **0.22°**, which occurred at **60°** degrees of elbow flexion. There was no statistical difference in the motion pathways between active and passive elbow flexion for the WF – 0 N condition, for the valgus position ($p = 0.596$).

(2) For the WF – 10 N condition, the passive motion pathway tracked in greater valgus than the active motion pathway at all degrees of elbow flexion; however, the largest difference between passive and active valgus angulations was only approximately **0.38°**, which occurred at **50°** degrees of elbow flexion. There was no statistical difference in the motion pathways between active and passive elbow flexion for the WF – 10 N condition, for the valgus position ($p = 0.061$).

(3) For the WF – 30 N condition, the passive motion pathway tracked in greater valgus than the active motion pathway (except at 30° and 40° of elbow flexion where active and passive valgus angulations were approximately equal); however, the largest difference between passive and active valgus angulations was only approximately **0.48°**, which occurred at **100°** degrees of elbow flexion. There was no statistical difference in the motion pathways between active and passive elbow flexion for the WF – 30 N condition, for the valgus position ($p = 0.109$).

(4) For the WF – 50 N condition, the passive motion pathway tracked in greater valgus than the active motion pathway after approximately 40° of elbow flexion; however, the largest difference between passive and active valgus angulations was only approximately **0.43°**, which occurred at **80°** degrees of elbow flexion. There was no statistical difference in the motion pathways between active and passive elbow flexion for the WF – 50 N condition, for the valgus position ($p = 0.431$).

A8.2.4 Dependent Position: Active Elbow Flexion

A8.2.4.1 *AMCL Tension (Figure 4.5)*

Table A8.23: AMCL tension two-way repeated measures ANOVA statistical analysis results (p-value) for active dependent neutral flexion for the WF study

There was no significant main effect of WF load condition on AMCL tension.

Main effect of WF load condition on AMCL tension	$p = 0.171$

Table A8.24: Minimum and maximum AMCL tension magnitudes for active dependent neutral flexion for the WF study

Ranges of AMCL tension magnitudes (considering all degrees of elbow flexion) for the WF – 0 N, the WF – 10 N, the WF – 30 N, and the WF – 50 N conditions.

WF – 0 N	
minimum:	7.3 ± 11.4 N at 20º of flexion
maximum:	64.0 ± 9.8 N at 120º of flexion
WF – 10 N	
minimum:	3.1 ± 2.2 N at 20º of flexion
maximum:	50.9 ± 15.6 N at 120º of flexion
WF – 30 N	
minimum:	3.2 ± 2.2 N at 20º of flexion
maximum:	33.5 ± 19.0 N at 120º of flexion
WF – 50 N	
minimum:	2.4 ± 1.9 N at 20º of flexion
maximum:	35.1 ± 13.6 N at 118º of flexion

Table A8.25: AMCL tension at every 10° of elbow flexion for each WF load condition for active dependent neutral flexion

Flexion Angle [Degrees]	WF 0 N		WF 10 N		WF 30 N		WF 50 N	
	Mean AMCL Tension [N]	Standard Deviation [N]	Mean AMCL Tension [N]	Standard Deviation [N]	Mean AMCL Tension [N]	Standard Deviation [N]	Mean AMCL Tension [N]	Standard Deviation [N]
20	7.3	± 11.4	3.1	± 2.2	3.2	± 2.2	2.4	± 1.9
30	11.5	± 17.7	5.1	± 4.8	5.2	± 3.3	4.1	± 3.0
40	15.9	± 23.7	7.9	± 8.0	7.6	± 6.2	7.0	± 6.7
50	19.0	± 26.3	11.0	± 11.0	10.2	± 8.5	9.5	± 9.6
60	22.1	± 27.5	14.4	± 14.0	11.8	± 9.3	12.4	± 12.6
70	26.0	± 27.0	17.3	± 14.1	13.8	± 9.3	15.0	± 14.4
80	30.5	± 21.3	20.8	± 10.6	16.8	± 7.5	17.8	± 13.9
90	37.9	± 13.2	26.6	± 4.7	20.6	± 3.5	22.3	± 11.6
100	48.1	± 9.0	35.1	± 9.1	26.3	± 4.7	27.8	± 6.4
110	52.9	± 7.5	38.9	± 13.2	29.5	± 9.1	32.6	± 4.5
120	64.0	± 9.8	50.9	± 15.6	33.5	± 19.0	34.8	± 15.9

Table A8.26: Minimum and maximum AMCL tension standard deviations for active dependent neutral flexion for the WF study

Ranges of AMCL tension standard deviations (considering all degrees of elbow flexion) for the WF – 0 N, the WF – 10 N, the WF – 30 N, and the WF – 50 N conditions.

WF Load Condition	Range of Standard Deviations
WF – 0 N	±4.6 N – ±28.0 N
WF – 10 N	±2.2 N – ±15.6 N
WF – 30 N	±2.1 N – ±19.0 N
WF – 50 N	±1.9 N – ±15.9 N

Table A8.27: The average AMCL tension level (considering all degrees of elbow flexion) for each WF load condition for active dependent neutral flexion

	WF 0 N	WF 10 N	WF 30 N	WF 50 N
Average AMCL tension throughout elbow flexion [N]	29.9 ± 18.1	20.4 ± 9.8	16.0 ± 7.1	16.9 ± 9.1

A8.2.4.2 *Kinematics – Valgus Angulation (Figure 4.6)*

Table A8.28: Valgus angulation two-way repeated measures ANOVA statistical analysis results (p-value) for active dependent neutral flexion for the WF study

There was no significant main effect of WF load condition on valgus angulation.

Main effect of WF load condition on valgus angulation	p = 0.073

Table A8.29: Minimum and maximum valgus angulations for active dependent neutral flexion for the WF study

Ranges of valgus angulations (considering all degrees of elbow flexion) for the WF – 0 N, the WF – 10 N, the WF – 30 N, and the WF – 50 N conditions.

WF – 0 N	
maximum:	11.2 ± 2.6º at both 20º and 30º of flexion
minimum:	9.5 ± 3.3º at 110º of flexion
WF – 10 N	
maximum:	10.4 ± 2.5º at both 30º and 40º of flexion
minimum:	9.3 ± 3.5º at 110º of flexion
WF – 30 N	
maximum:	9.4 ± 2.9º at 50º of flexion
minimum:	8.1 ± 3.3º at both 110º and 120º of flexion
WF – 50 N	
maximum:	8.3 ± 2.7º and 8.3 ± 3.0º at 40º and 60º of flexion, respectively
minimum:	6.7 ± 2.7 º at 110º of flexion

Table A8.30: Valgus angulation at every 10° of elbow flexion for each WF load condition for active dependent neutral flexion

Flexion Angle [Degrees]	WF 0 N		WF 10 N		WF 30 N		WF 50 N	
	Mean Valgus Angulation [Degrees]	Standard Deviation [Degrees]	Mean Valgus Angulation [Degrees]	Standard Deviation [Degrees]	Mean Valgus Angulation [Degrees]	Standard Deviation [Degrees]	Mean Valgus Angulation [Degrees]	Standard Deviation [Degrees]
20	11.2	± 2.6	10.1	± 2.4	8.5	± 2.8	7.4	± 2.6
30	11.2	± 2.6	10.4	± 2.5	9.2	± 2.7	8.1	± 2.7
40	11.1	± 2.7	10.4	± 2.5	9.2	± 2.7	8.3	± 2.7
50	10.9	± 2.7	10.3	± 2.5	9.4	± 2.9	8.2	± 2.9
60	10.6	± 2.7	10.2	± 2.7	9.2	± 3.0	8.3	± 3.0
70	10.3	± 2.8	10.0	± 2.9	9.0	± 3.2	8.2	± 3.3
80	10.0	± 2.9	9.7	± 2.9	9.1	± 3.3	8.0	± 3.2
90	9.8	± 3.1	9.5	± 3.1	8.6	± 3.3	7.6	± 3.0
100	9.6	± 3.2	9.5	± 3.3	8.4	± 3.4	7.0	± 2.8
110	9.5	± 3.3	9.3	± 3.5	8.1	± 3.3	6.7	± 2.7
120	9.8	± 4.0	9.7	± 4.1	8.1	± 3.3	6.8	± 2.9

Table A8.31: Minimum and maximum valgus angulation standard deviations for active dependent neutral flexion for the WF study

Ranges of valgus angulation standard deviations (considering all degrees of elbow flexion) for the WF – 0 N, the WF – 10 N, the WF – 30 N, and the WF – 50 N conditions.

WF Load Condition	Range of Standard Deviations
WF – 0 N	±2.6º – ±4.0º
WF – 10 N	±2.4º – ±4.1º
WF – 30 N	±2.7º – ±3.4º
WF – 50 N	±2.6º – ±3.3º

Table A8.32: The average valgus angulation (considering all degrees of elbow flexion) for each WF load condition for active dependent neutral flexion

	WF 0 N	WF 10 N	WF 30 N	WF 50 N
Average valgus angulation throughout elbow flexion [Degrees]	10.4 ± 3.0	9.9 ± 3.0	8.8 ± 3.1	7.7 ± 2.9

A8.2.5 Dependent Position: Passive Elbow Flexion

A8.2.5.1 *AMCL Tension (Figure 4.7)*

Table A8.33: AMCL tension two-way repeated measures ANOVA statistical analysis results (p-value) for passive dependent neutral flexion for the WF study

There was no significant main effect of WF load condition on AMCL tension.

Main effect of WF load condition on AMCL tension	p = 0.079

Table A8.34: Minimum and maximum AMCL tension magnitudes for passive dependent neutral flexion for the WF study

Ranges of AMCL tension magnitudes (considering all degrees of elbow flexion) for the WF – 0 N, the WF – 10 N, the WF – 30 N, and the WF – 50 N conditions.

WF – 0 N	
minimum:	2.4 ± 2.0 N at 20º of flexion
maximum:	57.4 ± 29.4 N at 120º of flexion
WF – 10 N	
minimum:	2.3 ± 2.4 N and 2.3 ± 2.3 N at 20º and 21º of flexion, respectively
maximum:	49.5 ± 20.7 N at 120º of flexion
WF – 30 N	
minimum:	2.9 ± 3.1 N at 20º of flexion
maximum:	40.7 ± 22.5 N at 120º of flexion
WF – 50 N	
minimum:	3.1 ± 3.2 N at 21º of flexion
maximum:	44.5 ± 25.6 N at 120º of flexion

Table A8.35: AMCL tension at every 10° of elbow flexion for each WF load condition for passive dependent neutral flexion

Flexion Angle [Degrees]	WF 0 N		WF 10 N		WF 30 N		WF 50 N	
	Mean AMCL Tension [N]	Standard Deviation [N]	Mean AMCL Tension [N]	Standard Deviation [N]	Mean AMCL Tension [N]	Standard Deviation [N]	Mean AMCL Tension [N]	Standard Deviation [N]
20	2.4	± 2.0	2.3	± 2.4	2.9	± 3.1	3.2	± 3.1
30	5.3	± 5.0	3.6	± 2.5	4.0	± 3.0	4.5	± 3.5
40	10.1	± 11.4	5.1	± 4.2	5.0	± 3.5	5.7	± 4.2
50	15.2	± 16.9	7.6	± 7.2	6.2	± 4.4	6.9	± 5.5
60	19.4	± 20.0	9.4	± 11.2	7.6	± 5.5	8.5	± 6.8
70	22.3	± 19.3	14.4	± 15.1	10.1	± 6.8	10.5	± 8.1
80	27.8	± 15.7	19.5	± 14.9	14.0	± 7.2	14.3	± 8.9
90	36.1	± 12.7	25.9	± 9.3	21.5	± 4.5	20.3	± 6.4
100	44.2	± 13.4	33.0	± 5.3	30.8	± 6.1	30.6	± 2.8
110	50.8	± 20.1	41.0	± 10.5	36.6	± 13.2	39.3	± 14.5
120	57.4	± 29.4	49.5	± 20.7	40.7	± 22.5	44.5	± 25.6

Table A8.36: Minimum and maximum AMCL tension standard deviations for passive dependent neutral flexion for the WF study

Ranges of AMCL tension standard deviations (considering all degrees of elbow flexion) for the WF – 0 N, the WF – 10 N, the WF – 30 N, and the WF – 50 N conditions.

WF Load Condition	Range of Standard Deviations
WF – 0 N	±2.0 N – ±29.4 N
WF – 10 N	±2.2 N – ±20.7 N
WF – 30 N	±2.9 N – ±22.5 N
WF – 50 N	±0.3 N – ±25.6 N

Table A8.37: The average AMCL tension level (considering all degrees of elbow flexion) for each WF load condition for passive dependent neutral flexion

	WF 0 N	WF 10 N	WF 30 N	WF 50 N
Average AMCL tension throughout elbow flexion [N]	26.1 ± 15.0	18.6 ± 9.1	15.8 ± 6.7	16.4 ± 7.5

A8.2.5.2 *Kinematics – Valgus Angulation (Figure 4.8)*

Table A8.38: Valgus angulation two-way repeated measures ANOVA statistical analysis results (p-values) for passive dependent neutral flexion for the WF study

Main effect of WF load condition on valgus angulation			p = 0.040
Pairwise Comparison Results *(no statistically significant differences)*			
WF 0 N	vs.	WF 10 N	p = 0.367
	vs.	WF 30 N	p = 0.341
	vs.	WF 50 N	p = 0.270
All other combinations of the WF load conditions			p > 0.050

Table A8.39: Minimum and maximum valgus angulations for passive dependent neutral flexion for the WF study

Ranges of valgus angulations (considering all degrees of elbow flexion) for the WF – 0 N, the WF – 10 N, the WF – 30 N, and the WF – 50 N conditions.

WF – 0 N	
maximum:	9.6 ± 3.3º and 9.6 ± 3.5º at 110º and 120º of flexion, respectively
minimum:	8.0 ± 1.9º at 20º of flexion
WF – 10 N	
maximum:	9.0 ± 3.4º at 120º of flexion
minimum:	6.4 ± 1.3º at both 20º and 30º of flexion
WF – 30 N	
maximum:	7.0 ± 2.7º at 120º of flexion
minimum:	5.1 ± 1.0º at 30º of flexion
WF – 50 N	
maximum:	6.4 ± 2.6º at 120º of flexion
minimum:	4.4 ± 1.0º at 30º of flexion

Table A8.40: Valgus angulation at every 10° of elbow flexion for each WF load condition for passive dependent neutral flexion

Flexion Angle [Degrees]	WF 0 N		WF 10 N		WF 30 N		WF 50 N	
	Mean Valgus Angulation [Degrees]	Standard Deviation [Degrees]	Mean Valgus Angulation [Degrees]	Standard Deviation [Degrees]	Mean Valgus Angulation [Degrees]	Standard Deviation [Degrees]	Mean Valgus Angulation [Degrees]	Standard Deviation [Degrees]
20	8.0	± 1.9	6.4	± 1.3	5.3	± 1.0	4.5	± 1.1
30	8.5	± 2.4	6.4	± 1.3	5.1	± 1.0	4.4	± 1.0
40	9.0	± 2.7	6.5	± 1.6	5.4	± 1.6	4.6	± 1.5
50	9.0	± 2.6	7.0	± 1.9	5.9	± 2.0	4.8	± 2.1
60	9.2	± 2.7	7.6	± 2.1	6.3	± 2.4	5.4	± 2.3
70	9.3	± 2.7	8.0	± 2.3	6.5	± 2.7	5.5	± 2.4
80	9.2	± 2.7	7.8	± 2.4	6.5	± 2.6	6.0	± 2.3
90	9.1	± 2.9	8.0	± 2.5	6.5	± 2.6	5.9	± 2.4
100	9.3	± 3.0	8.0	± 2.5	6.9	± 2.8	6.0	± 2.3
110	9.6	± 3.3	8.8	± 3.0	6.9	± 2.8	6.1	± 2.2
120	9.6	± 3.5	9.0	± 3.4	7.0	± 2.7	6.4	± 2.6

Table A8.41: Minimum and maximum valgus angulation standard deviations for passive dependent neutral flexion for the WF study

Ranges of valgus angulation standard deviations (considering all degrees of elbow flexion) for the WF – 0 N, the WF – 10 N, the WF – 30 N, and the WF – 50 N conditions.

WF Load Condition	Range of Standard Deviations
WF – 0 N	±1.9º – ±3.5º
WF – 10 N	±1.3º – ±3.4º
WF – 30 N	±1.0º – ±2.8º
WF – 50 N	±1.0º – ±2.6º

Table A8.42: The average valgus angulation (considering all degrees of elbow flexion) for each WF load condition for passive dependent neutral flexion

	WF 0 N	WF 10 N	WF 30 N	WF 50 N
Average valgus angulation throughout elbow flexion [Degrees]	9.1 ± 2.8	7.6 ± 2.2	6.2 ± 2.2	5.4 ± 2.0

A8.2.6 Dependent Position: Active versus Passive Elbow Flexion

A8.2.6.1 *Comparison of Active and Passive AMCL Tensions*

Comparing the passive AMCL tension levels (Figure 4.7) with their respective active AMCL tension levels (Figure 4.5), for the dependent position, the following observations were made:

(1) For the WF – 0 N condition, passive and active tension trends were similar. Passive tensions were less than active tensions at all degrees of elbow flexion; the largest difference between passive and active AMCL tensions was approximately **6.7 N**, which occurred at **118°** of elbow flexion. There was no statistical difference in the AMCL tension levels between active and passive elbow flexion for the WF – 0 N condition, for the dependent position ($p = 0.591$).

(2) For the WF – 10 N condition, passive and active tension trends were similar. Passive tensions were less than active tensions at all degrees of elbow flexion (except within approximately 105° to 115° of elbow flexion); the largest difference between passive and active AMCL tensions was approximately **5.0 N**, which occurred at **60°** of elbow flexion. There was no statistical difference in the AMCL tension levels between active and passive elbow flexion for the WF – 10 N condition, for the dependent position ($p = 0.111$).

(3) For the WF – 30 N condition, passive and active tension trends were similar. Passive tensions were less than active tensions within approximately 20° and 85° of elbow flexion, and for flexion angles greater than approximately 85°, passive tensions were greater than active tensions; the largest difference between passive and active AMCL tensions was approximately **7.3 N**, which occurred at **111°** of elbow flexion. There was no statistical difference in the AMCL tension levels between active and passive elbow flexion for the WF – 30 N condition, for the dependent position ($p = 0.964$).

(4) For the WF – 50 N condition, passive and active tension trends were similar. Passive tensions were less than active tensions within approximately 30° and 95° of elbow flexion, and for all other flexion angles, passive tensions were greater than active tensions; the largest difference between passive and active AMCL

tensions was approximately **9.7 N**, which occurred at **120°** of elbow flexion. There was no statistical difference in the AMCL tension levels between active and passive elbow flexion for the WF – 50 N condition, for the dependent position ($p = 0.952$).

A8.2.6.2 *Comparison of Active and Passive Motion Pathways*

Comparing the passive motion pathways (Figure 4.8) with their respective active motion pathways (Figure 4.6), for the dependent position, it was observed that the passive motion pathways for all WF load conditions tracked in greater varus than the active motion pathways, with the passive motion pathways having varus to valgus slopes and the active motion pathways having valgus to varus slopes. Statistical differences were found in the motion pathways between the active and passive elbow flexion for the WF – 0 N, the WF – 10 N, the WF – 30 N, and the WF – 50 N conditions (p-values were 0.006, 0.036, 0.039, and 0.045, for the WF – 0 N, the WF – 10 N, the WF – 30 N, and the WF – 50 N conditions, respectively).

APPENDIX 9

Appendix to Chapter 5

Effect of Radial Excision and Arthroplasty on Medial Collateral Ligament Tension in the Elbow

A9.1 METHODS AND MATERIALS

A9.1.1 Specimen Preparation

Table A9.1: Number of specimens analysed for the valgus and dependent positions for the RH study

Five specimens were tested for both the valgus and dependent positions; however, due to data acquisition difficulties, data from only four of the five specimens were analysed for the dependent position.

Valgus Position	5 specimens (mean age 72 ± 10 years; range: 62-82 years; 3 female; 1 right specimen)
Dependent Position	4 specimens (mean age 74 ± 9 years; range: 65-82 years; 2 female; 1 right specimen)

A9.1.2 Testing Protocol

Table A9.2: Motion protocol for the RH study

There were two test conditions: (1) active flexion in the dependent position; and (2) active flexion in the valgus position. For each RH condition, AMCL tension and elbow kinematic data from only the third flexion (Flex) cycle were analysed. Extension (Ext) data were not analysed.

RH Condition	Surgical Approach	Active Motion			
		Dependent Position		Valgus Position	
		Ext	Flex	Ext	Flex
Intact	N/A	×5	×5	×5	×5
AL Repaired	1 Anterior aspect of elbow exposed 2 AL and elbow capsule severed 3 AL and elbow capsule repaired	×3	×3	×3	×3
RH Excised	1 AL and elbow capsule severed 2 RH excised 3 AL and elbow capsule repaired	×3	×3	×3	×3
RH Arthroplasty	1 AL and elbow capsule severed 2 RH replacement inserted 3 AL and elbow capsule repaired	×3	×3	×3	×3

Table A9.3: Head and stem sizes of the RH arthroplasty used for each specimen

Specimen	Head Size [mm]	Stem Size [mm]
1	24 + 2	5.5
2	26 + 2	
3	20	
4	20	
5	20	

Anterior Surgical Approach

AL Repaired Condition

1) AL and joint capsule severed
2) AL and joint capsule repaired

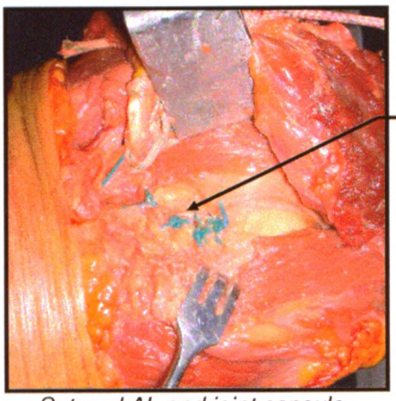

Sutured AL and joint capsule.

RH Excised Condition

3) AL and joint capsule severed
4) RH excision

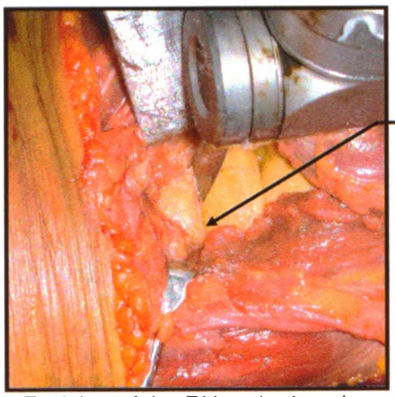

Excision of the RH at the junction of the RH and neck.

5) RH removed

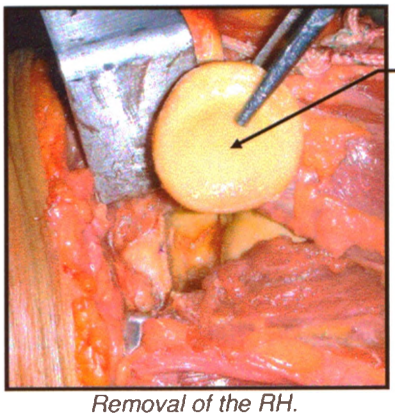

Removal of the RH.

6) AL and joint capsule repaired

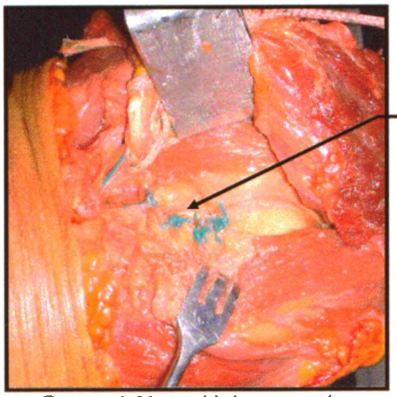

Sutured AL and joint capsule.

RH Arthroplasty Condition

7) Selected RH replacement

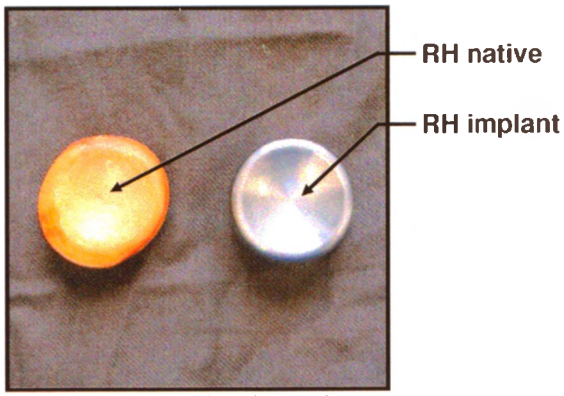

RH implant (right) chosen by closely matching the diameter and thickness of the articular surface to that of the resected RH (left).

8) Insertion of RH replacement

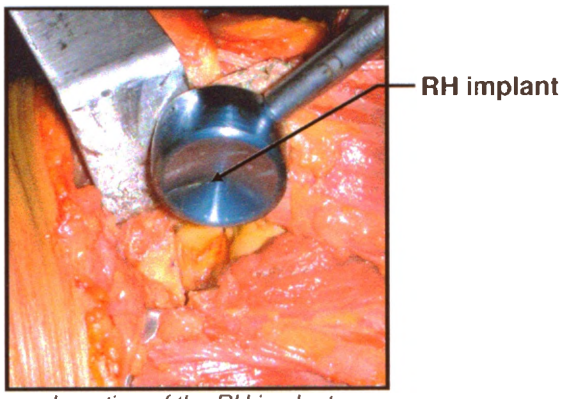

Insertion of the RH implant.

9) RH replacement inserted

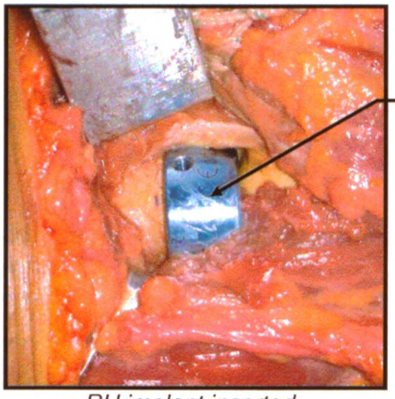

RH implant inserted.

10) AL and joint capsule repaired

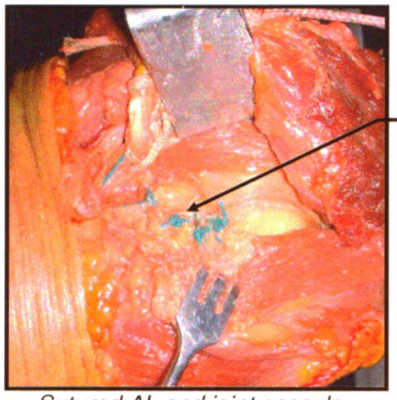

Sutured AL and joint capsule.

A9.2 RESULTS

A9.2.1 Valgus Position: Active Elbow Flexion

A9.2.1.1 *AMCL Tension (Figure 5.1)*

Table A9.4: AMCL tension two-way repeated measures ANOVA statistical analysis results (p-values) for active valgus neutral flexion for the RH study

Main effect of RH condition on AMCL tension			p = 0.003
Pairwise Comparison Results			
Intact	vs.	AL Repaired	p = 0.425
	vs.	RH Excised	p = 0.006
	vs.	RH Arthroplasty	p = 0.142
All other combinations of the RH conditions			p > 0.050

Table A9.5: Minimum and maximum AMCL tension magnitudes for active valgus neutral flexion for the RH study

Ranges of AMCL tension magnitudes (considering all degrees of elbow flexion) for the intact, the AL repaired, the RH excised, and the RH arthroplasty conditions.

Intact	
minimum:	43.4 ± 9.3 N at 20º of flexion
maximum:	94.3 ± 40.5 N at 120º of flexion
AL Repaired	
minimum:	47.8 ± 14.2 N at 20º of flexion
maximum:	95.2 ± 34.2 N at 97º of flexion
RH Excised	
minimum:	64.4 ± 11.8 N at 20º of flexion
maximum:	104.2 ± 31.5 N at 82º of flexion
RH Arthroplasty	
minimum:	54.3 ± 12.6 N at 20º of flexion
maximum:	95.9 ± 38.5 N at 89º of flexion

Table A9.6: AMCL tension at every 10° of elbow flexion for each RH condition for active valgus neutral flexion

Flexion Angle [Degrees]	Intact		AL Repaired		RH Excised		RH Arthroplasty	
	Mean AMCL Tension [N]	Standard Deviation [N]	Mean AMCL Tension [N]	Standard Deviation [N]	Mean AMCL Tension [N]	Standard Deviation [N]	Mean AMCL Tension [N]	Standard Deviation [N]
20	43.4	± 9.3	47.8	± 14.2	64.4	± 11.8	54.3	± 12.6
30	56.0	± 9.7	61.0	± 14.7	82.2	± 17.0	69.8	± 14.7
40	67.0	± 15.6	73.7	± 19.7	93.3	± 21.5	80.8	± 22.4
50	76.1	± 23.3	81.9	± 24.3	99.5	± 23.4	88.0	± 29.0
60	82.0	± 29.5	87.6	± 29.0	102.3	± 26.1	91.6	± 33.2
70	86.2	± 34.0	91.5	± 32.2	103.6	± 28.7	94.2	± 35.4
80	88.4	± 36.4	93.7	± 33.6	104.1	± 31.0	95.4	± 37.5
90	90.0	± 38.4	95.0	± 34.3	103.9	± 32.7	95.8	± 38.6
100	91.5	± 39.0	95.1	± 34.1	102.4	± 34.0	95.7	± 39.1
110	92.1	± 39.6	94.4	± 34.1	100.0	± 34.5	94.8	± 38.8
120	94.3	± 40.5	94.9	± 34.4	99.0	± 33.9	94.5	± 37.4

Table A9.7: Minimum and maximum AMCL tension standard deviations for active valgus neutral flexion for the RH study

Ranges of AMCL tension standard deviations (considering all degrees of elbow flexion) for the intact, the AL repaired, the RH excised, and the RH arthroplasty conditions.

RH Condition	Range of Standard Deviations
Intact	±8.7 N – ±40.5 N
AL Repaired	±14.2 N – ±34.4 N
RH Excised	±11.8 N – ±34.6 N
RH Arthroplasty	±12.3 N – ±39.1 N

Table A9.8: The average AMCL tension level (considering all degrees of elbow flexion) for each RH condition for active valgus neutral flexion

	Intact	AL Repaired	RH Excised	RH Arthroplasty
Average AMCL tension throughout elbow flexion [N]	79.7 ± 29.0	84.4 ± 28.0	97.3 ± 27.2	88.0 ± 31.2

A9.2.1.2 *Kinematics – Valgus Angulation (Figure 5.2)*

Table A9.9: Valgus angulation two-way repeated measures ANOVA statistical analysis results (p-values) for active valgus neutral flexion for the RH study

Main effect of RH condition on valgus angulation			p = 0.023
Pairwise Comparison Results			
Intact	vs.	AL Repaired	p = 0.772
	vs.	RH Excised	p = 0.051
	vs.	RH Arthroplasty	p = 1.000
AL Repaired	vs.	RH Excised	p = 0.045
All other combinations of the RH conditions			p > 0.050

Table A9.10: Minimum and maximum valgus angulations for active valgus neutral flexion for the RH study

Ranges of valgus angulations (considering all degrees of elbow flexion) for the intact, the AL repaired, the RH excised, and the RH arthroplasty conditions.

Intact	
maximum:	14.0 ± 2.8º at 20º of flexion
minimum:	12.8 ± 2.9º, 12.8 ± 3.2º, and 12.8 ± 3.5º at 90º, 100º and 110º of flexion, respectively
AL Repaired	
maximum:	14.1 ± 2.8º at 20º of flexion
minimum:	12.9 ± 3.2º and 12.9 ± 3.5º at 100º and 110º of flexion, respectively
RH Excised	
maximum:	16.4 ± 3.6º at 20º of flexion
minimum:	13.5 ± 4.1º at 120º of flexion
RH Arthroplasty	
maximum:	14.4 ± 3.6º at both 20º and 30º of flexion
minimum:	13.0 ± 4.0º at 120º of flexion

Table A9.11: Valgus angulation at every 10° of elbow flexion for each RH condition for active valgus neutral flexion

Flexion Angle [Degrees]	Intact		AL Repaired		RH Excised		RH Arthroplasty	
	Mean Valgus Angulation [Degrees]	Standard Deviation [Degrees]	Mean Valgus Angulation [Degrees]	Standard Deviation [Degrees]	Mean Valgus Angulation [Degrees]	Standard Deviation [Degrees]	Mean Valgus Angulation [Degrees]	Standard Deviation [Degrees]
20	14.0	± 2.8	14.1	± 2.8	16.4	± 3.6	14.4	± 3.6
30	13.9	± 2.7	14.0	± 2.7	16.3	± 3.5	14.4	± 3.6
40	13.6	± 2.6	13.8	± 2.6	15.8	± 3.4	14.2	± 3.5
50	13.3	± 2.6	13.6	± 2.6	15.4	± 3.3	13.9	± 3.5
60	13.1	± 2.5	13.4	± 2.6	14.9	± 3.3	13.7	± 3.4
70	13.0	± 2.6	13.2	± 2.7	14.6	± 3.2	13.5	± 3.3
80	12.9	± 2.8	13.0	± 2.8	14.2	± 3.2	13.4	± 3.3
90	12.8	± 2.9	13.0	± 3.0	13.9	± 3.3	13.2	± 3.3
100	12.8	± 3.2	12.9	± 3.2	13.8	± 3.5	13.1	± 3.4
110	12.8	± 3.5	12.9	± 3.5	13.6	± 3.8	13.1	± 3.7
120	12.9	± 3.9	13.0	± 3.9	13.5	± 4.1	13.0	± 4.0

Table A9.12: Minimum and maximum valgus angulation standard deviations for active valgus neutral flexion for the RH study

Ranges of valgus angulation standard deviations (considering all degrees of elbow flexion) for the intact, the AL repaired, the RH excised, and the RH arthroplasty conditions.

RH Condition	Range of Standard Deviations
Intact	±2.5º – ±3.9º
AL Repaired	±2.6º – ±3.9º
RH Excised	±3.2º – ±4.1º
RH Arthroplasty	±3.3º – ±4.0º

Table A9.13: The average valgus angulation (considering all degrees of elbow flexion) for each RH condition for active valgus neutral flexion

	Intact	AL Repaired	RH Excised	RH Arthroplasty
Average valgus angulation throughout elbow flexion [Degrees]	13.2 ± 2.9	13.4 ± 2.9	14.8 ± 3.5	13.6 ± 3.5

A9.2.2 Dependent Position: Active Elbow Flexion

A9.2.2.1 *AMCL Tension (Figure 5.3)*

Table A9.14: AMCL tension two-way repeated measures ANOVA statistical analysis results (p-value) for active dependent neutral flexion for the RH study

There was no significant main effect of RH condition on AMCL tension.

Main effect of RH condition on AMCL tension	p = 0.064

Table A9.15: Minimum and maximum AMCL tension magnitudes for active dependent neutral flexion for the RH study

Ranges of AMCL tension magnitudes (considering all degrees of elbow flexion) for the intact, the AL repaired, the RH excised, and the RH arthroplasty conditions.

Intact	
minimum:	5.5 ± 10.0 N at 20º of flexion
maximum:	56.0 ± 17.9 N at 120º of flexion
AL Repaired	
minimum:	4.0 ± 6.7 N at 20º of flexion
maximum:	52.5 ± 18.1 N at 120º of flexion
RH Excised	
minimum:	14.6 ± 16.5 N at 20º of flexion
maximum:	55.5 ± 21.7 N at 91º of flexion
RH Arthroplasty	
minimum:	5.0 ± 8.6 N at 20º of flexion
maximum:	44.9 ± 11.5 N at 120º of flexion

Table A9.16: AMCL tension at every 10° of elbow flexion for each RH condition for active dependent neutral flexion

Flexion Angle [Degrees]	Intact		AL Repaired		RH Excised		RH Arthroplasty	
	Mean AMCL Tension [N]	Standard Deviation [N]	Mean AMCL Tension [N]	Standard Deviation [N]	Mean AMCL Tension [N]	Standard Deviation [N]	Mean AMCL Tension [N]	Standard Deviation [N]
20	5.5	± 10.0	4.0	± 6.7	14.6	± 16.5	5.0	± 8.6
30	8.7	± 15.5	6.8	± 11.1	25.9	± 26.5	10.0	± 17.0
40	11.9	± 20.9	9.7	± 15.0	35.6	± 34.9	15.0	± 23.0
50	14.3	± 23.4	12.5	± 17.0	41.0	± 35.6	21.2	± 26.5
60	16.9	± 24.8	15.1	± 18.4	44.5	± 32.4	27.8	± 30.7
70	20.2	± 24.9	18.3	± 19.3	49.4	± 28.9	33.1	± 32.2
80	24.2	± 21.4	21.4	± 18.1	54.3	± 24.8	38.2	± 32.1
90	30.9	± 17.6	25.5	± 15.1	55.5	± 22.2	41.2	± 30.5
100	40.5	± 16.9	32.6	± 10.3	54.4	± 19.2	43.4	± 25.4
110	46.3	± 14.6	41.6	± 11.5	52.6	± 15.1	43.9	± 19.2
120	56.0	± 17.9	52.5	± 18.1	50.1	± 13.8	44.9	± 11.5

Table A9.17: Minimum and maximum AMCL tension standard deviations for active dependent neutral flexion for the RH study

Ranges of AMCL tension standard deviations (considering all degrees of elbow flexion) for the intact, the AL repaired, the RH excised, and the RH arthroplasty conditions.

RH Condition	Range of Standard Deviations
Intact	±10.0 N – ±25.3 N
AL Repaired	±6.7 N – ±19.3 N
RH Excised	±13.2 N – ±36.0 N
RH Arthroplasty	±8.6 N – ±32.4 N

Table A9.18: The average AMCL tension level (considering all degrees of elbow flexion) for each RH condition for active dependent neutral flexion

	Intact	AL Repaired	RH Excised	RH Arthroplasty
Average AMCL tension throughout elbow flexion [N]	24.4 ± 19.2	21.2 ± 14.8	44.5 ± 24.4	29.9 ± 24.8

A9.2.2.2 *Kinematics – Valgus Angulation (Figure 5.4)*

Table A9.19: Valgus angulation two-way repeated measures ANOVA statistical analysis results (p-value) for active dependent neutral flexion for the RH study

There was no significant main effect of RH condition on valgus angulation.

Main effect of RH condition on valgus angulation	p = 0.091

Table A9.20: Minimum and maximum valgus angulations for active dependent neutral flexion for the RH study

Ranges of valgus angulations (considering all degrees of elbow flexion) for the intact, the AL repaired, the RH excised, and the RH arthroplasty conditions.

Intact	
maximum:	10.7 ± 2.4º at 40º of flexion
minimum:	9.5 ± 2.7º at 110º of flexion
AL Repaired	
maximum:	10.5 ± 2.2º and 10.5 ± 2.0º at 30º and 40º of flexion, respectively
minimum:	9.5 ± 2.6º and 9.5 ± 2.8º at 100º and 110º of flexion, respectively
RH Excised	
maximum:	13.2 ± 3.7º at 30º of flexion
minimum:	9.9 ± 3.4º at 120º of flexion
RH Arthroplasty	
maximum:	11.3 ± 3.9º at 40º of elbow flexion
minimum:	9.7 ± 3.6º and 9.7 ± 3.8º at 110º and 120º of flexion, respectively

Table A9.21: AMCL tension at every 10° of elbow flexion for each RH condition for active dependent neutral flexion

	Intact		AL Repaired		RH Excised		RH Arthroplasty	
Flexion Angle [Degrees]	Mean Valgus Angulation [Degrees]	Standard Deviation [Degrees]	Mean Valgus Angulation [Degrees]	Standard Deviation [Degrees]	Mean Valgus Angulation [Degrees]	Standard Deviation [Degrees]	Mean Valgus Angulation [Degrees]	Standard Deviation [Degrees]
20	10.5	± 2.5	10.4	± 2.3	13.0	± 3.7	10.8	± 3.6
30	10.6	± 2.4	10.5	± 2.2	13.2	± 3.7	11.2	± 3.8
40	10.7	± 2.4	10.5	± 2.0	13.0	± 3.5	11.3	± 3.9
50	10.6	± 2.3	10.4	± 2.1	12.7	± 3.3	11.2	± 3.9
60	10.4	± 2.3	10.2	± 2.0	12.1	± 3.0	11.0	± 3.8
70	10.2	± 2.3	10.0	± 2.1	11.5	± 2.8	10.8	± 3.5
80	9.9	± 2.4	9.9	± 2.3	11.1	± 2.7	10.5	± 3.5
90	9.8	± 2.5	9.6	± 2.4	10.7	± 2.7	10.2	± 3.4
100	9.6	± 2.6	9.5	± 2.6	10.3	± 2.8	9.9	± 3.5
110	9.5	± 2.7	9.5	± 2.8	10.1	± 3.0	9.7	± 3.6
120	9.7	± 3.2	9.7	± 3.3	9.9	± 3.4	9.7	± 3.8

Table A9.22: Minimum and maximum valgus angulation standard deviations for active dependent neutral flexion for the RH study

Ranges of valgus angulation standard deviations (considering all degrees of elbow flexion) for the intact, the AL repaired, the RH excised, and the RH arthroplasty conditions.

RH Condition	Range of Standard Deviations
Intact	±2.3º – ±3.2º
AL Repaired	±2.0º – ±3.3º
RH Excised	±2.7º – ±3.7º
RH Arthroplasty	±3.4º – ±3.9º

Table A9.23: The average AMCL tension level (considering all degrees of elbow flexion) for each RH condition for active dependent neutral flexion

	Intact	AL Repaired	RH Excised	RH Arthroplasty
Average valgus angulation throughout elbow flexion [Degrees]	10.1 ± 2.5	10.0 ± 2.4	11.6 ± 3.1	10.6 ± 3.7

APPENDIX 10

Functionality Assessment of the Buckle Transducer

The functionality of the buckle transducer was assessed by performing several investigations, including repeatability, reproducibility, and invasiveness. The results of the reproducibility and invasiveness investigations are presented in the following section; recall that the results of the repeatability investigation were presented in Chapter 3 (Section 3.3.1).

A10.1 REPRODUCIBILITY

The reproducibility investigation assessed the buckle transducer's ability to produce consistent AMCL tension measurements after several cycles of insertion and removal of the transducer. Reproducibility of the buckle transducer was investigated at the end of the testing protocol (*i.e.* after the wrist flexor and radial head studies described in Chapters 4 and 5, respectively). Reproducibility was investigated for three specimens (specimens 1, 2, and 5). Testing was conducted with the arm oriented in the valgus position, with the elbow under active motion. For each insertion, three active flexion cycles were performed with the forearm in neutral rotation. Table A10.1 summarizes the testing protocol. For each insertion, the AMCL tension measurements from the third flexion cycle were analysed.

Table A10.1: Motion protocol for the reproducibility investigation

There was one test condition: active flexion in the valgus position. Data from only the third flexion cycle (of three) were analysed. Extension data were not analysed. It should be noted that for insertion 1 the buckle transducer was sutured to the adjacent joint capsule to maintain its alignment with the ligament during motion; however, for insertions 2 through 4 the transducer was not sutured to the capsule.

VALGUS POSITION							
Active Motion							
Insertion 1		**Insertion 2**		**Insertion 3**		**Insertion 4**	
Extension (×3)	Flexion (×3)	Extension (×3)	Flexion (×3)	Extension (×3)	Flexion (×3)	Extension (×3)	Flexion (×3)

The data presented here corresponds to that of the measurements obtained from specimen 2. To be consistent with the repeatability investigation, specimen 2 was also chosen to illustrate the results of the reproducibility investigation; however, it should be noted that all other specimens tested were analysed in the same manner. Figure A10.1 shows the results of the reproducibility investigation for specimen 2. All four measurements were similar, hence indicating good reproducibility of the buckle transducer; however, in particular, the curves corresponding to the measurements taken on insertions 2 through 4 were most equivalent throughout the arc of elbow flexion. The net effect of all four AMCL tension measurements is shown by the average curve (± one standard deviation) (Figure A10.1).

The reproducibility of the buckle transducer was quantified in terms of the standard deviations. The minimum and maximum magnitudes of standard deviations were found to be approximately ±0.6 N and ±2.6 N, respectively. Expressing the standard deviations as a percentage of the mean AMCL tensions, the minimum and maximum standard deviations as percentages were approximately ±0.8% (or ±1.0 N / 117.9 N) and ±4.2% (or ±0.7 N / 17.2 N), respectively.

In particular for this specimen, the difference in AMCL tensions between insertion 1 and insertions 2 through 4 may possibly be explained by the presence of the suture during insertion 1 (recall that for insertion 1 the transducer was sutured to the adjacent joint capsule, whereas for insertions 2 through 4 it was not). However, this trend was not observed for the other specimens (specimens 1 and 5) investigated for reproducibility.

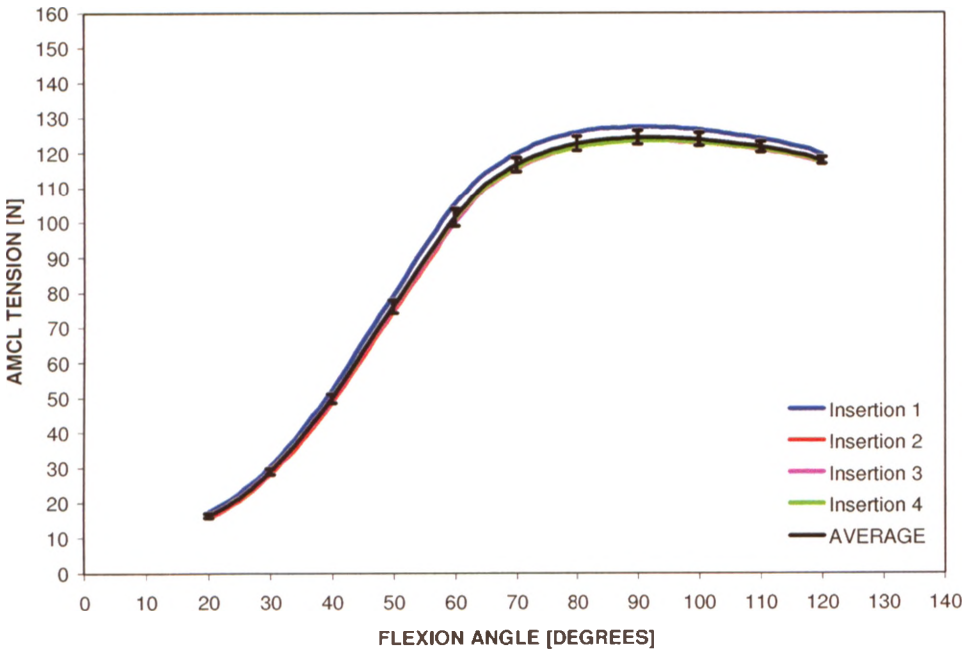

Figure A10.1: AMCL tension measurements of one specimen tested in active flexion in the valgus position for the reproducibility investigation

For each of the four insertions, the AMCL tension measurements throughout the arc of elbow flexion are shown for one specimen (specimen 2). All four measurements were similar, hence indicating good reproducibility of the buckle transducer. The average curve shows the standard deviations at every 10° of elbow flexion, which ranged from ±0.6 N to ±2.6 N throughout the arc of elbow flexion.

Table A10.2: Minimum and maximum standard deviations of the average AMCL tension for the three specimens tested in active valgus neutral flexion for the reproducibility investigation

Specimen No.	Standard Deviation [N]		Standard Deviation Expressed as a Percentage of the Average Tension [%]	
	minimum	maximum	minimum	maximum
1	± 0.25	± 2.47	± 0.27 (± 0.2510 N / 91.6485 N)	± 3.15 (± 2.4490 N / 77.7980 N)
2	± 0.59	± 2.58	± 0.85 (± 0.9993 N / 117.8507 N)	± 4.20 (± 0.7210 N / 17.1559 N)
5	± 1.27	± 3.65	± 0.99 (± 1.2661 N / 127.9076 N)	± 3.95 (± 3.6456 N / 92.2495 N)

A10.2 INVASIVENESS

Invasiveness of the buckle transducer was assessed in two ways. First, an investigation was performed to determine whether the presence of the buckle transducer within the AMCL caused damage to the tissue during the testing protocol, and as a result, altered the loading response of the tissue. The second investigation compared the kinematics of the forearm with the buckle transducer in the tissue to the kinematics of the forearm without the transducer present, to determine whether the presence of the buckle transducer within the AMCL altered the motion pathways of the forearm.

A10.2.1 Invasiveness Investigation Part I – Investigation of AMCL Loading Response Due to the Presence of the Buckle Transducer

In this study, two AMCL tension and valgus angulation measurements were taken in active flexion in the valgus position, as well as in active flexion in the dependent position. The first measurement was taken with the buckle transducer in the AMCL prior to the wrist flexor study (the *beginning* condition) and the second measurement was also taken with the buckle transducer in the AMCL, but at the end of the wrist flexor study (the *end* condition); the wrist flexors were not loaded when these measurements were obtained. For each test condition, three flexion cycles were performed in the valgus and dependent positions, with the forearm in neutral rotation. All AMCL tension and elbow kinematic data correspond to the measurements obtained from the third flexion cycle. This investigation was performed on four specimens (specimens 2 through 5) for the valgus position, and on three specimens (specimens 2, 3, and 5) for the dependent position.

The *beginning* and *end* data were analysed using a two-way repeated measures analysis of variance (ANOVA) with $\alpha = 0.05$, and *post hoc* paired *t*-tests using the Bonferroni correction for family-wise error (SPSS V16.0.1, Chicago, IL). There was no statistical difference in the AMCL tension levels between the *beginning* and the *end* conditions, for both the valgus and dependent positions ($p = 0.285$ and $p = 0.188$, respectively). Furthermore, there was no statistical difference in the motion pathways between the *beginning* and the *end* conditions, for both the valgus and dependent

positions ($p = 0.504$ and $p = 0.224$, respectively). For the valgus position, the largest difference between *beginning* and *end* AMCL tensions was approximately **4.1 N** (at **44°** of elbow flexion) (Figure A10.2), whereas the largest difference between *beginning* and *end* valgus angulations was approximately **0.3°** (at **50°** of elbow flexion) (Figure A10.4). For the dependent position, the largest difference between *beginning* and *end* AMCL tensions was approximately **14.0 N** (at **118°** of elbow flexion) (Figure A10.3), whereas the largest difference between *beginning* and *end* valgus angulations was approximately **0.3°** (at **120°** of elbow flexion) (Figure A10.5). Therefore, it can be concluded that the presence of the buckle transducer within the AMCL did not alter the loading response of the tissue, both in terms of tension and kinematics, as no significant difference was found between the tissue response at the beginning and end of the wrist flexor study.

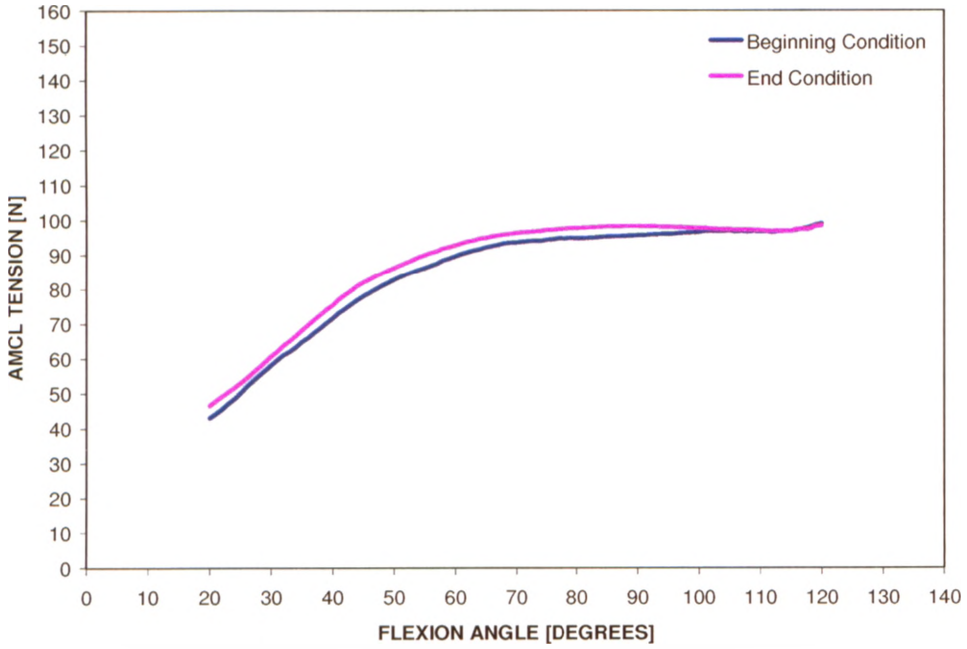

Figure A10.2: Mean AMCL tension levels for active flexion in the valgus position for the beginning and end of the WF study

Mean AMCL tension levels throughout the arc of elbow flexion are shown for the beginning of the WF study (*beginning* condition) and for the end of the WF study (*end* condition) ($n = 4$). There was no statistical difference in the AMCL tension levels between the *beginning* and the *end* conditions ($p = 0.285$). Standard deviations are omitted for clarity but ranged from ±9.7 N to ±45.2 N for the *beginning* curve, and from ±17.0 N to ±41.1 N for the *end* curve.

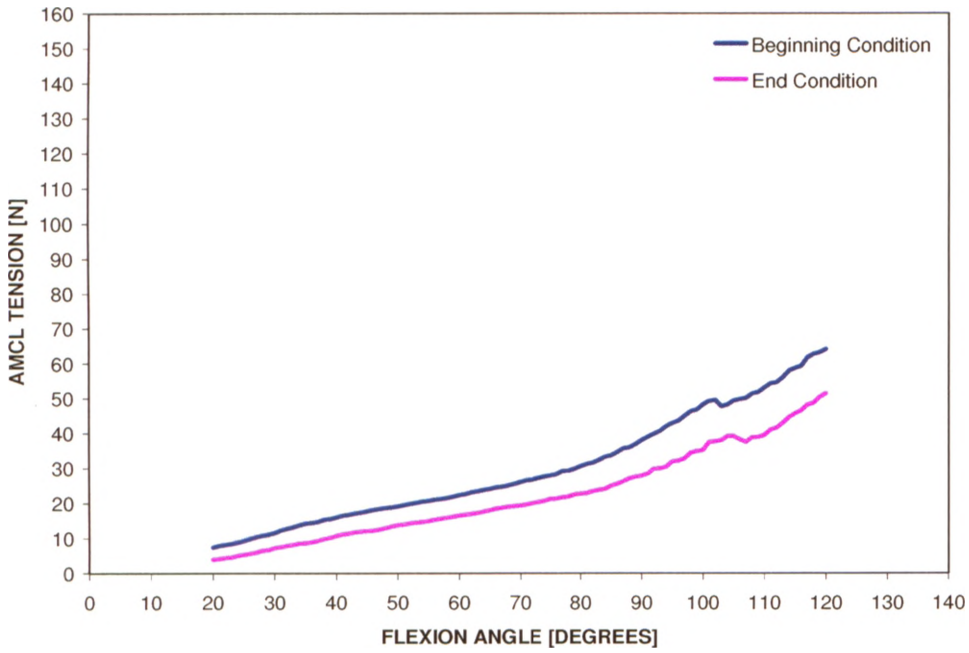

Figure A10.3: Mean AMCL tension levels for active flexion in the dependent position for the beginning and end of the WF study

Mean AMCL tension levels throughout the arc of elbow flexion are shown for the beginning of the WF study (*beginning* condition) and for the end of the WF study (*end* condition) (n = 3). There was no statistical difference in the AMCL tension levels between the *beginning* and the *end* conditions (p = 0.188). Standard deviations are omitted for clarity but ranged from ±4.6 N to ±28.0 N for the *beginning* curve, and from ±0.5 N to ±18.0 N for the *end* curve.

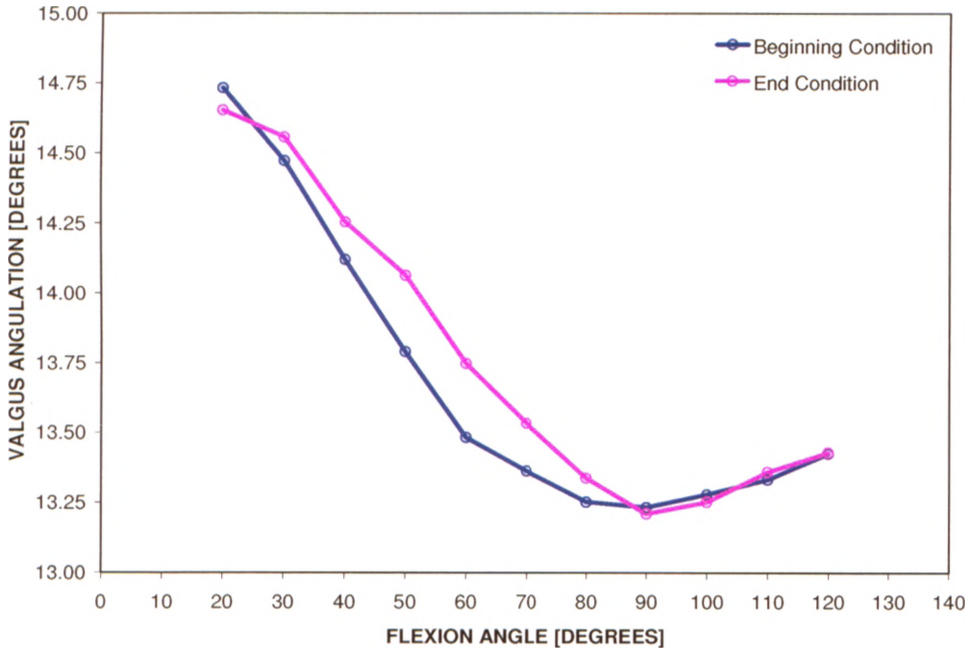

Figure A10.4: Mean elbow kinematic pathways for active flexion in the valgus position for the beginning and end of the WF study

Mean valgus angulation of the ulna relative to the humerus at every 10° of elbow flexion is shown for the beginning of the WF study (*beginning* condition) and for the end of the WF study (*end* condition) (n = 4). There was no statistical difference in the motion pathways between the *beginning* and the *end* conditions (p = 0.504). Standard deviations are omitted for clarity but ranged from ±2.6° to ±4.3° for both the *beginning* and *end* curves.

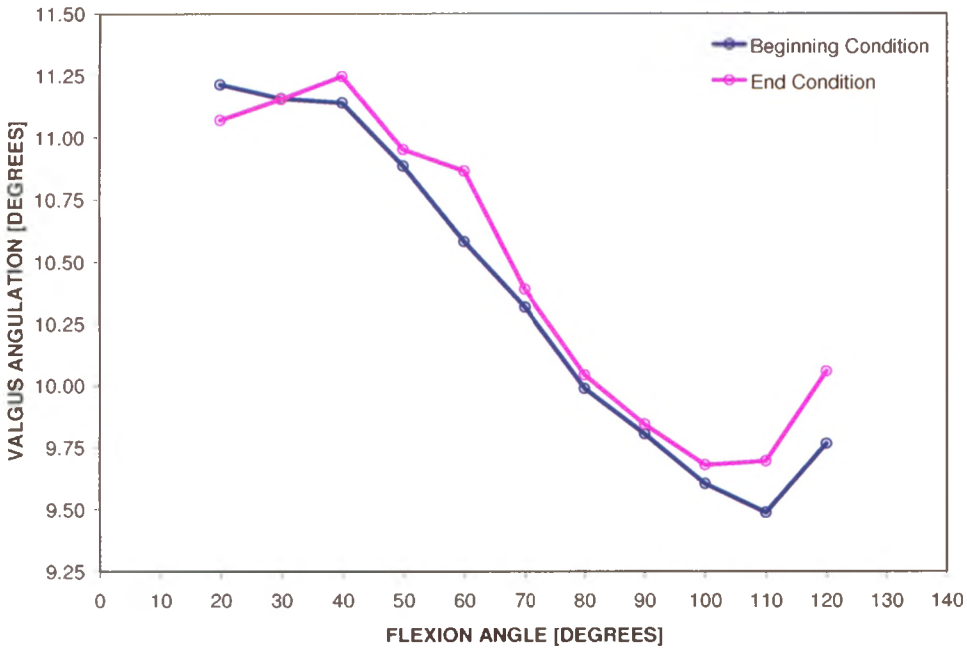

Figure A10.5: Mean elbow kinematic pathways for active flexion in the dependent position for the beginning and end of the WF study

Mean valgus angulation of the ulna relative to the humerus at every 10° of elbow flexion is shown for the beginning of the WF study (*beginning* condition) and for the end of the WF study (*end* condition) (n = 3). There was no statistical difference in the motion pathways between the *beginning* and the *end* conditions (p = 0.224). Standard deviations are omitted for clarity but ranged from ±2.6° to ±4.0° for the *beginning* curve, and from ±2.5° to ±4.3° for the *end* curve.

A10.2.2 Invasiveness Investigation Part II – Investigation of Elbow Kinematic Pathways Due to the Presence of the Buckle Transducer

In this study, two valgus angulation measurements were taken in active flexion in the valgus position; both measurements were taken at the end of the testing protocol (*i.e.* after the wrist flexor and radial head studies). The first valgus angulation measurement was taken with the buckle transducer in the AMCL (the *buckle-in* condition) and the second valgus angulation measurement was taken with the buckle transducer out of the AMCL (the *buckle-out* condition). For each test condition, three active flexion cycles were performed in the valgus position, with the forearm in neutral rotation. Both valgus angulations correspond to the measurements obtained from the third flexion cycle. This investigation was performed on all five specimens.

The *buckle-in* and *buckle-out* data were analysed using a two-way repeated measures analysis of variance (ANOVA) with $\alpha = 0.05$, and relevant *post hoc* paired *t*-tests using the Bonferroni correction for family-wise error (SPSS V16.0.1, Chicago, IL). There was a statistical difference in the motion pathways between the *buckle-in* and the *buckle-out* conditions ($p = 0.001$); however, the largest difference between *buckle-in* and *buckle-out* valgus angulations was only approximately **0.6°**, which occurred at **80°** of elbow flexion (Figure A10.6). Therefore, it can be concluded that the presence of the buckle transducer within the AMCL did slightly alter the kinematics of the forearm, as a significant difference was found between the motion pathways of the forearm with and without the transducer present.

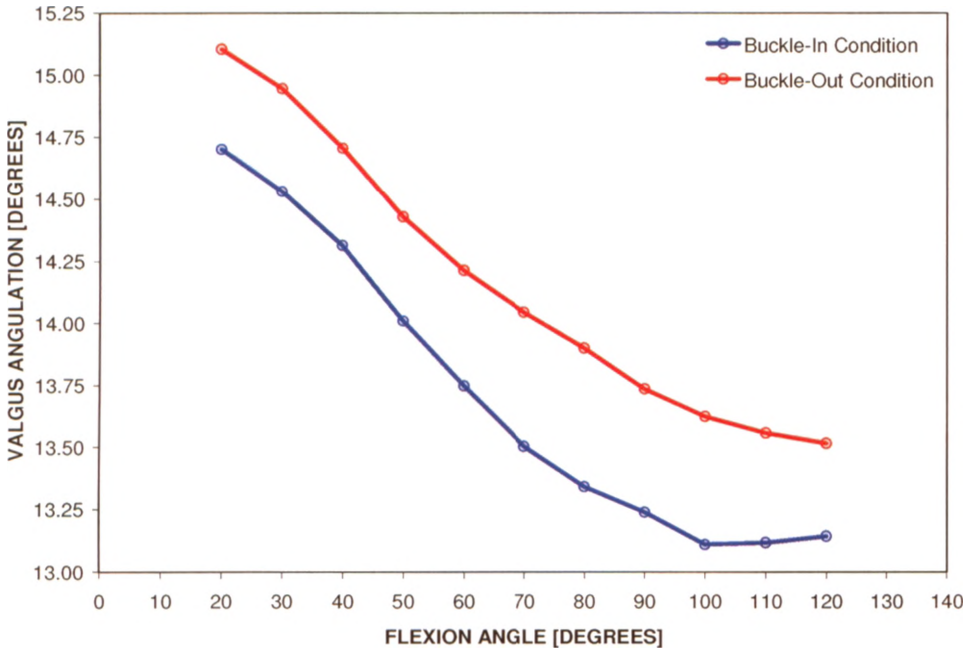

Figure A10.6: Mean elbow kinematic pathways for active flexion in the valgus position for the buckle transducer in and out of the AMCL

Mean valgus angulation of the ulna relative to the humerus at every 10° of elbow flexion is shown for when the buckle transducer was in the AMCL (*buckle-in* condition) and for when the buckle transducer was out of the AMCL (*buckle-out* condition) (n = 5). There was a statistical difference in the motion pathways between the *buckle-in* and the *buckle-out* conditions ($p = 0.001$). Standard deviations are omitted for clarity but ranged from ±3.2° to ±4.0° for the *buckle-in* curve, and from ±3.4° to ±4.1° for the *buckle-out* curve.

A10.2.3 Summary of Invasiveness Investigation

Thus, based on the results of this investigation, it should be noted that all tension and valgus angulation measurements presented in this thesis will vary from those found physiologically (based on the results of the second investigation of invasiveness). This aforementioned statement is based on the fact that AMCL tension and valgus angulation are correlated, as discussed in Chapters 4 and 5. Based on the results of the first investigation of invasiveness, all data presented in this thesis will consistently differ from the physiological, as it has been shown that once the buckle transducer is in the tissue, tensions and valgus angulations remain consistent with multiple flexion cycles.

APPENDIX 11

Photographs of the Buckle Transducer in the AMCL

Full Extension

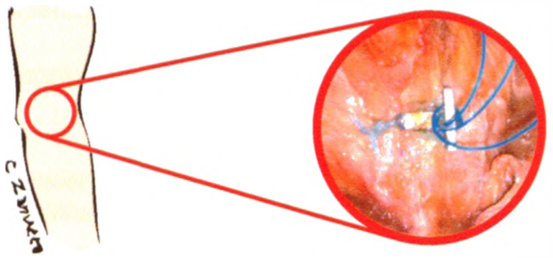

Mid Flexion

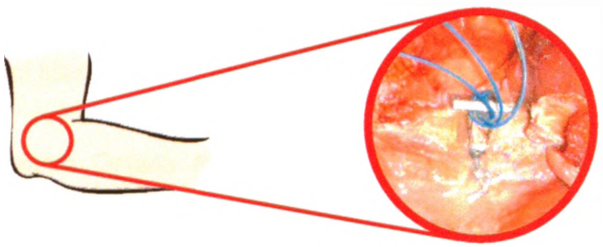

Full Flexion

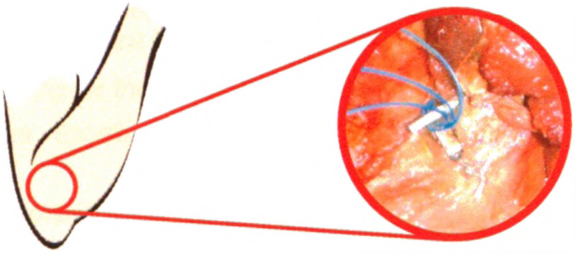

Note: Alignment of buckle transducer with the AMCL was maintained throughout the arc of elbow flexion. Insertion of the buckle transducer was anteriorly directed.